



**HAL**  
open science

# Optimization of the infrastructure cost of hydrogen transported at different states of aggregation in France and Germany.

Amin Lahnaoui

► **To cite this version:**

Amin Lahnaoui. Optimization of the infrastructure cost of hydrogen transported at different states of aggregation in France and Germany.. Chemical and Process Engineering. Institut Polytechnique de Paris; Forschungszentrum (Jülich, Allemagne), 2020. English. NNT : 2020IPPAE008 . tel-03506254

**HAL Id: tel-03506254**

**<https://theses.hal.science/tel-03506254>**

Submitted on 2 Jan 2022

**HAL** is a multi-disciplinary open access archive for the deposit and dissemination of scientific research documents, whether they are published or not. The documents may come from teaching and research institutions in France or abroad, or from public or private research centers.

L'archive ouverte pluridisciplinaire **HAL**, est destinée au dépôt et à la diffusion de documents scientifiques de niveau recherche, publiés ou non, émanant des établissements d'enseignement et de recherche français ou étrangers, des laboratoires publics ou privés.

# Optimization of the infrastructure cost of hydrogen transported at different states of aggregation in France and Germany

Thèse de doctorat de l'Institut Polytechnique de Paris  
Préparée à l'ENSTA en collaboration avec Forschungszentrum Jülich

École doctorale n°626 : Ecole Doctorale de l'Institut Polytechnique de  
Paris (ED IP Paris)  
Spécialité de doctorat: Ingénierie, mécanique et énergétique

Thèse présentée et soutenue à Paris le 25/09/2020, par

**Amin Lahnaoui**

Composition du Jury :

Richard LE GOFF Professeur, ENSTA Paris (– UEA)	Président du jury
Didier DALMAZZONE Professeur, ENSTA Paris (– UCP)	Directeur de thèse
Alain THOREL Directeur de recherche, Mines ParisTech (– MAT)	Rapporteur
Frederic LANTZ Professeur, IFP School	Rapporteur
Oifa TLILI Ingénieur de recherche, CEA	Examinatrice
Christina WULF Ingénieur de recherche, FZJ (– IEK-STE),	Co-Directrice de thèse
Patrice PARICAUD Professeur, ENSTA Paris (– UCP)	Co-Directeur de thèse

# ACKNOWLEDGMENT

First, I would like to express my sincere gratitude to my professor Prof. Didier Dalmazzone for his supervision and guidance, and Dr. Christina Wulf, for her support and help during my thesis program. It was an honor to work under your supervision and learn from you.

I would also like to acknowledge all the colleagues and friends at the Institute of Energy and Climate Research at IEK-STE for welcoming me. Special thanks to Dr. Peter Stenzel, my master thesis supervisor, who encouraged me to start this adventure, Mrs. Müller-Pohlers, Fabian, and Thomas for the help and guidance during my stay in Germany, to all other colleagues, and IEK football team. I would also like to thank the HITEC program and institute Polytechnique of Paris that have made the realization of this work possible.

Needless to say, that I would like to thank my parents to all the love they have given to me throughout the years, Anaheim and Bassam, for their unlimited patience and encouragement throughout the Ph.D. period. This work would not have been possible without their endless support and assistance from the whole family and friends.

# RESUME

L'hydrogène vert pour la mobilité via les véhicules électriques à pile à combustible représente une alternative au carburant conventionnel pour décarboniser le secteur des transports et développer un système énergétique durable. Néanmoins, les propriétés thermodynamiques de l'hydrogène rendent inefficaces le transport et le stockage de ce vecteur d'énergie à ses conditions de pression et de température standard. Par conséquent, cette thèse vise à étudier les techniques de transport de l'hydrogène et à modéliser l'infrastructure optimale pour différents scénarios de production et de demande en France et en Allemagne, couplée à une visualisation géographique de la distribution.

Pour le cadre considéré et pour permettre la comparaison entre les deux pays, l'énergie éolienne en tant que source de production d'hydrogène a été considéré pour répondre à la demande. Le réseau de transport a été limité à l'infrastructure routière pour étudier l'impact de différents états d'agrégation sur le flux d'hydrogène transporté pour 15 scénarios.

Dans un premier plan, plusieurs technologies de transport et de stockage d'hydrogène sont analysées en calculant les besoins énergétiques de transformation pour déduire les coûts de traitement, de stockage et de transport d'hydrogène. Ainsi, le travail de compression a été modélisé à l'aide d'un compresseur à plusieurs étages et comparé à 875 compresseurs industriels ; le travail de liquéfaction a été calculé en utilisant le travail idéal associé à différents processus de liquéfaction ; tandis que les processus d'hydrogénation et de déshydrogénation ont été simulés à l'aide d'ASPEN. Cela a permis de déduire les différents coûts d'investissement et d'exploitation.

Dans un second plan, ces coûts sont formulés comme des fonctions de coûts unitaires annuels basés sur la valeur actuelle nette et incluant le stockage, le transport routier, la liquéfaction, la compression et la déshydrogénation. Enfin, pour conclure quant à la part des sept technologies utilisées pour transporter et stocker l'hydrogène, une optimisation, basée sur une programmation linéaire a été réalisée. Ce sous-modèle a ensuite été inclus dans une optimisation générale pour relier les sites de production aux sites de distribution en utilisant le réseau routier. Ce modèle a permis ainsi de conclure aux différents coûts de déploiement des infrastructures, associés à une visualisation géographique de l'hydrogène transporté en Allemagne et en France.

Les résultats du sous-modèle ont montré qu'en moyenne, le gaz comprimé à haute pression est principalement utilisé à une distance de transport inférieure à 250 km contrairement à l'hydrogène liquide qui a des coûts énergétiques plus élevés. Le modèle a montré que le choix de la technologie est plus critique à court terme, et que les coûts de déploiement de l'infrastructure peuvent être amorties, en remplaçant le transport et le stockage du gaz comprimé à faible et moyenne pression par les liquides organiques porteurs d'hydrogène. Enfin, l'analyse des 15 scénarios a montré une meilleure répartition géographique de l'hydrogène en France, contrairement à l'Allemagne qu'a connue une disparité entre les éventuels points de production et de consommation.

# ABSTRACT

Green hydrogen for mobility via fuel cell electric vehicles represent an alternative to conventional fuel to decarbonize transportation sector and develop a sustainable future energy system. Nevertheless, the thermodynamic properties make the transport and the storage of this energy carrier at its standard conditions inefficient. Therefore, this thesis aims to investigate hydrogen transport technologies and to model the optimal infrastructure for different production and demand scenarios in France and Germany, coupled with geographical visualization of the distribution.

For the framework considered, and to allow the comparison between the two countries, wind power as an energy source was considered for hydrogen production to fuel the demand for. The network to transport hydrogen is restrained to the road infrastructure to investigate the impact of different state of aggregations on the hydrogen flow transported between different hydrogen production and distribution locations and capacities defined from 15 scenarios.

First, several technologies for transporting and storing hydrogen at its liquid and gas states are analyzed by calculating the energy requirements to deduce the costs of processing, storing and transporting hydrogen using trucks. Thus, compression work has been modelled using a multistage compressor and compared to 875 industrial compressors; Liquefaction work was calculated using the ideal work associated to a literature review on different liquefaction processes; While hydrogenation and de-hydrogenation process work has been simulated using ASPEN. This allowed defining the cost parameters chosen for investment and operation.

Then, these costs are formulated as annual levelized costs functions that include storage, road transport, liquefaction, compression, and de-hydrogenation costs based on the net present value methodology. Finally, to conclude to the share of the seven different technologies used to transport and store hydrogen between the locations, an optimization based on linear programming formulation was performed. This sub-model was then included in a more general cost flow optimization to link a set of production nodes to the distribution ones using the road network. This model allowed to conclude to the different cost of infrastructure deployment, associated to a geographical visualization of the hydrogen flow transported in Germany and France.

The sub-model results showed that in average compressed gas at a high-pressure level is mainly used at transport distance below 250 km in contrast to liquid hydrogen that has higher energy costs. Concerning early-stage infrastructure deployment, costs could be further minimized by substituting compressed gas at low to medium pressure levels by liquid organic hydrogen carrier. Finally, the analysis of the 15 scenarios showed a better geographical distribution of hydrogen in France, in contrast to the case of Germany that suffered from a disparity between production and eventual consumption locations.

<b>INTRODUCTION .....</b>	<b>2</b>
<b>1 HYDROGEN ECONOMY STATE OF THE ART .....</b>	<b>7</b>
I HYDROGEN ECONOMY AND PERSPECTIVE IN THE EUROPEAN UNION .....	10
II THE CASE OF FRANCE .....	14
III THE CASE OF GERMANY .....	17
IV HYDROGEN FOR TRANSPORT LITERATURE REVIEW.....	20
<b>2 HYDROGEN SUPPLY CHAIN AND FRAMEWORK.....</b>	<b>33</b>
I HYDROGEN PRODUCTION .....	41
II HYDROGEN DEMAND .....	53
III HYDROGEN TRANSPORT USING THE ROAD INFRASTRUCTURE .....	59
<b>3 TECHNICAL AND ECONOMIC ASSASSEMENT .....</b>	<b>67</b>
I TECHNICAL ASSESSMENT .....	75
II COST PARAMETERS .....	107
<b>4 MODEL AND METHODOLOGY .....</b>	<b>114</b>
I COST FUNCTIONS CALCULATION .....	121
II OPTIMIZATION MODEL .....	141
<b>5 MODEL RESULTS .....</b>	<b>150</b>
I MODEL RESULTS.....	156
II INFRASTRUCTURE MINIMUM COST.....	169
III FLOW RESULTS .....	176
<b>CONCLUSION.....</b>	<b>185</b>
<b>ANNEX .....</b>	<b>191</b>
A1. HYDROGEN PRODUCTION .....	191
A2. HYDROGEN DEMAND.....	194
A3. TECHNICAL PARAMETERS .....	196
A4. ECONOMIC PARAMETRS.....	201
A5. RESULTS.....	205
<b>FIGURES .....</b>	<b>208</b>
<b>REFERENCE.....</b>	<b>216</b>

# INTRODUCTION

**T**he current energy system is dealing with three interconnected problems, an increasing final energy demand, a high share of fossil fuels in the energy mix, and a growing impact of greenhouse gas emissions on the environment.

On the one hand, final energy demand has rapidly grown with more than 40% dependency on fossil fuels in the last decades [European-Commission, 2018a] and is expected to increase by 2040 from about 12% to 31% in case of 2°C Scenario and new policy scenario respectively [IEA, 2017]. This is mainly because of the continuously growing world population, as in the case of Africa, where the population is expected to increase by 800 million in the next coming 35 years [IEA, 2017]. Moreover, the developing nations are experiencing progressive industrialization, making them a future big energy consumer.

On the other hand, the limited resources of fossil fuels, and the geopolitical problems linked to their exploitation push to energy security improvement in order to reduce the dependency on fossil fuels and increase the supply using available and sustainable energy sources. Moreover, there is an increase of global consensus towards the increase of greenhouse gases and their impact on climate change and the rise of global temperature. The Intergovernmental Panel on Climate Change alarmed against the rising of global temperature due to climate change leading to rising sea level, water shortage problem, and significant diversity losses [Masson-Delmotte et al., 2018].

Thus, a significant international awareness raised to face the environmental problem; One example is the 21st Conference of the Parties (COP21) held in Paris in December 2015 set to fix the milestone to achieve the goal of maintaining the average global temperature below 2°C [Agency, 2015] by lowering carbon dioxide emissions to less than 45% by 2030 compared to the reference year 2010, and to have neutral to negative emission by 2050. This will severely affect the energy infrastructure system. In fact, all the newly constructed infrastructure has to have a neutral or negative carbon-emitting balance applying the use of new alternative fuels and energy sources and/ or carbon capture technologies [Pfeiffer et al., 2016].

## *Future energy system*

If the overall target of the necessity of lowering carbon emission is mainly approved, the development of the future energy system framework adequate to reach the target will still be dictated by the political, social, economic, and historical context of each country. Thus, two main

alternatives can be distinguished, ranging from the use of modified conventional resources to the adoption of alternative ones.

The first option, guided mainly by historical and geopolitical choices, fall mainly under the use of nuclear power or the use of fossil fuel associated with carbon capture and storage technologies. The second option applies the use of renewable energy sources, which enables the transformation of the entire energy system because of the potential of coupling between the different sectors. The sector coupling concept to inter-connect different sectors to each other's allows mainly to merge the transport and power sectors into a single energy vector and, therefore, increases the flexibility of the energy use. This concept can be introduced using gases like hydrogen and methane, creating the concept of power-to-gas, or different states of matter as a liquid, generalizing it to power-to-X.

### *The energy in the European Union*

The problem related to secure the energy sector and lower the dependency on fossil fuels and the export associated with it is mainly apparent in the context of the European Union context. The share of energy imports within the 28 European countries in 2016 reached 40.2%, 86.7%, and 70.4%, respectively, for solid fuel, petroleum products, and natural gas [European-Commission, 2018a], which impacts mainly the transport and household sector. For instance, 40% of households in the European Union uses natural gas for heating, which will be impacted by the increasing Geopolitical South and West. In fact, Russia is one of the main suppliers of natural gas to the EU-market [Sieminski, 2014], which requires crossing the territory of other countries, like Ukraine and thus taking the risk of a complete disruption of the transit due to geopolitics instabilities [Stern et al., 2009]. Moreover, the recent strategies to diversify the consumer portfolio towards east Asian [Stern et al., 2014] will mainly impact on the final consumer by increasing the gas prices [Bouwmeester & Oosterhaven, 2017]. South, the recent Algerian crisis and instability [CFR, 2019] will mainly have an impact on Spain and Italy as both countries export half of its demand from North Africa [European-Commission, 2018a].

Concerning greenhouse gas emissions, the European Union achieved a total reduction of 22.4% in 2016 compared to the reference year 1990 [European-Commission, 2018a]. Significant policies were adopted after the Kyoto Protocol in 1997 [Grubb et al., 1997] towards reducing carbon emissions. This resulted in the first common sustainable energy policy with the action plan and the treaty of Lisbon, commonly known for setting three 20-targets to be achieved by the signing countries in 2020 [Commission, 2007]. The first target aims to reach a total share of 20% renewable energy sources in the energy mix by 2020. The second one sets for the same year a total reduction of 20% of total carbon emission compared to the reference year 1990. The last one concerns the energy efficiency to be improved by 20% by the same year. Long term targets and policies later on followed this 2020 targets by 2030 [Commission, 2014] and 2050 [Commission, 2011] aiming to promote renewable energy sources as the main axis to achieve both

carbon emission reduction and secure the energy problem by lowering the dependency on fossil fuels and the export associated to it. For instance, only renewable energy sources were affected by the generation increase between 2017 and 2018, while nuclear generation was unchanged and hard coal decreased because of renewable energy sources (RES) in Germany and the U.K, and the switch to hydropower in Spain and Italy [Jones et al., 2019].

### *Transportation sector challenge*

The challenges of finding a balance between the increasing demand for energy, the limited conventional resources, and the necessity to lower the carbon emissions is particularly apparent in the transportation sector. At present, this sector is a high energy-intensive sector, and its share on energy consumption is still increasing. In the case of European Union countries, it represented 32% of the final energy demand in 2016. The increase of population of 30 million in the last 25 years within the E.U increases as well the need for transportation, especially the road one by adding 84 million new cars to the car park during the same period [Thomas, 2016]. In fact, road transportation is the most energy-intensive sector, with a total share of 81.7% of the total transport sector [European-Commission, 2018a].

Another problem related to the expansion of the transportation sector is the dependence increase in conventional fuel. In fact, rail transport has been the only one decarbonized by switching to electric mobility, while aviation and road transportation still struggle with the high dependency on oil products exceeding 90%. Thus, in opposition to other energy user sectors, the transportation sector is still highly not decarbonized. In fact, while total emissions of European countries have decreased by 17% in the last 25 years, the transportation sector still the only one that had its emissions increased by 20.35% [European-Commission, 2018a] during the same period. In addition to global carbon emission, the road transportation sector plays a crucial role in affecting local air pollution by increasing the concentration of particles in the air and contributing to acid rains, which are the primary concerns in urban air quality.

It seems urgent, in order to solve the energy problem, to give priority to the transportation sector and especially the road one by finding a balance between the increasing demand for energy, the limited conventional resources and the necessity to lower the carbon emissions. Consequently, the European Union, via the 2011 White Paper, pushed towards decarbonizing the transportation sector by fixing the threshold of oil dependency in transportation in 2050 to 70% less compared to 2008 [Commission, 2011].

As for the general energy problematic, the choice of the alternative strategy and substituting fuel is left to the local authorities as population growth, oil dependency, and carbon emissions reduction change from one country to another.

### *Decarbonizing road transportation*

For light-duty vehicles, a first transition phase can be accomplished using internal combustion engines (ICE) with the increased efficiency as well as smaller prototype cars for more aerodynamic efficiency. However, in the long run, alternative fuels and more efficient propulsion systems seem to be the only solution to decarbonize the road transport sector completely. In this optic, fuel cell electric vehicles (FCEV) and battery electric vehicles (BEV) constitute the main alternatives to the current gasoline and diesel vehicles.

Concerning the second category, the classic operating battery capacities range between 14 and 30 kWh for a driving distance below 250 km [Robinius et al., 2017]. However, the current market battery shows a maturity of the technology leading to the decrease of batteries cost expecting to average 300 €/kWh in 2020 for mobile applications [Nykvist & Nilsson, 2015], which is pushing constructors to equip new upper-class cars with battery capacities exceeding 60 kWh, with operational range for instance up to 363 km for new Nissan Leaf [Nissan, 2019], below 408 km for new Tesla S and X [Motors, 2019b, Motors, 2019a], and of maximum driving distance reaching 450 km for Kia E-Niro [Motor1, 2018] or Mercedes EQC [Mercedes-Benz, 2019].

However, the low energy density and by consequence the size and the weight of the internal propulsion engine are still constraining the driving range of electric vehicles. Thus, even with the increase of the battery capacity, BEVs are still more adapted to short-range distances such as urban driving and have the disadvantage of high charging time, which limits their flexibility. Moreover, using the power sector to fuel the road transportation, pushes to rethink the current electrical infrastructure to meet the additional demand, including mainly distributed storage solutions, because of the unsolved large-scale electric storage option. In fact, the increase of final energy consumption that reached 33.1% in 2016 [European-Commission, 2018a] applies investment costs that can be higher than the required one for hydrogen [Reis, 2010].

The long-term storage is the main problem because of the absence of technology to store electricity for longer periods (superior to one month). The only solution, being pumped hydroelectric energy storage, which is used at a share of more than 99% for large scale storage [Blanco et al., 2018], but being constrained to geographical aspects as it has to be constructed using gravitational potential between lower elevation reservoir to a higher elevation.

On the other hand, FCEV can be based on PEM fuel cells in the range of 80 kWh, which can guarantee a driving range of 500 km with approximatively only 6 kg of on-board hydrogen. Moreover, the charging time of about three minutes is comparable to those typical of conventional diesel automobiles. Therefore, major car manufactures already developed and commercialized their own FCEV prototype. For instance, Hyundai commercialized the first SUV fuel cell car ix35 and with the sixth generation FCEV 6 reached a driving range up to 594 km with 5.64 kg on-board hydrogen transported, and recently the Hyundai Nexo has been introduced

with a driven range up to 756 km for 6.33 kg tank capacity [Hyundai, 2019]. Honda and Toyota commercialized their own Saloon FCEVs as well, Clarity Fuel Cell 201 [Honda, 2018] and 2019 TOYOTA MIRA [Toyota, 2019], with a driving range of 589 and 500 km, respectively, and with a tank capacity of 5 kg. Finally, prototypes and commercialized hybrid cars mixing fuel cell and battery electric technologies have been launched, like Mercedes-Benz GLC F-CELL and KANGOO ZE H2 [H2, 2019a].

All taken into consideration, FCEV is a good combination of what makes the success of BEV and ICE light-duty cars; A good comfort and benefits of electric driving, including high efficiency, environmentally friendly, and silent technology, all associated to the advantage of conventional ICE cars including the refueling time and driving range. Nonetheless, the physical and chemical properties of hydrogen are a disadvantage to make it a good energy carrier for the transport sector compared to conventional fuels as it is still mainly handled as compressed gas with the drawback of low energy density and higher storage system weights and costs.

# CHAPTER ONE

## 1 HYDROGEN ECONOMY STATE OF THE ART

### **Abstract**

The chapter aims first to give a general introduction into the current energy system situation and prospects by focusing on the European contest. Then deals with transportation, as the main consumer and polluting sector by discussing the state of the art and the effort made to decarbonize the transportation sector, especially the road one. This sets the ground for hydrogen as an alternative fuel solution and as a merging vector between the different energy sectors. Thus, the current European initiatives and position towards the hydrogen economy are investigated, and an example of successful cooperation between European countries aiming to support the infrastructure deployment is developed. Finally, the case of France and Germany, as a framework for this study, are then investigated following the same methodology that is energy system, transport sector, and the hydrogen economy.

In the second part, hydrogen in the transportation sector is investigated at the academic level by performing a literature review of the main aspects with a focus on hydrogen infrastructure and supply chains. This allows investigating the main current studies gaps and include them in the scope of this work, and thus underlining the novelty of the analysis.

# Hydrogen economy of the art

- I HYDROGEN ECONOMY AND PERSPECTIVE IN THE EUROPEAN UNION**
  - I.1 Hydrogen perspective and scenarios.....10*
  - I.2 Hydrogen mobility in Europe.....11*
- II THE CASE OF FRANCE**
  - II.1 France future energy system.....14*
  - II.2 Hydrogen economy in France .....14*
  - II.3 Current hydrogen infrastructure .....15*
- III THE CASE OF GERMANY**
  - III.1 German future energy system .....17*
  - III.2 Hydrogen economy in Germany.....18*
  - III.3 Current hydrogen infrastructure .....18*
- IV HYDROGEN FOR TRANSPORT LITERATURE REVIEW**
  - IV.1 Hydrogen technologies .....20*
    - IV.1.1 Delivery.....20*
    - IV.1.2 Storage .....21*
    - IV.1.3 Production .....21*
  - IV.2 Hydrogen infrastructure. ....22*
    - IV.2.1 Cost assessment of hydrogen infrastructure .....23*
    - IV.2.2 Infrastructure cost optimization.....24*
      - IV.2.2.1 Focus on production and storage optimization .....24*
      - IV.2.2.2 Optimization of the total supply chain .....25*
      - IV.2.2.3 Multi-objective optimization .....26*
      - IV.2.2.4 Environmental assessment .....26*
  - IV.3 Geographical distribution .....28*
  - IV.4 Scientific motivation and novelty of the study.....29*

## Acronyms

2DS	2°C Scenario
COP21	The 21st Conference of the Parties
RES	Renewable energy sources
ZEV	Zero-emission vehicles
ICE	Internal combustion engines
FECV	Fuel electric cell vehicles
BEV	Battery electric vehicles
PEM	Proton-exchange membrane fuel cell
HRS	Hydrogen refueling station
MTPA	Milion tonnes per annum
EU4	Referring to four European countries (France, Germany, Italy and the United Kingdom)
H2ME	Hydrogen Mobility Europe project
SHHP	Scandinavian hydrogen highway partnership
HYWAY	Hydrogen project located in Auvergne-Rhône-Alpes region, France
EasHyMob	Hydrogen project located in la Manche, in Normandie region, France
H2Piy	Hydrogen project at the French Spanish border
HySA	National South African hydrogen program
PV	Photovoltaic power system
MOFs	Metal-organic frameworks
LOHC	Liquid organic hydrogen carrier
TPD	Tonnes per day

# H

ydrogen is described as one of the alternative solutions for existing fuel that will allow lowering the carbon emission in the transport sector by the use of fuel cell technology [Council, 2004, IEA, 2009]. In parallel, hydrogen can be used as a short- and long-term storage option that allows facing the intermittence character of renewable sources using electrolysis technology. Thus, in addition to being used directly as a chemical component in ammonia and methanol production, for example, hydrogen could be viewed as a single merged energy vector that connects three sectors, transport, power, and industry.

The other main advantage of using hydrogen for sector coupling is that it contributes to energy security and lower the dependency on fossil fuels and thus reduce the market volatility. In fact, hydrogen produced from the electrolyzer can be an option that will favour producing hydrogen from local renewable energy sources, while lowering the dependency on the fluctuating oil global market affected by geopolitical interests.

## **I Hydrogen economy and perspective in the European Union**

The current hydrogen production in the European Union reaches 7 MTPA used mainly at a share of 90% for industrial applications [Blanco et al., 2018]. The highest share goes for ammonia and methanol that are produced using hydrogen at a share of 63% of total annual production, followed by refineries at a share of 30%, while only 9% is used to process metal [Fraile et al., 2015]. Thus, the share of the energy and transport sector in the hydrogen market is still marginal and only related to activities from research and development.

### **I.1 Hydrogen perspective and scenarios**

In E.U, the main breakthrough in academia came after the HYWAYS study [L-B-Systemtechnik, 2008] based on the beginning of the commercialization of FCEV by 2015, that projected 2.5 million FCEV cars to be sold by 2020, and a penetration of the technology up to 70% by 2050. In term of scenarios; on the one hand, the European Union reference scenario [Capros et al., 2016], based on greenhouse gas reduction of only 48% by 2050 to the reference year 1990, projected very low penetration of hydrogen of less than 1%. On the other hand, the energy roadmap 2050 [Commission, 2012], considering a higher greenhouse gas reduction of 80%, only pointed out the importance of biomass and consumer behavior on transportation sector decarbonization. A scenario EU4 has been developed by the IEA [IEA, 2015] for four European countries, including France, Germany, Italy, and the United Kingdom, that projected a penetration of fuel cell technologies in the road transportation of 2.4% in 2020 and up to 28.5% by 2050. Finally, recent roadmap highlight the benefits of an ambitious energy scenario in the European Union based on the hydrogen economy to reach the target of 2 °C by 2050. It underline the potential of hydrogen, mainly in transportation sector, to close the gap fixed by lowering carbon emissions however

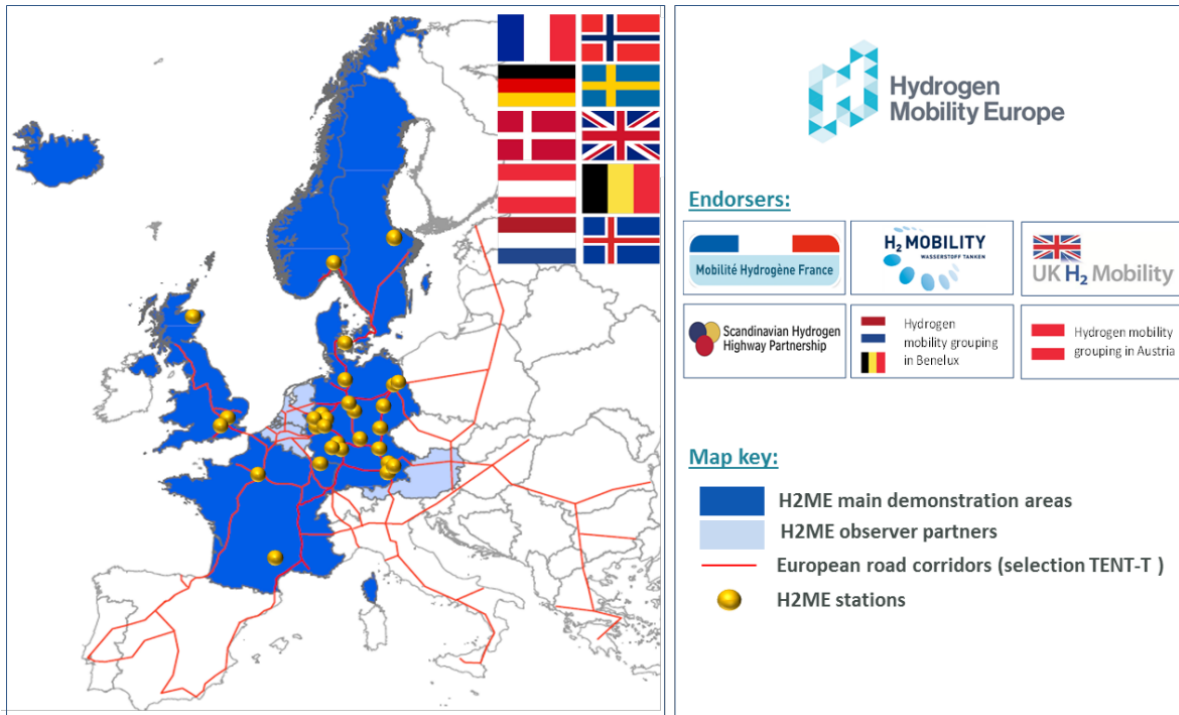
with a shift in priority for road transportation between 2017 (Council 2017) and 2019 (FCH 2019); where public transportation and heavy duty starting to be prioritized compared to private cars. For instance in case of 2DS scenario the roadmap hydrogen council (Council 2017) projected a 25% share by 2050. While the recent hydrogen technical report in 2019, (FCH 2019) and the communication from the commission in 2020 (Comission 2020) projected 14 % in the whole transportation sector under the same assumption for the share of transport sector in energy demand. This potential can allow to fuel more than 40 million cars and provide heat for more than 50 million households.

In terms of policies, hydrogen is still not directly targeted, as the renewable energy directive [Commission, 2009] pointed out a share of 6.8% of advanced renewable fuels in the transportation sector, but did not specify any requirement for fuel cell technology. The directive was revised and extended the share of renewable energy in transport to a mandatory minimum of 14% [Commission, 2018]. Although biofuels were the main target of the European directive in transport, fixing it to a maximum of 7% in the revised version, which leaves the same share for other technologies in the whole transport sector. Which translates in an even higher share for passenger cars that opens perspectives for mainly BEV and FCEV.

## **I.2 Hydrogen mobility in Europe**

Even if the European Union does not provide strong support to hydrogen as an alternative fuel in the transportation sector, a large European cooperative under the Hydrogen Mobility Europe project (H2ME) is supporting the deployment of hydrogen infrastructure across Europe (Figure 1.1) and take the lead to set up an economy based on hydrogen.

**Figure 1.1:** Main hydrogen project endorsers [Markillie, 2015]



A current example is the Scandinavian hydrogen highway partnership [SHHP, 2006]. This common strategy developed by Scandinavian countries, including Sweden, Norway, and Denmark is involving major and small industries, research institutions, and local, regional, and national authorities in order to set strategies toward hydrogen infrastructure deployment. The choice of this region was taken because of the strong taxation policy on zero-emission vehicles (ZEV) that make these countries highly attractive for an early market introduction of FCEV.

For instance, Norway [Ang, 2009] concluded on its report that hydrogen could be competitive at around 5% of market penetration, which can be achieved by 2025. As more than 95% of electricity production in Norway is carbon-free and mainly comes from hydropower [FuelCellToday, 2013], water electrolysis is considered as one of the two main alternatives for hydrogen production.

The oil reserves as well make hydrogen from natural gas and steam reforming with or without carbon capture and storage a good alternative for export to Europe’s mainland as well. It is why pipelines are considered as an attractive transport option besides compressed gas trucks, the routing to the continent can be shipped as liquid hydrogen. Concerning Denmark, the energy mix by 2050 will be focused on fluctuating renewable electricity from mainly wind turbines [HIT, 2014]; thus, hydrogen production in Denmark is therefore expected to be based on centralized

production from renewable electricity and onsite production. The market roll-out as projected is expected to be more homogenous than the Norwegian one because the country is located on the main European highway corridors [Stiller et al., 2010].

In conclusion, the Scandinavian region set a good example of how different the strategies to deploy hydrogen infrastructure could be depending on the potential resources and energy system strategies, but still can be under a dynamic common outlook. Norway, by a good hydropower potential and oil and gas resources, places hydrogen production as a main driver for the hydrogen economy and aims to build the infrastructure around the export of hydrogen to the European mainland. A vision that must be achieved by collaborating with Denmark and Sweden, as the main European corridor crosses these two countries. While Denmark's hydrogen economy is driven by mobility and stabilization of the grid as the country aims for a free carbon electricity production driven mainly by wind farms.

## **II The case of France**

The energy system in France has many similarities to the one in Sweden in the Scandinavian hydrogen highway partnership, as both countries have a higher share of nuclear power in electricity generation, followed by hydropower. In 2017, 71.6% of electricity generation was based on nuclear power, followed by hydropower at a share of 10.1%, while wind presented only a share of 4.5% [DATA LAB, 2018]. As for the European Union, the transport sector is still highly oil dependent and carbonized. For instance, light-duty vehicles, including passenger cars and duty cars, were responsible for 72.3% of total carbon emissions in the road transport sector [DATA LAB, 2018]. Finally, concerning hydrogen economy, the total hydrogen production in France is based on fossil fuels, contributing at 3% of total carbon emissions, and currently reaches 2500 TPD, 60% is used for refineries, and 35% for Ammonia production.

### **II.1 France future energy system**

COP21 led to the climate plan, pushing to rethink the energy system in France by decreasing the share of nuclear power in the electricity mix and increasing the contribution of renewable energy in the energy mix. The nuclear share has to be brought to a maximum of 50% in power generation by 2050 [Gouv, 2017], and the exploitation of fossil fuels should be stopped by 2040, which will increase the share of renewable sources in the energy mix by 2030 to a minimum of 32%. The part of RES in the electricity mix is expected to increase as well, as it is projected to range in 2035 between 45% and 71%, affecting mainly the installed wind capacity. Thus, onshore wind capacity is expected to range between 40 and 52, and offshore wind between 10 and 15 GW by 2035.

In parallel, the climate plan main priority was to deal with light-duty cars by setting the deadline for selling the carbon-emitting vehicles to 2040 [Gouv, 2017] by gradually replacing them with alternative fuel.

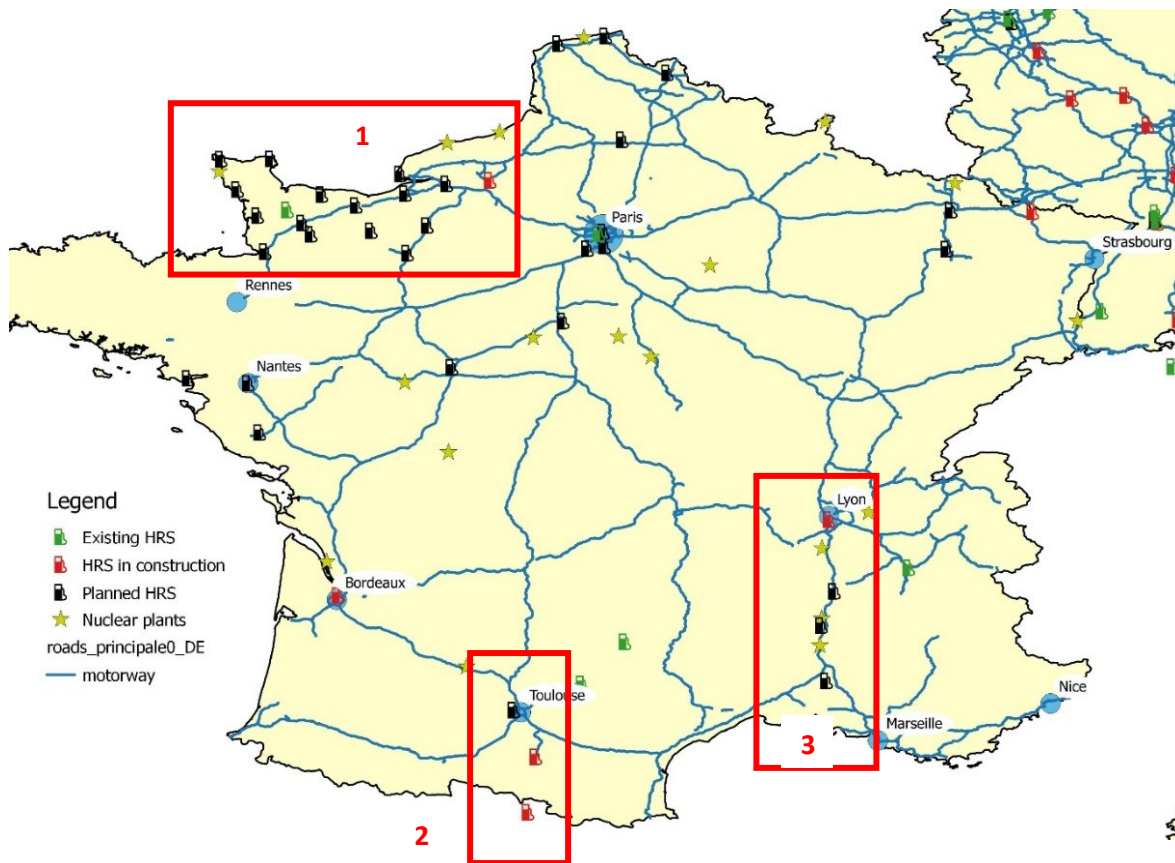
### **II.2 Hydrogen economy in France**

The hydrogen is at the center of the energy transition in France because it is coupled to renewable energy, and its deployment is flowing three main axes [Afhyac, 2018b]. The first one aims to decarbonize 40% of hydrogen production by 2028. The second one concerns the transport sector and aims to reach a share of 10% of hydrogen and ammonia in alternative fuel for transport by 2030. This will impact mainly road transport, and light-duty vehicles, as under the 2DS scenario, hydrogen could fuel over 18% of the car park by 2050 [Afhyac, 2018a] and already reach a car park of 200,000 vehicles by 2028. That concerns mainly the public transportation and utility service, as 1/10 of the cars will be an FCEV [Afhyac, 2018a]. The third axis concerns the use of hydrogen to increase the storage capacity of renewable energy, which can allow covering 15% of the final energy demand [Afhyac, 2018a].

### II.3 Current hydrogen infrastructure

However, the national deployment of the hydrogen consisting of locating the future hydrogen refueling station (HRS) is more difficult to predict as its hydrogen economy is mainly driven by local initiatives ((1) and (3) in Figure 1.2) and European projects ((2) in Figure 1.2).

**Figure 1.2:** France existing and planned hydrogen HRS [H2, 2018]



The two main national projects, HYWAY (3) and EasHyMob (1), currently in development are both linked to local initiatives and their proximity of nuclear power plants but differ concerning the populations and the European corridors' priorities. The HYWAY (3) project is located in the Auvergne-Rhône-Alpes region, the second biggest region by the number of the population after Île-de-France around Paris [HyWay, 2018]. The first step of this project will be focused on Lyon and Grenoble with hydrogen trucked as compressed hydrogen. The second step, consist of creating an ax following one of the main European corridors to the Mediterranean Sea through the Rhône river and extending the hydrogen project to the whole Auvergne-Rhône-Alpes region by building 20 HRS, 15 electrolyzers and reaching a car park of 1000 FCEV by 2020 [HyWay, 2018]. This ax will cross other cities where projects of HRS construction are planned, but more

importantly, will allow taking advantage of the hydropower stations and the four nuclear power stations along the Rhône. It is why one of the goals of this second phase deployment is to switch from compressed gas trucks to a local hydrogen production with electrolysis. The *EasHyMob* (1) [Brunet & Ponsard, 2016] project, on the other hand, takes place in la Manche, in Normandie region on of the less populated regions in France as the main projects are taken place in communes with less than 10,000 habitants. Although this project has the particularity to not being on a main European corridor nor on a populated area, it shares with the *HYWAY* the energy potential. In fact, besides the proximity of three nuclear power plants, the region has a significant wind energy potential of the current total installed capacity of 815 MW and an offshore project calvados of total capacity of 450 MW [Thewindpower, 2018].

Finally, the *H2Pyr* project (2) is a project that will link Rodez in France to Saragosse in Spain by developing ten hydrogen refueling stations in total [Hidrogenoaragon, 2018]. This corridor of 900 km will experiment the first one between two countries in the European Union. Besides the two existing stations in Huesca and Saragosse in Spain and in Albi and Rodez in France, four others are under construction in Spain, two in France and one in Andorra, and a network planned in Toulouse.

### **III The case of Germany**

The energy system in Germany is entirely different compared to the current situation in France, as the first phase of Energiewende is pushing out nuclear power from the electricity mix. Despite that, recently, Germany only closed Gundremmingen B at the end of 2017, which did not have an impact on the nuclear electricity generation because of the improved capacity of the other installed capacity. Thus, the main change is projected at the end of 2019 by the following German nuclear closure [Jones et al., 2019]. In parallel, this nuclear phase-out strategy increased the share of coal in the electricity mix despite enhanced renewable energy sources strategies. On the one hand, 39.72% of electricity generation by 2017 was based on fossil fuels with mainly 146 TWh electricity generation from lignite counting for half of Europe's generation from this source [Jones et al., 2019]. On the other hand, the increase of the share of renewable energy sources placed onshore and offshore wind as the second electricity producer with a total share of 20.4% by 2018 [Burger, 2018].

Similar to the case of the European Union and France, the transport sector is the less decarbonized sector and still highly oil dependent. For instance, by 2016, the transport sector released about 201.5 million tons of carbon emissions, increasing its share in greenhouse gas emission by 10% compared to its level in 1990. In the meantime, fossil fuel represented 95.3% of total fuel consumption in the transport sector [European-Commission, 2018b].

#### **III.1 German future energy system**

Besides the plan to phase out from nuclear power by 2022, the second phase of the energy transition in Germany targets mainly the increase of renewable energy sources in the energy mix and reducing greenhouse gas emissions as the main solutions against climate change and for energy security. The security of supply is targeted by lowering the import from its current level of 70% to 60% by 2030 [Agora, 2018]. Thus, combined to a nuclear and lignite phase-out by 2022 and 2038 respectively [Jones et al., 2019], which can only be achieved by doubling the share of renewable sources in the energy mix to reach 30% by 2030, and in increasing the renewable electricity to 65% compared to 38% in 2018. This will impact mainly the installed wind capacity as the total electricity generation for onshore and offshore wind is projected to increase from 71 and 8 TWh, respectively, by 2015 to 170 and 80 TWh, respectively, by 2030 [Agora, 2018].

Concerning the transport sector, the main objective concerns reducing the greenhouse gas emissions in the transport sector by a minimum of 39% by 2030 compared to its level in 2015, resulting in a 40% reduction of petrol and diesel consumption [Agora, 2018]. This energy transition in the transport sector consists of two parts, increasing efficiency and increasing the share of renewables in the transport sector [Agora, 2017] by reducing the energy demand by 30% in the transport sector and increase the use of railways and cities public transport and renewable-powered electric cars.

### **III.2 Hydrogen economy in Germany**

Thus, by increasing efficiency as one of the main targets of the transport energy transition, fuel cell vehicles are mainly targeted as the second most efficient alternative to conventional fuel. Moreover, it allows covering the second target by diversifying the fuel sources mix. Concerning production, hydrogen is seen as a potential vector in the energy transition to store excess electricity from renewable energy and achieve more flexibility and electricity balance. Meanwhile, hydrogen produced from electrolysis can be used directly as a fuel or implemented in a more coupled energy system allowing it to be used, for instance, to produce methane or liquid fuels via the use of power-to-gas and power-to-liquid technologies to link other sectors.

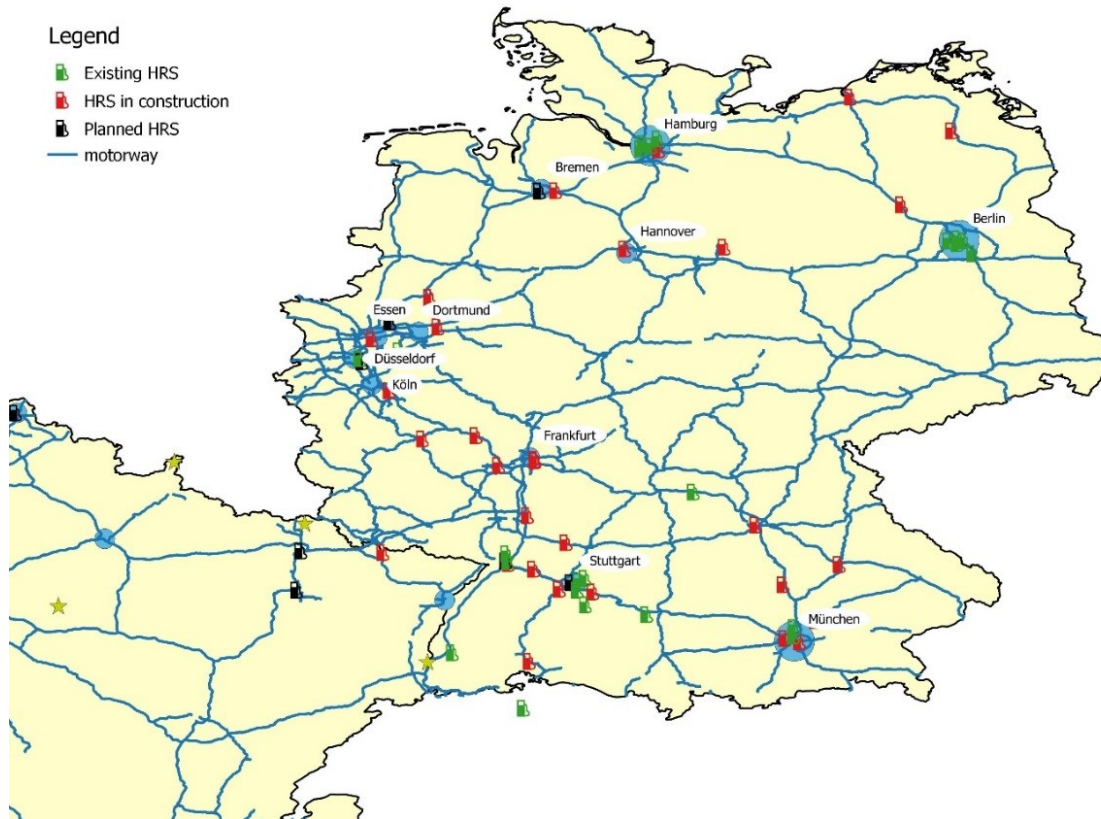
Concerning the infrastructure, the German federal government set a new regulation on the alternative fuel stations, which will allow defining an appropriate corresponding infrastructure aiming to establish 400 HRS by 2025 using public funds through 2026 [Agora, 2017]. In contrast to France, which sets targets on fuel cell vehicle deployment, Germany focuses on the hydrogen infrastructure by setting targets for the HRS. Thus, along the private investment station planned to reach 100 by 2020, the association of the public funds can allow reaching a target of 1000 HRS by 2030. Investment in prototype projects for decarbonized hydrogen is planned as well by 2020 as the example of Shell Rheinland refinery that plans to implement a 10 MW electrolyzer in order to reduce emission due to hydrogen production using fossil fuel products [IEA, 2019].

### **III.3 Current hydrogen infrastructure**

In Germany, the infrastructure development for hydrogen mobility follows the main European corridors, giving priority to the cities with a high population (Berlin, Hamburg, Cologne, Frankfurt, Stuttgart, and Munich), as shown in Figure 1.3.

By the end of 2018, 64 HRS were already operating, making Germany the second country by the number of hydrogen fueling stations and number one by the infrastructure deployment increase compared to 2017 [H2, 2019b]. The stations were gathered in the most populated cities along the Rheine between Dortmund and Bonn with nine HRS. In the meantime, five HRS are implemented around Frankfurt, Stuttgart, and Berlin, while respectively seven and three are operating in the area of Munich and Hamburg. Meanwhile, the hydrogen infrastructure is deployed along the main German highways and European corridors; from West to East linking Berlin to the North Rhine-Westphalia region via Hannover; from North to South linking Berlin to Austria via Munich and Nurnberg; and finally linking the North West Germany to Switzerland via Frankfurt and Stuttgart.

**Figure 1.3:** Germany existing and planned hydrogen *HRS*[H2, 2018]



Besides hydrogen for mobility, Germany is investing in hydrogen as a sector linking vector using power-to-gas technology with an overall performance reaching 30.4 MW of total installed capacity in operation and planned projects [Braunsdorf, 2018]. For instance, in the north of Germany in the Brandenburg region, the first power to gas project was developed in 2016 at the megawatt scale [Hydrogeneuropa, 2018]. The project aims to investigate the potential of storing excess electricity from wind. For that, first, the hydrogen is produced via alkaline electrolyzer before being injected using a pipeline system into the gas grid to be used in the household, industry and mobility sectors.

## **IV Hydrogen for transport literature review**

Studies in the field of hydrogen as an energy vector to decarbonize the transport sector can be classified into four main categories, one is dealing with the technology involving mainly electrolysis and fuel cell technology and their performance and operating conditions. A second one is investigating the optimum infrastructure and supply chain, and the different options for producing, transporting, and storing hydrogen. One dealing with the geographical information system, to show the exclusive transport of hydrogen between production and demand. Finally, one assessing hydrogen economy and policy to analyze the roadmap and the different scenarios to hydrogen roll-up strategies.

### **IV.1 Hydrogen technologies**

The studies dealing with hydrogen technologies assess technically and economically different aspects related to hydrogen production technologies including mainly one based on renewable energy sources [Hollmuller et al., 2000, Barbir, 2005, Kotay & Das, 2008, Boudries & Dizene, 2011, Boudries, 2013, Al-Sharafi et al., 2017, Bhattacharyya et al., 2017, Rezaei-Shouroki et al., 2017, Duman & Güler, 2018, Jung et al., 2018, Kikuchi et al., 2019], hydrogen storage focusing mainly on the short term storage and transport application [Brückner et al., 2014, Bellotti et al., 2015a, Fikrt et al., 2017, Zaitsau et al., 2018, Zheng et al., 2012] or hydrogen delivery investigating the operating conditions to deliver hydrogen to the end-user [Lin et al., 2018, Reddi et al., 2014, Nistor et al., 2016].

More general studies investigate as well, within a scope of national or regional programs, different technical solutions related to the hydrogen economy before defining a roll-up and deployment strategies. For instance, the technical aspects behind the national South African HySA program were developed, and the different technologies of producing and storing hydrogen involved in the project were investigated [Bessarabov et al., 2017]. This included, for instance, hydrogen production system consisting of an array of PV modules coupled to lead-acid batteries for the short-term storage, all connected to a PEM electrolyzer. While, the development of metal-organic frameworks (MOFs) and their composites were investigated as a storage option due to their high surface and porosities with particular focus on zinc-based, chromium-based MOFs, and composites MOFs. The research focused as well on developing LOHC, as the solar to hydrogen facility is planned to integrate a hydrogenation plant to store hydrogen, which can be released when needed via a dehydrogenation process and converted to electricity using a fuel cell [Bessarabov et al., 2017].

#### *IV.1.1 Delivery*

Concerning delivery, studies investigate the optimum delivery options and operating strategies and their impact on the end-user. For instance, the optimal delivery pressure at the hydrogen

refueling station was investigated using three operating pressure of 350, 500, and 700 bar for six driving patterns that depend on the frequency and the commute distance [Lin et al., 2018]. The results showed that for regional strategy, 700 bar was the optimal delivery pressure independently of the driving pattern, especially at the early market stage when the number of hydrogens refueling stations is limited. Meanwhile, for cluster strategies, 350 bar and 500 bar were assessed as optimum pressure for less frequent commute patterns, independently of the distance. Two different scenarios of hydrogen refueling stations were compared as well at different operating strategies [Reddi et al., 2014], and the impact of refueling compression and storage configurations on the delivery cost was investigated. The results showed that for both scenarios, a five-cascade storage system and a higher tube trailer return pressure reduce the cost, and the system can be further optimized by using the second scenario where the tube trailers are used first to fill the vehicle tank before supplying the hydrogen station storage system. In the meantime, studies assessed delivery as well in the case of distributed production. For instance, [Nistor et al., 2016] investigated the cost of delivering hydrogen for hydrogen mobility in the case of United Kingdom using onsite electrolysis from combined wind electricity and power grid, and [Gökçek & Kale, 2018] performed a techno-economic study on a wind-PV hybrid power system associated to hydrogen refueling station and applied it for a case study in Çeşme in Izmir, Turkey.

#### *IV.1.2 Storage*

Concerning storage options, new technologies were assessed in the last years, mainly the use of liquid organic hydrogen carrier as a storage alternative was the scope of various analyses. Thus, several studies investigate thermodynamic properties of potential hydrogen carriers [Zaitsau et al., 2018, Brückner et al., 2014], and the optimum temperature reaction conditions of de- and hydrogenation processes and the optimum catalyst capacities [Shi et al., 2019], [Fikrt et al., 2017]. Concerning the assessment of components as liquid organic hydrogen carrier using experimental and computational methods, benzylaniline, dibenzyltoluene mixture, and biphenyl were mainly investigated [Brückner et al., 2014],[Zaitsau et al., 2018].

Other conventional ways of storing hydrogen still attract studies' attention as [Bellotti et al., 2015b], for instance, focused on the hydrogen storage process taking into account two different alternatives. The first alternative consists of a conventional method, in which the hydrogen is stored in high pressure tanks, and the second alternative uses storage in hydro-methane form.

#### *IV.1.3 Production*

Concerning renewable hydrogen production, electrolysis using solar and wind energy were mainly investigated as an energy source for decarbonized hydrogen production. Studies investigate the potential of hydrogen production using both energy sources on [Duman & Güler, 2018, Al-Sharafi et al., 2017]. While other analyses focused on wind energy systems [Jung et al.,

2018, Rezaei-Shouroki et al., 2017], or solar energy potential via the use of PV systems [Kikuchi et al., 2019, Boudries & Dizene, 2011, Bhattacharyya et al., 2017, Hollmuller et al., 2000], concentrating photovoltaic system [Boudries, 2013] or solar thermal technologies [Pregger et al., 2009, Hoffmann, 2019].

For instance, a techno-economic analysis of hydrogen production from solar energy using PV coupled to a battery system was performed by giving priority to the PEM electrolyzer in Nagano, Japan, in order to assess the electrical storage impact on hydrogen production cost reduction [Kikuchi et al., 2019]. The impact of PV panel orientation on hydrogen production cost in the Ardar region, Algeria, was investigated by looking at the configurations east/west, north/south, and tilted panels [Boudries & Dizene, 2011]. Finally, alkaline water electrolysis were technically investigated as well as hydrogen production technology using inclined PV modules located in Mumbai, India [Bhattacharyya et al., 2017].

Electrolysis system has been investigated as a potential grid balancing system as well by injecting the excess electricity converted to hydrogen into the natural gas grid and comparing it to other technologies like a gas turbine system for instance [Guandalini et al., 2015]

## **IV.2 Hydrogen infrastructure.**

Concerning hydrogen infrastructure and supply chain cost, a complete analysis of various transformation and transport hydrogen options was performed, including compressed gas and liquid, using rail, road, maritime, and pipeline infrastructure [Amos, 1999]. This study was a pioneer reference that gave a cost review of the different investment costs and operations and maintenance costs. This work was later used as a reference point for many studies that assessed and compared different transport and storage pathways [Yang & Ogden, 2007, Simbeck & Chang, 2002, Council, 2004]. The last work investigated, for instance, the cost-effective configuration to transport and distribute hydrogen from a centralized production plant to a direct transmission point or local distribution network of refueling stations using compressed gas trucks, liquid trailers, and a pipeline system. The analysis [Yang & Ogden, 2007] assumed for compressed hydrogen that the transformation and storage occurs at the central production plant, then hydrogen is transported using a compressed gaseous truck filled at 162.1 bar of total net capacity of 243.75 kg or via a pipeline system, for both cases an additional compression is needed to bring hydrogen to the refueling conditions of 344.7 bar. Concerning liquid transport, additional liquefaction plants and storage is needed, the tank truck is considered to have a total capacity of 4000 kg with additional losses due to transport and boil off, and the hydrogen is pumped after transport at the delivery point before vaporization at the refueling pressure. Concerning the point to point results where the transport distance varied between 25 and 500 km, and hydrogen demand from 2 to 100 TPD; Compressed gas truck was found out to be the minimum cost option at low demand below 14 TPD and low average transport distance below 350 km; liquid tanker was used at higher average transport distance above 250 km and average demand below 50 TPD;

While the pipeline system was optimal from higher demand above 50 TPD. Concerning local distribution, gaseous compressed gas was mainly used to deliver hydrogen for hydrogen station of 0.5 TPD capacity, while a pipeline system and liquid tankers were the delivery option for higher station capacity above 1 TPD. The city radius impact on the transmission choice was found out to increase with the increase of refueling stations capacity, as pipeline system transmission is used in lower city radius compared to liquid tanker transmission for higher city radius.

The study gives a complete analysis of the cost-effective option used to transport hydrogen in point-to-point cases, as well as an insight of the distribution mode in a simplified city configuration with homogeneous population distribution and fixed refueling station capacity and delivery mode using a compressed gas truck, liquid tankers and a pipeline system. Nevertheless, the methodology is based on a simple cost comparison and does not optimize the overall transport infrastructure. Moreover, other transport options raised in the recent ten years, and compressed gas hydrogen technologies maturity increased, allowing higher pressure ranges, increased transported capacities, and higher delivery pressures. Thus, many contributions in hydrogen infrastructure and supply chain reviewed and updated the hydrogen state of aggregation [Brey et al., 2012, Reuß et al., 2017, Xu et al., 2017, Lin et al., 2008, Anex et al., 2010], while other work-integrated linear programming to investigate a cost-effective infrastructure deployment and applied it at national and regional cases [Almansoori & Shah, 2006, Almansoori & Shah, 2009, Han et al., 2012, Hwangbo et al., 2017, Kim & Kim, 2016, Moreno-Benito et al., 2017, Nunes et al., 2015, Woo et al., 2016, Maroufmashat et al., 2016, Li et al., 2008].

#### *IV.2.1 Cost assessment of hydrogen infrastructure*

Similar to Yang and Ogden's work, the cost of total hydrogen infrastructure considering additional types of hydrogen storage and transportation modes was analyzed [Reuß et al., 2017]. The model considered seasonal storage using caverns, and on-ground storage using modules as compressed gas, as liquid hydrogen, and as liquid organic hydrogen carrier. The results showed, in case of the use of the transport and the storage mode at the same state of aggregation, that the cost varied at a minimum level range of 7.2 to 8.0 €/kg, at a medium cost range of 8.0 to 8.8 €/kg, and high total cost range of 8.8 to 10.4 €/kg. The minimum cost range occurs at hydrogen demand above 10 TPD and distance below 200 km and uses hydrogen as compressed gas using a truck for transport, and seasonal storage. The medium cost range occurs at hydrogen demand above 40 TPD and distance above 200 km and uses hydrogen as compressed gas using a pipeline for transport, and seasonal storage. Finally, the highest cost range occurs at low hydrogen demand and uses hydrogen as LOHC for transport and storage.

In the same optic, other studies focused on the distribution phase of the supply chains and the deployment of hydrogen refueling stations. For instance, a roll-out strategy to deploy steam methane reforming refueling station in the region of Shenzhen, China, was analyzed using three different FCEV share scenarios in the new vehicle sales by 2025 [Xu et al., 2017]; While a

sequential roll-out of hydrogen infrastructure in five time periods in Andalusia, Spain, was investigated by estimating the size, the number and the region location of the fueling station that will be constructed in order to cover 30% of the total population by 2030 [Brey et al., 2012].

The results for Shenzhen [Xu et al., 2017] estimated a total cost of 1.08, 4.45, and 8.49 M€ for small, medium, and large fueling stations of 0.1, 0.5, and 1 TPD respectively. This corresponded to a Levelized cost of hydrogen per station of 7, 6.3, and 6 €/ kg by 2050 for small, medium, and large stations. Concerning the regional distribution of the fueling station, the ten regions of Shenzhen were organized by the area, population, and average wage by sector to identify three regions for refueling station location organized at three medium ones and seven small ones. Meanwhile, the results for Andalusia [Brey et al., 2012] showed that 525 fueling stations will be constructed to fuel an average of 2000 vehicles per station by 2030, costing 2236.4 M€ for the deployment of the total infrastructure by 2030 using mainly delivered renewable energy, which resulted in a cost of 4.7 M€ per station. Concerning the regional distribution, Andalusia was broken down to 770 sub-regions corresponding to the municipalities, and each one was ranked by the most favorable to hydrogen penetration to the least favorable one, and only the first 35 were chosen as they represented 30% of the population.

If the majority of studies can access different storage technologies and transport and distribution options with and without state transformation between the two, and thus allowing a complete comparison of the cost between the different pathways, it still does not assure to give the optimal cost, and a linear optimization, in this case, may be needed.

#### *IV.2.2 Infrastructure cost optimization*

Many studies in the literature used linear programming to investigate the optimum infrastructure solution and apply it in regional and national cases but differ concerning the scope of application and the functions optimized. For instance, in some analyses the whole infrastructure was optimized [Almansoori & Shah, 2006, Almansoori & Shah, 2009, Moreno-Benito et al., 2017, Nunes et al., 2015], while other work focused on distinctive aspects of the supply chain as production, storage or distribution importance may vary with geographical and regional resource and energy systems [Han et al., 2012, Hwangbo et al., 2017, Kim & Kim, 2016, Woo et al., 2016]. Finally, risk optimization besides cost minimization was addressed as well using multi-objective optimization [Almaraz et al., 2014, Sabio et al., 2010].

##### *IV.2.2.1 Focus on production and storage optimization*

Concerning hydrogen production optimization, electricity production using solar, wind and biomass technologies were studied for hydrogen production to be transported for the mobility sector in South Korea investigating three different scenarios for the market share of ICE, BEV, and FCEV [Kim & Kim, 2016]. The results showed that for high penetration of FCEV corresponding to a total demand of 8108.1 thousand tons by 2040, the main hydrogen is produced using

electrolysis, and hydrogen storage in large facilities was used. Concerning the cost, the Levelized cost reached 6.0 €/ kg in this case scenario and is reduced to 5.3 €/ kg in case of 34.5% less hydrogen demand. Hydrogen produced using only biomass was studied as well for the transportation sector in Jeju island, South Korea [Woo et al., 2016]. This analysis was performed by dividing the total supply chain to be optimized into two sub-chains, one related to biomass feedstock for hydrogen production, which took into account four types of regional suppliers and oversea export, and one related to hydrogen, which took into account gasification plants, storage systems, and refueling stations. The results, in this case, showed that the hydrogen cost ranged between 4.83 and 5.21 €/ kg for four different scenarios and that hydrogen export was needed when the demand exceeded 34 TPD.

The storage location and state of aggregation were optimized as well in South Korea for hydrogen demand in order to perform a carbon reduction of 20% and 30% [Han et al., 2012]. The model focused on the storage as compressed gas and liquid hydrogen next to production facilities or transported using trucks, ships, or pipeline system. The results showed that for both carbon emission reduction targets, the storage facilities implementation and transport option depended on the period of storage. At five days, the hydrogen was stored as compressed gas and mainly transported using the pipeline system, while at 15 days the hydrogen was stored in its liquid form and equally transported using pipeline system and tanker trucks.

#### *IV.2.2.2 Optimization of the total supply chain*

Optimization of the whole supply chain allows to invest the different parts of hydrogen delivery pathways, including the stages of hydrogen production, storage, transmission, and distribution, and was the main scoop of several analyses. For instance, the total infrastructure cost was minimized for the United Kingdom case [Moreno-Benito et al., 2017] by decomposing the country in 36 grids, to investigate the connections between the regions, and to analyze the type, the size and the location associated to the different production, storage, and transport technologies. Thus, liquid hydrogen import was considered along with natural gas, coal, and biomass processes with and without carbon and storage technology and electrolysis. The transport and storage technologies include mainly liquid and compressed gas trucks and pipelines associated with the appropriate storage option, along with carbon reservoirs and pipelines for captured carbon. The results showed that for hydrogen penetration of 2.5% and 50% in transport by 2035 and 2050 resulting a total demand of 50 thousand TPD the total cost was found to reach 3180 million£ resulting in cost of delivery ranging between 4.5 – 2.4 €/ kg by 2050, and with methane reforming at large scale as main production option. The infrastructure without pipelines resulted in a total cost of 4280 M€ and a replacement of 25% of large-scale methane reforming by medium scale facilities with liquid hydrogen import at the north. For the same case of Great Britain, the uncertainty related to the hydrogen demand was also included in the analysis based on liquid hydrogen as a transport carrier using railway and road infrastructure [Nunes et al., 2015]. The

results showed that, in this case, the mean cost of infrastructure deployment varied between 29,315.21 and 31,200.51 M€. Concerning hydrogen deployment, methane-reforming small production plants are suitable at the beginning, while the increase of the demand adds larger plants using the same technology. In the meantime, medium-size storages are the most suitable alternative, independently from the demand.

#### *IV.2.2.3 Multi-objective optimization*

Besides cost minimization, other parameters were optimized using multi-objective optimization, mainly risk minimization and environmental impact assessment. For instance, the optimization problem in terms of cost and financial risk of hydrogen network delivery was developed in Spain [Sabio et al., 2010], taking into consideration the implementation of different production plants and storage facilities in a set of potential locations with known hydrogen demand. For that, Spain was decomposed into 19 grids, and the results were simulated for two scenarios, a minimum cost one and a minimum worst-case one. The results showed that steam methane reforming and coal gasification was the suitable production option for the minimum cost scenario and worst-case scenario, respectively, while only cryogenic tanks were a storage option for both scenarios.

Due to the rising awareness towards the environmental impact, several studies introduced this parameter in their existing optimization model as a cost function [Han et al., 2013, Hwangbo et al., 2018]. For instance, the initial optimization study of hydrogen production from imported natural gas and from biomethane production transported using a pipeline system [Hwangbo et al., 2017] was extended to a multi-objective stochastic mixed-integer linear programming to optimize both annual cost and environmental cost [Hwangbo et al., 2018]. The results showed that the minimum cost solution applied only natural gas import but was the less environmentally friendly option, while a share of 56% and 44% of biomethane and natural gas, respectively, had a less environmental impact but was the most expensive option. Another alternative to assess environmental impact is done by including it as constraints for the optimization problem or assesses it independently by performing a life cycle assessment.

#### *IV.2.2.4 Environmental assessment*

The environmental impact can be introduced in the cost function to minimize e.g. [Almaraz et al., 2014] or as an environmental constraint e.g. [Almansoori & Betancourt-Torcat, 2016]. In the first work, for instance, a hydrogen supply chain applied to the region of Midi-Pyrénées in France by 2020 and 2050 was investigated by optimizing the total costs, the carbon emissions, and the risk associated with the infrastructure deployment for two scenarios considering hydrogen. The comparison of two scenarios with hydrogen penetration of 25% and 50%, respectively, in the transport sector by 2050 revealed an optimum cost of about 5.3 €/ kg and 5.8 €/ kg, respectively, and carbon emission of 1.9 kg CO<sub>2</sub> and 1.97 kg CO<sub>2</sub>, respectively. In the second work, the total network cost of distributing hydrogen in Germany by 2030 was minimized under environmental constraints [Almansoori & Betancourt-Torcat, 2016]. The model considered production from

three different feedstocks, including coal, natural gas, and biomass, with and without carbon capture and storage. The distribution was performed using compressed gas and liquid hydrogen following two infrastructures, the road one and the railway one, to meet the demand in Germany for road transportation considering a hydrogen vehicle penetration of 10% corresponding to a total demand of 2785 TPD. The base case scenario placed three production plants at Munich, Hannover, and Cologne, to meet the demand respectively in southeast, north and central region, and west Germany [Almansoori & Betancourt-Torcat, 2016]. The overall scenario results show that coal gasification is the preferred production option and that carbon capture storage is added when the scenario considered environmental constraints. For the transport option, hydrogen as its liquid form is preferred, while the railway infrastructure is the most suitable one. The minimal cost of implementing the infrastructure without environmental constraints was 7.72 M€/ day corresponding to 2.93 €/ kg.

On the contrary, several studies estimated the environmental impacts using different transport and storage pathways without optimizing the overall infrastructure. [Demir & Dincer, 2018], for instance, investigated their different hydrogen infrastructure scenarios that use different transport modes and storage technologies, and compared their respective cost, and the environmental impact by assessing the greenhouse gas emission. Two scenarios can be directly compared as they deliver the same hydrogen demand of 1596 tonnes per year. In the first one, the hydrogen is compressed before being delivered via the pipeline system at the city gate and then liquefied to be distributed to the fueling station, while in the second scenario compressed hydrogen stored in large scale geological storage to be transported via hydrogen tube trailers as compressed gas is used. The results showed that over 18.47 M€ are needed to construct the pipeline system in the first scenario compared to only 2.67 M€ for transmission investment in the second one using the tube trailers. The terminal costs were higher for the case of the first scenario because of liquefaction expenses that consist of 20.32 M€, while only 1.48 M€ are needed for the cavern compressors. This results in a higher Levelized cost of hydrogen of 7.02 €/ kg for the first scenario compared to only 2.64 €/ kg for the second one. Concerning the environmental impact, the use of the liquefier in the first scenario results in higher emissions, while the main environmental impact in the second scenario accounts for truck transport and compressor operations. Thus, pipeline transmission is the most environmentally friendly option. Nevertheless, the scenario implementing liquefaction is the most emitting one of a total of 10,709 g CO<sub>2</sub> per MJ hydrogen energy compared to only 736 for the second scenario.

Recent studies turn into new modes of storing and transporting hydrogen and their environmental impact using a life cycle assessment comparison. [Wulf et al., 2018] for instance, considering the future energy mix of Germany and the coupling sector potential, production was limited to electrolysis and distribution to fueling station for road transportation while different transport and storage pathways were investigated. For the hydrogen storage option, the

hydrogen was stored as compressed gas in caverns before being transported in a pipeline or via truck, or in LOHC storage tank before being transported in the corresponding trucks. The results showed that for climate change, the environmental impact of storage is marginal. However, for the different options considered, the one involving the pipeline system has the lower impact of less than 2 kg CO<sub>2</sub>/ kg H<sub>2</sub> followed by compressed gas trucks at 500 bar and a transport distance of 100 km, while LOHC at 400 km was the most emitting option with more than 5 kg CO<sub>2</sub>/ kg H<sub>2</sub>.

### **IV.3 Geographical distribution**

Geographical distribution allows visualizing the optimum transport network within a region or a country, mainly based on an integer linear programming results performed in parallel. In these cases, the infrastructure chosen has a significant impact on the results as it has to be at the same time representative of reality and not too complex due to time calculation management. Thus, several studies focus on the pipeline network deployment because of its flexibility e.g. [André et al., 2014], or restrain the transport via road infrastructure to the main highway system e.g. [Almaraz et al., 2015]. Moreover, geographical distribution can only be performed in the optic of representing final hydrogen distribution infrastructure at the city scale level. In this case, a more complex road system is taken into account e.g. [Stephens-Romero et al., 2010].

For this purpose, the early investment for deploying hydrogen infrastructure was optimized by adequate spatial and temporal HRS distribution in Irvine, California [Stephens-Romero et al., 2010]. The model uses a linear program to optimize the number of HRS, taking into account travel-time analysis that guarantees the minimum travel time between the stations, a land-use by applying constraints to the location already commercially available, vehicle density to identify the regions with the highest vehicle use, a service coverage and finally a temporal analysis to investigate the optimum strategy for the stations time deployment that will correspond to the need of the early adopters of fuel cell vehicles. The results showed that eight HRS could serve a comparable population portion as the 34 existing gasoline stations within three to five minutes of travel distance. Concerning California state environmental framework, the hydrogen was assessed to be likely produced mainly from localized plants using gas production and solar energy and transported using gaseous trucks.

A constrained nonlinear optimization program was developed to determine the minimum cost topology of the pipeline network and the corresponding optimal pipes diameter to transport the hydrogen from a given production plant to the main 78 cities in France and for hydrogen penetration of 100% in passenger car mobility by 2050 [André et al., 2013]. At the national level, one production point was considered located near Paris with an inlet pressure of 100 bar, while at the regional level, four production points were considered. The results showed that the minimal pipeline network at the national level was 5274 km long with an average diameter of 300 mm and a total cost of 2.472 billion €, while for the regional one, the total investment cost dropped by 30%. This model was then used as an input parameter for the north region of France

[André et al., 2014] and considered backward all the preceding periods till 2010 at five years' time step, to justify every time the pipeline development by comparing it to the truck transport option. The results show that for mid-term, the trucks are the most economical option at low hydrogen penetration share, while the deployment of the pipeline is developed when the share exceeds 10%. Thus, the pipeline infrastructure deployment occurs between 2030 and 2040 for a low demand scenario, and between 2025 and 2030 at the high demand scenario.

Concerning the use of road infrastructure at the national level, [Almaraz et al., 2015] proposed a work to design an optimal hydrogen supply chain at the national level with geographical visualization in France based on a regional optimization cost model [Almaraz et al., 2014] by 2020 and 2050. The network flow is simplified by considering the center of the 21 grids used for the optimization problem to correspond to the cities used for the transported flow. This applies a transport distance ranging between 98 km and 1182 km and an average one of 555 km. Thus, the flow between the grids is found out to range between 3.5 TPD and 88.3 TPD by 2030 and between 22.2 and 237.1 TPD by 2050 for a total transported flow at the national level of 105.1 TPD and 2372.3 TPD by 2030 and 2050, respectively, which applied, for the transport distance considered, an average flow per transport distance of 0.01 TPD/ km and 0.25 TPD/ km by 2030 and 2050, respectively.

#### **IV.4 Scientific motivation and novelty of the study**

The main proposed approach aims to develop a cost-effective infrastructure transport system following the road infrastructure for hydrogen. The methodology will be using as well linear programming to minimize the cost and geographical distribution to visualize the different flows transported. For that, different states of aggregation are considered, and the results are applied to the case of France and Germany. The primary motivation of the study aims to counter the few studies that couple cost optimization and geographical distribution at this scale level, and the lack of a complete comparison of various hydrogen states of aggregations.

Thus, Table 1.1 summarized the main benefits and drawbacks of the relevant literature review to the case study, to overcome the gaps in the methodologies used.

**Table 1.1:** Benefits and drawbacks of the leading literature reviews relevant to the study

Reference	Main results	Methodology benefits and drawback
[Demir & Dincer, 2018]	<ul style="list-style-type: none"> <li>- Over 18.47 M€ to construct the pipeline system (7.02 €/ kg) and 2.67 M€ for transmission investment in the second one using the tube trailers (2.64 €/ kg)</li> <li>. Pipeline transmission is the most environmentally friendly option.</li> </ul>	<ul style="list-style-type: none"> <li>- Various hydrogen transport and delivery cost</li> <li>- Greenhouse emissions associated</li> <li>▪ <u>Restricted to cost comparison</u></li> </ul>
[Yang & Ogden, 2007]	<ul style="list-style-type: none"> <li>-- Compressed gas truck with the minimum transport cost at low demand below 14 TPD and low average transport distance below 350 km</li> <li>- Liquid tanker for average to high transport distance above 250 km and average demand below 50 TPD</li> <li>- Pipeline system for high demand above 50 TPD</li> </ul>	<ul style="list-style-type: none"> <li>- Complete analysis of the cost-effective transport option</li> <li>▪ <u>Restricted to cost comparison</u></li> </ul>
[Kim & Kim, 2016]	<ul style="list-style-type: none"> <li>- At high penetration of FCEV in South Korea corresponding to a total demand of 8108.1 thousand tons by 2040, the main hydrogen is produced using electrolysis, and hydrogen storage in large facilities was used.</li> <li>- A Levelized cost of 6.0 €/ kg in high penetration scenario and is reduced to 5.3 €/ kg in case of 34.5% less hydrogen demand.</li> </ul>	<ul style="list-style-type: none"> <li>- Various hydrogen production sources</li> <li>- Mixed-integer formulation</li> <li>▪ <u>One transportation option was investigated</u></li> <li>▪ <u>Only export/ import hydrogen between the grid was analyzed without setting the exact locations</u></li> </ul>
[Sabio et al., 2010]	<ul style="list-style-type: none"> <li>- Steam methane reforming as a minimum cost production option in the case of Spain</li> <li>- Coal gasification as a suitable production option for the worst-case scenario.</li> <li>- Cryogenic tanks as a storage option for both optimum cost and risk scenarios.</li> </ul>	<ul style="list-style-type: none"> <li>- Cost and risk optimization</li> <li>- Multi-objective optimization</li> <li>▪ <u>Hydrogen transport impact on cost reduction is missing</u></li> <li>▪ <u>Transported considered as an option only in the worst-case scenario</u></li> </ul>
[Nunes et al., 2015]	<ul style="list-style-type: none"> <li>- A mean cost of infrastructure deployment in UK between 29,315.21 and 31,200.51 M€.</li> <li>- Methane-reforming production plants as a suitable option, ranging from small to medium size depending on the demand</li> <li>- Medium-size storages as the most suitable alternative for all scenarios</li> </ul>	<ul style="list-style-type: none"> <li>- Optimization of the total supply chain</li> <li>- Mixed-integer formulation</li> <li>▪ <u>Only liquid hydrogen is considered for the transport option</u></li> </ul>

Reference	Main results	Methodology benefits and drawback
[Almaraz et al., 2015]	<ul style="list-style-type: none"> <li>- A flow of hydrogen transported between the 21 grids decomposition of France ranging between 3.5 TPD and 88.3 TPD by 2030, and between 22.2 and 237.1 TPD by 2050</li> <li>- A total transported flow at the national level of 105.1 TPD and 2372.3 TPD by 2030 and 2050, respectively.</li> <li>- An average flow per transport distance of 0.01 TPD/ km and 0.25 TPD/ km by 2030 and 2050, respectively</li> </ul>	<ul style="list-style-type: none"> <li>- optimization of the total supply chain</li> <li>- Mixed-integer formulation</li> <li>- Flow visualization using geographical information system</li> <li>▪ <u>Simplified road infrastructure,</u></li> <li>▪ <u>High transport distance,</u></li> <li>▪ <u>overestimating the costs</u></li> <li>▪ <u>Simplified demand locations</u></li> </ul>
[André et al., 2013]	<ul style="list-style-type: none"> <li>- Pipeline transport system for the main 78 cities in France and for hydrogen penetration of 100% in passenger car mobility by 2050</li> <li>- A minimal pipeline network at the national level of 5274 km long with an average diameter of 300 mm and a total cost of 2.472 billion €.</li> <li>- A total investment cost reduction of 30%, when going from national to regional distribution</li> </ul>	<ul style="list-style-type: none"> <li>- optimization of the pipeline system</li> <li>- Nonlinear optimization</li> <li>- Flow visualization using geographical information system</li> <li>▪ <u>Restricted to only one mode of transport</u></li> <li>▪ <u>A maximum of only four production sites is considered</u></li> </ul>
[André et al., 2014]	<ul style="list-style-type: none"> <li>- For mid-term, the trucks are the most economical option at low hydrogen penetration share.</li> <li>- The deployment of the pipeline occurs when the share on hydrogen for mobility exceeds 10%.</li> <li>- The pipeline infrastructure deployment occurs between 2030 and 2040 for a low demand scenario, and between 2025 and 2030 at the high demand scenarios.</li> </ul>	<ul style="list-style-type: none"> <li>- optimization of the pipeline system and the road system</li> <li>- Nonlinear optimization</li> <li>- Flow visualization using geographical information system</li> <li>▪ <u>Simplified geometry,</u></li> <li>▪ <u>restricted to regional analysis</u></li> <li>▪ <u>Only one production point is considered</u></li> </ul>

The first aspect related to the optimization problem was covered by performing both a simple cost comparison and a linear optimization to find not only the minimum cost within an input transport mode range but as well the optimum one. Moreover, a case was added where a linear optimization was associated with daily technical analysis to minimize the cost further, and its impact was assessed.

Concerning the limitation of the transport mode and the state of aggregation, this was overcome by investigating seven different options and three states of aggregation. In addition to compressed gas and liquid hydrogen, liquid organic hydrogen carrier as novelty storage and transport options are considered as well. Furthermore, the different optimizations available in the literature showed that the studies focused on one pressure level. For instance, [Yang & Ogden, 2007] investigate the cost of transporting hydrogen using a compressed gas truck at low operating pressure of 162 bar pressure transporting a total net capacity of 300 kg when [Demir & Dincer, 2017] investigate a higher operating pressure of 486 bar but only at a fixed round-trip distance of 100 km. The middle range pressure of 200 bar was investigated as well by developing a model based on life cycle cost for implementing a general refueling station siting [Sun et al., 2017] or along the expressway [He et al., 2017]. Thus, five different pressure levels were considered, two at low pressure level, one at medium pressure level, and two at higher pressure level.

For the road infrastructure, a complete European road map including highways, first and the secondary road was used. The enormous number of data that should be treated to calculate the optimum transport network solution was overcome by adding two parallel models that deal with the flow transported, and the cost associated with each link and/or road. Finally, a solution was found as well concerning the limited hydrogen production and the simplified demand location. In fact, different scenarios considering different numbers of production plants and locations were considered, and the demand hub was chosen proportional to both regional hydrogen demand for mobility and the existing conventional fueling stations to tend towards a real case scenario.

Another novelty of the work resides on the fact that the detailed transport analysis and optimization performed were maintained and coupled to geographical visualization at a scale of two countries. Moreover, the two countries in question France and Germany do not have any common hydrogen economy initiatives and differ by their energy and power systems, which allows investigating the results in the scope of a single European hydrogen market.

# CHAPTER TWO

## 2 HYDROGEN SUPPLY CHAIN AND FRAMEWORK

### **Abstract**

In this chapter, the model framework that includes hydrogen production, demand, and transport modes is defined, which allows setting different scenarios for the optimum infrastructure calculation. Concerning hydrogen production, the capacity and the location are set proportional to wind electricity generation, and different scenarios are investigated depending on the total installed capacity and regional location in case of distributed or located production. The hydrogen demand is considered only for mobility, and two scenarios are considered depending on the hydrogen penetration for fuel cell electric vehicles. Finally, hydrogen is transported using the road infrastructure, and seven transport modes are considered linked to liquid hydrogen, liquid organic carrier, and different compressed gas pressure levels. Thus, the road infrastructure complicity and simplification are discussed, and the transport system using trucks is defined.

## Hydrogen supply chain and framework

### I HYDROGEN PRODUCTION

<i>I.1 Wind electricity generation</i> .....	43
I.1.1 Current status review .....	43
I.1.1.1 Capacity factor .....	43
I.1.1.2 Wind farm data information .....	44
I.1.2 Installed capacity growth .....	46
<i>I.2 Hydrogen production</i> .....	47
I.2.1 Literature overview .....	48
I.2.2 Hydrogen production cost .....	48
<i>I.3 Hydrogen production plants location and data</i> .....	50
I.3.1 Initial data set .....	50
I.3.2 New data set .....	51

### II HYDROGEN DEMAND

<i>II.1 Demand by NUTS-2 region</i> .....	53
II.1.1 Population growth .....	53
II.1.2 Car park and need of transportation .....	54
II.1.3 FCEV share on road transportation .....	55
<i>II.2 Distribution hubs demand and location</i> .....	56
II.2.1 Initial data set .....	56
II.2.2 New data set .....	56

### III HYDROGEN TRANSPORT USING THE ROAD INFRASTRUCTURE

<i>III.1 State of transport</i> .....	59
<i>III.2 Road infrastructure</i> .....	61
III.2.1 Data sources and comparison .....	61
III.2.2 Road input data .....	62
III.2.2.1 Modified distribution and production nodes .....	63
III.2.2.2 Road network .....	64

## Acronyms

RES	Renewable energy sources
FCEV	Fuel cell electric vehicles
CGH	Compressed gas hydrogen
LH	Liquid hydrogen
LOHC	Liquid organic hydrogen carrier
SMR	Steam methane reforming
ATR	Autothermal reforming
PEM	Polymer electrolyte membrane
PV	Photovoltaic power
NUTS	Nomenclature of Territorial Units for Statistics
SoT	State of Transport
QGIS	Open-source geographical information system
PostgreSQL	Open-source relational database management system
OSM	OpenStreetMap
SHP	Shapefile
ROAD 2	The road data network of Germany and France and neighboring countries
BORDER	The road data network of Germany and France border countries
ROAD 1	The road data network of Germany and France
CS1	The scenario of high distributed hydrogen production
CS2	The scenario of low distributed hydrogen production
CS3	The scenario of centralized hydrogen production

## Nomenclature

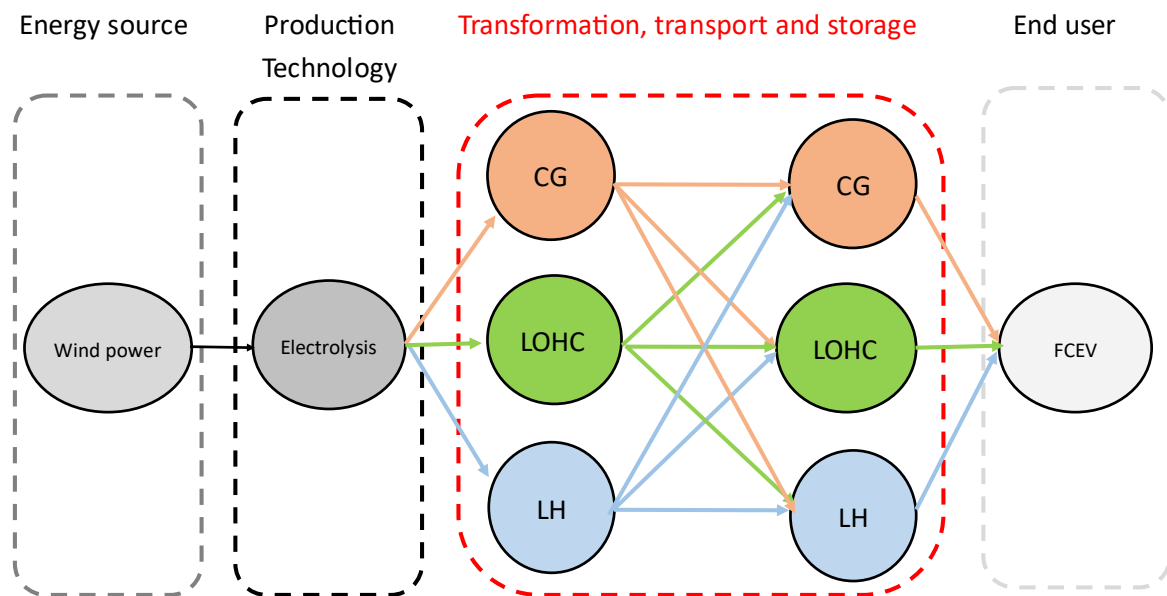
Parameter		First appearance	Unit
$CF_{wind}$	Wind capacity factor	Equation 2.1	-
$G_{pd,wind}$	Electricity generation produced from wind farm during a period $pd$	Equation 2.1	$GWh$
$E_{wind}$	Wind farm installed capacity	Equation 2.1	$MW$
$Th_{pd}$	Number of hours during a specific period $pd$	Equation 2.1	$hour$
$CF_{windOff,G}$	Offshore wind capacity factor in Germany	Table 2.1	-
$CF_{windOn,G}$	Onshore wind capacity factor in Germany	Table 2.1	-
$CF_{windOff,F}$	Offshore wind capacity factor in France	Table 2.1	-
$CF_{windOn,F}$	Onshore wind capacity factor in France	Table 2.1	-
$G_{y_{wind,y16}}(i)$	Wind generation in 2016 of a wind farm located in $i$	Equation 2.2	$GWh$
$E_{wind,y16}(i)$	Wind farm installed capacity of the reference year 2016	Equation 2.2	$MW$
$E_{windOff,G,y}$	Projected offshore wind installed capacity in Germany for the year $y$	Equation 2.3	$MW$
$E_{windOn,G,y}$	Projected onshore wind installed capacity in Germany for the year $y$	Equation 2.3	$MW$
$E_{windOff,F,y}$	Projected offshore wind installed capacity in France for the year $y$	Equation 2.3	$MW$
$E_{windOn,F,y}$	Projected onshore wind installed capacity in France for the year $y$	Equation 2.3	$MW$
$E_{windOff,G,y16}$	Offshore wind installed capacity in Germany in 2016	Equation 2.3	$MW$
$E_{windOn,G,y16}$	Onshore wind installed capacity in Germany in 2016	Equation 2.3	$MW$
$E_{windOff,F,y16}$	Offshore wind installed capacity in France in 2016	Equation 2.3	$MW$

$E_{windOn,F,y16}$	Onshore wind installed capacity in France in 2016	Equation 2.3	MW
$\Delta I_{yF,on}(i)$	Increased onshore wind installed capacity in $i$ located France	Equation 2.3	-
$\Delta I_{yF,off}(i)$	Increased offshore wind installed capacity in $i$ located in France	Equation 2.3	-
$\Delta I_{yG,on}(i)$	Increased onshore wind installed capacity in $i$ located in Germany	Equation 2.3	-
$\Delta I_{yG,off}(i)$	Increased offshore wind installed capacity in $i$ located in Germany	Equation 2.3	-
$G_{ywind,y}(i)$	Projected wind generation for the year $y$ of a wind farm in $i$	Equation 2.4	GWh
$p_{pd}$	Hydrogen potential produced during a period $pd$	Equation 2.5	Kg/ $pd$
$Er_{elec,HHV}$	Electrolysis energy requirement	Equation 2.5	kWh/ kg
$Td_y$	Number of days during the year	Equation 2.5	-
$Cp_d(p_d)$	Cost of a given production plant of size $p_d$	Equation 2.6	€
$LCOPH$	Levelized cost of producing hydrogen	Equation 2.7	€/ kg
$Tce$	Electricity price	Equation 2.7	€
$Lat(i)$	Latitude of the location $i$	Table 2.4	°
$Long(i)$	Longitude of the location $i$	Table 2.4	°
$p_d(i)$	Daily hydrogen production of the location $i$	Table 2.4	TPD
$(\varphi, \lambda)$	Geographical coordinates	Equation 2.8	-
$Tp_d(i)$	Total daily plant production of the location $i$	Equation 2.9	TPD
$LatT(i)$	Latitude of the total production plant of the location $i$	Equation 2.10	°
$LongT(i)$	Longitude of the total production plant of the location $i$	Equation 2.10	°
$d_y(r)$	Projected hydrogen demand for a region $r$ and during a year $y$	Equation 2.11	TPD
$Sc_2(r)$	Share of cars per capita	Equation 2.11	-
$Sp_2(r)$	Share of the regional population distribution to the national one	Equation 2.11	-
$Pop_y(N)$	The projected population at the national level for the year $y$	Equation 2.11	-
$D_{travel,y}(r)$	Yearly average distance traveled per capita for a region $r$ and during a year $y$	Equation 2.11	pKm/ year
$p_{FCEV,y}$	Share of Fuel Cell Electric Vehicle in light-duty road transportation during a year $y$	Equation 2.11	-
$Pop_y(r)$	The projected population at the NUTS – 2 regional level for the year $y$	Equation 2.12	-
$Sp_2(r)$	Share of the regional population distribution to the national one	Equation 2.12	-
$Pop_{16}(r)$	The population at the NUTS – 2 regional level for 2016	Equation 2.13	-
$Pop_{16}(N)$	The population at the national level for 2016	Equation 2.13	-
$Sc_2(r)$	The car share per capita	Equation 2.14	-
$CAR_{16}(r)$	The car park at the NUTS – 2 regional level for 2016	Equation 2.14	-
$N_{FuelS}(r)$	Number of fuel stations per NUTS – 2 region	Table 2.7	-
$LatH(i)$	Latitude demand hub of the location $i$	Equation 2.17	°
$LongH(i)$	Longitude demand hub of the location $i$	Equation 2.17	°
$d_y(i)$	The demand of the hydrogen hub for a given year	Equation 2.18	TPD
$\bar{E}_2$	Set of edge of the European road shapefile	Equation 2.19	-
$\bar{E}_1$	Set of edge of the France and Germany road shapefile	Equation 2.19	-
$\bar{E}_{BOR}$	Set of edge of the border road shapefile	Equation 2.19	-
$N_{BOR}$	Set of nodes of the European road shapefile	Equation 2.19	-
$N_2$	Set of nodes of the France and Germany road shapefile	Equation 2.19	-
$N_1$	Set of nodes of the border road shapefile	Equation 2.19	-
$D$	Set of demand nodes	Figure 2.10	-

$P$	Set of production nodes	Figure 2.10	-
$H$	Set of hubs nodes	Figure 2.10	-
$\bar{u}(i, j)$	Edge defined by its extremities nodes $i$ and $j$	Figure 2.11	-

The hydrogen supply chain can be broken down into production, storage, transportation, and distribution to the end-user. In the analysis, hydrogen transport and storage infrastructure using the road system is the focus of the optimization method. Thus, hydrogen production and demand are considered fixed and proportional respectively to wind electricity generation and mobility use, as shown in Figure 2.1.

**Figure 2.1:** Hydrogen supply chain considered

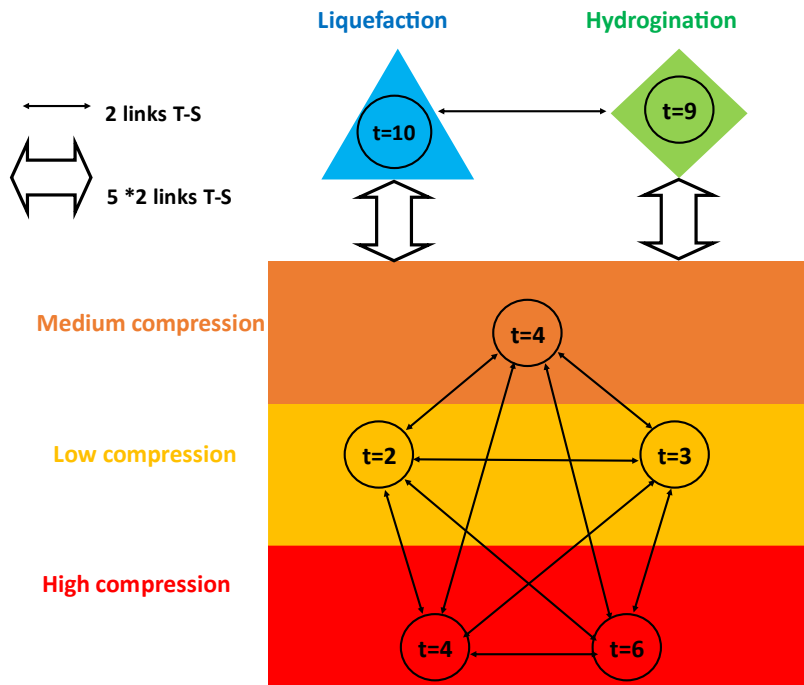


In fact, for the framework considered for France and Germany and to allow the comparison between the two countries, wind power as an energy source is considered for hydrogen production using electrolyzer. In France, the national plan to maintain the installed nuclear power capacity and increase the renewable energy sources (RES) in the electricity mix will increase the potential generation from wind power [Eolienne, 2017]. In Germany, the high share of wind power in the electricity mix justifies the choice of the source for hydrogen production.

Concerning the hydrogen demand for France and Germany, it will be restrained to the demand for fuel cell electric vehicles (FCEV) in order to decarbonize the transport sector (Figure 2.1). This will be done by assessing the growth potential of the car park associated with the population projection for 2030 and 2050, considering a penetration of FCEV in passenger car mobility of 2.4% and 28.5%, respectively, for the two years considered.

Finally, hydrogen transport is restrained to the use of road infrastructure via truck to investigate the impact of different states of aggregation. Thus, three states are considered in hydrogen transport, as compressed gas CGH, as a liquid LH, and bound in a liquid organic carrier LOHC (Figure 2.1) and a total of seven states of transport  $t$  accounting as well for five different pressure levels. Concerning the storage option, and to allow the flexibility associated with road transportation, hydrogen is considered stored in-ground tubes in different states as well. Therefore, by allowing transformation between transport and storage, 49 links are identified between each transport and storage pathways consisting of seven without transformation 42 with transformation. The 42 links are shown in Figure 2.2 and are broken down to 20 within compressed gas states, 20 between liquid, LOHC and gas states, and two between LH and LOHC.

**Figure 2.2:** Different links combinations between transport and storage (T-S)



$t$  refers to the state of transport index ranging between 2 and 10.

←→ The link translate on a single transformation on both ways (from Liquid hydrogen to LOHC and vice versa).

↔ The link translate on five transformation between the different presser level and liquid hydrogen or LOHC in both ways (from a single state to five gas states and vice versa).

↔ The link translate on a single transformation on both ways (from lower to higher pressure level and vice versa).

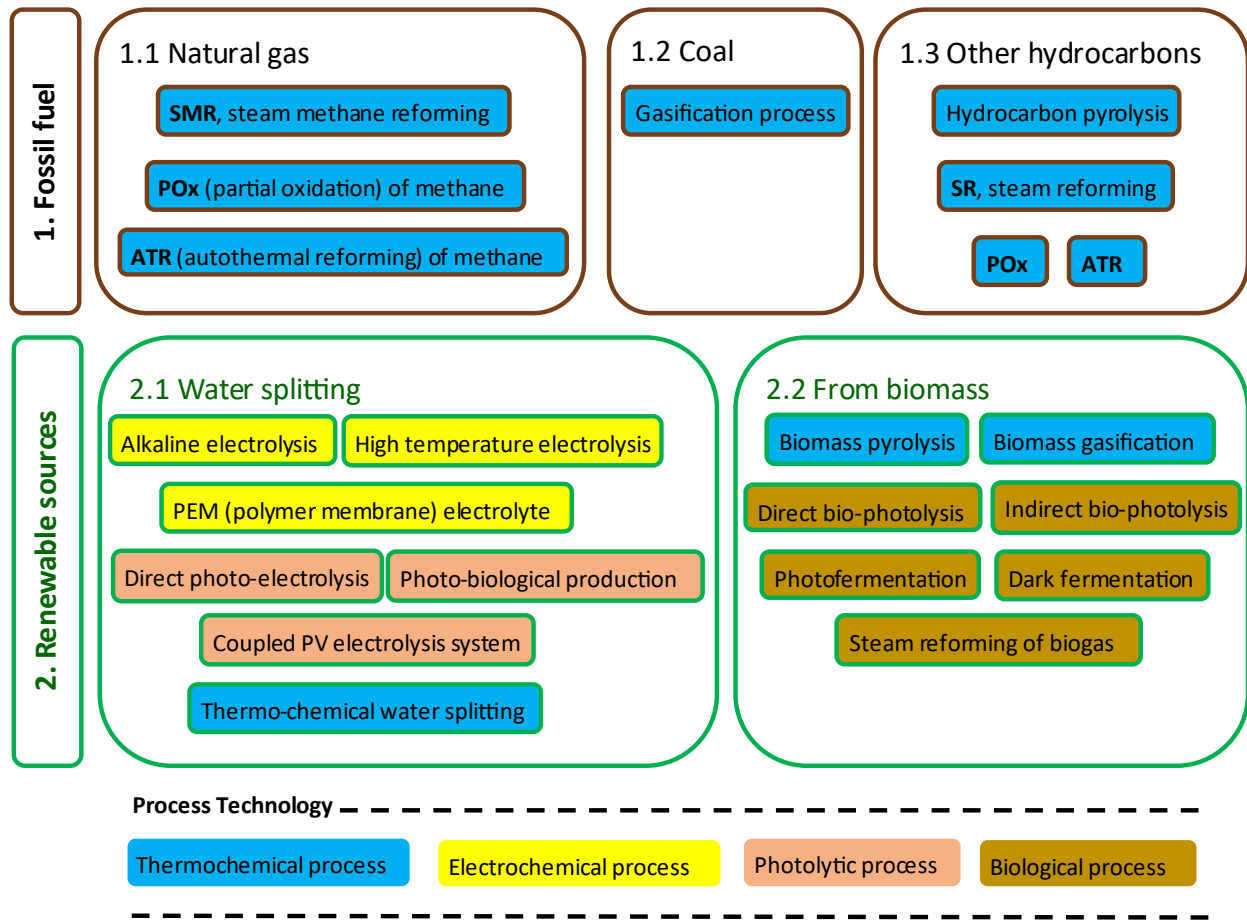
Concerning the state of aggregation at the initial production site and at the finale use, hydrogen is taken at atmospheric pressure  $t = 0$  or 20 bar  $t = 1$  when the cost of production is considered to be delivered at its final state as a compressed gas at 700 bar  $t = 7$  for hydrogen refueling

Stations

# I Hydrogen production

Hydrogen can be produced using two categories of feedstocks, a carbon one from fossil fuels (Figure 2.3, 1) using mainly natural gas and coal, or a green one from renewable sources (Figure 2.3, 2). The last source, although it still at the research stage with low energy efficiency and higher cost, offers the best alternative to fossil fuels and allows the use of different source RES such as wind, solar, or hydropower.

**Figure 2.3:** Main hydrogen production sources and technologies



As shown in Figure 2.3, the main process technology used for hydrogen produced from fossil fuel is thermochemical processing. These processes are the most developed and widely used as 48% of hydrogen was produced in 2016 using natural gas, 30% using naphtha, and 18% using coal [Nikolaidis & Poullikkas, 2017].

Using natural gas (Figure 2.3, 1.1), the hydrogen can currently be produced by the mean of three different thermochemical processes, steam methane reforming SMR, partial oxidation, and autothermal reforming (ATR). The first one involves mainly an endothermic reaction to transform methane and water vapor into hydrogen and carbon monoxide. Where the second one is an exothermic reaction of the partial combustion of methane with oxygen gas resulting in carbon monoxide and hydrogen. Finally, ATR is a combination of both steam reforming and partial oxidation [Riis et al., 2006]. Partial oxidation and ATR can be adapted to other hydrocarbons [Nikolaidis & Poullikkas, 2017].

Hydrogen can be produced as well from water splitting (Figure 2.3, 2.1) using water electrolysis. The leading current technologies include alkaline electrolysis, polymer electrolyte membrane (PEM), and high-temperature electrolysis. The first one uses an aqueous alkaline solution, while the second one, although less mature, has the advantage to provide hydrogen at high compression and purity rates, and with flexible operation and response time, which makes it suitable for intermittent sources (Schmidt, Gambhir et al. 2017). The high-temperature electrolysis is used to split water at a higher temperature ranging between 373 and 1123 Kelvin. Water can be splitted as well using, a photolytic process technology (Figure 2.3, 2.1) designed mainly for PV, and thermochemical water splitting designed for nuclear applications.

Finally, hydrogen production from renewable sources can be processed directly from biomass using thermochemical processes or biological processes (Figure 2.3, 2.2).

In order to achieve energy security, electricity balance, and carbon emissions reduction, hydrogen is chosen to be produced from renewable electricity sources in the model framework. On the one hand, RESs allow diversifying the hydrogen production and lower import and carbon emissions associated with hydrocarbons. On the other hand, hydrogen can be used as a storage option to balance the excess electricity often linked to renewable sources.

In France, and despite the goal of maintaining the nuclear share under 50% of the total electricity mix by 2025 [Gouvernement, August 2017], the country will have the main hydrogen production based on nuclear power. In contrast, Germany has a high share of RES in the electricity mix and will consequently have its hydrogen economy driven by these technologies. For the regions considered on the border and to allow the comparison between the two countries, the study is restrained to production from wind electricity. The 'Grande Est' at the French-German border has the particularity of having the two nuclear power plants Fessenheim and Cattenom planned to be shut down by 2020 and 2025, respectively. This region has as well a high wind potential pushed by a national plan to reach an installed capacity of 45 GW onshore wind power by 2030 [Eolienne, 2017]. Germany, in contrast, already has a high wind energy share, mainly centralized in the north with the populated and industrial areas mostly located in the south.

To calculate the hydrogen production and location for both countries, and for the different regions studied, the wind electricity generation is calculated based on the reference year 2016.

### I.1 Wind electricity generation

First, all the parameters associated with wind electricity generation are defined and used to approximate the projected for a given year  $y$  at a given region  $i$ .

#### I.1.1 Current status review

The data associated with electricity generation from wind electricity for France and Germany are gathered. Thus, it includes the average capacity factor of the total wind farms depending on the technology and the location, and the installed capacities for the different wind farms.

##### I.1.1.1 Capacity factor

The wind capacity factor ( $CF_{wind}$ ) is defined as the ratio of the actual electricity generation from a wind turbine (wind farm) during a specific period  $pd$   $G_{pd\_wind}$  in GWh, and the ideal electricity generation that could be generated if it would have been running for the whole period. This last parameter is deduced from the wind turbine (wind farm) installed capacity  $E_{wind}$  in MW. This can be generalized by Equation 2.1.

$$CF_{wind} = \frac{G_{pd\_wind}}{E_{wind} * Th_{pd} * UNITS}$$

**Equation 2.1**

$Th_{pd}$  represents the number of hours during the period  $pd$  and  $UNITS$  represents the unit change from MW to GW.

As the capacity factor for a wind farm reflects the meteorological condition as well, and the wind turbines technologies, the projected capacity factor is taken constant equal to the average one from 2006 to the reference year 2016. This was calculated based on the data shown in Table A.1 for France and Germany and both onshore and offshore farms. The results are shown in Table 2.1.

**Table 2.1:** Capacity factor for offshore and onshore wind in Germany and France

Germany		France	
offshore	onshore	offshore	onshore
$CF_{windOff,G}$	$CF_{windOn,G}$	$CF_{windOff,F}$	$CF_{windOn,F}$
0.33	0.19	0.45	0.24

Calculated from Annex (Table A.1)

### *1.1.1.2 Wind farm data information*

Different data were investigated to collect information about the different wind farm installed capacity at the reference year 2016 on both countries.

The first data investigated was [OPSD, 2018]. To check the completeness of the sources, the installed capacities, containing the geographical information, of the different farms were summed depending on the technology (onshore or offshore) or the region (France or Germany) and compared to the total installed one given by [Europe, 2018]. The difference between the dataset information and total national installed capacity review gives an error difference of 0.72%, 71.47%, and 25.95% for onshore German wind farms, German offshore windfarms, and onshore French wind farms respectively; and no detailed data was found concerning offshore French wind farms. Following these outcomes, only the data concerning onshore wind in Germany was kept then and other sources were investigated.

For the offshore wind in Germany, the data were scraped using python and BeautifulSoup library [Richardson, 2012] from different webpages. The new data contained a total of 13.946 GW offshore data for a total of only 5.355 GW installed in 2017 [Europe, 2018]. This is because the data sets contain as well the planned, approved, the under construction, and the operational projects. The data were reorganized under the installed one and expected one and showed a new error difference of only 0.67%.

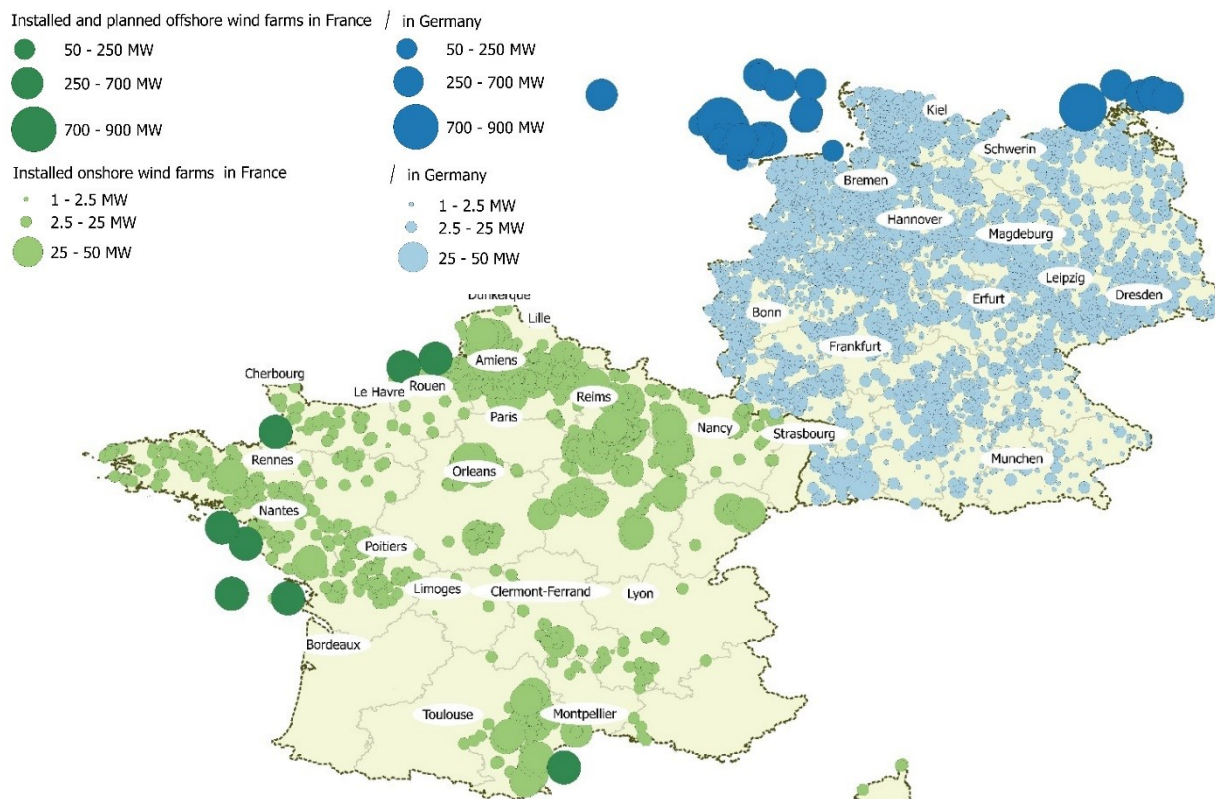
The same methodology was used to extract data from various sources for the case of onshore wind in France, which gives a new error difference of only 1.3%. For offshore wind, the current installed capacity gathered (16 MW) is negligible compared to the total planned and projected data (4043 MW). Thus, only the planned one was considered, and Table 2.2 below summarizes the total installed capacity of the wind farms where the geographical information was available, along with the values that were taken for the reference year 2016, and Figure 2.4 shows the geographical distribution for the reference year along with the offshore projects.

**Table 2.2:** Wind dataset that contains geographical information

	France		Germany	
	Onshore	Offshore	Onshore	Offshore
Data set of installed wind farms	13.57 GW	-	50.42 GW	5.32 GW
Data set of Planned wind farms	-	4.05 GW	-	8.596 GW
Difference Error to the total national installed capacity [Europe, 2018]	1.30%	-	0.72%	0.67%
Reference value taken	$E_{windOn,F_{y16}}$	$E_{windOff,F_{y16}}$	$E_{windOn,D_{y16}}$	$E_{windOff,D_{y16}}$
	13.57 GW	4.05 GW	50.42 GW	13.92 GW

Calculated based on [Europe, 2018, OPSD, 2018, Power, 2016, WindPower, 2017]

**Figure 2.4:** Wind onshore and offshore wind farm taken for the reference year 2016



Based on the database summed in Table 2.2

The parameters introduced before are used to calculate the annual wind generation of the reference year 2016  $Gy_{wind,y16}(i)$  of a wind farm located in  $i$  (given by its geographical localization and installed capacity  $E_{wind,y16}(i)$ ) using Equation 2.1.

Since not all the capacity factors related to each wind farm were available, the ones defined in Table 2.1 are used for calculation,, as shown in Equation 2.2.

$$\begin{aligned} \text{For } i \in F \quad & \begin{cases} Gy_{wind,y16}(i) = E_{wind,y16}(i) * CF_{windOn,F} * Th_{pd} * UNITS \\ Gy_{wind,y16}(i) = E_{wind,y16}(i) * CF_{windOff,F} * Th_{pd} * UNITS \end{cases} \\ \text{For } i \in G \quad & \begin{cases} Gy_{wind,y16}(i) = E_{wind,y16}(i) * CF_{windOn,G} * Th_{pd} * UNITS \\ Gy_{wind,y16}(i) = E_{wind,y16}(i) * CF_{windOff,G} * Th_{pd} * UNITS \end{cases} \end{aligned}$$

**Equation 2.2**

### 1.1.2 Installed capacity growth

As the literature review gives only the national or regional projection of offshore and onshore wind, an assumption has to be made concerning the projection of each wind farm installed capacity. For that, projected capacity has been considered installed in the existing location, respecting the same ratio to the reference year.

These ratios represent the increased total installed wind capacity of the year  $y$  compared to the reference year 2016 in France and Germany and for onshore and offshore capacity, as shown by Equation 2.3.

$$\begin{aligned} \text{For } i \in F \quad & \begin{cases} \Delta I_{F,On}(i) = CF_{windOn,F} / E_{windOn,F,y16} \\ \Delta I_{F,Off}(i) = CF_{windOff,F} / E_{windOff,F,y16} \end{cases} \\ \text{For } i \in G \quad & \begin{cases} \Delta I_{G,On}(i) = CF_{windOn,G} / E_{windOn,G,y16} \\ \Delta I_{G,Off}(i) = CF_{windOff,G} / E_{windOff,G,y16} \end{cases} \end{aligned}$$

**Equation 2.3**

The projected installed capacities  $E_{windOn,F,y}$ ,  $E_{windOff,F,y}$ ,  $E_{windOn,D,y}$  and  $E_{windOff,D,y}$  are calculated based on the total projected installed capacity for the year  $y$  for France and Germany [Corbetta et al., 2015]. Meanwhile, the current onshore installed capacities are based on the data for the year 2016 [Europe, 2018], while the current offshore installed capacities are based on the share of offshore to total wind power for the same year [Ho et al., 2016]. This assumptions

translate on different ratios of 2.64, 1.73, 1.38 and 1.08 corresponding, respectively, to  $\Delta I_{yF,On}(i)$ ,  $\Delta I_{yF,Off}(i)$ ,  $\Delta I_{yD,On}(i)$  and  $\Delta I_{yD,Off}(i)$ . Thus, the projected annual generation  $Gy_{wind_y}(i)$  of a given year  $y > 2020$  of a wind farm located in  $i$  is given by Equation 2.4.

$$\begin{aligned} \text{For } i \in F \quad & \begin{cases} Gy_{wind_y}(i) = E_{wind_{y16}}(i) * CF_{windOn,F} * \Delta I_{yF,On} * Th_{pd} * UNITS \\ Gy_{wind_y}(i) = E_{wind_{y16}}(i) * CF_{windOff,F} * \Delta I_{yF,Off} * Th_{pd} * UNITS \end{cases} \\ \text{For } i \in G \quad & \begin{cases} Gy_{wind_y}(i) = E_{wind_{y16}}(i) * CF_{windOn,G} * \Delta I_{yG,On} * Th_{pd} * UNITS \\ Gy_{wind_y}(i) = E_{wind_{y16}}(i) * CF_{windOff,G} * \Delta I_{yG,Off} * Th_{pd} * UNITS \end{cases} \end{aligned}$$

**Equation 2.4**

## 1.2 Hydrogen production

The generated wind electricity  $Gy_{wind_y}(i)$  is then conducted to the electrolyzer to drive the electrochemical splitting of water. A proton exchange membrane electrolyzer (PEM) is considered because of its reduced cost perspective, and efficiency increases potential [Riis et al., 2006].

The main parameters associated with the electrolyzer are its electricity demand  $Er_{elec,HHV}$  in kWh/ kg, its efficiency  $\eta_{elec,HHV}$  in%, and its capacity factor  $CF_{elec}$ . As electricity is considered to be generated by only wind power, the last parameter can be considered equal to the wind capacity factor defined in Table 2.1. For the efficiency of electrolyzers, it is mainly based on the higher heating value  $HHV_{H_2}$  (39 kWh/kg) to calculate the efficiency [Turner, 2004]. This corresponds to the isothermal potential and represents the assumption that all the energy needed to split water comes from the electricity.

Thus, a maximum hydrogen potential  $p_{pd}$  can be produced during a period  $pd$  using the electricity generation from wind power as expressed in Equation 2.5 for yearly production.

$$p_d = \frac{1}{Er_{elec,HHV}} * \frac{Gy_{wind_y}(i) * UNITS}{Td_y}$$

**Equation 2.5**

Where  $UNITS$  represent the unit change from kW to GW, and  $Td_y$  is the number of days during the year, as the electricity generation  $Gy_{wind_y}(i)$  is a yearly parameter, and the hydrogen production  $p_d$  is calculated daily.

### 1.2.1 Literature overview

Hydrogen production from wind electricity was compared to other sources of electricity, such as nuclear, solar thermal, and solar PV [Nikolaidis & Poullikkas, 2017]. The results showed that hydrogen production from wind was less cost-effective compared to nuclear and hydrogen cost for high production rated between 38 and 63 TPD ranged between 4.6 and 5.8 €/ kg.

Hydrogen production from only wind sources were investigated as well depending on the wind speed and the scenario projection year using an electrolyzer producing a daily amount  $p_d$  of 1000 kg/ day [Bartels et al., 2010]. For a mid-term scenario calculated for a year before 2020, the electrolyzer efficiency  $\eta_{elec,HHV}$  was taken equal to 78% corresponding to energy requirement  $Er_{elec,HHV}$  of 47.9 kWh/kg. The hydrogen production cost based on electricity cost of 30 €/ MWh was found equal to 2.14 €/ kg for a region where the wind speed reached 7.41 m/s and 1.8 €/ kg for a wind speed of 8.5 m/s. For a long term scenario about a year between 2020 and 2030, the electrolyzer efficiency  $\eta_{elec,HHV}$  was taken equal to 83% corresponding to an energy requirement  $Er_{elec,HHV}$  of 44.7 kWh/kg. The hydrogen production cost based on electricity cost of 30 €/ MWh was found equal to 2.7 €/ kg for a region where the wind speed reached 7.41 m/s and 2.3 €/ kg for a wind speed of 8.5 m/s.

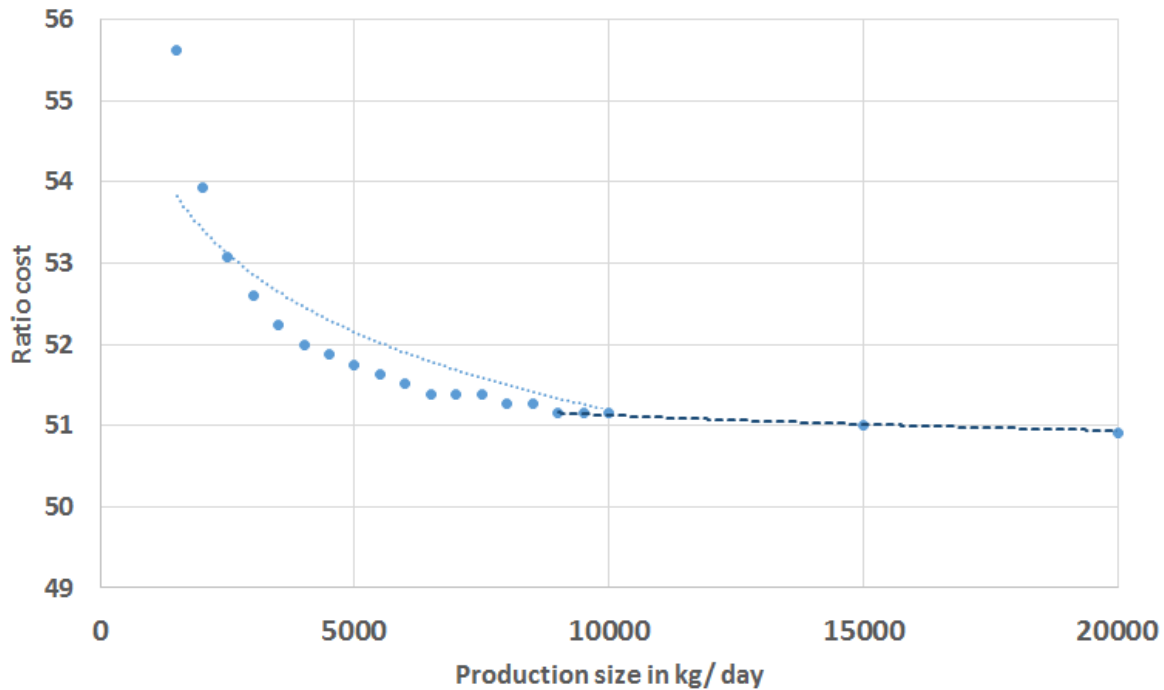
Finally, hydrogen production was assessed for different scenarios with and without electricity production from a wind farm of 278 MW total installed capacity and 41% capacity factor [Levene, 2005]. The cost of hydrogen production without electricity co-production dropped from 5.21 €/ kg in the near term to 2.17 €/ kg in the long term.

### 1.2.2 Hydrogen production cost

The results were calculated based on the [NREL, 2015] model for future central hydrogen production from PEM electrolysis. The costs were adapted from the basis of 2000 dollar for a reference year of 2004, and hydrogen production costs were simulated at different plant design capacity to show the variation of cost as a function of capacity and electricity cost.

The minimum hydrogen plant capacity  $p_d$  was fixed at 1000 kg/ day and the maximum one at 200,000 kg/ day. Figure 2.5 gives the ratio of different plant size cost to the reference cost at 1000 kg/ day as a function of production size.

**Figure 2.5:** Cost ratios of different production size to the reference one of 1000 kg/ day, along with the two fitting curves below and above 10000 kg/ day (limited in this figure to 20000 kg/ day for better visualization)



The logarithmic fitting of the results gives a relation between the cost of a given production plant  $Cp_d(p_d)$  of size  $p_d$  and the reference cost  $Cp_1(p_1)$  of the reference plant of size 1000 kg/ day,, as shown in Equation 2.6.

$$\frac{Cp_d(p_d)}{Cp_1(p_1)} = -13.11 * \ln(p_d) + 174 \quad \text{if } 1000 \text{ kg/ day} < p_d \leq 10000 \text{ kg/ day}$$

$$\frac{Cp_d(p_d)}{Cp_1(p_1)} = -1.74 * \ln(p_d) + 67 \quad \text{if } 10,000 \text{ kg/ day} < p_d \leq 200000 \text{ kg/ day}$$

**Equation 2.6**

The same model [NREL, 2015] was used to calculate the Levelized Cost of producing hydrogen at different electricity price  $TCE$  for the reference production plant of 1000 kg/ day.

The results are then introduced in Equation 2.6 to model the Levelized cost of producing hydrogen  $LCOPH$  as a function of production plant size  $p_d$  and electricity prices  $TCE$ , as shown in Equation 2.7.

if  $1000 \text{ kg/day} < p_d \leq 10,000 \text{ kg/day}$ :

$$LCOPH(p_d, TCe) = \frac{1}{100} [55 * TCe + 1.6] * [-13.11 * \ln(p_d) + 174]$$

if  $10,000 \text{ kg/day} < p_d \leq 200,000 \text{ kg/day}$ :

$$LCOHP(p_d, TCe) = \frac{1}{100} [55 * TCe + 1.6] * [-1.742 * \ln(p_d) + 67]$$

**Equation 2.7**

The electricity cost was taken as those of France  $TCe^{FR}$  or Germany  $TCe^{DE}$  depending on the location of the production plant. In both cases, correspondence has to be found between the annual electrical demand and the plant production size. In fact, the electricity costs vary depending on the Bands that are defined using the maximum annual electrical demand (Table A.13). Thus, Table 2.3 shows the corresponding maximum production plant size  $p_d$  that could be run using the different Bands.

**Table 2.3:** Production plant size for different Bands

Band (Table A.13)	IA	IB	IC	ID	IE	IF	IG
Maximum production plant size $p_d$ in kg/ day	-	31	122	1224	4287	97,187	-

### I.3 Hydrogen production plants location and data

The location organized the different wind farms in France and Germany, and the different parameters associated with them, including the amount of electricity generation and hydrogen production, were calculated.

As the production plants are constrained by a minimum and maximum production plant size, different wind farms electricity generation were gathered by proximity, and the hydrogen production is re-calculated to include all the wind farms.

#### I.3.1 Initial data set

The data of the different wind farms in France and Germany were gathered by the type of technology (onshore or offshore). For onshore wind farms, the data were organized by country, in France (0) or Germany (1), and included the location  $i$  of the wind farm defined by its coordinates  $Lat(i)$  and  $Long(i)$ , its installed capacity in MW in the reference year 2016  $E_{wind,y16}(i)$ , the electricity generation  $Gy_{wind,y}(i)$  and the hydrogen production  $p_d(i)$  of the scenario years,, as shown in Table 2.4.

**Table 2.4:** Initial data set of onshore wind farms

Country	Latitude	Longitude	Installed capacity in MW	Generation in GWh/year	Hydrogen production in kg/day
$\{F, G\}$	$Lat(i)$	$Long(i)$	$E_{wind_{y16}}(i)$	$G_{ywind_y}(i)$	$p_d(i)$

The data were then reorganized and clustered by summing different wind farm capacities to one hydrogen production capacity, considering two criteria, total hydrogen production and location.

The productions sum should always be between a minimum  $p_{min}$  and a maximum  $p_{max}$  respectively, set by the production plant reference size of 1000 kg/ day, and the maximum production cost model of 200 TPD.

The locations are gathered by proximity, by setting a circle radius  $rAd$  where the size of the production capacities was summed. The new plant location of the new total capacity is set equal to the center of the capacities mass of the summed wind farms.

### 1.3.2 New data set

The location condition is associated with an input circle radius  $rAd$ . Thus, every two wind farms of latitude and longitude coordinates difference  $(\Delta\phi, \Delta\lambda)$  are within a circle radius  $rAd$  if they verify Equation 2.8.

$$\sqrt{\Delta\phi^2 + \Delta\lambda^2} \leq rAd$$

**Equation 2.8**

By respecting the minimum and maximum capacity constraints, the new total plant production of total capacity  $Tp_d(i)$  will be the sum of the different wind farms hydrogen production  $p_d(i)$  respecting the location condition,, as shown in Equation 2.9.

$$\begin{cases} Tp_d(i) = \sum_{j \leq rAd} p_d(j) \\ p_{min} \leq Tp_y(i) \leq p_{max} \end{cases}$$

**Equation 2.9**

The associated cost of producing hydrogen  $LCOPH(Tp_d, TCe)$  is calculated using Equation 2.7, by replacing  $p_d$  with  $Tp_d$ .

Finally, the new location of the production plant defined by its geographical coordinates latitude and longitude  $(LatT(i), LongT(i))$  is set equal to the center of capacities mass of the different production plants located inside the circle radius condition  $rAd$ , as shown in Equation 2.10.

$$LatT(i) = \sum_{j \leq rAd} \frac{p_d(j)}{Tp_d(i)} * Lat(j)$$

$$LongT(i) = \sum_{j \leq rAd} \frac{p_d(j)}{Tp_d(i)} * Long(j)$$

**Equation 2.10**

The different parameters calculated are summed in a new data set and reorganized, as shown in Table 2.5.

**Table 2.5:** New data set of onshore wind farms

Country	Latitude	Longitude	Hydrogen production in kg/day	Production cost in €/ kg
{F, G}	LatT(i)	LongT(i)	$Tp_d(i)$	$LCOPH(Tp_d, TCe)$

For offshore wind electricity, the same methodology was applied to calculate the new production plant size, and the location was chosen as the closest one to the continent.

The circle radius within the different wind farms gathered was changed to obtain different scenarios for hydrogen production. In Table 2.6, the information corresponding to the results of four different hydrogen production location scenarios is summed up, and the corresponding geographical distribution is shown in the annex (Figure A.1, Figure A.2, and Figure A.3).

**Table 2.6:** Summary of hydrogen production for different scenarios

	Distributed hydrogen production				Centralized hydrogen production	
	High		Low		production	
	FR	DE	FR	DE	FR	DE
<b>Number of plants</b>	32	41	15	20	9	12
<b>Minimum LCOPH in €/ kg</b>	2.32	3.88	2.32	3.88	2.32	3.88
<b>Maximum LCOPH in €/ kg</b>	3.17	6.87	2.54	5.48	2.38	4.06

Based on the results of Figure A.1, Figure A.2 and Figure A.3

## II Hydrogen demand

The projected hydrogen demand  $d_y(r)$  for a given region  $r$  and during a given year  $y$  in both France and Germany will be based only on the light-duty road transportation sector demand, and will not include other forms and modes of transport or heavy industries which use hydrogen.

The hydrogen demand projections are calculated, taking into account the population distribution and the need for transport. These parameters include  $Pop_y(N)$ , the total population of the country at the corresponding year  $y$ ;  $D_{travel,y}(r)$ , yearly average distance per capita; and  $p_{FCEV,y}$ , the share of Fuel Cell Electric Vehicle (FCEV) in light-duty road transportation,, as shown in Equation 2.11.

$$d_y(r) = Sc_2(r) * Sp_2(r) * Pop_y(N) * D_{travel,y}(r) * p_{FCEV,y}$$

**Equation 2.11**

---

$Sc_2(r)$  and  $Sp_2(r)$  are variable parameters linked to the regional population and the car park and will be defined by population growth and car park projection.

### II.1 Demand by NUTS-2 region

All the demand projections are calculated per region defined by the population distribution. Each region corresponds to the NUTS-2 regions as defined by Eurostat [Eurostat, 2017b, Eurostat, 2017a].

First, the population distribution and projection are calculated for each NUTS-2 region, then the car park and the share of transportation are defined for each country. Finally, the share of FCEV is taken as an assumed parameter to calculate the projected hydrogen demand.

#### II.1.1 Population growth

First the population  $Pop_{16}(r)$  of each NUTS-2 region  $r$  for the first of January, 2016 [Eurostat, 2018a] was taken. This regional distribution is used then to project the population distribution  $Pop_y(r)$  at a given year  $y$  using the main scenario of population projection at a national level  $Pop_y(N)$  [Eurostat, 2016b], as defined by Equation 2.12.

$$Pop_y(r) = Sp_2(r) * Pop_y(N)$$

**Equation 2.12**

---

Equation 2.12 uses the assumption that the share  $Sp_2(r)$  (Equation 2.13) of the regional population distribution to the national one is constant. In fact, the main indicators used for population projection were fertility, death rate and age dynamic, and because of low fertility and death rates in the investigate countries, population projection is mainly driven by age dynamic

that has, in the case of France and Germany, a proportional increase between national and different regional levels.

$$Sp_2(r) = Pop_{16}(r)/Pop_{16}(N)$$

**Equation 2.13**

### II.1.2 Car park and need for transportation

Concerning the population distribution in 2016, the number of passenger cars  $CAR_{16}(r)$  is taken for each NUTS -2 region  $r$  [Eurostat, 2018b]. This parameter is used to calculate the car share per capita  $Sc_2(r)$  considered constant as defined by Equation 2.14.

$$Sc_2(r) = CAR_{16}(r)/Pop_{16}(r)$$

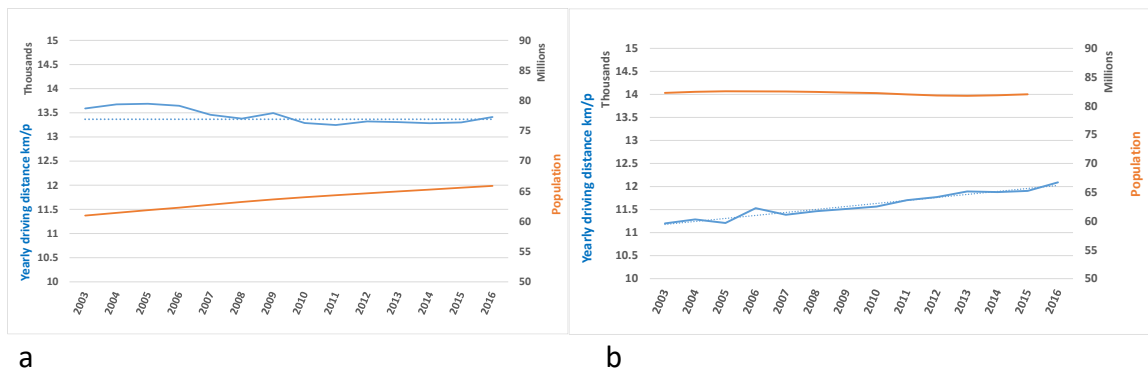
**Equation 2.14**

Along with the number of cars, the annual hydrogen consumption of each car has to be calculated to estimate the annual demand needed to fuel the car park.

In France and Germany, this need for transportation can be estimated by looking at the yearly average distance in km traveled by a person, deduced from the number of populations in a million people, and the total traveled distance in million-person km. The main projection of European population growth [Eurostat, 2016b], is used to project the need for transportation in the coming ten to 35 years.

Figure 2.6 shows the yearly average traveled distance per capita and the yearly population in France (a) and Germany (b) for ten years beginning from 1994.

**Figure 2.6:** Population and need for transportation growth in France (a) and Germany (b) [Eurostat, 2016c]



---

The yearly average distance traveled per capita  $D_{travel,y}(r)$  is constant in France since 2000 [Eurostat, 2016a] reaching its maximum value  $D_{max}$  of 13,366 km per capita. Which suggests that the car park growth can be taken proportional to population growth [Eurostat, 2016b]. This will apply a total population reaching 34.4 million by 2030 and 35.7 million by 2050.

For Germany, the yearly average distance traveled per capita is still increasing [Eurostat, 2016a] and is considered as an increasing function with a limit tending towards  $D_{max}$ . Therefore, the car park will be proportional to population decrease of Germany [Eurostat, 2016b] reaching 42.5 million by 2030 and 39.8 million by 2050.

The yearly average distance traveled per capita  $D_{travel,y}(r)$  in a given year  $y$  used for the model calculation is expressed in Equation 2.15.

$$\begin{cases} D_{travel,y}(r) = D_{max} & \text{for } r \in FR \\ D_{travel,y}(r) = 44.3 * y - 77407 & \text{for } r \in DE \end{cases}$$

**Equation 2.15**

---

### II.1.3 FCEV share on-road transportation

The car park prediction associated with the share of fuel cell electric vehicles (FCEV) in oil transportation can give an idea about the number of cars using conventional fuel that should be replaced. However, the penetration of the alternative fuels in the market is at its early commercialization phase, which makes it challenging to have an estimation about the share of new car technologies, mainly electric and hydrogen, in the car park projections.

For this study, the share of alternative fuels until 2050 is deduced from the report about hydrogen technology and fuel cells [IEA, 2015]. These results are used as a base case study for the calculations.

The scenario called EU4 was done for four European countries (France, Germany, Italy, and UK) and gives the number of FCEV till 2050 for PLDV in case of high penetration of hydrogen. From this number, the share of FCEV  $p_{FCEV,y}$  is deduced and taken equally for the four countries as a first approximation, which gives a share of 2.4% by 2030 and 28.5% by 2050 in case of high penetration of hydrogen [IEA, 2015]. Recent scenarios matched to a certain extent the EU4 scenario, where the hydrogen council projected a share of 25 % of hydrogen in passenger cars (Council 2017), and (FCH 2019) accounted for 14 % of hydrogen in the total transportation sector, which translates in even higher number for private mobility.

FCEVs, in general, have a driving range of 500 km for 4 to 6 kg of hydrogen [Stolten, 2016]. These values allow constraining the hydrogen flow in France and Germany for the two years between a minimum and maximum values.

## II.2 Distribution hubs demand and location

The distribution hubs locations are based on the refueling stations, while the demand is based on the NUTS-2 demand region. Thus, the different refueling stations in France and Germany are organized by their locations.

### II.2.1 Initial data set

All the primary refueling station geographical data [Esso, 2016] including in total more than 13,567 stations are first sorted depending on the country, in France (0) or Germany (1), and by geographical location ( $Lat(i)$  and  $Long(i)$ ).

The stations are then organized by their NUTS-2 regional location  $r$ . For each region  $r$ , the number of refueling stations located in the NUTS-2 region  $N_{Fuels}(r)$  is calculated. All the parameters were gathered, as shown in Table 2.7, including as well the regional hydrogen demand for a giving year  $d_y(r)$ .

**Table 2.7:** Initial data set of refueling station

Country	NUTS-2 region	Number of Fuel station	Fuel station location		Hydrogen demand projection
			Latitude	Longitude	
{F, G}	$r$	$N_{Fuels}(r)$	$Lat(i)$	$Long(i)$	$d_y(r)$

The data are then reorganized and gathered by associating different refueling station locations to one hydrogen distribution hub location, considering two criteria, regional hydrogen demand and the number of refueling stations.

The locations are gathered by proximity, by defining a circle radius  $rDs$  where the refueling stations are summed within the circle  $N_{Fuels}(i \leq rDs)$ , and by setting the distribution hub location and demand as the center of mass of the different refueling stations.

### II.2.2 New data set

The location defined by the geographical coordinates  $(\varphi, \lambda)$  condition is set as mentioned above. Thus, every two refueling stations of latitude and longitude coordinates difference  $(\Delta\varphi, \Delta\lambda)$  are within a circle radius  $rDs$  if they verify Equation 2.16.

$$\sqrt{\Delta\varphi^2 + \Delta\lambda^2} \leq rDs$$

**Equation 2.16**

By respecting that the distribution hub location is the center of mass of the different refueling station locations within the circle  $rDs$ , the latitude  $LatH(i)$  and the longitude  $LongH(i)$  associated with the hub can be defined from the refueling station geographical location using Equation 2.17.

$$\begin{cases} LatH(i) = Average_{i \leq rDs} Lat(i) \\ LotH(i) = Average_{i \leq rDs} Long(i) \end{cases}$$

**Equation 2.17**

The demand of the hydrogen hub for a given year  $d_y(i)$  is set equal to the ratio between the number of refueling stations within the circle  $N_{FuelS}(i \leq rDs)$  and the total number of refueling stations  $N_{FuelS}(r)$  for each region  $r$  as expressed by Equation 2.18.

$$d_y(i) = \frac{N_{FuelS}(i \leq rDs)}{N_{FuelS}(r)} * d_y(r)$$

**Equation 2.18**

The different parameters calculated are summed in new data set and reorganized, as shown in Table 2.8.

**Table 2.8:** New data set of the distribution hub

Country	Latitude	Longitude	NUTS—2 region	Hydrogen demand projection
{F, G}	$LatH(i)$	$LongH(i)$	$r$	$d_y(i)$

The hydrogen demand corresponding to the two different years 2030 and 2050 allows defining two scenarios representing the impact of hydrogen penetration in passenger car mobility. Table 2.9 sum up the information corresponding to the results of two scenarios based on the detailed results in Table A.2.

**Table 2.9:** Summary of regional hydrogen demand and demand hubs

Regional		FR		DE	
		2030	2050	2030	2050
	<b>Maximum demand in TPD</b>	36.95	462.72	15.34	178.04
	<b>Maximum demand location</b>	Île de France, FR10		Dusseldorf, DEA1	
	<b>Minimum demand in TPD</b>	1.99	23.11	1.58	18.33
	<b>Minimum demand location</b>	Limousin, FR63		Trier, DEB2	
	<b>Number of demand hubs</b>	144		126	

Based on the Annex results (Table A.2)

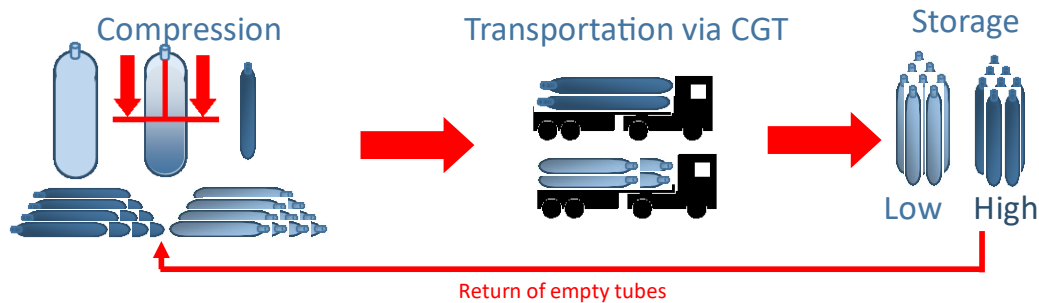
### III Hydrogen transport using the road infrastructure

The hydrogen is transported using three states of aggregation as compressed gas, as a liquid, and as bounded to a liquid organic hydrogen carrier corresponding to seven states of transport SoT as hydrogen is compressed at five different pressure level corresponding to low, medium and high rates. In this model, to allow the comparison of the different SoT, only road transportation is considered. Thus, in the first part, how hydrogen is stored and transported is described depending on the state of aggregation. Then, the adequate road system used to transport hydrogen using QGIS and PostgreSQL is detailed in the second part.

#### III.1 State of transport

Different methodologies are used when dealing with the transport of hydrogen, which depends on the state of aggregation. Common to all SoT, a specific flow  $X_{ij}$  of hydrogen is transported using tube or tanks between two locations  $i$  and  $j$  far from each other by a total distance  $d_{ij}$ . The hydrogen is at a transport state  $s$  at the initial location and then transported at SoT  $t$  where it is stored before further use. The different steps associated with the use of a compressed gas truck, a liquid hydrogen truck, and a liquid organic hydrogen carrier truck are shown in Figure 2.7, Figure 2.8, and Figure 2.9, respectively.

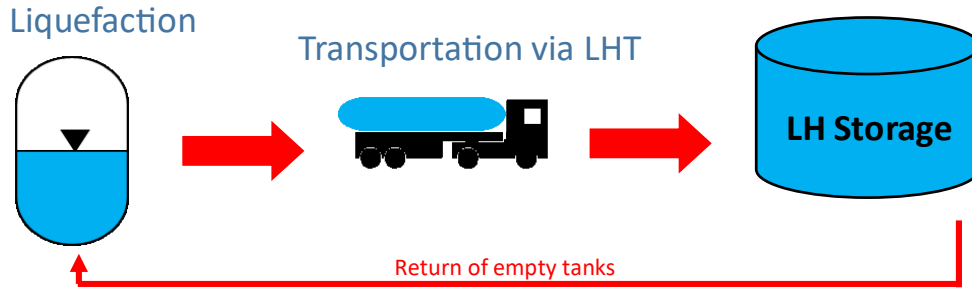
**Figure 2.7:** Transport components of compressed hydrogen



As a compressed gas (Figure 2.7), hydrogen can be transported using five different pressure levels; low ones at  $t = 2 = 180 \text{ bar}$  and  $t = 3 = 250 \text{ bar}$ ; medium one at  $t = 4 = 350 \text{ bar}$ ; and high ones at  $t = 5 = 500 \text{ bar}$  and  $t = 6 = 550 \text{ bar}$ . First the total hydrogen flow  $X_{ij}$  is compressed from its initial pressure corresponding to its SoT  $s$  to its transport pressure corresponding to the SoT  $t$ . The total capacity is distributed over the adequate number of tubes and loaded in different trucks. This is done considering that each truck can transport a total net capacity  $m[t]$  that depends on the pressure level. Hydrogen is transported afterward over the distance  $d_{ij}$  to the destination  $j$  where it is unloaded and stored until further use at the same

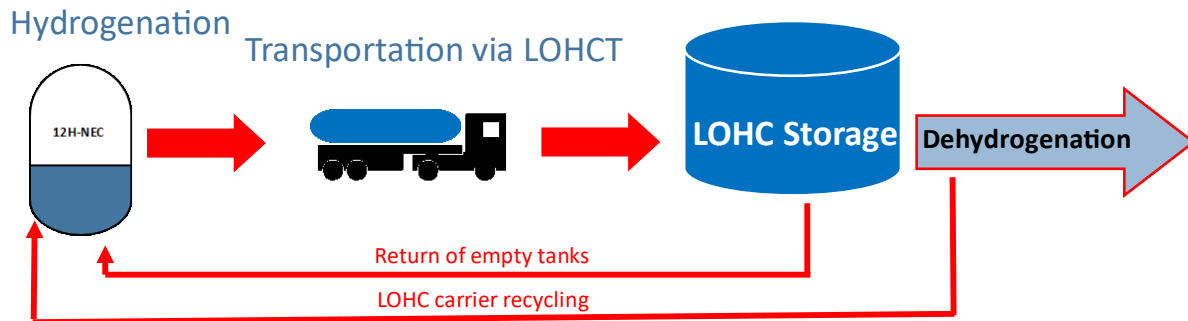
state of transport  $t$ . At the same time, the same number of empty tubes are picked from the location  $j$  to be returned at the initial transport location.

**Figure 2.8:** Transport components of liquid hydrogen



Concerning the liquid hydrogen, the same hydrogen flow  $X_{ij}$  is liquified from its initial pressure corresponding to its SoT. In the case where hydrogen is already at its liquid phase, no further transformation is needed. The total capacity is distributed over the corresponding number of tanks, then loaded in different trucks, each one of them can transport one tank of a total net capacity of 3600 kg [Tamhankar, 2014]. Hydrogen is transported over the distance  $d_{ij}$  to the location  $j$  where it is unloaded and emptied into an existing tank storage system till further use, while the empty tank is transported back to the liquefaction plant.

**Figure 2.9:** Transport components of liquid organic hydrogen carrier



Finally, concerning liquid organic hydrogen carrier, two facilities to process the hydrogen are needed one hydrogenation plant at the location  $i$  and one dehydrogenation plant associated with an existing storage system at the location  $j$ . The same hydrogen flow  $X_{ij}$  is transformed via hydrogenation to be bounded to a liquid carrier. The total capacity is distributed over the corresponding number of tanks, then loaded in different trucks, each one of them can transport one tank of total net capacity of 1500 kg. Hydrogen is transported then over the distance  $d_{ij}$  to

the location  $j$  where it is unloaded and emptied into an existing tank storage system till further use, while the empty tank is transported back to the liquefaction plant for further use. The dehydrogenation process is located in  $j$  only in the case where hydrogen has to be transformed into a different SoT. In this case, the carrier is transported back to the location  $i$  after the process.

In the three cases, the truck needs to use an adequate road system representative of reality. Thus, different road systems data had to be analyzed, gathered and merged into a single road network that will allow the transport between a given set of locations.

### **III.2 Road infrastructure**

The main framework impacting the choice of an adequate truck operating at the SoT is the road infrastructure that would be used to transport hydrogen, as a complete road system would increase the modeling time in contrast to the simplified one that would give wrong results.

For instance, the main open geographical reference system can be downloaded as OSM file from open street map, but the fact that the data are as detailed as in Google Maps for comparison, makes the analysis over France and Germany impossible to handle; as an example, the data information contained between Bonn Hauptbahnhof and Bonn Beuel station of 3 km diagonal [OpenStreetMap, 2019] can be downloaded as an OSM file of 20 MB size.

Another way to simplify the road infrastructure is to download the main roads in France, Germany, and border countries as a SHP file. For instance, the Socioeconomic Data and Applications Center allows downloading the road system in Europe as SHP file of 82 MB size [SEDAC, 2010]. This reduces the processing time, yet the number of roads to be analyzed accounts for more than 20,000 edges and contains bridges, double roads, end roads and repeated roads that need be corrected.

#### *III.2.1 Data sources and comparison*

For the road data shapefile, two different data sets for infrastructure are used for the model developed. The first one, ROAD 2, simulate the transported hydrogen and the second one, ROAD 1, is used to project the different production hubs and demand hubs. The main difference comes from the border roads BORDER along France and Germany, including Netherlands, Belgium, Luxembourg, Spain, Italy, Switzerland, Austria, and the Czech Republic, which are included in the first data file.

The ROAD 2 shapefile was used to simulate hydrogen transport using a truck, allowing the use of roads at the border counties, in contrast, production hubs and demand are located only in Germany and France and their projection (if not located in the road system) should remain within the two countries.

As the analysis will not consider the direction of the transport and will allow transport in both directions, first, only the primary, secondary, and local urban roads with dual ways were kept.

ROAD 1 and ROAD 2 files contained two roads associated with each highway in a single way, so only one was kept and was set as a dual way as well.

The next step is to delete or connect all the dead-end roads to the network [GRASS, 2003]. In fact, some errors can be found in the shapefiles as some roads are not connected when zoomed. For that, a threshold corresponding to 500 meters is set, so all the edges that are disconnected from the road network are reconnected.

Then, the bridges have to be defined and specified as not all of them are mentioned within the shapefile. In fact, some nodes could be declared as intersection nodes between two roads, while they are not in reality. As a matter of fact, it just two overlapped roads corresponding in reality to two roads one of the top of each other creating a bridge.

Finally, as the road shapefile is organized as a union of more than 20,000 edges linking different nodes, the number of edges has to be reduced. So, the edges that are part of the same line and does not intersect with another line are merged in a new line to reduce the number of edges to simulate. Another way to do it, is to merge all the lines of the road in one single geometry and then to break the lines again at each intersection [GRASS, 2003]. This allows us to reduce the geometry of ROAD 1 to 9641 edges, and of ROAD 2 to 11,506 edges.

### III.2.2 Road input data

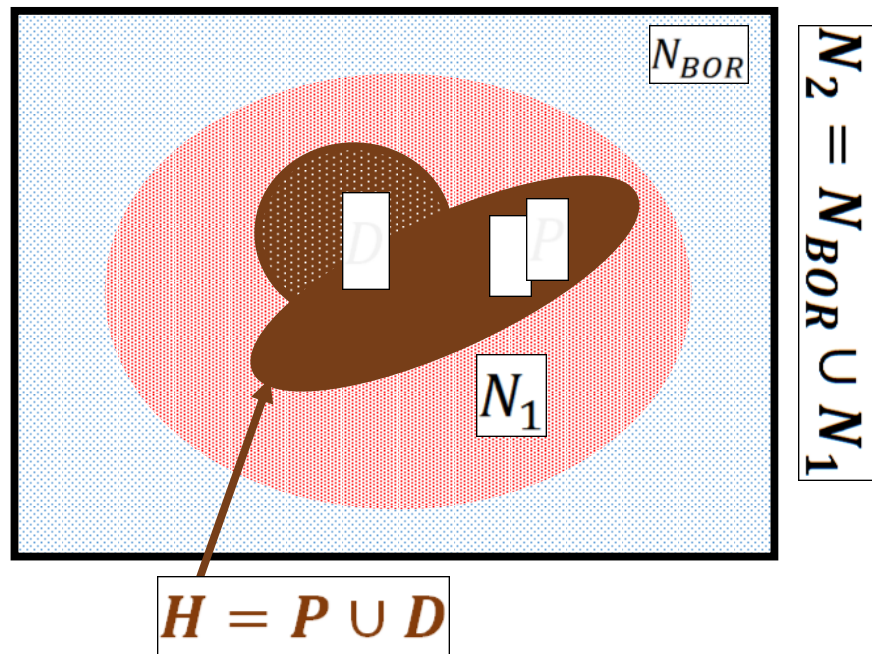
Thus, each final geometry ROAD 1 or ROAD 2 can be defined as a road network  $(N_1, \bar{E}_1)$  or  $(N_2, \bar{E}_2)$ , of edges  $(\bar{u}(i, j) \in \bar{E}_1)$  and  $(\bar{u}(i, j) \in \bar{E}_2)$  that connects  $n_1$  nodes  $(i \in N_1)$  and  $n_2$  nodes  $(i \in N_2)$ , respectively. The network  $(N_{BOR}, \bar{E}_{BOR})$  associated with the *BORDER* geometries can be defined then as expressed in Equation 2.19.

$$\begin{cases} \bar{E}_{BOR} = \bar{E}_2 \setminus \bar{E}_1 \\ N_{BOR} = N_2 \setminus N_1 \end{cases}$$

**Equation 2.19**

Both networks  $(N_1, \bar{E}_1)$  and  $(N_2, \bar{E}_2)$  have to include the information related to the production plants and distribution hubs. In fact, as these plants are located only in France and Germany, the nodes associated with the first network  $(i \in N_1)$  should include the production plants  $(i \in P)$  and distribution hubs  $(i \in D)$ . If not, the node has to be added via minimum projection to include all the information, as shown in Figure 2.10.

**Figure 2.10:** Different set nodes used for road networks



**III.2.2.1 Modified distribution and production nodes**

The different production plants ( $i \in P$ ) as defined in the four different scenarios and the distribution hubs ( $j \in D$ ) are used to create four sets points called hubs (Figure 2.10) corresponding to four scenarios, a low and high distributed one, and a centralized one as defined by Equation 2.20.

$$H = \{i \in P\} \cup \{j \in D\}$$

**Equation 2.20**

First, the hubs nodes ( $i \in H$ ) are placed on the edges of ROAD 1. This network was used to keep the nodes projection within the two countries. For that, the shapefile was uploaded on PostgreSQL [PostgreSQL, 1996] using the projection 4326 - GCS\_WGS\_1984 in the spatial reference system SRS [Spatialreference, 2013] for posttreatment.

For that, the nodes that are not on the ROAD 1 network are projected as the minimum distance to the closest edge. The original data information ( $i \in H$ ), including mainly whether it is a production or distribution node and all the technical data associated with production and demand, were linked to the displaced data on the edges ( $i \in NinE$ ).

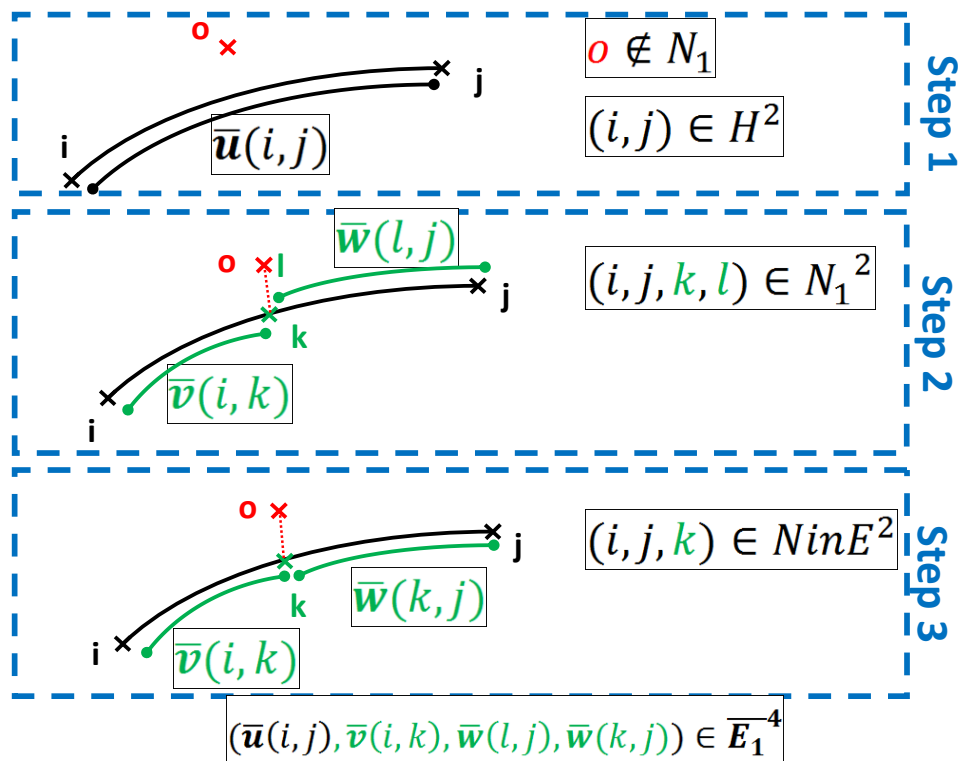
The results showed that some original nodes ( $i \in H$ ) that are close to each other but could not be gathered as a single production plant, due to the constraint of maximum production capacity below 200 thousand TPD, were projected as a single point ( $i \in NinE$ ). To avoid confusion and to

keep the same original results, the new node is marked as a multiple production node ( $i \in MP$ ), and the total production capacity of the new node is set as the sum of the other, but the cost of production corresponds to the maximum capacity of 200 thousand TPD.

### III.2.2.2 Road network

If a node  $o$  is not on the road edges, the associated closest edge ( $(\bar{u}(i, j) \in \bar{E})$  of ROAD 1 and ROAD 2 are splitted then on a set of new edges  $\bar{v}(i, k)$  and  $\bar{w}(l, j)$  with a unique id number  $k$  and  $l$  associated with each edge (primary key). In fact, for each two new splitted edges, a different id is associated with each one of them corresponding in reality to the same node (as shown in step 2 in the example of Figure 2.11).

**Figure 2.11:** Example of the different steps to add a node not located on the edge



To identify the newly added node, two columns  $\bar{E}.source$  and  $\bar{E}.target$  are added to each edge ( $\bar{u}(i, j) \in \bar{E}$ ) corresponding to the source id node and the target id node. Finally,  $\bar{E}.source$  and  $\bar{E}.target$  are filled with a unique location number  $N.id$  that correspond to the newly added node ( $k \in NinE$ ), as shown in step 3 in the example of Figure 2.11, and verifies for each set of two edges Equation 2.21.

$$\forall(\vec{v}(i, k), \vec{w}(l, j)) \in \vec{E}^2 \quad N.id(\vec{v}.source) = N.id(\vec{w}.target) \text{ if } l = k$$

**Equation 2.21**

As the roads are defined as two-way streets, the flow can be transported both ways so that Equation 2.22 is valid as well for the same set of edges  $\vec{v}(i, k)$  and  $\vec{w}(l, j)$ .

$$N.id(\vec{v}.target) = N.id(\vec{w}.source) \text{ if } l = k$$

**Equation 2.22**

A new topology is created then using the set of the new edges ( $\vec{u}(i, j) \in \vec{E}$ ) and the new nodes ( $i \in NinE$ ) and the remaining intersection nodes ( $i \in N \setminus NinE$ ). The primary key associated with all the nodes  $i \in N$  corresponds to the source and targets location number  $N.id$ .

All the information contained in the network  $(N, \vec{E})$  and the type of each data are summed up in Table 2.11.

**Table 2.11:** Main information contained in the network shapefile

Name	Type	Description
Edges set $\vec{E}$	LineString	ROAD 1 and ROAD 2 splitted in the $NinE$ nodes and indexed with two entries $\vec{E}.source$ and $\vec{E}.target$
Nodes set $N$	Point	Each Edge $\vec{E}$ is transformed in a set of two points with one entry $N.id$ corresponding to both $\vec{E}.source$ and $\vec{E}.target$
New nodes $NinE$	Point	Hub displaced at the closest point on the roads $NinE \subset N$
Hub nodes $H$	Point	The original distribution and production nodes $H = P \cup D$

The different hydrogen production and demand locations and sizes were organized depending on the years and the distribution. The corresponding total hubs are then introduced in the different road infrastructures to create different scenarios that will be used to simulate the minimum cost. Since the results aim to investigate the impact of the hydrogen export on the flow transported, a case scenario was added at high demand for isolated German road infrastructure. Finally, because hydrogen production is not included in the cost optimization, the impact of production cost was assessed as well as summed up in Table 2.12.

**Table 2.12: Different scenarios used for calculation**

	Demand		Productions			<i>LCOHP</i>	Country	
	2030	2050	CS1 [*]	CS2 [*]	CS3 [*]		F+G	G
$S_1$	X		X				X	
$S_2$		X	X				X	
$S_3$		X	X					X
$S_4$	X			X			X	
$S_5$		X		X			X	
$S_6$		X		X				X
$S_7$	X				X		X	
$S_8$		X			X		X	
$S_9$		X			X			X
$Sp_1$	X		X			X	X	
$Sp_2$		X	X			X	X	
$Sp_3$		X	X			X		X
$Sp_7$	X				X	X	X	
$Sp_8$		X			X	X	X	
$Sp_9$		X			X	X		X

**[\*] CS1** Corresponds to the first case scenario of high distributed hydrogen production (Figure A.3), corresponding to 73 production plants with 41 in Germany

**CS2** Corresponds to the second case scenario of low distributed hydrogen production (Figure A.2), corresponding to 35 production plants with 20 in Germany

**CS3** Corresponds to the case scenario of centralized hydrogen production (Figure A.1), corresponding to 22 production plants with 12 in Germany

# CHAPTER THREE

## 3 TECHNICAL AND ECONOMIC ASSASSMENT

### **Abstract**

This chapter aims to perform a technical assessment associated with the different parts of the optimized supply chain, including storage transformation and road transport. Thus, first, a storage review is performed in order to investigate their potential and the associated transformation. This allows calculating the energy requirement associated with compression, liquefaction, hydrogenation and dehydrogenation. Finally, the different parameters associated with truck transportation are defined and calculated as a function of different states of aggregation. This technical assessment allows, in a second part, to define the main parameters used for the economical one. Thus, the different sources and estimations used for costs associated with capital investment and variable operation and maintenance of the different transformation and storage plants are introduced. Finally, the different energy requirements and technical truck parameters are used to calculate the different costs associated with fixed operation and maintenance and fuel costs.

## Technical and economic assessment

### I TECHNICAL ASSESSMENT

<i>I.1 Hydrogen thermodynamic properties</i> .....	75
I.1.1 Compressibility coefficients .....	75
I.1.2 Enthalpy and entropy .....	76
I.1.3 Specific heat ratios.....	77
I.1.4 Ortho and para mixture:.....	77
<i>I.2 Hydrogen storage</i> .....	78
I.2.1 Compressed hydrogen .....	78
I.2.2 Liquid hydrogen .....	80
I.2.3 Liquid organic hydrogen carrier .....	80
<i>I.3 Hydrogen transformation work</i> .....	82
I.3.1 Ideal work review .....	82
I.3.1.1 Isentropic and isothermal compression .....	82
I.3.1.2 Polytrophic compression.....	83
I.3.1.3 Ideal liquefaction work.....	84
I.3.2 Multistage compression .....	86
I.3.2.1 System work.....	88
I.3.2.2 System cooling requirement .....	89
I.3.2.3 Conclusion.....	91
I.3.3 Liquefaction work .....	92
I.3.3.1 Liquefaction system work .....	92
I.3.3.2 State of art of different liquefaction plants and processes:.....	93
I.3.4 De- and hydrogenation work .....	96
I.3.4.1 De- and hydrogenation reaction .....	96
I.3.4.2 De- and hydrogenation simulation.....	97
I.3.4.2.1 Hydrogenation simulation .....	97
I.3.4.2.2 Dehydrogenation simulation .....	99
I.3.4.2.3 Simulation results .....	99
<i>I.4 Hydrogen truck transportation</i> .....	100
I.4.1 Hydrogen state of aggregation and storage .....	101
I.4.2 Transformation matrix.....	102
I.4.3 Transportation parameters.....	104
I.4.3.1 Technical parameters.....	104
I.4.3.2 Daily and yearly technical parameters .....	106

### II COST PARAMETERS

<i>II.1 Compressor and liquefier capital cost</i> .....	107
<i>II.2 Capital cost of hydrogenation</i> .....	109
<i>II.3 Storage capital cost</i> .....	110
<i>II.4 Operations and maintenance cost</i> .....	111
<i>II.5 Road transport cost</i> .....	112

## Acronyms

CGH	Compressed gas hydrogen
FCEV	Fuel cell electric vehicles
LOHC	Liquid organic hydrogen carrier
LH	Liquid hydrogen
TPD	Ton per day
US	United States
RK	Redlich–Kwong equation of state
NEC	N-Ethylcarbazole
12H-NEC	Dodecahydro-N-Ethylcarbazole
SoT	State of transport
RTT	Road transportation truck
DOE	The US Department of Energy
EUR	Euro currency
USD	US Dollar currency

## Nomenclature

Parameter		First appearance	Unit
$Z$	Compressibility coefficient	Equation 33.1	-
$V_m$	Gas molar volume	Equation 33.1	$m^3/mol$
$T$	Gas temperature	Equation 33.1	K
$P$	Gas pressure	Equation 33.1	bar
$\beta_T$	Isothermal compressibility	Equation 3.2	MPa
$\beta_S$	Adiabatic compressibility	Equation 3.2	MPa
$\gamma$	Specific heat ratio	Equation 3.2	-
$H$	Enthalpy	Equation 3.4	J
$h$	Specific enthalpy	Equation 3.4	$kJ/kg$
$U$	Internal energy	Equation 3.4	J
$S$	Entropy	Equation 3.5	J/K
$Q$	Heat	Equation 3.5	J
$s$	Specific entropy	Equation 3.5	$kJ/(kg \cdot K)$
$C_p$	Heat capacity at constant pressure	Equation 3.7	J/K
$c_v$	Heat capacity at constant volume	Equation 3.7	J/K
$h_{mix}$	Specific enthalpy of the hydrogen mixture	Equation 3.8	$kJ/kg$
$h_o$	Specific enthalpy of ortho hydrogen	Equation 3.8	$kJ/kg$
$h_p$	Specific enthalpy of para hydrogen	Equation 3.8	$kJ/kg$
$s_{mix}$	Specific entropy of the hydrogen mixture	Equation 3.8	$kJ/(kg \cdot K)$
$s_o$	Specific entropy of ortho hydrogen	Equation 3.8	$kJ/(kg \cdot K)$
$s_p$	Specific entropy of para hydrogen	Equation 3.8	$kJ/(kg \cdot K)$
$r$	Individual gas constant	Equation 3.8	$kJ/(kg \cdot K)$
$x_{mix}$	Mass fraction of the hydrogen mixture	Equation 3.8	-
$x_o$	Mass fraction of ortho hydrogen	Equation 3.8	-
$x_p$	Mass fraction of para hydrogen	Equation 3.8	-
$h_n$	Specific enthalpy of normal hydrogen	Equation 3.9	$kJ/kg$

$s_n$	Specific entropy of normal hydrogen	Equation 3.9	$\text{kJ}/(\text{kg}\cdot\text{K})$
$W$	Work	Equation 3.11	<i>Joule</i>
$P$	Pressure	Equation 3.11	<i>Pa</i>
$t, t'$	Hydrogen state of aggregation	Equation 3.11	-
$V$	Volume	Equation 3.11	$\text{m}^3$
$V_{in}$	Inlet volume	Equation 3.13	$\text{m}^3$
$\gamma$	Heat ratio	Equation 3.13	-
$P_{in}, P_{out}$	Inlet and outlet pressure	Equation 3.13	<i>Pa</i>
$W_{\Delta S \rightarrow 0, ideal}$	Isentropic work	Equation 3.13	<i>Joule</i>
$W_{iso, ideal}$	Isothermal work	Equation 3.14	<i>Joule</i>
$W_p$	Polytropic work	Equation 3.16	<i>Joule</i>
$n$	Polytropic exponent	Equation 3.16	-
$T_{in}, T_{out}$	Inlet and outlet temperature	Equation 3.17	<i>K</i>
$\dot{w}_{ideal, l}$	Specific ideal liquefaction work	Equation 3.18	$\text{kJ}/\text{kWh}$
$Q_L$	Quantity of heat removed	Equation 3.18	<i>J</i>
$Q_H$	Isothermal heat rejection	Equation 3.18	<i>J</i>
$h_f$	Final specific enthalpy	Equation 3.19	$\text{kJ}/\text{kg}$
$h_i$	Initial specific enthalpy	Equation 3.19	$\text{kJ}/\text{kg}$
$T_i$	Initial temperature	Equation 3.19	<i>K</i>
$s_f$	Final specific entropy	Equation 3.19	$\text{kJ}/(\text{kg}\cdot\text{K})$
$s_i$	Initial specific entropy	Equation 3.19	$\text{kJ}/(\text{kg}\cdot\text{K})$
$h_{mix, f}$	Specific final enthalpy of the hydrogen mixture	Equation 3.20	$\text{kJ}/\text{kg}$
$h_{p, f}$	Specific final enthalpy of para hydrogen	Equation 3.20	$\text{kJ}/\text{kg}$
$h_{n, f}$	Specific final enthalpy of normal hydrogen	Equation 3.20	$\text{kJ}/\text{kg}$
$s_{mix, f}$	Specific final entropy of the hydrogen mixture	Equation 3.20	$\text{kJ}/(\text{kg}\cdot\text{K})$
$s_{p, f}$	Specific final entropy of para hydrogen	Equation 3.20	$\text{kJ}/(\text{kg}\cdot\text{K})$
$s_{n, f}$	Specific final entropy of normal hydrogen	Equation 3.20	$\text{kJ}/(\text{kg}\cdot\text{K})$
$r$	Individual gas constant	Equation 3.20	$\text{J}/(\text{kg}\cdot\text{K})$
$h_{n, i}$	Specific initial enthalpy of normal hydrogen	Equation 3.21	$\text{kJ}/\text{kg}$
$s_{n, i}$	Specific initial entropy of normal hydrogen	Equation 3.21	$\text{kJ}/(\text{kg}\cdot\text{K})$
$P_i$	Inlet pressure	Equation 3.22	<i>bar</i>
$j$	Stage of compression between 2 and $N$	Equation 3.23	-
$W_{p, j}$	Polytropic work of stage $j$	Equation 3.23	<i>Joule</i>
$V_{in, j}$	Volume at the stage $j$	Equation 3.23	$\text{m}^3$
$r_j$	Compression ratio at the stage $j$	Equation 3.23	-
$P_{in, j}, P_{out, j}$	Inlet and outlet pressure at the stage $j$	Equation 3.24	<i>Pa</i>
$P_{i, j}$	Intermediate pressure between stage $j$ and $j + 1$	Equation 3.24	<i>Pa</i>
$\dot{w}_{p, N}(P_{in}, P_{out})$	Specific multistage compressor work	Equation 3.28	$\text{kWh}/\text{kg}$
$P_{in}$	Inlet pressure	Equation 3.28	<i>bar</i>
$\vartheta_{in}$	Specific volume	Equation 3.28	$\text{m}^3/\text{kg}$
$r_N$	Compression ratio	Equation 3.29	-
$T_0$	Ambient temperature	Figure 3.3	<i>K</i>
$\dot{m}_w$	Cooling water flow	Figure 3.3	$\text{kg}/\text{day}$
$\dot{m}_{H_2}$	Hydrogen compressed flow	Figure 3.3	$\text{kg}/\text{day}$

$T_{iw}, T_{ow}$	Inlet and outlet cooling water temperature	Figure 3.3	K
$\eta_p$	Polytropic efficiency	Equation 3.30	-
$\dot{w}_{aw}(P_{in}, P_{out})$	Actual specific work	Equation 3.31	kWh/ kg
$\dot{w}_{mw}(P_{in}, P_{out})$	Specific mechanical work	Equation 3.32	kWh/ kg
$\eta_{mc}$	Mechanical efficiency	Equation 3.32	-
$\dot{w}_c$	Specific compressor system work	Equation 3.32	kWh/ kg
$\eta_e$	Electricity motor efficiency	Equation 3.32	-
$\dot{V}_w$	The volume flow of cooling water	Equation 3.33	l/ day
$\dot{w}_{cl}$	Specific cooling work	Equation 3.33	kWh/ kg
$Cp_w$	Heat capacity of water	Equation 3.33	J/K
$W_d$	Daily energy consumed	Equation 3.34	kWh/ day
$CF_c$	Compressor capacity factor	Equation 3.34	-
$P_0$	Atmospheric pressure	Figure 3.6	bar
$T_0$	Ambient temperature	Figure 3.6	K
$T_l$	Saturated state temperature	Figure 3.6	K
$\dot{w}_s$	System work	Equation 3.36	kWh/ kg
$\eta_s$	System efficiency	Equation 3.37	-
$\dot{w}_{ideal,s}$	Ideal system work	Equation 3.37	kWh/ kg
$\dot{w}_p$	Work of compression	Equation 3.38	kWh/ kg
$\dot{w}_{pc}$	Ideal work of compression	Equation 3.38	kWh/ kg
$\eta_{pc}$	Compression efficiency	Equation 3.38	-
$\dot{w}_l$	Liquefaction work	Equation 3.39	kWh/ kg
$\eta_l$	Liquefaction efficiency	Equation 3.39	-
$a$	Attractive term that considers interactions between particles	Equation 3.44	-
$b$	Repulsive term that considers the volume of the particles	Equation 3.44	-
$St, St'$	Hydrogen state of aggregation	Figure 2.1	-
$t, t'$	Index related to hydrogen state of aggregation	Figure 2.1	-
$i, j$	Locations	Figure 2.1	-
$d_{ij}$	Distance between the locations $i, j$	Figure 2.1	km
$tt_{l/u}[t]$	Total loading and unloading time	Figure 2.1	hour
$Pt$	Tube design pressure	Table 2.1	bar
$m[t]$	Total net truck capacity	Table 2.1	kg
$\dot{w}_s(St, St')$	Total work of transformation from $S^t$ to $S^{t'}$	Equation 3.45	kWh/ kg
$\dot{w}_c(P^t, P^{t'})$	Compression work from $P^t$ to $P^{t'}$		kWh/ kg
$\dot{w}_l(P^t)$	Liquefaction work at an inlet pressure $P^t$		kWh/ kg
$\dot{w}_h(P^t)$	Total work of de- and hydrogenation	Equation 3.47	kWh/ kg
$\dot{w}_s[t, t']$	Total work of transformation from $S^t$ to $S^{t'}$	Equation 3.48	kWh/ kg
$\dot{w}_c[t, t']$	Compression work from $P^t$ to $P^{t'}$	Equation 3.48	kWh/ kg
$\dot{w}_l[t]$	Liquefaction work at an inlet pressure $P^t$	Equation 3.48	kWh/ kg
$\dot{w}_h[t]$	Total work of de- and hydrogenation and	Equation 3.48	kWh/ kg
$Av_{pd,RTT}$	Total time of truck availability during $pd$	Equation 3.49	hours
$CF_{RTT}$	Truck capacity factor	Equation 3.49	-
$Th_{pd}$	Duration of the period $pd$	Equation 3.49	hours
$Nrt_{pd,max}[t](i, j)$	Maximum number of roundtrips over a period $pd$	Equation 3.50	-

$Nrt_{pd}[t](i,j)$	Number of roundtrips performed by one truck	Equation 3.51	-
$Dpd_j$	Demand at the location $j$ over a period $pd$	Equation 3.51	kg
$Nt_{pd}[t](i,j)$	Number of trucks needed	Equation 3.52	-
$TNrt_{pd}[t](i,j)$	Number of roundtrips performed by all trucks	Equation 3.53	-
$Ndr[t](i,j)$	Numbers of drivers needed	Equation 3.54	-
$Nwh$	Maximum number of working hours	Equation 3.54	hours
$Dy_j$	Yearly demand	Equation 3.55	kg
$Dd_j$	Daily demand	Equation 3.55	kg
$Th_y$	Yearly hours	Table 3.8	hours
$Th_d$	Daily hours	Table 3.8	hours
$Av_{y,RTT}$	Yearly truck availability	Table 3.8	hours
$Av_{d,RTT}$	Daily truck availability	Table 3.8	hours
$Nrt_{y,max}[t](i,j)$	Yearly maximum number of roundtrips	Table 3.8	-
$Nrt_{d,max}[t](i,j)$	Daily maximum number of roundtrips	Table 3.8	-
$Nrt_y[t](i,j)$	Number of roundtrips performed by one truck per year	Table 3.8	-
$Nrt_d[t](i,j)$	Number of roundtrips performed by one truck per day	Table 3.8	-
$Nt_y[t](i,j)$	Number of trucks needed per year	Table 3.8	-
$Nt_d[t](i,j)$	Number of trucks needed per day	Table 3.8	-
$TNrt_y[t](i,j)$	Number of roundtrips performed by all trucks per year	Table 3.8	-
$TNrt_d[t](i,j)$	Number of roundtrips performed by all trucks per day	Table 3.8	-
$CC_{c,1}$	Compressor capital cost 1	Equation 3.56	€
$CF_{Tc}$	Compressor capacity factor	Equation 3.56	-
$P_c$	Compressor power	Equation 3.56	kWh
$CC_{c,2}$	Compressor capital cost 2	Equation 3.57	€
$C$	System cost	Equation 3.58	€
$S$	System size	Equation 3.58	Variable
$\alpha_{sc}$	Cost scale coefficient	Equation 3.58	NAN
$C_b$	Base compressor cost	Equation 3.58	€/size
$S_b$	Base compressor size	Equation 3.58	Variable
$CC_{c,3}$	Compressor capital cost 3	Equation 3.59	€
$CC_c$	Compressor capital cost modeled	Equation 3.60	€
$C_{b,c}$	Base compressor cost	Equation 3.60	€/kW
$S_{b,c}$	Base compressor size	Equation 3.60	kW
$r_c[t]$	Ratio compression to the base case	Equation 3.60	-
$Pt$	Operating pressure	Equation 3.60	bar
$P_{b,c}$	Baseline operating pressure	Equation 3.60	bar
$Pr_{h,net}$	Liquefier net production rate	Equation 3.61	kg/hour
$Pr_h$	Production rate	Equation 3.61	kg/hour
$BoR$	Boil-off rate	Equation 3.61	-
$Th_{st}$	Total liquid storage time	Equation 3.61	hour
$CC_l$	The capital cost of the liquefier	Equation 3.62	€
$C_{b,l}$	Base liquefier cost	Equation 3.62	€/kW
$S_{b,l}$	Base liquefier size	Equation 3.62	kW
$CC_h$	The capital cost of the hydrogenation process	Equation 3.62	€

$C_{b,h}$	Base hydrogenation cost	Equation 3.62	€/kW
$S_{b,h}$	Base hydrogenation size	Equation 3.62	kW
$CC_{Sc}$	Compressor storage capital cost	Equation 3.64	€
$C_{b,sc}$	Base compressor storage cost	Equation 3.64	€/kW
$S_{b,sc}$	Base compressor storage size	Equation 3.64	kW
$P_{b,sc}$	Baseline storage operating pressure	Equation 3.64	bar
$CC_{Sl}$	Liquefier storage capital cost	Equation 3.64	€
$C_{b,sl}$	Base liquefier storage cost	Equation 3.64	€/kW
$S_{b,sl}$	Base liquefier storage size	Equation 3.64	kW
$CC_S[t]$	Storage capital cost	Equation 3.65	€
$C_{tube}[t]$	Cost of the tube trailer	Equation 3.65	€
$m[t]$	Total net truck capacity	Equation 3.65	kg
$\alpha_{sc}[t]$	Sizing factor	Equation 3.65	-
$O\&M_{Sc}$	Fixed operations and maintenance cost associated with	Equation 3.66	€
$O\&M_{Tc}$	Compression storage and transformation		
$O\&M_{Sl}, O\&M_{Tl}$	Fixed operations and maintenance cost associated with	Equation 3.66	€
	Liquefaction storage and transformation		
$O\&M_{Sh}$	Fixed operations and maintenance cost associated with de- and	Equation 3.66	€
$O\&M_{Th}$	hydrogenation storage and transformation		
$OM_c$	Share of $O\&M_{Sc}$ and $O\&M_{Tc}$ to the capital cost	Equation 3.66	-
$OM_l$	Share of $O\&M_{Sl}$ and $O\&M_{Tl}$ to the capital cost	Equation 3.66	-
$OM_h$	Share of $O\&M_{Sh}$ and $O\&M_{Th}$ to the capital cost	Equation 3.66	-
$Tce^F[t, t']$	Specific cost of work transformation in France	Equation 3.67	€/kg
$Tce^G[t, t']$	Specific cost of work transformation in Germany	Equation 3.67	€/kg
$\dot{w}_s[t, t']$	Work of transformation	Equation 3.67	kWh/kg
$CF_h$	Liquefaction capacity factor	Equation 3.67	-
$CF_l$	De- and hydrogenation capacity factor	Equation 3.67	-
$Ce^{FR}$	Electricity cost in France	Equation 3.67	€/kWh
$Ce^{DE}$	Electricity cost in Germany	Equation 3.67	€/kWh
$TCw$	Cooling cost	Equation 3.68	€
$\dot{V}_w$	Cooling water requirement	Equation 3.68	m <sup>3</sup> /day
$CF_T$	Capacity factor of transformation	Equation 3.68	-
$Tdy$	Number of days during the year	Equation 3.68	day
$Cw$	Water cost	Equation 3.68	€/m <sup>3</sup>
$FC[t](i, j)$	Fuel cost for one truck	Equation 3.69	€
$F_p$	Unit fuel cost	Equation 3.69	€/km
$LC[t](i, j)$	Labor cost for one truck	Equation 3.70	€
$TC_{driver}$	Driver wage	Equation 3.70	€/hour

# H

Hydrogen is the most abundant element on earth as more than 90% of all atoms are hydrogen, and because of its single valence electron, it is very reactive and found mostly bounded to other elements and very rarely in the pure form, mainly bounded to oxygen as water. It is the lightest of all gases and has an atomic weight of 1.008 g/mol (McCarty, Hord, & Roder, 1981b), the first element of the periodic table, and the simplest one presented mainly (99.985%) at its ordinary form called light hydrogen consisting of one electron and one proton.

Hydrogen is presented at its dimerized form  $H_2$  at standard operating conditions of 288.15 K and atmospheric pressure. In this form, hydrogen presents a molecular weight of 2.016 g/mol (McCarty et al., 1981b) and high bond energy of 436 kJ/mol (McCarty et al., 1981b) allowing it to be stable. Moreover, hydrogen has a low density of only 0.089 g/l. As a comparison, the air has a density of 1.29 g/l, which makes it very volatile. These chemical aspects make hydrogen challenging to use at standard operating conditions and have to be transformed to increase its density and efficiency. The simplest way is high compression in the order of 350 to 500 bar for gaseous transport and in the order of 350 bar and 700 bar for on-board storage.

Hydrogen can be as well transformed in other states of aggregation to gain on density in the form of liquid hydrogen, but with the drawback of product loss via evaporation and massive energy intake. Besides, hydrogen can be transported not at its molecular form but rather bounded a liquid organic carrier via the hydrogenation process. All the states of aggregation present benefits and drawbacks depending on the hydrogen capacity needed, the transport distance, and the storage period. Thus, they are considered as potential transport options in the model performed and have to be technically and economically assessed to be introduced in the optimization model.

First, the different storage options (I.2) are presented to initially investigate their potential and the associated transformation (I.3). Thus, the technical assessment focuses on giving a useful modeling tool based on literature review, developed models, and simulation to investigate the energy needs associated with each transformation. This includes the different work of compressing hydrogen at different pressure level, the liquefaction process work, and the work needed for de- and hydrogenation.

As the hydrogen at its different states of aggregation is transported using trucks, a technical assessment is performed to investigate and define the parameters associated to truck transportation (I.4), including mainly the number of trucks needed in the case of the use of one state of aggregation and the number of roundtrips performed to transport a specific needed flow.

Finally, the technical assessment is associated with an economic one to define the different cost parameters associated with the capital investment of the different transformation and storage plants as well as those associated with the use of truck transportation.

## I Technical assessment

The hydrogen molecule is composed of two hydrogen atoms. These two atoms can appear in two modifications ortho and para hydrogen. The difference between the two is due to the relative orientation of the nuclear spin of the individual atoms, they can be in the same direction, or they may be in opposite directions. Associated with this quantization are quantum numbers for the spin and the corresponding energy levels. The molecules with antiparallel nuclear spins, called parahydrogen, are in the lowest energy state. Conversely, the molecules with parallel nuclear spins, called ortho hydrogen, have odd quantum numbers and are at a higher energy level.

Hydrogen may then be a binary mixture of two different species of molecules differing from each other in physical properties. The percentage of the ortho and para concentrations in the mixture is temperature-dependent. The term equilibrium hydrogen is, as the name implies, the equilibrium concentration at a given temperature. For example, near ambient temperature, the composition is 75% ortho and 25% para called normal hydrogen, while liquid hydrogen presents a concentration of 99.8% para.

Since the percentage of the ortho and para composition is temperature dependent, the rate of conversion is of interest in a variety of problems. The conversion of a nonequilibrium ortho and para composition to an equilibrium composition is a very slow process in the absence of a catalyst called self-conversion.

### I.1 Hydrogen thermodynamic properties

As the transportation of hydrogen is considered in different conditions and different phases, the thermodynamic properties, mainly at liquid and gas and different temperature-pressure conditions, are presented. This includes compressibility and specific heat coefficients, entropy, and enthalpy.

#### I.1.1 Compressibility coefficients

Compressibility coefficient  $Z$  is defined (Equation 33.1) as the ratio of the molar volume of a gas  $V_m$  to the molar volume of an ideal gas at the same temperature  $T$  and pressure  $P$ .

$$Z = -\frac{P}{V} \left( \frac{\partial V_m}{\partial P} \right)_T$$

**Equation 33.1**

---

This ratio  $Z$  can be linked to the isothermal compressibility  $\beta_T$  using Equation 3.2:

$$\beta_T = -\frac{Z}{P} = -\frac{1}{V} \left( \frac{\partial V_m}{\partial P} \right)_T$$

---

**Equation 3.2**

Finally, the isentropic or adiabatic compressibility  $\beta_S$  (Equation 3.3) can be defined from the isothermal one by the specific heat ratio  $\gamma$  defined later:

$$\beta_S = \frac{1}{\gamma} \beta_T = -\frac{1}{V} \left( \frac{\partial V_m}{\partial P} \right)_S$$

---

**Equation 3.3**

Table A.3 in the annex summarizes the different compressibility coefficients used for the modeling chapter at the main pressure conditions at 300 K temperature. Uncertainty varies from 0% in the low-density limit to about 3 to 4% at 350 bar and 10% at 1000 bar.

### 1.1.2 Enthalpy and entropy

On the one hand, using the first law of thermodynamics allows defining the enthalpy  $H$  using the internal energy  $U$  (Equation 3.4).

The entropy  $S$  of a system, on the other hand, is defined using the second law of thermodynamics as the heat  $Q$  which is absorbed divided by the absolute temperature (Equation 3.5)

$$H = U + P * V$$

---

**Equation 3.4**

$$dS = \frac{dQ}{T}$$

---

**Equation 3.5**

Table A.4 in annex summarizes the specific enthalpy  $h$  in kJ/ kg, and the specific entropy  $s$  in kJ/ (kg\*K) at the main temperature and pressure conditions used for the modeling part.

For the specific enthalpy, the uncertainties vary with pressure and temperature. In the region where the temperature is below 300 K, uncertainty is estimated to range from 1.2 kJ/ kg at low densities to about 5.0 kJ/ kg in the liquid phase. For all temperatures ranging between 300 and 500 K, the uncertainty is estimated to vary from 1 kJ/ kg at low pressure to about 15 kJ/ kg at the highest pressure.

For the specific entropy, the uncertainties vary with pressure and temperature as well. In the region where the temperature is below 300 K, uncertainty is estimated to range from 0.04 kJ/ (kg\*K) at low pressure to about 0.17 kJ/ (kg\*K) at higher pressure. For all temperatures between

300 and 500 K, the uncertainty is estimated to vary from 0.05 kJ/ (kg\*K) at low pressure to about one kJ/ (kg\*K) at the highest pressure.

### 1.1.3 Specific heat ratios

The specific heat ratio  $\gamma$  introduced in the compressibility factors (Equation 3.3) is defined by Equation 3.6:

$$\gamma = \frac{C_p}{C_v}$$

**Equation 3.6**

The two parameters  $c_p$  and  $c_v$  are the heat capacity at constant pressure and the heat capacity at constant volume, respectively, and are defined by Equation 3.7:

$$c_p = \left(\frac{\partial H}{\partial T}\right)_P; \quad c_v = \left(\frac{\partial U}{\partial T}\right)_V$$

**Equation 3.7**

Table A.3 in Annex summarizes the specific heat ratio at the main pressure conditions at 300 K. The uncertainty is estimated to vary from 0.02% in the low density limit to 3% at 350 bar and 8% at 1000 bar.

### 1.1.4 Ortho and para mixture:

For ideal gas mixtures of ortho and para hydrogen, the properties of the mixture can be determined using a mixing equation (Compilation of thermal properties of Hydrogen in its various isotopic and ortho and para modifications (Staats, 2008)):

$$\begin{cases} h_{mix} = x_p * h_p + x_o * h_o \\ s_{mix} = x_p * s_p + x_o * s_o - * (x_p * \ln x_p + x_o * \ln x_o) \end{cases}$$

**Equation 3.8**

Where  $p/o$  corresponds to para/ortho hydrogen,  $x_{p/o}$  the mass fraction,  $h_{p/o}$  the specific enthalpy and  $s_{p/o}$  the specific entropy and  $r$ , the individual gas constant in J/ (kg\*K), and the third term in the mixture entropy represents the entropy of mixing.

For normal hydrogen  $n$  where the composition is 75% ortho ( $x_o = 3/4$ ) and 25% para ( $x_p = 1/4$ ), Equation 3.8 is equivalent to Equation 3.9:

$$\begin{cases} h_o = \frac{4}{3} * h_n - \frac{1}{3} * h_p \\ s_o = \frac{4}{3} * s_n - \frac{1}{3} * s_p - 0.562335 * r \end{cases}$$

**Equation 3.9**

Which gives by replacing the definitions of  $h_o$  and  $s_o$  shown by Equation 3.9 on Equation 3.8:

$$\begin{cases} h_{mix} = (x_p - \frac{1}{3} * x_o) * h_p + \frac{4}{3} * x_o * h_n \\ s_{mix} = (x_p - \frac{1}{3} * x_o) * s_p + \frac{4}{3} * x_o (s_n - 0.562335 * r) - r * (x_p * \ln x_p + x_o * \ln x_o) \end{cases}$$

**Equation 3.10**

## 1.2 Hydrogen storage

The thermodynamic properties of hydrogen at different states of aggregation allow calculating the work associated with transformation. To investigate the possible transformation options, a review is performed on how hydrogen is stored and transported in vessels to enumerate the different hydrogen states  $t$ .

### 1.2.1 Compressed hydrogen

The simplest way to increase hydrogen density is compression. Compressed gas hydrogen (CGH) is stored at ambient temperature and in vessels at pressure way above the ambient pressure, in the order of 350 to 500 bar for gaseous transport, and in the order of 350 bar and 700 bar for on-board storage. Table 3.1 shows the density of normal hydrogen at ambient temperature and different pressure levels.

**Table 3.1:** Density of normal hydrogen

Pressure in bar	20	50	100	200	300	400	500
density of normal hydrogen in kg/ m <sup>3</sup>	1.59	3.92	7.62	14.39	20.40	25.79	30.65
density of normal hydrogen increase in%	-	145	94	89	42	26	19

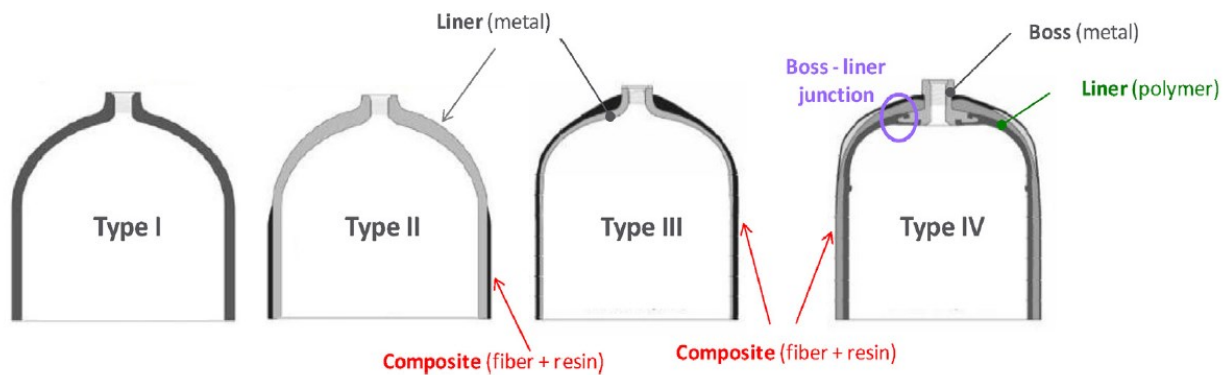
Calculated from Table A.3

It can be noticed that the density has a logarithmic increase, and the improvement related to compression decreases with the pressure level. In fact, high-pressure storage allows reducing the storage volume needed to fuel a FCEV for 500 km (Stolten, 2016) to 200 l on average, when a volume of 3145 l would have been needed for the same distance at a pressure of 20 bar. This volume saving decreases when the pressure reaches 500 bar as the volume is reduced by only 40 l for the same driving range.

After compressing hydrogen, the hydrogen has to be stored using an appropriate lightweight material, which can resist the higher pressure level and the effects of hydrogen embrittlement, as well as low hydrogen permeability (Léon, 2008). In fact, the high-pressure levels apply constraints concerning the component dimensioning, safety, material, and vessel choice. This choice differs on the specific application; For instance, depending on whether the vessels are used for bulk transportation, for stationary storage and vehicular application.

Thus, the hydrogen can be stored as CGH in four different types of pressure vessels, as shown in Figure 3.1, Type I, type II, type III, and type IV. The first one is the most mature technology and the most cost-effective, but can only resist to pressure below 500 bar and has a considerable weight (Barthelemy, Weber, & Barbier, 2017) due to use of only metallic parts. The type II tank is the best compromise between cost performance and weight performance and allows unlimited pressure levels due to the use of composite materials. Finally, type III and IV are at the early commercial stage for pressure levels up to 450 bar and 1000 bar, respectively (Barthelemy et al., 2017).

**Figure 3.1:** The four different type of pressure vessels (Barthelemy et al., 2017)



The most common materials included in the construction of the vessels are metallic, polymer, and composite parts. The metallic parts, which are in direct contact with hydrogen, can suffer from degradation due to the hydrogen embrittlement (Furtado & Barbier, 2014). The composite parts of type II, III, and IV can be subject to damage accumulation due to the pressure loads and accidental environment impact and accidents, which can lead to fiber breaks and matrix cracking (Barthelemy et al., 2017). Finally, because of the small size of hydrogen molecules, the polymer parts of type IV are more exposed to permeation of gas molecules, which enhances the diffusion in the polymer matrix (Klopffer & Flaconnèche, 2001).

In addition to vessel problems, and despite the storage volume decrease, the storage using hydrogen of 30 kg/ m<sup>3</sup> density is still way below a density of conventional gasoline that ranges

between 720 and 770 kg/ m<sup>3</sup>. Thus, one solution can be to store hydrogen as another aggregate form.

### *1.2.2 Liquid hydrogen*

Liquid hydrogen is an alternative solution to CGH with higher density and purity, which increases the storage capacity and efficiency, but because of product loss via evaporation, it is used more as a transport option than a long-term storage option.

In order to manage the extreme temperature of 30 K, highly insulated vessels are used, mainly a dual one with spacer material between the two in order to minimize losses due to the different forms of heat transfer (Wolf, 2002). Thus, the interior part has a multilayer insulation, consisting of different metallic foil layers, which are separated by a glass fiber to reduce heat radiation. The air compromised between the two vessels is evacuated to create a vacuum, which reduces the thermal conductivity.

Nevertheless, heat transfer from the ambient air is inevitable, which causes the evaporation of hydrogen. This evaporation, known as boil-off losses, depends on the tank dimensions and causes an increase in pressure. Therefore, liquid containers are always equipped with valves to release pressure.

The evaporation problem can be dealt with by increasing the volume of the tanks to minimize the contact surface in comparison to the transported capacity. For instance, losses are in the order of 0.3% / day for a vacuum insulated 320,00 l tank in comparison of 5% / day for a 102 l cryogenic vehicular (Léon, 2008).

Another problem is the evaporation of the liquid during the loading and unloading process when filling the tanks due to the temperature difference between the inside and outside vessels consisting on three main types of losses. (1) Loss of heat input and the heat transfer from the ambient environment to the inside vessel; (2) Loss due to the filling volume, as a volume of hydrogen as gas has to be removed from the tank in order to allow the filling with liquid hydrogen; and (3) loss due to a pressure drop, which causes a decrease of the boiling temperature releasing more hydrogen.

Moreover, liquid hydrogen can be subject as well to another common problem consisting of hydrogen embrittlement that can be observed at low temperatures, especially around -100 °C. This change of mechanical vessel properties at low temperatures leads as well to expansion and contraction phenomena and brittleness (Barthelemy et al., 2017).

### *1.2.3 Liquid organic hydrogen carrier*

Another way to store hydrogen as an energy-carrying compound is to use hydrogen, not at its molecular form but rather bounded to a liquid organic hydrogen carrier LOHC via hydrogenation process (Luo, Campbell, Zakharov, & Liu, 2011). These consist of unsaturated organic compounds,

which can store hydrogen at ambient temperature and pressure conditions. Nowadays, possible LOHC include mainly decalin, carbazole derivatives, and dibenzyltoluene. These hydrogenated compounds have thermophysical properties close to those of diesel fuel, allowing it to be stored accordingly.

The feasibility of LOHC storage depends mainly on the choice of the liquid carrier. The main parameters considered when selecting the adequate hydrogen carrier are the gravimetric storage density, the boiling point, and the melting point.

The first parameter corresponds to the percentage of hydrogen mass in the hydrogen carrier compound that has to be optimized. On the one hand, higher gravimetric storage reduces the amount of material needed to store a certain amount of hydrogen. On the other hand, the hydrogen capacity is limited by the number of chemical bonds that the organic molecule can establish with the hydrogen atom.

Theoretically speaking, every unsaturated organic compound can be used to store hydrogen, but an ideal organic carrier compound should have a higher boiling point and a lower melting point to keep the liquid state of storage at all operating conditions.

Early-stage research investigated cycloalkanes as a possible hydrogen carrier as they showed a high gravimetric capacity up to 8 wt%, a high boiling point, and a low melting point. However, a dehydrogenation has to be performed at a temperature above 300° C (He, Pei, & Chen, 2015).

Other research later proposed the exploitation of industrially applied heat transfer fluids such as the isomeric mixture of dibenzyltoluene and benzyltoluene (Brückner et al., 2014; Preuster, Alekseev, & Wasserscheid, 2017; Teichmann, Arlt, Schlücker, & Wasserscheid, 2016) as these components offer high hydrogen storage without solidification but with unfavorable thermodynamics consisting of high reaction heat.

In the meantime, the research investigated the alteration as well of the LOHC composition to reduce the enthalpy of reaction and thus, increasing the efficiency of dehydrogenation. For instance, the presence of an N atom reduces the aromaticity, which reduces the temperature of dehydrogenation and, therefore, the enthalpy of reaction (Sotoodeh, Huber, & Smith, 2012). However, N-Ethylcarazole for instance, which has favorable thermodynamics making it a good LOHC candidate, has a high melting point, making it solid at ambient temperature and pressure conditions. Nonetheless, the melting point depression can be easily achieved by adding a solvent, but with the drawback of decreasing the storage capacity (Crabtree, 2008; Emel'yanenko et al., 2015).

Taking into consideration as well the relatively low environmental impact and low operating costs, N-Ethylcarazole is taken as a LOHC candidate. Moreover, as discussed before, high volumetric and gravimetric hydrogen capacity is still achievable through binary mixtures (Stark et al., 2016).

### I.3 Hydrogen transformation work

The three ways of storing hydrogen, as CGH, LH, and LOHC, offer three different associated transformation work to estimate. The first one concerns compression work and has been calculated based on the work of a multistage compressor. The liquefaction work is done by calculating the ideal work associated with a literature review on different liquefaction processes. Finally, de- and hydrogenation work has been simulated using ASPEN as the process is still in its early research stage.

#### I.3.1 Ideal work review

When hydrogen is used in a gaseous form, it usually has to be compressed to elevated pressure, a process that requires work to be done on the gas. This work calculation can be simplified, considering that there is no heat exchange between the compressor and the environment and that the process is reversible (isentropic process).

The work  $W$  required to increase the pressure  $P$  of a gas of volume  $V$ , from a state  $t$  to a state  $t'$  is defined by Equation 3.11:

$$W = \int_{V_{t'}}^{V_t} P \cdot dV$$

---

**Equation 3.11**

#### I.3.1.1 Isentropic and isothermal compression

Under isentropic conditions, an equation for ideal gases links the pressure to the volume of a gas using the specific heat ratio  $\gamma$ , as shown below in Equation 3.12:

$$\int P * V^\gamma \cdot dV = 0$$

---

**Equation 3.12**

The work to compress an inlet gas from  $P_{in}$  to an outlet pressure  $P_{out}$  ( $P_{in} < P_{out}$ ) is given then by integrating the work equation (Equation 3.11) between initial conditions and the outlet pressure, which gives the relation shown in Equation 3.13.

$$W_{\Delta S \rightarrow 0, ideal} = \frac{\gamma}{\gamma - 1} * P_{in} * V_{in} * \left[ \left( \frac{P_{out}}{P_{in}} \right)^{\frac{\gamma-1}{\gamma}} - 1 \right]$$

---

**Equation 3.13**

Another simplification is to consider the whole process isothermal; this calculation is commonly used for the cost calculation and will be used only as a comparison.

The work of compression using the ideal gas model and real gas models and considering the temperature constant is using the same methodology for isentropic compression with  $\gamma = 1$ , which gives the expression shown in Equation 3.14.

$$W_{iso,ideal} = P_{in} * V_{in} * \ln\left(\frac{P_{out}}{P_{in}}\right)$$

**Equation 3.14**

---

### 1.3.1.2 Polytropic compression

In practical applications, the actual form of compression will usually be between the theoretical conditions of isothermal compression and isentropic compression (Jensen, Li, & Bjerrum, 2010), which represents a lower limit and an upper limit of the work of compression.

This actual work of compression is calculated using a reversible polytropic path, which links pressure to the volume using the polytropic index  $n$  (Equation 3.15). This index depends on the nature of the gas and the details of the compression process.

$$\int P * V^n . dV = 0$$

**Equation 3.15**

---

On the one hand, if the polytropic index is higher than the heat ratio, heat is supplied to the gas during compression. On the other hand, heat is released by the gas during compression. The work of polytropic compression is calculated like the isentropic process by replacing the specific heat ratio  $\gamma$  in Equation 3.13 by the polytropic index  $n$ :

$$W_p = \frac{n}{n-1} * P_{in} * V_{in} * \left[ \left( \frac{P_{out}}{P_{in}} \right)^{\frac{n-1}{n}} - 1 \right]$$

**Equation 3.16**

---

Since the compression of hydrogen is a polytropic process, the temperature of the gas is not constant and changes during the process from  $T_{in}$  to  $T_{out}$  according to Equation 3.17:

$$T_{out} = T_{in} * \left( \frac{P_{out}}{P_{in}} \right)^{(n-1)/n}$$

**Equation 3.17**

---

A direct consequence is that the final temperature increases with the pressure ratio  $\left( \frac{P_{out}}{P_{in}} \right)$ . Therefore, cooling during the compression process can reduce the actual work required. The case

of ideal isothermal compression can only be achieved if cooling is continuous throughout the compression process.

### 1.3.1.3 Ideal liquefaction work

Transforming a quantity of hydrogen from a gas at ambient temperature and pressure  $P_{in}$  to a saturated liquid requires work input. This work input is used to extract entropy from the low-temperature hydrogen and rejects it at ambient temperature (Staats, 2008).

The specific ideal work  $\dot{w}_{ideal}$  is defined using the first Law of thermodynamics,, as shown in Equation 3.18:

$$\dot{w}_{ideal,l} = \frac{Q_H - Q_L}{m}$$

**Equation 3.18**

The two parameters  $Q_L$  and  $Q_H$  expressed in Equation 3.19 represent, respectively, the quantity of heat removed expressed by the first law of thermodynamics and the isothermal heat rejection expressed by the second law.

$$\left\{ \begin{array}{l} -\frac{Q_L}{m} = h_f - h_i \\ \frac{Q_H}{m} = -T_i * (s_f - s_i) \end{array} \right.$$

**Equation 3.19**

The amount of work required by a reversible cycle to bring 25% para hydrogen from the starting conditions of 300 K and  $P_i$ , to the final saturated liquid state of 1 bar and an equilibrium of 99.8% para hydrogen concentration (at a temperature of 20.268 K) can be calculated from the mixture equations expressed in Equation 3.10.

The final conditions of the hydrogen at 99.8% para hydrogen concentration applies that Equation 3.10 can be re-written as expressed in Equation 3.20.

$$\left\{ \begin{array}{l} h_{mix,f} = \frac{2.992}{3} * h_{p,f} + \frac{0.008}{3} h_{n,f} \\ s_{mix,f} = \frac{2.992}{3} * s_{p,f} + \frac{0.008}{3} (s_{n,f} - 0.562335 * r) + 0.0144 * r \end{array} \right.$$

**Equation 3.20**

At initial conditions, hydrogen is at 25% para hydrogen known as normal hydrogen with enthalpy  $h_{n,i}$  and entropy  $s_{n,i}$ . Thus, the work of conversion with para and ortho conversion in kWh/kg can be expressed using Equation 3.21.

$$\dot{W}_{ideal,l} = \frac{h_{mix,f} - h_{n,i} - T_i * (s_{mix,f} - s_{n,i})}{3600}$$

**Equation 3.21**

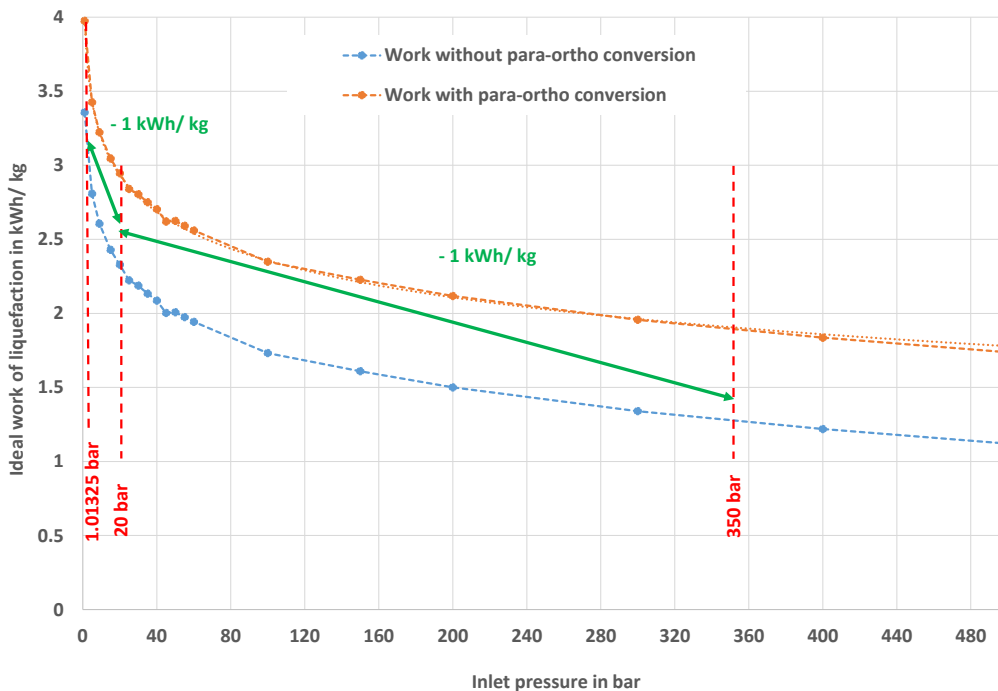
The values of entropy and enthalpy were taken at the conditions summarized in Table 3.2 using the values in Annex (Table A.4 and Table A.5).

**Table 3.2:** Temperature and pressure conditions for entropy and enthalpy calculation

Entropy/Enthalpy index	Para hydrogen concentration	Temperature	Pressure
<i>n, i</i>	Normal (25%)	300 K	$P_i$
<i>n, f</i>	Normal (25%)	20.268 K	Atmospheric
<i>p, f</i>	Para (99.8%)	20.268 K	Atmospheric

Figure 3.2 shows the specific ideal work of liquefaction of hydrogen in kWh/ kg with and without para hydrogen conversion. This work is calculated for different inlet gas pressure level, but for the same outlet saturated pressure and the same temperature.

**Figure 3.2:** Ideal work of liquefaction with and without para and ortho conversion



The results show that the ideal work taking into account para and ortho conversion can be modeled as a power function of the inlet pressure with an R-squared of 99.7%, as shown in Equation 3.22:

$$\dot{w}_{ideal,l} = -0.359 * \ln(P_i) + 4.0102$$

**Equation 3.22**

---

The results display as well that pre-compression of the feed-in hydrogen can reduce the work of liquefaction. For instance, a pre-compression to 20 bar before the liquefaction process, can reduce the specific liquefaction work by 1 kWh/ kg.

This specific liquefaction work can be reduced even further if the pre-compression is increased. For instance, the same specific work reduction of 1 kWh/ kg is achieved by pre-compressing hydrogen to 350 bar instead of 20 bar (green arrow in Figure 3.2).

Taking that into account, the majority of liquefaction processes benefit from a pre-compression ranging between 20 and 60 bar (Table A.7 in annex).

### 1.3.2 Multistage compression

A multistage compression of  $N$  stages is often used to cool the gas between the compression stages, using an intercooler and reducing, therefore, the work. This type of compressor was chosen and compared at different stages  $N$ , and one model was kept for the system compression work.

The polytropic compression is used for each stage  $j \in [2, N]$  using Equation 3.16:

$$W_{p,j} = \frac{n}{n-1} * P_{in,j} * V_{in,j} * \left[ r_j^{\frac{n-1}{n}} - 1 \right]$$

**Equation 3.23**

---

With the pressure ratio at each stage defined by  $r_j = \left( \frac{P_{out,j}}{P_{in,j}} \right)$

For this case study, the intercooling is considered perfect, meaning that the intermediate pressure  $P_{i,j}$  is constant (Equation 3.24), and that the temperature of the gas is reduced to the initial temperature after each compression stage.

$$\begin{cases} P_{in,j+1} = P_{out,j} = P_{i,j} \\ P_{in,j} * V_{in,j} = P_{in,j+1} * V_{in,j+1} \end{cases} \quad \text{with } j \in [1, N - 1]$$

**Equation 3.24**

The total work can be written then, as a sum of the work at each stage (Equation 3.23), as defined in Equation 3.25:

$$W_{p,N} = \sum_j^{N-2} \frac{n}{n-1} * P_{in,j} * V_{in,j} * \left[ \left( \frac{P_{i,j}}{P_{in,j}} \right)^{\frac{n-1}{n}} + \left( \frac{P_{out,j+2}}{P_{i,j}} \right)^{\frac{n-1}{n}} - 2 \right]$$

**Equation 3.25**

The total work function is minimal if the intercooling at each stage is minimal. Thus applies, the derivative of Equation 3.25 with respect to  $P_{i,j}$  is equal to 0:

$$\frac{dW_{p,j}}{dP_{i,j}} = \sum_j^{N-2} \left[ \left( \frac{P_{i,j}}{P_{in,j}} \right)^{\frac{n-1}{n}} * \frac{1}{P_{i,j}} - \left( \frac{P_{out,j+2}}{P_{i,j}} \right)^{\frac{n-1}{n}} * \frac{1}{P_{i,j}} \right] = 0$$

**Equation 3.26**

The simplification of Equation 3.26 applies the equality at each inter-stage expressed by Equation 3.27.

$$r_j^2 = r_{j+1} * r_{j-1}$$

**Equation 3.27**

The total work can be further simplified by replacing the intermediate pressure with the inlet and outlet pressure. In fact, the outlet pressure at the final stage is the outlet pressure of the compressor  $P_{out,N} = P_{out}$ , and the inlet pressure at the first stage is the inlet pressure of the compressor  $P_{in,1} = P_{in}$ .

Finally, the total specific compressor work  $\dot{w}_{p,N}$  needed to compress a kilogram of hydrogen can be given in kWh/ kg using Equation 3.28 and the specific volume  $\vartheta_{in}$  of hydrogen, which depends on the inlet pressure:

$$\dot{w}_{p,N}(P_{in}, P_{out}) = \frac{N}{36} * \frac{n}{n-1} * \vartheta_{in} * P_{in} * \left[ r_N^{\frac{n-1}{n}} - 1 \right]$$

**Equation 3.28**

Where the quotient  $\frac{1}{36}$  comes from unit conversion from J/ kg to kWh/ kg, and  $N$  is the number of stage of compression and  $r_N$  is the compression ratio defined by Equation 3.29.

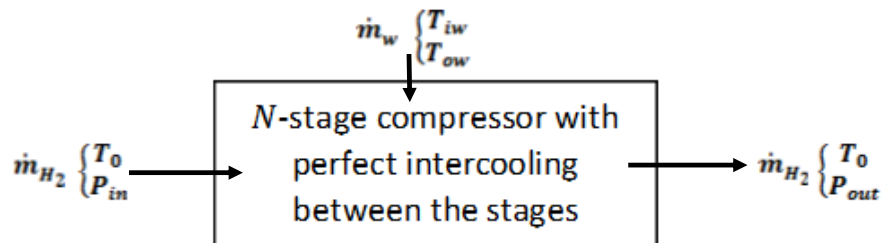
$$r_N = \sqrt[N]{\left(\frac{P_{out}}{P_{in}}\right)}$$

**Equation 3.29**

### 1.3.2.1 System work

The specific compressor work  $\dot{w}_{p,N}$  is used to deduce the total compressor system work  $\dot{w}_s$  using the different efficiencies, including the polytropic one, the mechanical one, and the electric one. For that, hydrogen is compressed from  $P_{in}$  at ambient temperature  $T_0$  to an output pressure  $P_{out}$ . A water flow  $\dot{m}_w$  is used to cool down the compressor; the water temperature varies from  $T_{iw}$  to  $T_{ow}$ , as shown in Figure 3.3.

**Figure 3.3:** Compressor system inputs and outputs



First, the polytropic exponent  $n$  is calculated using the specific heat ratio  $\gamma$  and polytropic efficiency  $\eta_p$  (Ozsaban, Midilli, & Dincer, 2011):

$$\frac{n}{n-1} = \frac{\gamma}{\gamma-1} \eta_p$$

**Equation 3.30**

The actual specific work of the compression stage is then deducted from the specific polytropic work of compression stage (Equation 3.28) and polytropic efficiency  $\eta_p$  (Brown, 1997) as expressed in Equation 3.31.

$$\dot{w}_{aw} = \frac{\dot{w}_{p,N}}{\eta_p}$$

**Equation 3.31**

The specific mechanical transmitted work to the compressor axis  $\dot{w}_{mw}$  is calculated using the mechanical efficiency  $\eta_{mc}$ . When the overall specific system work  $\dot{w}_s$  transmitted to the electric motor axis is deduced using the electric motor efficiency  $\eta_e$ :

$$\dot{w}_{mw} = \frac{\dot{w}_{aw}}{\eta_{mc}}; \quad \dot{w}_c(P_{in}, P_{out}) = \frac{\dot{w}_{mw}}{\eta_e}$$

**Equation 3.32**

### 1.3.2.2 System cooling requirement

The required volume flow of cooling water  $\dot{V}_w$  in liter/ day needed to reduce the temperature of hydrogen gas between the stages is deduced from the specific cooling work  $\dot{w}_{cl}$  in kWh/ kg and expressed by Equation 3.33:

$$\dot{m}_{H_2} * \dot{w}_{cl} = Cp_w * (T_{wo} - T_{wi}) * \dot{V}_w * \rho_w$$

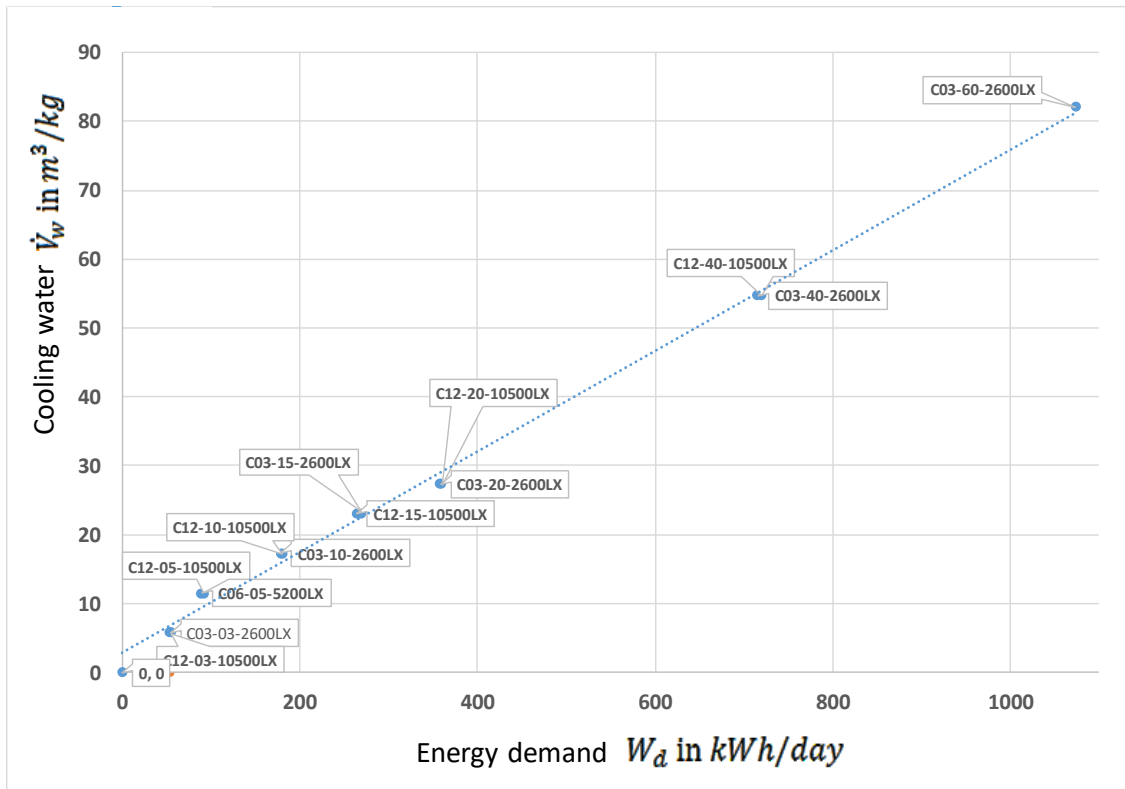
**Equation 3.33**

Where  $\dot{m}_{H_2}$  is the compressed hydrogen rate in kg/ day,  $Cp_w$  is the heat capacity at the average temperature  $\frac{T_{wo}+T_{wi}}{2}$  in kWh/ (kg K), and  $\rho_w$  water density in kg/liter

A literature review was done on commercial compressors to deduce the cooling water requirement as a function of electricity.

Figure 3.4 shows the trend line with the data (Hydro-Pac, 2007, 2008; L&W, 2016a, 2016b) mentioning the hydrogen temperature or cooling water requirements.

**Figure 3.4:** Daily cooling water requirements for industrial compressors ( $CF_c = 1$ )



(Hydro-Pac, 2007, 2008; L&W, 2016a, 2016b)

Figure 3.4 shows that the daily cooling water requirements  $\dot{V}_w$  in  $m^3/\text{day}$  can be expressed as a linear function of daily energy demand by the compressor  $W_d$  in  $\text{kWh}/\text{day}$  and the compressor capacity factor  $CF_c$ :

$$\dot{V}_w = 0.0731 * \frac{W_d}{CF_c} + 2.795$$

**Equation 3.34**

Which allows expressing the annual water requirement  $\dot{V}_{y_w}$  in  $m^3/\text{day}$  as a function of the annual energy consumed  $W_y$  in  $\text{kWh}/\text{year}$ .

$$\dot{V}_{y_w} \approx 0.0731 * \frac{W_y}{CF_c}$$

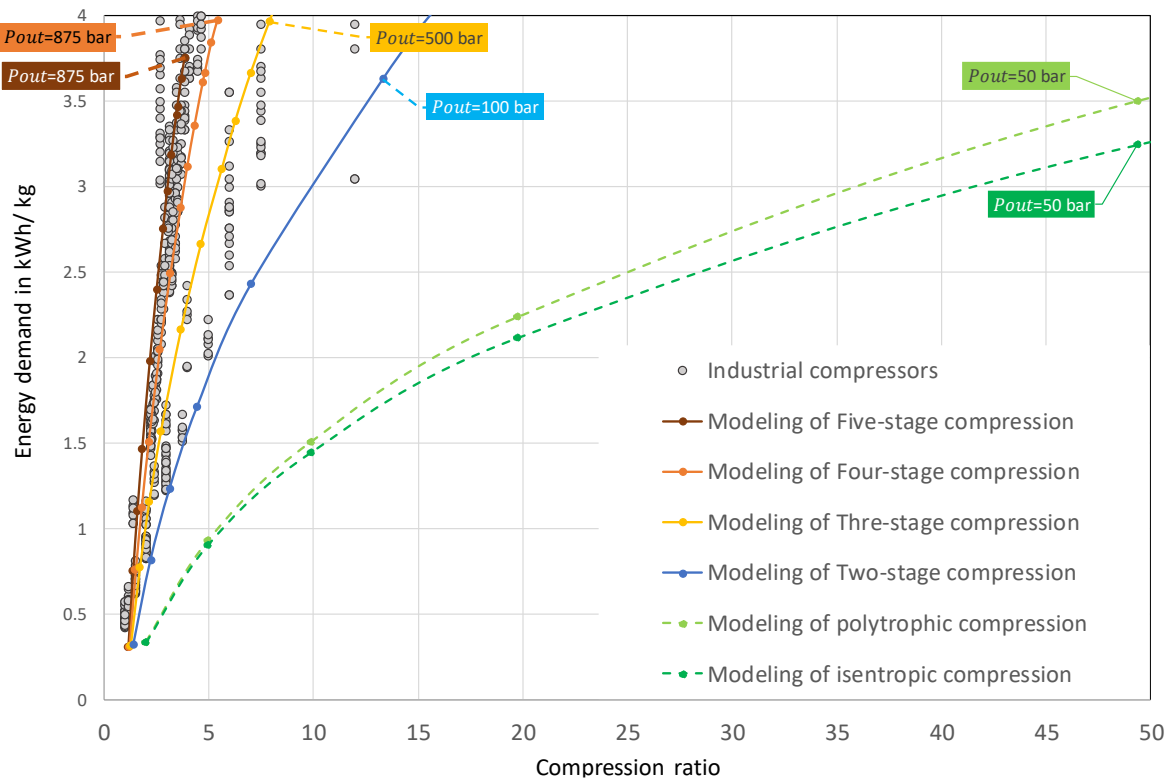
**Equation 3.35**

### 1.3.2.3 Conclusion

The work of a multi-stage compressor system (Equation 3.32) with  $N = [2,3,4,5]$ , based on the polytropic work at every single stage and perfect intercooling, was calculated and shown in Figure 3.5. The compressor isentropic and polytropic system works were modeled as well and compared to a data of 875 industrial compressors (Globalspec, 2016; Hydro-Pac, 2007, 2008; Johnsoncontrols, 2015; L&W, 2016a, 2016b; RIX, 2010).

The work is shown as a function of the compression ratio. For each compressor model, the maximum output pressure, which can be reached with compression energy below 4 kWh/ kg, is indicated.

**Figure 3.5:** Modeling of the compressor energy system



(Globalspec, 2016; Hydro-Pac, 2007, 2008; Johnsoncontrols, 2015; L&W, 2016a, 2016b; RIX, 2010) and own calculations

The results show that the five-stage and the four-stage compressor allow reaching the maximum output pressure of  $P_{out} = 875 \text{ bar}$ , compared to only 100 bar in case of two-stage compression and 50 bar in case of one stage polytropic and isentropic compression. Moreover, the energy modeling results for four and five stages match the energy output of the industrial compressors.

Therefore, these two compressors are considered for modeling compression energy; and the five-stage, with a lower energy requirement, was kept for the cost calculation functions.

### 1.3.3 Liquefaction work

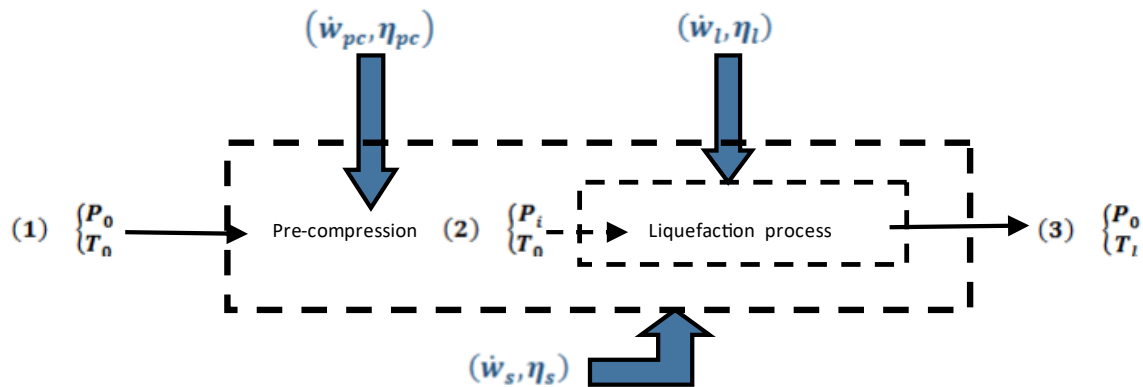
To allow comparison of the different liquefaction plants and processes, first, the feed-in steam and liquefied hydrogen have to be brought to the same temperature-pressure conditions.

#### 1.3.3.1 Liquefaction system work

For this comparison, the input hydrogen gas was chosen at the atmospheric pressure  $P_0$  and temperature  $T_0$  of 300 K. For the output liquefied hydrogen, it was at a saturated state temperature  $T_l$  of atmospheric pressure  $P_0$  (Figure 3.6).

For the process that uses compressed hydrogen as a feed-in gas, a pre-compression is needed to bring the hydrogen from atmospheric pressure to the pressure needed  $P_i$  (Figure 3.6). The total work is then calculated from the liquefaction process and a pre-compression process (David O Berstad, Stang, & Nekså, 2009)

**Figure 3.6:** The liquefaction process



Using the first and the second law over the system, the specific system work  $\dot{w}_s$  can be written, as shown in Equation 3.36.

$$\dot{w}_s = T_1 * (s_1 - s_3) - (h_1 - h_3)$$

**Equation 3.36**

The efficiency and the exergy of the whole processes  $\eta_s$  from (1) to (3) is defined as the ratio of the ideal specific work of the system  $\dot{w}_{ideal,s}$  and the net amount of specific work consumed in the  $\dot{w}_s$ :

$$\eta_s = \frac{\dot{W}_{ideal,S}}{\dot{W}_s}$$

**Equation 3.37**

---

The same efficiency definitions of exergy can be given for the pre-compression and the liquefaction processes alone:

$$\dot{W}_{p,N} = T_1 * (s_1 - s_2) - (h_1 - h_2) = \dot{W}_c * \eta_c$$

**Equation 3.38**

---

$$\dot{W}_{ideal,l} = T_1 * (s_2 - s_3) - (h_2 - h_3) = \dot{W}_l * \eta_l$$

**Equation 3.39**

---

Where  $\dot{W}_{p,N}$  represents the specific ideal compressor work defined in Equation 23 and  $\dot{W}_{ideal,l}$  the specific ideal work of liquefaction defined in Equation 3.20.

Summing Equation 3.38 and Equation 3.39 gives:

$$\dot{W}_{ideal,S} = \dot{W}_{p,N} + \dot{W}_{ideal,l} = \dot{W}_c * \eta_c + \dot{W}_l * \eta_l = \eta_s * \dot{W}_s$$

**Equation 3.40**

---

This allows us to write the system efficiency using the specific ideal work of liquefaction and compression, as shown in Equation 3.41:

$$\eta_s = \eta_c \frac{\dot{W}_{p,N}}{\dot{W}_{p,N} + \dot{W}_l} + \eta_l \frac{\dot{W}_l}{\dot{W}_{p,N} + \dot{W}_l}$$

**Equation 3.41**

---

### 1.3.3.2 State of the art of different liquefaction plants and processes:

Among the operating liquefaction companies, Praxair, for instance, has five hydrogen liquefaction plants in the US with production rates between 6 and 35 TPD. Typical electricity demand lies between 12.5 and 15.2 kWh/kg (Drnevich, 2003). Air Products has four hydrogen liquefaction plants capable of producing between 30 and 35 TPD in operation in North America (Krasae-in, 2013). Besides, two plants of 5 TPD capacity are located in the Netherlands and the USA with an optimum demand in the US of about 10.2 kWh/ kg (Drnevich, 2003)

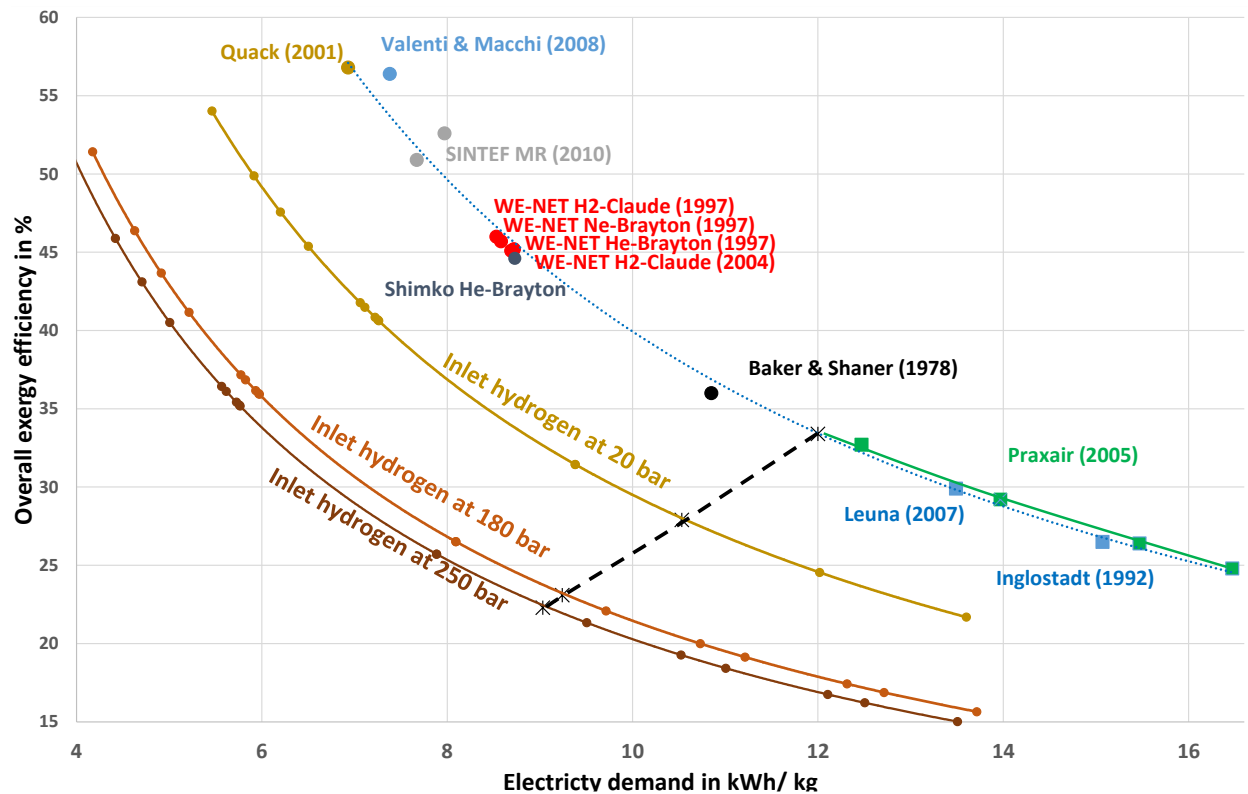
Among others, Air Liquide has a plant in France and one in Canada, and both have capacities of about 10 TPD (Krasae-in, 2013), and Linde, has two plants in Germany (David O. Berstad, Stang, & Nekså, 2010) of 4.4 and 5 TPD production capacities.

Besides these operating plants, many studies of liquefaction processes can be found in literature, their technical data (David O. Berstad et al., 2010; Bracha, Lorenz, Patzelt, & Wanner, 1994; Fukano, Fitzi, LÖHLEIN, & Vinage, 2007; Krasae-in, 2013; Kuendig, Loehlein, Kramer, & Huijsmans, 2006; Klaus Ohlig & Decker, 2000; K Ohlig & Decker, 2014) are summarized in annex (Table A.7).

To allow comparison between the different liquefaction plants and processes, the inlet and outlet temperature and pressure are brought to the same conditions. That corresponds to atmospheric pressure and ambient temperature at the feed-in conditions, and the saturated liquid for the hydrogen product. The missing plants and process data were calculated using Equation 3.22, Equation 3.28, Equation 3.39, Equation 3.40, and Equation 3.41, along with the results and shown in Table A.7 in the annex.

The efficiency results as a function of specific power are shown in Figure 3.7. The points corresponding to the liquefaction plants and processes studied in Table A.7 are brought to the same input pressure corresponding to atmospheric pressure. The results are then calculated for different inlet pressure using Equation 3.40 and Equation 3.41, to conclude to the new system efficiencies.

**Figure 3.7:** Overall exergy efficiency and specific power of current and studied plants and processes



The different graph correspond to different hydrogen feed in pressure ranging from atmospheric pressure (in dash) to 250 bar.

The calculation are based on existing and experimental liquefaction plants calculated in Table A.8 and compared to Table A.7, and brought to the same initial conditions

The results shown in Figure 3.7 confirm the impact of the inlet hydrogen pressure on the liquefaction process when calculating the ideal work. In fact, the specific work is reduced by 1.5 kWh/ kg when choosing an inlet pressure of 20 bar. The work reduction is not linear with the inlet pressure increase. In fact, when the hydrogen is compressed with an additional 160 bar, the reduction of work still constant and equal to 1.5 kWh/ kg.

Concerning the overall exergy efficiency, higher efficiency comes from the work of compression (76.9%). So, using pre-compressed hydrogen reduces the overall efficiency.

For the cost calculation, the specific liquefaction work is chosen lower than the Leuna liquefaction plant and the minimum of Paraxaire's future status. It is represented in Figure 3.7 by the dashed black line. Which gives a work of 12 kWh/ kg at atmospheric pressure, 10.53 kWh/ kg at 20 bar,

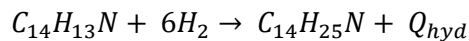
and 9.24 kWh/ kg at 180 bar (the results of the specific work at different pressure inlet used for the model calculation are available in the annex in Table A.8 and Table A.9).

### 1.3.4 De- and hydrogenation work

Although, the mixture of the carbazole-based compounds would be more suitable for future applications, the significant benefits linked to the use of N-Ethylcarbazole, led to choose this component as a LOHC candidate for transporting and storing hydrogen. In fact, this N-Alkylcarbazole has a high gravimetric and volumetric capacity, allowing it to store up to 5.8 wt% hydrogen. Moreover, it has as well a high reversibility process, and its degradation for hydrogenation cycling is marginal due to its high stability over time (Yang, Han, Ni, Wu, & Cheng, 2012). The only drawback is the melting point temperature that is reached at 342.25 K. It is why the dehydrogenation process was restricted to 90% discharging, which leads to an actual hydrogen storage capacity of 5.2 wt%.

#### 1.3.4.1 De- and hydrogenation reaction

The N-Ethylcarbazole hydrogenation reaction is exothermic, which releases heat  $Q_{hyd}$  equivalent to 53 kJ/ mol (Preuster et al., 2017) as expressed using Equation 3.42.

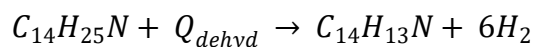


**Equation 3.42**

This reaction is heterogenic as well because it involves three phases, a gaseous one associated with hydrogen, a liquid one associated with the use of N-Ethylcarbazole as storing component and a solid phase linked to the use of the catalyst. Therefore, the hydrogen has first to reach the gas-liquid interface passing through the gas film before getting dissolved into the liquid and reaching the catalyst surface. It is why hydrogen solubility is a crucial parameter in the process evaluation, as the reaction cannot take place without hydrogen in the liquid phase.

The N-Ethylcarbazole reaction is subject to a volume reduction. Therefore, an increase of hydrogen inlet pressure shifts the reaction to product direction and accelerates the reaction by increasing the solubility. Thus, the optimum reaction condition (Wan, An, Xu, & Kong, 2012) was identified to be under a temperature of 413 K, and a pressure of 60 bar, and the use of  $Ru/Al_2O_3$  as a catalyst at 0.2 g per one gram of N-Ethylcarbazole used because the reaction kinetic is favored by an increase of the temperature up to 493 K.

In the other hand, the N-Ethylcarbazole dehydrogenation reaction is endothermic at a high temperature and lower pressure that needs heat  $Q_{dehyd}$  equivalent to 53 kJ/ mol (Preuster et al., 2017) of stored hydrogen as expressed using Equation 3.43.



**Equation 3.43**

As for the hydrogenation process, the reaction is heterogenic and includes molecular diffusion from the liquid phase to the solid phase of the catalyst, an absorption of the reactant, a surface reaction, and finally a product desorption from the catalyst surface. However, only the superficial reaction is considered in the kinetic model as it is the rate-determining step (Becatti, Dalmazzone, & Paricaud, 2018).

#### 1.3.4.2 De- and hydrogenation simulation

De- and hydrogenation simulation were carried out using Aspen Plus software. For that, first, the physical properties of the hydrogenated and dehydrogenated components were estimated (Marrero & Gani, 2001) as the properties of the recently discovered pure components such as Dodecahydro-N-Ethylcarbazole and N-Ethylcarbazole are not yet available. Thus, thermodynamic properties are calculated using an equation of state because direct measurements are not always possible because of the cost and time analysis.

Two thermodynamic property models widely industrially used, RK-SOAVE and RK-ASPEN, are based on the standard Save-Redlich Kwong equation of state (Soave, Gamba, & Pellegrini, 2010). For that, first, the state properties of a non-mixture component is expressed using van der Waals theory (Dzyaloshinskii, Lifshitz, Pitaevskii, & Priestley, 1992), as shown in Equation 3.44.

$$p = \frac{R * T}{V_m - b} + \frac{a}{V * (V_m + b)}$$

**Equation 3.44**

The parameters  $a$  and  $b$  correspond, respectively, to the attractive term and the repulsive term. The first one considers interactions between particles, while the second one considers the volume of the particles. These two parameters, when applied to mixtures, are calculated, linking each compound's constant through a mixture rule using the classical van der Waals mixing rule (Kwak & Mansoori, 1986) in case of RK-SOAVE for instance (Becatti et al., 2018).

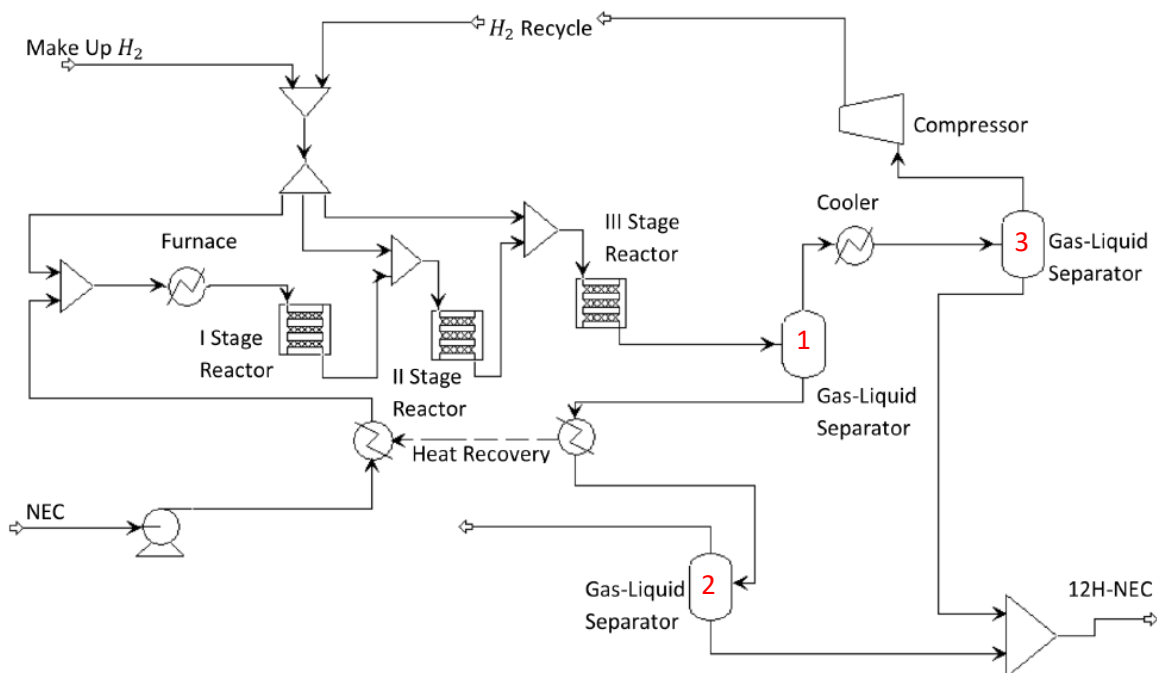
##### 1.3.4.2.1 Hydrogenation simulation

The design of the hydrogenation process plant developed by Argonne National Laboratory (Ahluwalia et al., 2011) was implemented using RK-ASPEN thermodynamic property method that has been proved to be the most appropriate for this case study (Becatti et al., 2018).

The hydrogenation was designed as a three-stage process, as shown in Figure 3.8; As introduced before, the hydrogenation reaction benefits from the increase of hydrogen pressure and feedstock. The hydrogen added absorbs the heat and allows to maintain the temperature within

the range of maximum reaction rates. Moreover, the excess of hydrogen can be subsequently separated from the products at the end of the process, recompressed and recycled. In parallel, the increase of the pressure fixed at the optimal value of 60 bar, further shifts the equilibrium reaction to the product.

**Figure 3.8:** Diagram of the hydrogenation process



Source: (Becatti et al., 2018)

NEC: N-Ethylcarbazole

12H-NEC: Dodecahydro-N-Ethylcarbazole

The hydrogen concentration in the liquid phase after the hydrogenation process at the exit of the third reactor is high, reaching a concentration of 21% mol. Thus, the surplus of hydrogen and Dodecahydro-N-Ethylcarbazole are separated using three adiabatic flashes at different pressure and temperature conditions.

A first flash **1** at high temperature and pressure of 50 bar allows to recover most of the hydrogen. Further separation is necessary since hydrogen remains dissolved within Dodecahydro-N-Ethylcarbazole. This flash **2** is carried out at nearly ambient pressure of 1 bar and effectuated to recuperate the excess of hydrogen dissolved at 10.5% mol. Finally, further separation is necessary since hydrogen was found out to be saturated with Dodecahydro-N-Ethylcarbazole using flash **3** at the pressure of 40 bar but at a lower temperature of 288.15 K to avoid additional

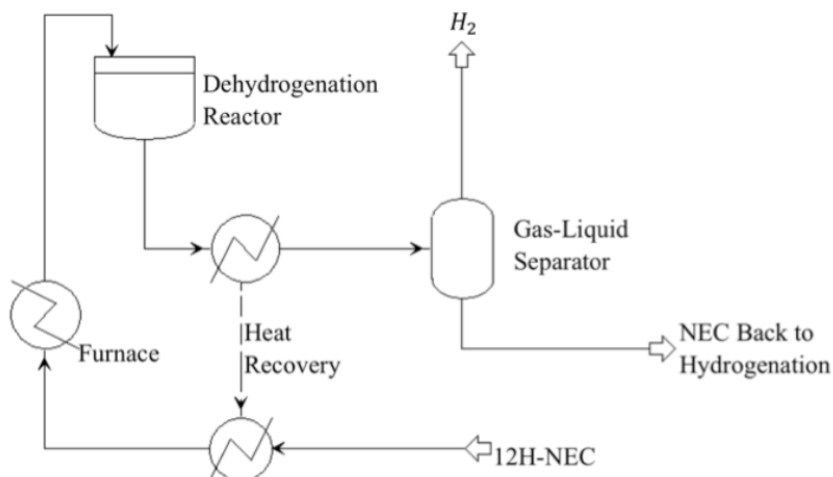
recompression energy costs. During the separation process, it is also possible to recover heat from hydrogen cooling before its compression at 3, and by preheating the reactants using Dodecahydro-N-Ethylcarbazole at 2.

#### 1.3.4.2.2 Dehydrogenation simulation

The dehydrogenation process requires pressure values close to ambient pressure. Thus, the simulation is less affected by the property method, and both RK-ASPEN and RK-SOAVE give similar results (Becatti et al., 2018).

The reaction of dehydrogenation is performed by using heat provided from the furnace, as shown in Figure 3.9. Heat recovery is performed as well before the separation using a single adiabatic flash. The endothermic reaction is then carried out for dehydrogenation and stopped at 90% of Dodecahydro-N-Ethylcarbazole conversion to maintain the liquid state of the carrier, which will be recycled for hydrogenation process use.

**Figure 3.9:** Diagram of the dehydrogenation process



Source: (Becatti et al., 2018)

NEC: N-Ethylcarbazole

12H-NEC: Dodecahydro-N-Ethylcarbazole

The dehydrogenation reaction requires pressure and temperature values close to the ambient conditions. Thus, hydrogen can be easily separated from the liquid carrier using only one single adiabatic flash.

#### 1.3.4.2.3 Simulation results

The hydrogenation process used a compressed gas at 60 bar, and the total work of hydrogenation, including the compression work, as summed up in Table 3.3.

**Table 3.3:** Hydrogenation energy demand (Becatti et al., 2018)

<b>Compression</b>	2.22	kWh/ kg
<b>NEC pump</b>	0.03	kWh/ kg
<b>Furnace</b>	3.56	kWh/ kg

For the dehydrogenation process, it is performed and produced at atmospheric pressure, and the results are shown in Table 3.4.

**Table 3.4:** Dehydrogenation energy demand (Becatti et al., 2018)

<b>Reactor</b>	0.1	kWh/ kg
<b>Furnace</b>	0.11	kWh/ kg

As the hydrogen is transported up to a pressure of 540 bar, the feed-in hydrogen pressure is above 60 bar, which results in lower energy demand. For that, the new energy system demand is deduced from the total energy of de- and hydrogenation for a feed-in hydrogen pressure at 60 bar, and the work of the transport compression, using the same methodology for liquefaction system work (chapter I.3.3.1 page 92). The results are shown in Table 3.5

**Table 3.5:** Total work of de- and hydrogenation as a function of the hydrogen feed-in pressure

<b>Input pressure in bar</b>	1.013	20	180	250	350	500	540
<b>Total work in kWh/ kg</b>	6.02	4.31	3.8	3.71	3.62	3.53	3.51

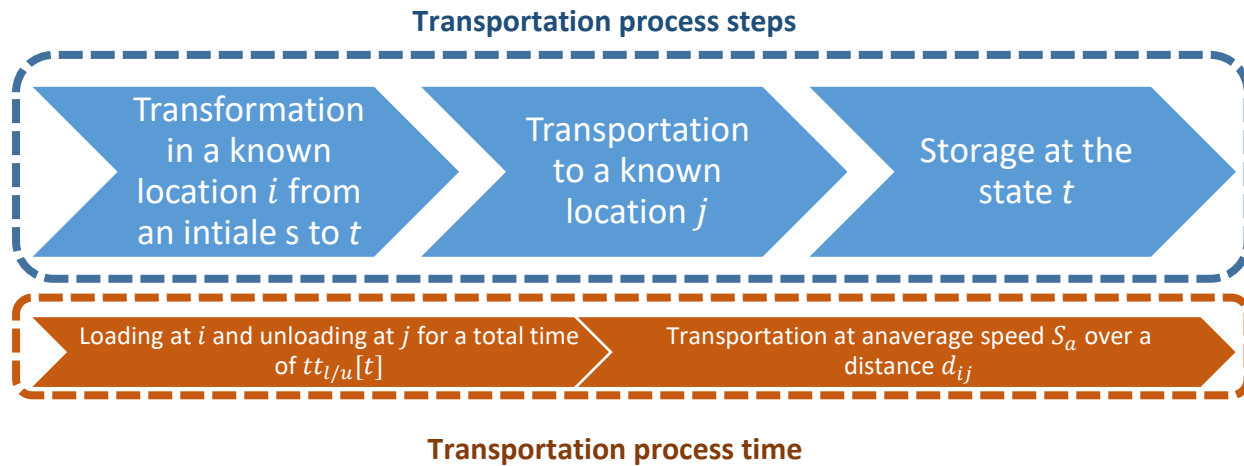
Calculated from Table A.9 in annex

#### I.4 Hydrogen truck transportation

The main steps to transport hydrogen using a truck via road transportation RTT is shown in Figure 2.1. The hydrogen is initially at a known location  $i$  and at an initial state of aggregation  $s$ . The hydrogen is then transformed to a new state of aggregation  $t$  using a corresponding system delivering a total specific work for transformation  $\dot{w}_s$ . If no transformation is needed, the hydrogen is transported at the same state of aggregation  $s = t$ .

The hydrogen results at the new state  $t$  are stored in different tube trailers, or tanks of a total net capacity  $m[t]$ , which depends on the hydrogen state of aggregation, and is afterward loaded to be transported by RTT to a location  $j$ .

**Figure 3.10:** Steps for hydrogen transportation via *RTT*



When transporting hydrogen to the site  $j$  over a distance  $d_{ij}$  at the average speed  $S_a$  from the storage site  $i$ , the truck is supposed to wait till it is unloaded adding a total loading and unloading time  $tt_{l/u}[t]$ , which depends on its hydrogen state of aggregation  $t$ .

The main technical parameters associated with the steps shown in Figure 2.1 are those associated with the transformation work, the storage in tube trailers and tanks, and the transportation using RTT.

The hydrogen is chosen to be transported using three different states of transport SoT, as compressed gas hydrogen CGH, as liquid hydrogen LH, or in a liquid organic hydrogen carrier LOHC.

#### 1.4.1 Hydrogen state of aggregation and storage

For CGH, the literature review showed that optimizing the overall hydrogen supply chain shifted the focus away from the transportation using compressed gas. This way of transporting hydrogen could be further optimized by investigating different pressure levels.

This is done by investigating a set of pressure levels instead of restraining the study to only one. The current CGH market and prospects give a range of five possible operation pressure level of 180, 250, 350, 500, and 540 bar, which could be used for RTT transportation.

The choice was made by investigating current operating CGH in the market, literature reviews and reports (Composites, 2006; Simbeck & Chang, 2002; Steward, Ramsden, Zuboy, & National Renewable Energy, 2008; Tamhankar, 2014) as summed up in annex (Table A.10).

As the study aims to build a scenario of hydrogen penetration by 2030 and 2050, the analysis uses as well the target set by the US DOE for the year 2020 to reach economic feasibility of a

filling pressure of 520 bar (Gerboni, 2016) along with other prospects (Hexagon, 2013; Zerhusen, 2013) shown in annex (Table A.10).

Table 2.1 summarized the different tube trailers, which will be used to store and transport hydrogen at different state of aggregation  $St$  defined by the corresponding state of transport SoT and the operating pressure  $Pt$ , along with the corresponding capacity  $m(St)$  and the total loading and unloading time  $tt_{l/u}(St)$ .

**Table 3.6:** Variable transport parameters for a different state of aggregation

State of transport $SoT$	CGH					LH	LOHC
Design pressure $Pt$ in bar	180	250	350	500	540	1.013	
Total net truck capacity $m(St)$ in kg	350	668	885	1100	1230	3600	1500
Loading and unloading time $tt_{l/u}^t$ in hours	2.5	2	1.5	1	1	3	1.5

Adjusted from (Table A.10)

Along with the state of aggregation used for storage and transportation, additional states are needed corresponding to the outlet state from the hydrogen production sites and the inlet state for the distribution sites.

At the production phase, the hydrogen is chosen at two different pressure levels. One, where the gas is at atmospheric pressure and ambient temperature. Another one, where the gas is pre-compressed to 20 bars when hydrogen production costs are taken into account.

For the distribution phase, the hydrogen is investigated at two different pressure levels corresponding to the fuel cell use condition and hydrogen dispensing condition. That corresponds to a pressure level of 700 bar and 875 bar consecutively.

The hydrogen needs to be dispensed at a pressure of 875 bar and temperature of 350 K to reach atmospheric pressure and a pressure of 700 bar at equilibrium in the fuel cell (Rivkin, Buttner, & Burgess, 2016).

#### 1.4.2 Transformation matrix

The system work  $\dot{w}_s$  is defined as the work needed to bring hydrogen from a state of aggregation  $St$  to another state  $St'$ .

This transformation work is equal to compression work (Equation 3.32) if the hydrogen is kept as a gas but only compressed from an initial pressure  $P_{in} = Pt$  to an outlet pressure  $P_{out} = Pt'$ , as shown in Equation 3.45.

$$\dot{w}_s(St, St') = \dot{w}_c(Pt, Pt')$$

**Equation 3.45**

If the hydrogen state is changed from a gas at pressure  $Pt$  to a saturated liquid at the atmospheric pressure, then the transformation work is equal to a liquefaction work at an inlet pressure  $P_{in} = Pt$  (Equation 3.32),, as shown in Equation 3.46.

$$\dot{w}_s(St, St') = \dot{w}_l(Pt)$$

**Equation 3.46**

Finally, the transformation work is equal to the total work of de- and hydrogenation, if the process transforms hydrogen from a gas at a pressure  $P_{in} = Pt$  to a liquid organic hydrogen carrier at atmospheric pressure, as shown in Equation 3.47.

$$\dot{w}_s(St, St') = \dot{w}_h(Pt)$$

**Equation 3.47**

If the energy state of  $St$  is higher than the one of  $St'$ , then the transformation releases energy, and in this configuration, the transformation work is taken equal to 0.

For the mathematical modeling and for the clarity of the equations, each index  $t [t']$  was chosen equal to a different state and was summarized in Table 3.7

**Table 3.7:** Different state of aggregation

Index $t [t']$	0	1	2	3	4	5	6	7	8	9	10
Pressure in bar	1.013	20	180	250	350	500	540	700	875	1.013	
Temperature in K	300								350	300	20.28
State of transport	CGH								LOHC		LH
Work	$\dot{w}_c$								$\dot{w}_h$		$\dot{w}_l$

The system transformation work  $\dot{w}_s(St, St')$  can be then written using only the index  $t$  and  $t'$ , and the work  $\dot{w}_s[t, t']$  can be summarized in one equation, as shown in Equation 3.48.

$$\begin{aligned}
\dot{w}_s[t, t'] &= \dot{w}_c[t, t'] \quad \text{if } (t, t') \in [0, 8]^2 \\
\dot{w}_s[t, t'] &= \dot{w}_{LOHC}[t] \quad \text{if } t' = 9 \\
\dot{w}_s[t, t'] &= \dot{w}_L[t] \quad \text{if } t' = 10 \\
\dot{w}_s[t, t'] &= 0 \quad \text{if } t > t'
\end{aligned}$$

**Equation 3.48**

Alike, the transport capacity  $m(St)$  and the total loading and unloading time  $tt_{l/u}(St)$  can be written as well using the index  $t$ :  $m[t]$  and  $tt_{l/u}[t]$ , respectively.

#### 1.4.3 Transportation parameters

The tube trailers of capacity  $m[t]$  used to store hydrogen at the state of aggregation  $St$  (Table 2.1) are used afterward to transport hydrogen. This maximum tube trailer capacity limits the transported capacity. Hence, an RTT can perform a certain number of roundtrips  $Nrt[t]$  to increase the transported hydrogen.

Each single RTT of capacity  $m[t]$  can perform only a maximum number of roundtrips  $Nrt_{pd,max}[t]$  over a period time of operation  $pd$ . So, to meet the hydrogen demand at a location  $j$  additional trucks are needed increasing the total trucks operating at the same time during  $pd$  to  $Nt_{pd}[t]$ .

Finally, each truck running for one trip is operated by a number of drivers  $Ndr[t]$  limited by the driver working hours  $Nwh$ .

The total costs are simulated annually when different technical parameters can be calculated daily. This means that time of operation  $pd$  can be chosen equal from one day to one year, which will impact the total costs as will be discussed in the modeling part.

##### 1.4.3.1 Technical parameters

A RTT is not available to be operated during the whole time  $pd$  as a capacity factor  $CF_{RTT}$  is introduced to deduce the total time of truck availability  $Av_{pd,RTT}$ , as shown in Equation 3.49.

$$Av_{pd,RTT} = CF_{RTT} * Th_{pd}$$

**Equation 3.49**

Where both times,  $Av_{RTT}$  and  $Th_{pd}$  are expressed in the number of hours during the period  $pd$ .

The maximum number of roundtrips  $Nrt_{pd,max}[t](i, j)$  over a period  $pd$  between two locations  $i$  and  $j$  is the floor ratio of the truck availability and the time duration of one transportation process (Figure 2.1),, as shown in Equation 3.50.

$$Nrt_{pd,max}[t](i,j) = \left\lceil \frac{Av_{pd,RTT}}{\frac{2 * d_{ij}}{S_a} + tt_{l/u}[t]} \right\rceil$$

**Equation 3.50**

The number of roundtrips of one truck  $Nrt_{pd}[t](i,j)$  per period  $pd$  is limited by  $Nrt_{pd,max}[t](i,j)$  and is equal to the ceil ratio between the total hydrogen transported flow during the period  $pd$  from a location  $i$  the location  $j$   $Xpd_{ij}$  per period and the RTT capacity,, as shown in Equation 3.51.

$$\begin{cases} Nrt_{pd}[t](i,j) = \left\lceil \frac{Xpd_{ij}}{m^t} \right\rceil & \text{if } Nrt_{pd}[t](i,j) < Nrt_{pd,max}[t](i,j) \\ Nrt_{pd}[t](i,j) = Nrt_{pd,max}[t](i,j) & \text{if } Nrt_{pd}[t](i,j) > Nrt_{pd,max}[t](i,j) \end{cases}$$

**Equation 3.51**

In case of the use of RTT at the same state of aggregation for transport, then the number of trucks needed  $Nt_{pd}[t](i,j)$  per period  $pd$  is defined as the ceil ratio between total hydrogen flow transported to the location  $j$   $d_j$  and the total transported capacity by one RTT during the period  $pd$ ,, as shown in Equation 3.52.

$$Nt_{pd}[t](i,j) = \left\lceil \frac{Xpd_{ij}}{m[t] * Nrt_{pd,max}[t](i,j)} \right\rceil$$

**Equation 3.52**

This allows defining the total number of roundtrips performed by all trucks  $TNrt_{pd}[t](i,j)$  per period  $pd$  between the two locations over a period  $pd$  expressed by Equation 3.53

$$TNrt_{pd}[t](i,j) = \left\lceil \frac{Xpd_{ij}}{m[t]} \right\rceil$$

**Equation 3.53**

Finally, for transporting hydrogen, each driver cannot exceed a maximum number of working hours  $Nwh$  defining the number of drivers  $Ndr[t](i,j)$  needed in the same time to operate one RTT over one trip distance  $d_{ij}$  by Equation 3.54.

$$Ndr[t](i, j) = \left\lceil \frac{\frac{d_{ij}}{S_a} + tt_{l/u}[t]}{Nwh} \right\rceil$$

**Equation 3.54**

**1.4.3.2 Daily and yearly technical parameters**

On the one hand, the cost is calculated annually, allowing to adjust the operation period  $pd$  to 365 days. On the other hand, hydrogen stored and transported can be optimized by calculating them every day by setting  $pd$  equal to 24 hours. This is why both values are used in the modeling chapter.

Table 3.8 summarizes the parameters listed in Equation 3.49, Equation 3.50, Equation 3.51, Equation 3.52, and Equation 3.54, expressed as daily and yearly parameters as a function of the daily and yearly flow and linked by Equation 3.55.

$$Xd_{ij} = Xy_{ij}/365$$

**Equation 3.55**

**Table 3.8:** Daily and yearly parameters

	Symbol	Value
Yearly hours	$Th_y$	8640
Daily hours	$Th_d$	24
Yearly transported flow	$Xy_{ij}$	$Xd_{ij}$
Daily transported flow	$Xd_{ij}$	Input
Yearly truck availability	$Av_{y,RTT}$	Equation
Daily truck availability	$Av_{d,RTT}$	3.49
Yearly maximum number of roundtrips	$Nrt_{y,max}[t](i, j)$	Equation
Daily maximum number of roundtrips	$Nrt_{d,max}[t](i, j)$	3.50
Number of roundtrips performed by one truck per year	$Nrt_y[t](i, j)$	Equation
Number of roundtrips performed by one truck per day	$Nrt_d[t](i, j)$	3.51
Number of trucks needed per year	$Nt_y[t](i, j)$	Equation
Number of trucks needed per day	$Nt_d[t](i, j)$	3.52
Number of roundtrips performed by all trucks per year	$TNrt_y[t](i, j)$	Equation
Number of roundtrips performed by all trucks per day	$TNrt_d[t](i, j)$	3.53

## II Cost parameters

The cost parameters chosen for investment and operating the different plants and trucks are estimated based on different literature reviews and cost assessments. This includes the investment cost related to the different transformation processes and storage technologies, in addition to truck, tube and tank investment costs. The fixed and variable operation and maintenance cost for the different transport supply chains are defined, in addition to fuel and logistic costs for truck transportation.

### II.1 Compressor and liquefier capital cost

The cost data of several hydrogen compression technologies have been summarized (Weinert & Lipman, 2006) to establish a relation between the capital costs of the compressor  $CC_{c,1}$  in USD 2005 as a function of the capacity in kg/hour. The results are then converted to cost in EUR 2016 (Table A.11 and Table A.12 in annex) as a function of the annual hydrogen demand.

This model corresponds to the operating pressure of 345 bar. Thus, using Equation 3.32, the cost can be deduced as a function of the compressor power  $P_c$  and capacity factor  $CF_{Tc}$  (Table A.17) using the corresponding compressor work of 2.45 kWh/ kg., as shown in Equation 3.56 :

$$CC_{c,1} = 24661 * \left( \frac{P_c}{2.45 * CF_{Tc}} \right)^{0.5202} \quad \text{for } x_t \leq 7 * 10^4 \text{ kW}$$

---

**Equation 3.56**

The capital cost of the compressor  $CC_{c,2}$  as a function of the compressor power  $P_c$  was as well estimated using different sizing factors (True, 2000). This cost includes as well indirect capital costs as installation and property taxes for instance and was calculated for a power below  $2 * 10^4 \text{ kW}$ . Equation 3.57 shows the cost inflated to EUR 2016 (Table A.11 and Table A.12) as a function of compressor power:

$$CC_{c,2} = 36738 * P_c^{0.6674} \quad \text{for } P_c \leq 2 * 10^4 \text{ kW}$$

---

**Equation 3.57**

Another method uses a scaling coefficient  $\alpha_{sc}$  to scale the cost from a base known case cost  $C_b$  of a system of size  $S_b$ . This relation calculates the increase in capacity size  $S$  and cost  $C$  as given by Equation 3.58 (Tribe & Alpine, 1986).

$$\frac{C}{C_b} = \left( \frac{S}{S_b} \right)^{\alpha_{sc}}$$

---

**Equation 3.58**

In the case of the compressor capital cost, the capacity size  $S$  can be reduced to the compressor power  $P_c$  and the cost  $C$  to the capital cost of compression  $CC_c$ .

The main work cited in literature used a sizing factor of  $\alpha_{sc} = 0.9$  (Amos, 1998) to calculate the central plant compressors' costs,, as shown in Equation 3.59.

$$CC_{c,3} = 17,457 * \left(\frac{P_c}{10}\right)^{0.9}$$

**Equation 3.59**

The same sizing factor for compressor work has also been used but considering a different base compressor cost, which ranges between 2545 EUR/ kW and 3151 EUR/ kW for a compressor filled at a pressure 218 bar that corresponds to a system work of 2.12 kWh/ kg (Simbeck & Chang, 2002).

A more accurate way to calculate the capital cost is to use two sizing factors corresponding to the compressor power size  $P_c$  and operating pressure  $Pt$  (Drennen & Rosthal, 2007),, as shown in Equation 3.60 and was used for the cost functions calculation.

$$CC_c[t] = C_{b,c} * S_{b,c} * \left(\frac{P_c}{S_{b,c}}\right)^{0.8} * (r_c[t])^{0.18}$$

$$r_c[t] = Pt/P_{b,c}$$

**Equation 3.60**

The same method (Tribe & Alpine, 1986) was used to calculate the cost  $C$  corresponding to the capital cost of liquefaction  $CC_L$ .

In the case of the liquefaction capital cost, the capacity size  $S$  corresponds to the net production rate  $Pr_{h,net}$  expressed in kg/ hour. This net production accounts for the losses that accrue later on, during the storage process, due to the boil-off effect.

The hourly net production  $Ph_{h,net}$  can be expressed by the production rate  $Pr_h$ , taking into account the boil-off rate  $BoR$  fixed at 1%/hour and the total storage time  $Th_{st}$  in the unit of rate (hours in this case) as expressed by Equation 3.61.

$$Pr_{h,net} = Pr_h * (1 - e^{-BoR*Th_{st}})$$

**Equation 3.61**

The capital cost of the liquefier was determined using a sizing factor of  $\alpha_{sc} = 0.65$  to adjust from the baseline size  $S_{b,L}$  fixed at 454 kg/ hour (Drennen & Rosthal, 2007). Using Equation 3.58 the

capital cost of liquefaction  $CC_L$  can be expressed at different net production rates  $Pr_{h,net}$ , as shown in Equation 3.62.

$$CC_L = C_{b,l} * S_{b,l} * \left( \frac{Pr_{h,net}}{S_{b,l}} \right)^{0.65}$$

**Equation 3.62**

---

## II.2 The capital cost of hydrogenation

Even though the hydrogenation of LOHC for storage and transport does not exist yet at the commercial scale, the costs can be based on the applications in refineries and chemical plants (Teichmann, Arlt, & Wasserscheid, 2012) converting the costs to EUR 2016 (Table A.11 and Table A.12 in annex).

One example is to assess the cost of processing aromatic hydrocarbons, mainly used in the industry. In fact, diesel hydrodesulphurization and dehydroaromatization represent similarities to LOHC hydrogenation, which can be used for approximating the investment costs (Teichmann et al., 2012).

For instance, a capital cost for hydrodesulphurization per oil flow processed was found out to range between 7969 and 11,523 € / (kg/ h) (Yamaguchi, 2003), while the cost for both hydrodesulphurization and dehydroaromatization per oil flow processed was approximated to 8692 € / (kg/ h) (Teichmann et al., 2012).

Finally, the investment cost of LOHC was approximated to a total of 1584 € / (kg/ day) (Ahluwalia et al., 2011), which includes as well the storage capital cost (7.9% of the total investment cost) and the carrier material cost (49% of the total investment cost).

Following these studies, the base capital cost of hydrogenation was chosen equal to 11,000 € / (kg/ h), which corresponds to a base installed capacity of 12,500 kg/h with a sizing factor of 0.7. This cost excluded the storage cost and the carrier material cost.

For the catalyst material, 1 kg of catalytic material, costing 148 € /kg to produce 500 tonnes of LOHC was estimated (Ahluwalia et al., 2011). As the carrier material is not consumed during the process, it can be recycled, and hydrogenation cycles analyses showed a high stability cycle (Teichmann et al., 2012). Thus, the degradation of the catalytic material was supposed negligible, and the catalytic cost can be introduced in the capital cost of hydrogenation, as showed in Equation 3.63.

$$CC_h = C_{b,h} * S_{b,h} * \left( \frac{Pr_h}{S_{b,h}} \right)^{0.7}$$

**Equation 3.63**

---

### II.3 Storage capital cost

Gaseous pressure vessels, both for stationary and bulk transportation applications, are currently the most common means of storing hydrogen for meeting fuel demand at hydrogen stations.

Storage pressures may range from 135 bar to 930 bar corresponding to low pressure level around 160 bar, medium one around 430 bar, and a higher one around 860 bar. The cost associated with each of them for the prospects was 632 €, 678 €, and 903 € per kg of hydrogen stored, corresponding respectively to low, medium, and high compressed stored gas (Partnership., 2017).

Furthermore, cylindrical steel tanks with a volume of 765 l and operating at about 415 bar may cost about 11,912 €, yielding a specific cost of about 595 €/ kg of storage capacity (Simbeck & Chang, 2002). According to the same source, composite pressure vessels may cost about 321 €/ kg. Finally, the modern full-composite vessel with a volume of 150 l costs about 4000 €.

The same methodology used for calculating transformation capital cost (Tribe & Alpine, 1986) can also be applied to deduce the storage capital cost for both compression and liquefaction. In this case, the capacity size  $S$  will correspond to the storage capacity  $Cp$  in kg and the cost  $C$  to the capital cost of storage  $CC_S$ .

As for transformation capital cost, two sizing factors corresponding to the storage capacity and the operating pressure can be used to calculate the capital cost of storing compressed gas  $CC_{sc}$  (Drennen & Rosthal, 2007); and one sizing factor could be used to calculate the capital cost of storing liquid hydrogen  $CC_{sl}$ , or liquid organic hydrogen carrier  $CC_{sh}$ , as shown in Equation 3.64

$$CC_{Sc} = C_{b,sc} * S_{b,sc} * \left( \frac{Cp \frac{P_{b,sc}}{P_t}}{S_{b,sc}} \right)^{0.75} * \left( \frac{P_t}{P_{b,sc}} \right)^{0.44}$$

$$CC_{Sh} = C_{b,sh} * S_{b,sh} * \left( \frac{Cp}{S_{b,sh}} \right)^{0.7}$$

$$CC_{Sl} = C_{b,sl} * S_{b,sl} * \left( \frac{Cp}{S_{b,sl}} \right)^{0.7}$$

Equation 3.64

In this case study, the compressed tube trailers used to transport hydrogen have a fixed capacity  $m[t]$  corresponding to the operating pressure (Table A.15 in annex). These same tubes are used as well for the storage.

During the transport phase, losses will happen proportionally on the distance of the transport, reducing the transported capacity. This effect can be taken into account by introducing the losses of the storage phase and updating the capacity of the tube trailer  $m[t]$ . This is only valid when the production cost is considered.

Thus, a more general formulation to calculate the capital cost associated with storing a specific flow  $Xpd_{ij}$  during an amount period of time  $Tpd_S$  can be written for different states of aggregation of hydrogen by using only one sizing factor corresponding to the tank storage capacity  $m[t]$ , as shown in Equation 3.65

$$CC_S[t] = C_{tube}[t] * \left( \frac{Xpd_{ij} * Tpd_S}{m[t]} \right)^{\alpha_{sc}[t]}$$

**Equation 3.65**

The two parameters  $m[t]$  and  $C_{tube}[t]$  vary with the state of aggregation of hydrogen  $St$ , and the sizing factor  $\alpha_{sc}[t]$  varies whether the hydrogen is transported as a compressed gas, a liquid gas, or a liquid organic hydrogen carrier, as shown in Table 3.9.

**Table 3.9:** Variable parameters for different states of aggregation

State of transport	CGH					LOHC	LH
sizing factor $\alpha_{sc}[t]$	0.75					0.7	0.7
Index $t$ of state of aggregation	2	3	4	5	6	9	10
Total net truck capacity $m[t]$ in kg	350	668	885	1100	1230	1500	3600
Cost of the tube trailer $C_{tube}[t]$ in €	385,000	525,000	689,000	1,056,991	1,197,500	57,087	1,732,500

Adjusted from Annex (Table A.10 Table A.11 and Table A.12)

#### II.4 Operations and maintenance cost

Operation and maintenance costs are broken down into fixed and variable ones. The fixed ones include the operations and maintenance associated with the storage  $O\&M_S$  and the operations and maintenance associated with transformation  $O\&M_T$ . The parameters depend on the transformation process and refer to compression  $O\&M_{Sc}$  and  $O\&M_{Tc}$ ; or liquefaction  $O\&M_{Sl}$  and  $O\&M_{Tl}$ ; or de- and hydrogenation  $O\&M_{Sh}$  and  $O\&M_{Th}$  (Table A.17 in annex).

All the fixed operations and maintenance cost were taken as a percentage  $OM$  of the capital cost  $CC$ , as shown in Equation 3.66:

$$\begin{aligned}
O\&M_{Sc} + O\&M_{Tc} &= OM_c * (CC_c + CC_S[t]) & t = [2,6] \\
O\&M_{Sh} + O\&M_{Th} &= OM_h * (CC_h + CC_S[t]) & t = 9 \\
O\&M_{Sl} + O\&M_{Tl} &= OM_l * (CC_l + CC_S[t]) & t = 10
\end{aligned}$$

**Equation 3.66**

Concerning the variable operations and maintenance cost, it includes the cost of the work needed to transform hydrogen  $TCe[t, t']$  from a state  $St$  to another state  $St'$  and the cooling water requirement cost associated with both transformation operations  $TCw$ .

The specific work cost  $TCe$  is linked to electricity cost  $Ce$ , as shown in Equation 3.67 and varies depending on the annual demand and the country (France  $FR$  or Germany  $DE$ ) where the transformation occurs.

$$\begin{aligned}
\begin{bmatrix} TCe^G[t, t'] \\ TCe^F[t, t'] \end{bmatrix} &= \dot{w}_s[t, t'] * CF_c * \begin{bmatrix} Ce^G \\ Ce^F \end{bmatrix} & t' = [2,6] \\
\begin{bmatrix} TCe^G[t, t'] \\ TCe^F[t, t'] \end{bmatrix} &= \dot{w}_s[t, t'] * CF_h * \begin{bmatrix} Ce^G \\ Ce^F \end{bmatrix} & t' = 9 \\
\begin{bmatrix} TCe^G[t, t'] \\ TCe^F[t, t'] \end{bmatrix} &= \dot{w}_s[t, t'] * CF_l * \begin{bmatrix} Ce^G \\ Ce^F \end{bmatrix} & t' = 10
\end{aligned}$$

**Equation 3.67**

$\dot{w}_s[t, t']$  is the work associated with the transformation as defined by the matrix annexed in Table A.9 and  $CF_T$  is the capacity factor that depends on the type of transformation;  $CF_c$  in case of compression,  $CF_l$  in case of liquefaction and  $CF_h$  in case of de- and hydrogenation (Table A.17 in annex).

For the annual cooling cost  $TCw$ , it was calculated for compression using the annual cooling water requirement  $\dot{V}y_w$  as defined in Equation 3.35 for compression and hydrogenation and 12 times more in case of liquefaction. Considering that water cost  $Cw$  is constant for both countries,  $TCw$  is expressed using Equation 3.68.

$$TCw = \dot{V}y_w * CF_T * Cw$$

**Equation 3.68**

## II.5 Road transport cost

The capital cost related to the purchase of the truck components is defined as those for its two components the cab  $C_{Cab}$  (Table A.16 in annex) and the trailer that includes the undercarriage

$C_{und}$  (Table A.16 in annex) plus the tube corresponding to the tube used for storage  $C_{tube}[t]$  (Table A.15 in annex).

In addition to the different capital cost components, the fuel cost to perform  $Nrt_{pd}[t](i, j)$  roundtrips with one truck during a period  $pd$  depends on the distance between the two locations  $d_{ij}$  and the unit fuel cost  $F_p$  in € / km, as expressed in Equation 3.69.

$$FC[t](i, j) = Nrt_{pd}[t](i, j) * F_p * d_{ij}$$

**Equation 3.69**

---

Finally, labor cost associated with one truck performing  $Nrt_{pd}[t](i, j)$  roundtrips during a period  $pd$  are calculated using the numbers of drivers  $Ndr[t](i, j)$  and the driver wage  $TC_{driver}$ , as shown in Equation 3.70.

$$LC[t](i, j) = Nrt_{pd}[t](i, j) * Ndr[t](i, j) * TC_{driver} * \left( \frac{2 * d_{ij}}{S_a} + tt_{l/u}[t] \right)$$

**Equation 3.70**

---

# CHAPTER FOUR

## 4 MODEL AND METHODOLOGY

### **Abstract**

This chapter aims to develop the model behind the general optimization problem. First, the method to calculate the cost functions needed for the optimization model is introduced and defined. That includes the cost functions associated with storage cost, to transformation cost and road transport cost, these functions are then linearized to reduce the optimization problem time. A dynamical formulation is presented as well, where the technical assessment and the economical one is decoupled, the first one is calculated daily and the second one yearly. This method is found out to reduce the total cost by giving priority to storage over transport in daily base use. Finally, the general model is formulated as three connected problems; The first one gives the minimum cost for an input hydrogen flow and transport distance; The second one simulates the optimum flow to transport hydrogen for a set of production and distribution nodes corresponding to the different considered scenarios; The third one calculates the optimum hydrogen infrastructure by associating each edge to its minimum transport cost.

## Model and methodology

### I COST FUNCTIONS CALCULATION

<i>I.1 Annual cost functions</i> .....	123
I.1.1 Compression cost function .....	123
I.1.2 Liquefaction cost function .....	125
I.1.3 De- and hydrogenation cost function .....	127
I.1.4 Transformation and storage cost summary .....	128
I.1.5 Road transport cost function .....	130
<i>I.2 Cost function linearization</i> .....	132
<i>I.3 Dynamic transport cost</i> .....	136
I.3.1 Dynamic cost functions .....	137
I.3.2 Linearization .....	139

### II OPTIMIZATION MODEL

<i>II.1 Mathematical formulation of the minimum cost</i> .....	142
II.1.1 The objective function .....	142
II.1.2 Constrains and ILP formulation .....	143
II.1.3 Dynamic formulation .....	145
<i>II.2 Mathematical formulation of the optimum flow</i> .....	146
II.2.1 The objective function .....	146
II.2.2 Constrains .....	147
<i>II.3 Mathematical formulation of the minimum road network cost</i> .....	148

## Acronyms

SoT	State of transport
NPV	Net present value
CGH	Compressed gas hydrogen
LH	Liquid hydrogen
LOHC	Liquid organic hydrogen carrier
LP	Linear programming
ILP	Integer linear programming
MILP	Mixed-integer linear programming
TPD	Ton per day

## Nomenclature

Parameter		First appearance	Unit
$C_{an}$	Total annual cost occurring at each year $y$	Equation 4.1	€
$CC$	Initial investment	Equation 4.1	€
$O\&M$	Fixed operation and maintenance cost	Equation 4.1	€
$FC$	Fuel cost	Equation 4.1	€
$EC$	Electricity cost	Equation 4.1	€
$LC$	Labor cost	Equation 4.1	€
$yn$	Economic lives	Equation 4.1	-
$y$	Year	Equation 4.1	-
$i_{dr}$	Discount rate	Equation 4.1	-
$CRF$	Capital recovery factor	Equation 4.2	-
$Xy_{ij}$	Demand flow during the year	Equation 4.7	TPY
$C_{tot}$	Total cost of hydrogen	Equation 4.7	€
$LCOH$	Levelized cost of hydrogen	Equation 4.7	€/ kg
$LCOPH$	Levelized cost of producing hydrogen	Equation 4.7	€/ kg
$LCOTH$	Levelized cost of transporting hydrogen	Equation 4.7	€/ kg
$C_T$	Cost associated with transformation	Equation 4.8	€
$C_S$	Cost associated with storage	Equation 4.8	€
$C_R$	Cost associated with road transport	Equation 4.8	€
$LCOH_T$	Levelized cost associated with transformation	Equation 4.8	€/ kg
$LCOH_S$	Levelized cost associated with storage	Equation 4.8	€/ kg
$LCOH_R$	Levelized cost associated with road transport	Equation 4.8	€/ kg
$P_c$	Compressor power	Equation 4.10	kW
$Th_y$	Yearly hours	Equation 4.10	hours
$fCC_{Tc}[s, t]$	Compression capital cost function	Equation 4.11	NAN
$CC_{Tc}$	Compressor capital cost	Equation 4.11	€
$C_{b,c}$	Base compressor cost	Equation 4.11	€/kW
$S_{b,c}$	Base compressor size	Equation 4.11	kW
$r_c[t]$	Ratio compression to the base case	Equation 4.11	-
$CF_{Tc}$	Capacity factor of compression	Equation 4.11	-
$fCC_{Sc}[t]$	Storage capital cost function for the compressor	Equation 4.12	NAN
$CC_S[t]$	Storage capital cost	Equation 4.12	€
$C_{tube}[t]$	Cost of the tube trailer	Equation 4.12	€

$m[t]$	Total net truck capacity	Equation 4.12	kg
$CF_{Sc}$	Capacity factor of compression storage	Equation 4.12	-
$O\&M_{Sc}$ ,	Fixed operation and maintenance cost associated with compression	Equation 4.13	€
$O\&M_{Tc}$	storage and transformation		
$Tce^F[t, t']$	Specific cost of work transformation in France	Equation 4.14	€/kg
$Tce^G[t, t']$	Specific cost of work transformation in Germany	Equation 4.14	€/kg
$\dot{w}_c[s, t]$	Specific work of compression	Equation 4.14	kWh/kg
$Ce^{FR}$	Electricity cost in France	Equation 4.14	€/kWh
$Ce^{DE}$	Electricity cost in Germany	Equation 4.14	€/kWh
$Cw$	Water cost	Equation 4.14	€/m <sup>3</sup>
$fVom_c[s, t]$	Compressor variable operation and maintenance cost function	Equation 4.14	€
$C_c$	Total annual cost associated with compression	Equation 4.15	€
$Pr_h$	Production rate	Equation 4.16	kg/hour
$BoR$	Boil-off rate	Equation 4.17	-
$CC_{Tl}$	Capital cost of the liquefier	Equation 4.17	€
$C_{b,l}$	Base liquefier cost	Equation 4.17	€/kW
$S_{b,l}$	Base liquefier size	Equation 4.17	kW
$CF_{Tl}$	Capacity factor of liquefaction	Equation 4.17	-
$fCC_{Tl}[s, t]$	Liquefaction capital cost function	Equation 4.17	NAN
$fCC_{Sl}[t]$	Storage capital cost function for the liquefier	Equation 4.18	NAN
$CF_{Sl}$	Capacity factor of liquefaction storage	Equation 4.18	-
$O\&M_{Sl}$ ,	Fixed operation and maintenance cost associated with liquefaction	Equation 4.19	€
$O\&M_{Tl}$	storage and transformation		
$\dot{w}_l[s]$	Specific work of liquefaction	Equation 4.20	kWh/kg
$fVom_l[s]$	Liquefier variable operation and maintenance cost function	Equation 4.20	€
$C_l$	Total annual cost associated with liquefaction	Equation 4.21	€
$fCC_{Th}[s, t]$	Hydrogenation capital cost function	Equation 4.22	NAN
$CC_{Th}$	Capital cost of the hydrogenation process	Equation 4.22	€
$C_{b,h}$	Base hydrogenation cost	Equation 4.22	€/kW
$S_{b,h}$	Base hydrogenation size	Equation 4.22	kW
$CF_{Th}$	Capacity factor of de- and hydrogenation	Equation 4.22	-
$CF_{Sh}$	Capacity factor of de- and hydrogenation storage	Equation 4.23	-
$fCC_{Sh}[t]$	LOHC storage capital cost function	Equation 4.23	NAN
$fVom_h[s]$	De- and hydrogenation variable operation and maintenance cost function	Equation 4.25	€
$\dot{w}_h[s]$	Specific work of de- and hydrogenation	Equation 4.25	kWh/kg
$C_h$	Total annual cost associated with hydrogenation	Equation 4.26	€
$O\&M_{Sh}$ ,	Fixed operation and maintenance cost associated with de- and	Equation 4.26	€
$O\&M_{Th}$	hydrogenation storage and transformation		
$\alpha_{sc}[t]$	Sizing factor	Equation 4.27	NAN
$fCC_T$	Capital cost function of transformation	Equation 4.27	NAN
$fCC_S$	Capital cost function of storage	Equation 4.27	NAN
$fVom_T$	Transformation variable operation and maintenance cost function	Equation 4.27	€
$OM_T$	Share of $O\&M_{Tc}$ , $O\&M_{Tl}$ or $O\&M_{Th}$ to the capital cost	Equation 4.27	-
$OM_S$	Share of $O\&M_{Sc}$ , $O\&M_{Sl}$ or $O\&M_{Sh}$ to the capital cost	Equation 4.27	-
$\alpha_{tc}[t]$	Transformation sizing factor	Equation 4.27	-
$\alpha_{sc}[t]$	Storage sizing factor	Equation 4.27	-

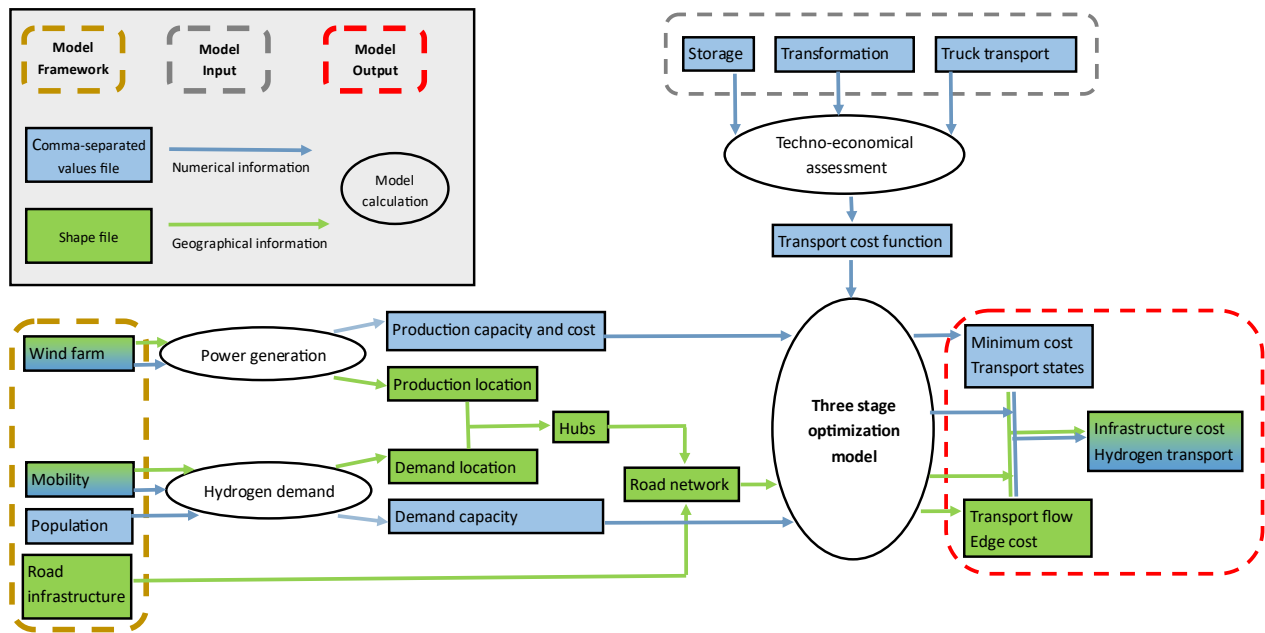
$CRF_T$	Transformation capital recovery factor ( $CRF_{Tc}, CRF_{Th}$ or $CRF_{Tl}$ )	Equation 4.27	-
$CRF_S$	Storage capital recovery factor ( $CRF_{Sc}, CRF_{Sh}$ or $CRF_{Sl}$ )	Equation 4.27	-
$CC_{Cab}$	Capital cost of the cabin	Equation 4.31	€
$Nt_y[t]$	Annual number of trucks at each transport state $t$	Equation 4.31	-
$C_{Cab}$	Cost of one cabin	Equation 4.31	€
$CC_{tra}$	Capital cost of the trailer	Equation 4.32	€
$C_{tra}$	Cost of one trailer	Equation 4.32	€
$C_{und}$	Cost of one undercarriage	Equation 4.32	€
$O\&M_{Cab}$	Fixed operation and maintenance cost associated with the cabin	Equation 4.33	€
$OM_{Cab}$	Share of $O\&M_{Cab}$ to the capital cost	Equation 4.33	-
$O\&M_{tra}$	Fixed operation and maintenance cost associated with the trailer	Equation 4.33	€
$OM_{tra}$	Share of $O\&M_{tra}$ to the capital cost	Equation 4.33	-
$FC[t]$	Fuel cost associated with the truck operating at $t$ state	Equation 4.34	€
$CF_{RTT}$	Truck capacity factor	Equation 4.34	-
$d_{ij}$	Distance between the locations $i, j$	Equation 4.34	km
$tt_{l/u}[t]$	Total loading and unloading time	Equation 4.34	hour
$FC[t]$	Fuel cost of a truck operating at the state of transport $t$ in €	Equation 4.34	€
$F_p$	Unit fuel cost	Equation 4.34	€/km
$TC_{driver}$	Driver wage	Equation 4.35	€/hour
$Nwh$	Maximum number of working hours	Equation 4.35	hours
$LC[t]$	Labor cost associated with the truck operating at $t$ state	Equation 4.35	€
$Dy_{min}$	Yearly minimum demand hub in France and Germany	Equation 4.37	TPY
$Dy_{max}$	Yearly maximum demand region in France and Germany	Equation 4.37	TPY
$g_n(Xy_{ij}, \alpha)$	Approximation of the power function $[Xy_{ij}]^\alpha$ on the interval $[Dy_{min}, Dy_{max}]$	Equation 4.38	-
$f_k(Xy_{ij}, \alpha, s)$	Approximation of the power function $[Xy_{ij}]^\alpha$ on the interval $[Dy_{k-1}, Dy_k]$	Equation 4.39	-
$s_k$	Middle of segment $[Dy_{k-1}, Dy_k]$	Equation 4.39	TPY
$A_T$	Fixed parameter associated with capital cost and $O\&M$ of Transformation	Equation 4.42	€
$A_S$	Fixed parameter associated with capital cost and $O\&M$ of storage	Equation 4.42	€
$h_n(Xy_{ij}, \alpha)$	Approximation of the step function $Nt_y[t]$ on the interval $[Dy_{min}, Dy_{max}]$	Equation 4.44	-
$A_r$	Fixed parameter associated with road transport cost	Equation 4.47	€
$Cd_R$	Dynamic annual cost of road transport	Equation 4.48	€
$Trd_{ij}$	Daily transported capacity	Equation 4.48	TPD
$Cd_T$	Dynamic annual cost of transformation	Equation 4.49	€
$Cd_S$	Dynamic annual cost of storage	Equation 4.49	€
$Std$	Daily stored capacity	Equation 4.50	TPD
$CCd_{Cab}$	Dynamic capital cost of the cab	Equation 4.52	€
$CCd_{tra}$	Dynamic capital cost of the trailer	Equation 4.52	€
$O\&Md_{Cab}$	Fixed operation and maintenance cost associated with the cabin	Equation 4.53	€
$O\&Md_{Tra}$	Fixed operation and maintenance cost associated with the trailer	Equation 4.53	€
$FCd$	Dynamic fuel cost	Equation 4.54	€
$FC_d[t]$	Daily fuel cost of a truck operating at state of transport $t$	Equation 4.54	€
$LCd$	Dynamic labor cost	Equation 4.55	€

$LC_d[t]$	Dynamic labor cost of a truck operating at state of transport $t$	Equation 4.55	€
$LCOHd_T$	Dynamic Levelized cost associated with transformation	Equation 4.57	€/ kg
$LCOHd_S$	Dynamic Levelized cost associated with storage	Equation 4.57	€/ kg
$LCOHd_R$	Dynamic Levelized cost associated with road transport	Equation 4.57	€/ kg
$Ad_r$	Fixed parameter associated with road transport cost	Equation 4.58	€
$i_p$	Production node	Equation 4.70	-
$j_d$	Distribution node	Equation 4.70	-
$x_{ij}$	Input demand flow to transport over a distance $d_{ij}$	Equation 4.60	
$Z(x_{ij}, d_{ij})$	Minimum cost model of transporting a flow $x_{ij}$	Equation 4.69	-
$Xy_{ij}[t]$	Output annual flow of the model $Z(x_{ij}, d_{ij})$	Equation 4.61	TPY
$Z_{i_p j_d}$	Optimum flow model between production and distribution nodes	Equation 4.71	-
$F_{i_p j_d}$	Output total network flow of the model $Z_{i_p j_d}$	Equation 4.71	TPY
$C_{ij}$	Minimum flow cost model along all connecting edges $\overline{u_{ij}}$	Equation 4.75	-
$c_{ij}[t]$	Cost function of the model $Z(x_{ij}, d_{ij})$	Equation 4.61	€/ kg
$T_s$	State of transport group	Equation 4.61	-
$\Delta x$	Flow step	Equation 4.64	TPD
$\Delta d$	Distance step	Equation 4.64	Km
$\Delta m$	Truck capacity step	Equation 4.65	Kg
$p_{i_p}$	Hydrogen flow produced at initial condition 0/1	Equation 4.72	TPD
$p_{i_p, max}$	Maximum installed capacity	Equation 4.72	TPD
$d_{i_p}$	Demand flow	Equation 4.73	TPD
$d(i, j)$	Euclidean distance between the nodes $i$ and $j$	Equation 4.76	km
$I_{(i, j)}$	Group of the summed edges	Equation 4.77	-

# T

he general model aims, for a network corresponding to the road one, to link a set of production nodes to a set of distribution nodes at the minimum cost using different transport cost function corresponding to seven states of transport (SoT). Thus, the model output for each edge gives the optimum capacity transported by each state using three parallel models, as shown in Figure 4.1. This optimization model allows finally to calculate the total infrastructure deployment cost.

**Figure 4.1:** General model



As shown in Figure 4.1, the model uses as framework the road infrastructure, the hydrogen production and demand scenarios defined in Chapter 2. Thus, the different wind farms numerical and geographical information allow defining the hydrogen production plant data. These data include the production plants capacities and costs and the locations for different scenarios. In the meantime, the mobility and population frameworks allow the definition of the different hydrogen demand hubs capacities and locations. Finally, using the European road infrastructure, and the different production and demand hubs, a road network is defined for the different scenarios that will be used to simulate the hydrogen flow transport between the nodes.

In parallel, the cost function calculation based on the net present value is presented in the first part, which allows calculating the different cost functions associated with transformation, storage and road transport. This function will be introduced as an input parameter for the model that will be described in detail in the second part.

## I Cost functions calculation

Based on the techno-economic assessment performed in chapter 3, different costs associated with the transport supply chain are calculated. These costs are formulated as functions of the transport state and include storage, road transport, liquefaction, compression, and de- and hydrogenation costs. For that, the cost methodology to define the different functions based on the net present value is presented. Then, the different costs are formulated as annual Levelized costs, linearized and then reformulated as dynamic functions. In the dynamic case study, the technical assessment is performed daily, and storage capacity is decoupled from transport capacity to reduce the cost of using road truck transport that is higher compared to storage cost.

To compare investments with different economic lives of  $yn$  years at a specified discount rate  $i_{dr}$ , and to account the differing points in time  $y$  in which they occur, the net present value ( $NPV$ ) method is used. Taking the notation used in the definition of [André et al., 2014], the net present value of the initial investment is written , as shown in Equation 4.1.

$$NPV = \sum_{y=1}^{yn} \frac{C_{an}}{(1 + i_{dr})^y} = CC + \sum_{y=1}^{yn} \frac{O\&M + EC + FC + LC}{(1 + i_{dr})^y}$$

**Equation 4.1**

Where  $C_{an}$  is the total annual cost occurring at each year  $y$  and accounts for different costs that include the capital cost brought down to the year  $y$  and the different operation and maintenance cost.

The capital cost  $CC$  corresponds to the initial investment. The capital recovery factor ( $CRF$ ) [Short et al., 2005] or fixed charge factor [EIA, 2016] is applied to determine the financial impact of the capital cost as it converts a present value into a stream of equal annual payments over a specified time  $yn$ , at a specified discount rate (interest)  $i_{dr}$ , and is calculated using Equation 4.2.

$$CRF = \frac{i_{dr}(1 + i)^{yn}}{(1 + i_{dr})^{yn} - 1} = \frac{i_{dr}}{1 - (1 + i_{dr})^{-yn}}$$

**Equation 4.2**

The fixed operation and maintenance costs  $O\&M$  include the total cost that remains relatively constant, regardless of plant utilization levels, such as maintenance or refurbishment costs that are scheduled on a calendar basis rather than an operating-hours basis.

The variable operation and maintenance costs include costs that are closely tied to the actual operating hours of the equipment, such as consumable maintenance items and refurbishment

costs that are scheduled based on operating hours. This cost includes mainly energy cost: fuel cost  $FC$  and electricity cost  $EC$ .

Other variable costs include the labor cost  $LC$  as well as various costs associated with each transformation process or storage technology and only occur in that specific context.

The sum of the power series of variable year  $y$  displayed in Equation 4.1 is expressed using Equation 4.3.

$$\sum_{y=1}^{yn} \frac{1}{(1 + i_{dr})^y} = \frac{1 - (1 + i_{dr})^{-yn}}{i_{dr}}$$

**Equation 4.3**

---

Replacing the sum of the power series in the NPV method (Equation 4.1) allows rewriting the equality, as shown in Equation 4.4.

$$\frac{1 - (1 + i_{dr})^{-yn}}{i_{dr}} * C_{an} = CC + \frac{1 - (1 + i_{dr})^{-yn}}{i_{dr}} * (O\&M + FC + EC + LC)$$

**Equation 4.4**

---

From the definition of the capital recovery factor (Equation 4.2), Equation 4.4 is equivalent to Equation 4.5.

$$\frac{1}{CRF} * C_{an} = CC + \frac{1}{CRF} * (O\&M + FC + EC + LC)$$

**Equation 4.5**

---

Equation 4.5 allows then to define the annual cost  $C_{an}$  directly from the capital cost  $CC$ , and the total operation and maintenance cost, including fixed ones  $O\&M$ , fuel cost  $FC$ , electricity cost  $EC$  and labor cost  $LC$ .

The fixed operation and maintenance cost is expressed as a percentage  $OM$  of the total capital cost, allowing to write the annual cost  $C_{an}$  as defined in Equation 4.6.

$$C_{an} = CC * (CRF + OM) + FC + EC + LC$$

**Equation 4.6**

---

The total cost of hydrogen  $C_{tot}$  is introduced via the Levelized cost of Hydrogen ( $LCOH$ ) as the total cost  $C_{tot}$  per mass hydrogen flow  $Xy_{ij}$  transported over a year  $y$  from a location  $i$  to a location  $j$  (Equation 4.7). This Levelized cost is the sum of the different  $LCOH$  of the hydrogen

supply chain excluding the dispensing on the fuel station. Thus, the total cost includes the one producing hydrogen ( $LCOPH$ ) and transporting it ( $LCOTH$ ), as shown in Equation 4.7.

$$C_{tot} = LCOH * Xy_{ij}$$

$$LCOH = LCOPH + LCOTH$$

**Equation 4.7**

The definition of  $LCOH$  is kept for all cost calculations and reflects the annual cost of transporting one-unit kg of hydrogen and as a sum of the different  $LCOH$  of the hydrogen chain.

For the cost calculation and because the production and consumption rates are assumed fixed, only the Levelized cost related to transporting hydrogen  $LCOTH$  will be minimized. These Levelized costs include  $LCOH_T$  associated with transformation cost  $C_T$ ,  $LCOH_S$  associated with storage cost  $C_S$  and  $LCOH_R$  associated with road transport cost  $C_R$ , as shown in Equation 4.8.

$$LCOTH = LCOH_T + LCOH_S + LCOH_R$$

$$\begin{cases} C_T = LCOH_T * Dpd_j \\ C_S = LCOH_S * Dpd_j \\ C_R = LCOH_R * Dpd_j \end{cases}$$

**Equation 4.8**

## 1.1 Annual cost functions

As the capital cost is brought down to its annual payment, all the costs are expressed in a period  $pd$  corresponding to a year  $y$ . For the different cost calculations, the hydrogen is set at the initial state of aggregation  $s$  and transported and stored at the SoT  $t$ . Thus, regarding energy requirement, the work of transformation  $\dot{w}_s[s, t]$  depends on the SoT as presented in Equation 4.9 and calculated in the annex (Table A.9).

$$\dot{w}_s[s, t] = \dot{w}_c[s, t] \quad \text{if } t \in [2,6]$$

$$\dot{w}_s[s, t] = \dot{w}_h[s] \quad \text{if } t = 9$$

$$\dot{w}_s[s, t] = \dot{w}_l[s] \quad \text{if } t = 10$$

**Equation 4.9**

### 1.1.1 Compression cost function

Setting the compressor annual operating hours as a product of its capacity factor  $CF_{Tc}$  (Table A.17 in Annex) and the total annual hours  $Th_y$ , the compressor power  $P_c$  can be deduced from the

specific work of compression  $\dot{w}_c[s, t]$  (Equation 4.9) and the yearly hydrogen transported flow from a location  $i$  to a location  $j$   $Xy_{ij}$ , as shown in Equation 4.10.

$$P_c = \frac{\dot{w}_c[s, t] * Xy_{ij}}{CF_{Tc} * Th_y}$$

**Equation 4.10**

Replacing  $P_c$  in Equation 3.60 the capital cost of compression  $CC_{Tc}$  can be expressed as a power product of compression capital cost function  $fCC_{Tc}[s, t]$  independently from the yearly hydrogen flow  $Xy_{ij}$ , as shown in Equation 4.11.

$$CC_{Tc} = fCC_{Tc}[s, t] * (Xy_{ij})^{0.8}$$

$$fCC_{Tc}[s, t] = C_{b,c} * S_{b,c} * \left( \frac{\dot{w}_c[s, t]}{S_{b,c} * CF_{Tc} * Th_y} \right)^{0.8} * (r_c[t])^{0.18}$$

**Equation 4.11**

The capital cost of the corresponding storage in compressed tubes expressed by Equation 3.65 can be written as well as a power product of the storage capital cost function  $fCC_{Sc}[t]$  and the yearly hydrogen demand  $Xy_{ij}$  as shown in Equation 4.12.

$$CC_{Sc} = fCC_{Sc}[t] * (Xy_{ij})^{0.75}$$

$$fCC_{Sc}[t] = C_{tube}[t] * \left( \frac{Th_s}{m[t] * CF_{Sc} * Th_y} \right)^{0.75}$$

**Equation 4.12**

In case of annual calculation, the hydrogen is stored just the time before its being transported to the distribution hubs, fixing the storage time  $Th_s$  to two hours corresponding to the maximum loading and unloading time.

Both fixed operation and maintenance costs associated with compression and storage using compressed tubes are expressed as a percentage of capital cost (Equation 3.66), as shown in Equation 4.13.

$$O\&M_{Tc} + O\&M_{Sc} = OM_{Tc} * CC_{Tc} + OM_{Sc} * CC_{Sc}$$

**Equation 4.13**

The variable operation and maintenance cost consists mainly of energy cost  $Vom_c$  as the sum of both electric cost (Equation 3.67) and water requirement cost (Equation 3.68). The total cost is

expressed as a product of the cost function associated with it  $fVom_c[s, t]$  and the yearly hydrogen demand  $Xy_{ij}$ , as shown in Equation 4.14.

$$Vom_c = fVom_c [s, t] * Xy_{ij}$$

$$fVom_c [s, t] = \dot{w}_c[s, t] * CF_{Tc} * \left[ \frac{Ce^G}{Ce^F} \right] + 0.0731 * \dot{w}_c[s, t] * Cw$$

**Equation 4.14**

Finally, using Equation 4.6 the total annual cost associated with compression  $C_c$  could be written using Equation 4.11, Equation 4.12, Equation 4.13, and Equation 4.14, as shown in Equation 4.15.

$$C_c = fCC_{Tc}[s, t] * (CRF_{Tc} + OM_{Tc}) * (Xy_{ij})^{0.8} + fCC_{Sc}[t] * (CRF_{Sc} + OM_{Sc}) * (Xy_{ij})^{0.75} + fVom_c [s, t] * Xy_{ij}$$

$$\left\{ \begin{array}{l} fCC_{Tc}[s, t] = C_{b,c} * S_{b,c} * \left( \frac{\dot{w}_c[s, t]}{S_{b,c} * CF_{Tc} * Th_y} \right)^{0.8} * (r_c[t])^{0.18} \\ fCC_{Sc}[t] = C_{tube}[t] * \left( \frac{Th_s}{m[t] * CF_{Sc} * Th_y} \right)^{0.75} \\ fVom_c [s, t] = \dot{w}_c[s, t] * CF_{Tc} * \left[ \frac{Ce^G}{Ce^F} \right] + 0.0731 * \dot{w}_c[s, t] * Cw \end{array} \right.$$

**Equation 4.15**

### 1.1.2 Liquefaction cost function

Setting the liquefier annual operating hours as a product of its capacity factor  $CF_{Tl}$  and the total annual hours  $Th_y$ , the net production rate  $Pr_h$  can be deduced from the yearly hydrogen flow  $Xy_{ij}$ , as shown in Equation 4.16.

$$Pr_h = \frac{Xy_{ij}}{CF_l * Th_y}$$

**Equation 4.16**

Replacing  $Pr_h$  in Equation 3.62, the capital cost of liquefaction  $CC_{Tl}$  can be expressed as the power product of the liquefaction cost function  $fCC_{Tl}$  independently from the yearly hydrogen flow  $Xy_{ij}$ , as shown in Equation 4.17.

$$CC_{Tl} = fCC_{Tl} * (Xy_{ij})^{0.65}$$

$$fCC_{Tl} = C_{b,l} * S_{b,l} * \left( \frac{(1 + (1 - e^{-BoR * Th_{St}}))}{CF_{Tl} * Th_y * S_{b,l}} \right)^{0.65}$$

**Equation 4.17**

The capital cost of the corresponding storage in liquid tanks expressed by Equation 3.65 is expressed as a power product of the storage cost function  $fCC_{Sl}[t]$  and the yearly hydrogen demand  $Xy_{ij}$ , as shown in Equation 4.18.

$$CC_{Sl} = fCC_{Sl}[t] * (Xy_{ij})^{0.7}$$

$$fCC_{Sl}[t] = C_{tube}[t] * \left( \frac{Th_s}{m[t] * CF_{Sl} * Th_y} \right)^{0.7}$$

**Equation 4.18**

Both fixed operations and maintenance associated with liquefaction and storage using liquid tanks are expressed as a percentage of capital cost (Equation 3.66), as shown in Equation 4.19.

$$O\&M_{Tl} + O\&M_{Sl} = OM_{Tl} * CC_c + OM_{Sl} * CC_{Sc}$$

**Equation 4.19**

The variable operation and maintenance cost  $Vom_l$  is broken down to electric cost (Equation 3.67) and water requirement cost (Equation 3.68) and expressed as a product of the cost function associated with it  $fVom_l[s]$  and the yearly hydrogen demand  $Xy_{ij}$ , as shown in Equation 4.20.

$$Vom = fVom_l [s] * Xy_{ij}$$

$$fom_l [s] = \dot{w}_l [s] * CF_{Tl} * \left[ \frac{Ce^G}{Ce^F} \right] + 0.8772 * \dot{w}_l [s] * Cw$$

**Equation 4.20**

Finally, using Equation 4.6 the total annual cost associated with liquefaction  $C_l$  can be written using Equation 4.17, Equation 4.18, Equation 4.19, and Equation 4.20 is expressed in Equation 4.21.

$$C_l = fCC_{Tl} * (CRF_{Tl} + OM_{Tl}) * (Xy_{ij})^{0.65} + fCC_{Sl} * (CRF_{Sl} + OM_{Sl}) * (Xy_{ij})^{0.7} + fVom [s] * Xy_{ij}$$

$$\left\{ \begin{array}{l} fCC_{Tl} = C_{b,l} * S_{b,l} * \left( \frac{1 + (1 - e^{-BoR * Th_{st}})}{CF_{Tl} * Th_y * S_{b,l}} \right)^{0.65} \\ fCC_{Sl}[t] = C_{tube}[t] * \left( \frac{Th_s}{m[t] * CF_{Sl} * Th_y} \right)^{0.7} \\ fVom_l [s] = \dot{w}_l[s] * CF_{Tl} * \left[ \frac{Ce^G}{Ce^F} \right] + 0.8772 * \dot{w}_l[s] * Cw \end{array} \right.$$

**Equation 4.21**

### 1.1.3 De- and hydrogenation cost function

Replacing  $Pr_h$  in Equation 3.63 by the expression of Equation 4.16, the capital cost of hydrogenation  $CC_{Th}$  is expressed as a power product of the compression cost function  $fCC_{Th}$  independently from the yearly hydrogen demand  $Xy_{ij}$ , as shown in Equation 4.22.

$$CC_{Th} = fCC_{Th} * (Xy_{ij})^{0.7}$$

$$fCC_{Th} = C_{b,h} * S_{b,h} * \left( \frac{1}{CF_{Th} * Th_y * S_{b,h}} \right)^{0.7}$$

**Equation 4.22**

The capital cost of the corresponding storage in liquid tanks expressed by Equation 3.65 is expressed as a power product of the storage cost function  $fCC_{Sh}[t]$  and the yearly hydrogen demand  $Xy_{ij}$ , as shown in Equation 4.23.

$$CC_{Sh}[t] = fCC_{Sh}[t] * (Xy_{ij})^{0.7}$$

$$fCC_{Sh}[t] = C_{tube}[t] * \left( \frac{Th_s}{m[t] * CF_{Sh} * Th_y} \right)^{0.7}$$

**Equation 4.23**

Both fixed operation and maintenance costs associated with de- and hydrogenation and storage using liquid organic carrier tanks are expressed as a percentage of capital cost (Equation 3.66), as shown in Equation 4.24.

$$O\&M_{Th} + O\&M_{Sh} = OM_{Th} * CC_{Th} + OM_{Sh} * CC_{Sh}$$

**Equation 4.24**

The variable operation and maintenance cost  $Vom_h$  is defined as the sum of electricity cost (Equation 3.67) and water requirement cost (Equation 3.68), and expressed as a product of the cost function associated with it  $fVom_h[s]$  and the yearly hydrogen demand  $Xy_{ij}$ , as shown in Equation 4.25.

$$Vom = fVom_h [s] * Xy_{ij}$$

$$fVom_l [s] = \dot{w}_h[s] * CF_{Th} * \left[ \frac{Ce^G}{Ce^F} \right] + 0.0731 * \dot{w}_h[s] * Cw$$

**Equation 4.25**

Finally, using Equation 4.6 the total annual cost associated with hydrogenation  $C_h$  is expressed using Equation 4.22, Equation 4.23, Equation 4.24, and Equation 4.25, as shown in Equation 4.26.

$$C_h = fCC_{Th} * (CRF_{Th} + OM_{Th}) * (Xy_{ij})^{0.7} + fCC_{Sh} * (CRF_{Sh} + OM_{Sh}) * (Xy_{ij})^{0.7} + fVom_h [s] * Xy_{ij}$$

$$\left\{ \begin{array}{l} fCC_{Th} = C_{b,h} * S_{b,h} * \left( \frac{1}{CF_{Th} * Th_y * S_{b,h}} \right)^{0.7} \\ fCC_{Sh}[t] = C_{tube}[t] * \left( \frac{Th_s}{m[t] * CF_{Sh} * Th_y} \right)^{0.7} \\ fVom_h [s] = \dot{w}_h[s] * CF_{Th} * \left[ \frac{Ce^G}{Ce^F} \right] + 0.0731 * \dot{w}_h[s] * Cw \end{array} \right.$$

**Equation 4.26**

#### 1.1.4 Transformation and storage cost summary

All the costs corresponding to compression, liquefaction and de- and hydrogenation are summed up under the cost of transformation and storage cost,  $C_T$  and  $C_S$  respectively, as shown in Equation 4.27.

The different economic parameters (summarized in Table 4.22) and cost functions are then defined using the indexes  $t$  corresponding to each state of aggregation and the corresponding work  $\dot{w}_s[s, t]$  (Equation 4.9).

$$C_T + C_S = fCC_T * (CRF_T + OM_T) * (Xy_{ij})^{\alpha_{tc}[t]} + fCC_S * (CRF_S + OM_S) * (Xy_{ij})^{\alpha_{sc}[t]} + fVom_T * Xy_{ij}$$

**Equation 4.27**

**Table 4.22:** Economic parameters correspondence

Index $t$ of state of aggregation	2, 3, 4, 5, 6	9	10
State of matter	CGH	LOHC	LH
Transformation sizing factor $\alpha_{tc}[t]$	0.8	0.7	0.65
Storage sizing factor $\alpha_{sc}[t]$	0.75	0.7	0.7
Transformation capital recovery factor $CRF_T$	$CRF_{Tc}$	$CRF_{Th}$	$CRF_{Tl}$
Storage capital recovery factor $CRF_T$	$CRF_{Sc}$	$CRF_{Sh}$	$CRF_{Sl}$
Transformation share of operation and maintenance cost $OM_T$	$OM_{Tc}$	$OM_{Th}$	$OM_{Tl}$
Storage share of operation and maintenance cost $OM_S$	$OM_{Sc}$	$OM_{Sh}$	$OM_{Sl}$

$fCC_T$  accounts for transformation capital cost and is defined by Equation 4.28.

$$fCC_T = \begin{cases} C_{b,c} * S_{b,c} * \left( \frac{\dot{w}_s[s, t]}{CF_{Tc} * Th_y * S_{b,c}} \right)^{0.8} * (r_c[t])^{0.18} & t \in [2,6] \\ C_{b,h} * S_{b,h} * \left( \frac{1}{CF_{Th} * Th_y * S_{b,h}} \right)^{0.7} & t = 9 \\ C_{b,l} * S_{b,l} * \left( \frac{\left( 1 + (1 - e^{-BoR * Th_{St}}) \right)}{CF_{Tl} * Th_y * S_{b,l}} \right)^{0.65} & t = 10 \end{cases}$$

**Equation 4.28**

$fCC_S$  accounts for storage capital cost and is defined by Equation 4.29.

$$fCC_S = \begin{cases} C_{tube}[t] * \left( \frac{Th_s}{m[t] * CF_{Sc} * Th_y} \right)^{0.75} & t \in [2,6] \\ C_{tube}[t] * \left( \frac{Th_s}{m[t] * CF_{Sl} * Th_y} \right)^{0.7} & t = 9 \\ C_{tube}[t] * \left( \frac{Th_s}{m[t] * CF_{Sh} * Th_y} \right)^{0.7} & t = 10 \end{cases}$$

**Equation 4.29**

$fVom_T$  accounts for variable operation and maintenance cost and is defined by Equation 4.30.

$$fVom_T = \begin{cases} \dot{w}_c[s, t] * \left( CF_{Tc} * \begin{bmatrix} Ce^G \\ Ce^F \end{bmatrix} + 0.0731 * Cw \right) & t' \in [2,6] \\ \dot{w}_l[s] * \left( CF_{Th} * \begin{bmatrix} Ce^G \\ Ce^F \end{bmatrix} + 0.0731 * Cw \right) & t' = 9 \\ \dot{w}_h[s] * \left( CF_{Tl} * \begin{bmatrix} Ce^G \\ Ce^F \end{bmatrix} + 0.8772 * Cw \right) & t' = 10 \end{cases}$$

**Equation 4.30**

### 1.1.5 Road transport cost function

The capital cost related to the purchase of the truck components is defined as that of its two components, the cab  $C_{Cab}$  and the trailer  $C_{tra}$  that includes the undercarriage  $C_{und}$  and the tube corresponding to the one used for storage  $C_{tube}[t]$ .

The annual capital cost of the cab  $CC_{Cab}$  is defined from the annual number of trucks  $Nt_y[t]$  (Equation 3.52 and Table 3.8) to meet the yearly hydrogen demand  $Xy_{ij}$  as expressed in Equation 4.31.

$$CC_{Cab} = Nt_y[t] * C_{Cab}$$

**Equation 4.31**

Similarly, the capital cost of the trailer is defined using the annual number of trucks  $Nt_y[t]$  and both undercarriage and tube costs  $C_{und}$  and  $C_{tube}[t]$ , as expressed in Equation 4.32.

$$CC_{tra} = Nt_y[t] * C_{tra} = Nt_y[t] * (C_{und} + C_{tube}[t])$$

**Equation 4.32**

As for transformation cost calculation, both fixed operation and maintenance costs associated with the cab and the undercarriage are expressed as a percentage of the two capital cost  $OM_{Cab}$  and  $OM_{und}$  respectively, as shown in Equation 4.33.

$$\begin{aligned} O\&M_{Cab} &= OM_{Cab} * CC_{Cab} \\ O\&M_{tra} &= OM_{tra} * CC_{tra} \end{aligned}$$

**Equation 4.33**

Additional truck cost includes the fuel cost  $FC$  and labor cost  $LC$ . In the case of annual cost calculation, each truck is used at its maximum annual capacity performing an annual roundtrip  $Nrt_y[t]$  corresponding to the maximum one (Equation 3.51 and Table 3.8).

The fuel cost  $FC$  is then calculated by multiplying the fuel cost associated with each truck  $FC[t]$  (Equation 3.69) and the number of trucks  $Nt_y[t]$  operating at the same SoT  $t$ , as expressed in Equation 4.34.

$$FC = FC[t] * Nt_y[t]$$

$$FC[t] = 2 * \left[ \frac{CF_{RTT} * Th_y}{\frac{2 * d_{ij}}{S_a} + tt_{l/u}[t]} \right] * F_p * d_{ij}$$

**Equation 4.34**

Using the same assumption, the labor cost  $LC$  is deduced from the labor cost associated with each truck  $LC[t]$  (Equation 3.70) and the number of trucks  $Nt_y[t]$  operating at the same SoT  $t$  as expressed in Equation 4.35.

$$LC = LC[t] * Nt_y[t]$$

$$LC[t] = \left[ \frac{CF_{RTT} * Th_y}{\frac{2 * d_{ij}}{S_a} + tt_{l/u}[t]} \right] * \left[ \frac{\frac{d_{ij}}{S_a} + tt_{l/u}[t]}{Nwh} \right] * TC_{driver} * \left( \frac{2 * d_{ij}}{S_a} + tt_{l/u}[t] \right)$$

**Equation 4.35**

Finally, using Equation 4.6 the total annual cost associated with road transport  $C_R$  is expressed using Equation 4.31, Equation 4.32, Equation 4.33, Equation 4.34, and Equation 4.35, as shown in Equation 4.36.

$$C_R = [(C_{Cab}) * (CRF_{Cab} + OM_{Cab}) + (C_{tra}) * (CRF_{tra} + OM_{tra}) + LC[t] + FC[t]] * Nt_y[t]$$

$$\left\{ \begin{array}{l} C_{tra} = C_{und} + C_{tube}[t] \\ FC[t] = 2 * \left[ \frac{CF_{RTT} * Th_y}{\frac{2 * d_{ij}}{S_a} + tt_{l/u}[t]} \right] * F_p * d_{ij} \\ LC[t] = \left[ \frac{CF_{RTT} * Th_y}{\frac{2 * d_{ij}}{S_a} + tt_{l/u}[t]} \right] * \left[ \frac{\frac{d_{ij}}{S_a} + tt_{l/u}[t]}{Nwh} \right] * TC_{driver} * \left( \frac{2 * d_{ij}}{S_a} + tt_{l/u}[t] \right) \end{array} \right.$$

**Equation 4.36**

## I.2 Cost function linearization

The total cost of transformation and storage  $C_T$  includes two power functions of a base  $Xy_{ij}$  and an exponent  $\alpha$  equal to  $\alpha_{tc}[t]$  or  $\alpha_{sc}[t]$ . Minimizing the power function is equivalent to minimizing the sum of the linear approximation over different periods [Vaziri et al., 2011].

The yearly transported flow  $Xy_{ij}$  between two locations  $i$  and  $j$  can be constrained between  $Dy_{min}$  and  $Dy_{max}$  corresponding respectively to the minimum demand hub and the maximum demand region in all France and Germany for low and high penetration of hydrogen. These values are chosen respectively as the minimum distribution hub located in Bretagne, in the West of France and the total demand of Île-de-France region (representing the most populated region in both countries).

Thus, the power function minimization problem expressed in Equation 4.37 can be written equivalent to the minimization of the sum of the linear approximation over different periods constrained between  $Dy_{min}$  and  $Dy_{max}$  (expressed in Equation 4.38).

$$\begin{aligned} & \min [Xy_{ij}]^\alpha \\ & Dy_{min} \leq Xy_{ij} \leq Dy_{max} \end{aligned}$$

**Equation 4.37**

$$\begin{aligned} & \min g_n(Xy_{ij}, \alpha) \\ & Dy_{min} \leq Xy_{ij} \leq Dy_{max} \end{aligned}$$

**Equation 4.38**

Where  $g_n(Xy_{ij}, \alpha)$  is the sum of the approximation functions  $f_k(Xy_{ij}, \alpha, s_k)$  at each interval  $[Dy_{k-1}, Dy_k]$ , as expressed by Equation 4.39.

$$\begin{aligned} g_n(Xy_{ij}, \alpha) &= \sum_{k=1}^n [f_k(Xy_{ij}, \alpha, s_k) * \chi_{[Dy_{k-1}, Dy_k]}(Xy_{ij})] \\ \chi_{[Dy_{k-1}, Dy_k]}(Xy_{ij}) &= \begin{cases} 1 & \text{if } Xy_{ij} \in [Dy_{k-1}, Dy_k] \\ 0 & \text{if not} \end{cases} \end{aligned}$$

**Equation 4.39**

The function  $f_k(Xy_{ij}, \alpha, s_k)$  is defined by Taylor's theorem as the derivative of the power function, as expressed in Equation 4.40.

$$f_k(Xy_{ij}, \alpha, s_k) = s_k^\alpha + \alpha * s_k^{\alpha-1} * (Xy_{ij} - s_k) \text{ defined in } [Dy_{k-1}, Dy_k]$$

$$s_k \in [Dy_{k-1}, Dy_k]$$

$$s_k = Dy_{min} + k * \frac{Dy_{max} - Dy_{min}}{n}$$

**Equation 4.40**

---

For the case where  $\alpha$  is close to 1, the segments are chosen with variable length corresponding to a small repartition, and  $s_k$  is fixed as the middle of each segment. This is equivalent to re-define  $f_k(Xy_{ij}, \alpha, s_k)$  with the parameters shown in Equation 4.41.

$$s_k = \frac{Dy_{k-1} + Dy_k}{2}$$

$$Dy_k = \varepsilon_k * Dy_{max} + (1 - \varepsilon_k) * Dy_{min}$$

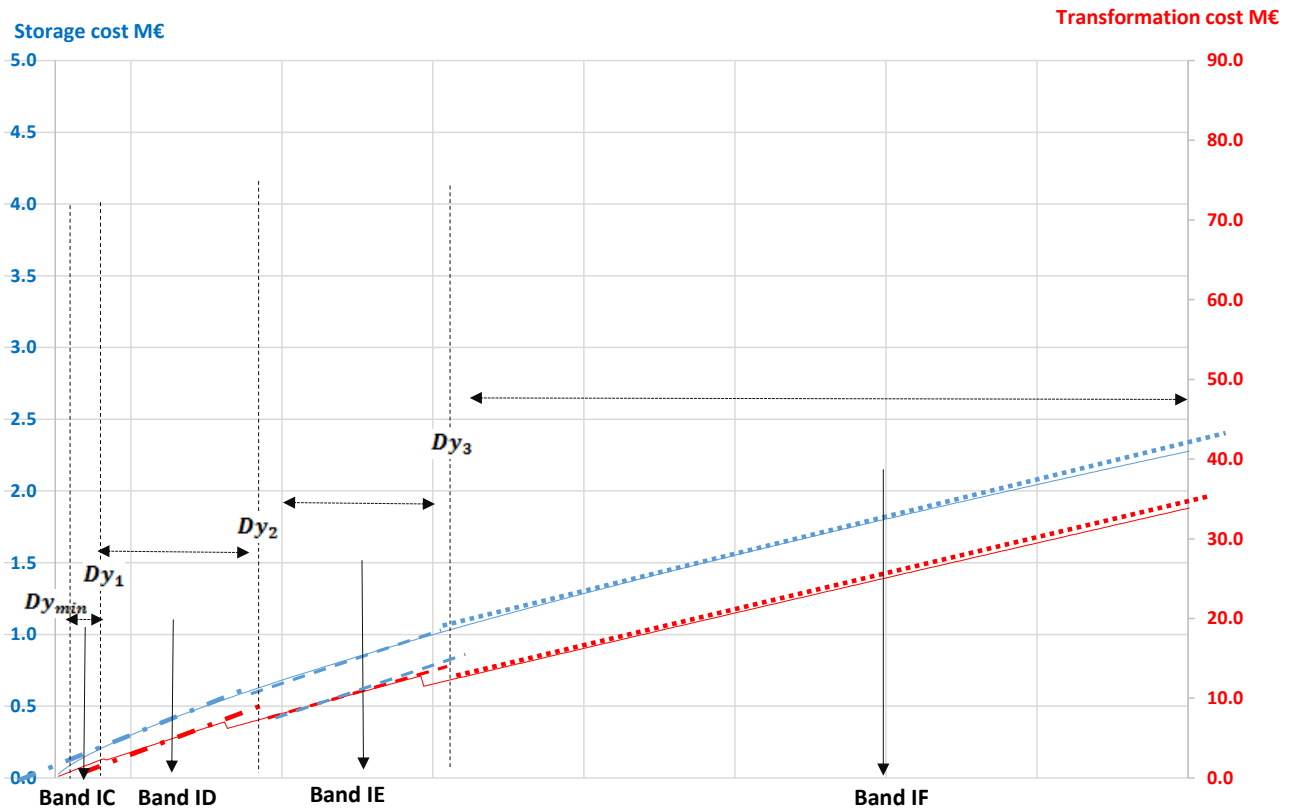
$$\varepsilon_0 = 0 \leq \varepsilon_1 \dots \leq \varepsilon_i \leq \varepsilon_{i+1} \dots \leq \varepsilon_n = 1$$

**Equation 4.41**

---

In both transformation and storage equations, the intervals were chosen equivalent to the limit of the maximum annual consumption defined by the different bands (Annex A4), as shown in Figure 4.2

**Figure 4.2:** Linearization of storage and transformation cost functions



The variable intervals  $Dy_k$  and the middle segments  $s_k$  depend on the state of aggregation of hydrogen, and the interval limits are fixed to  $Dy_{max}$  and  $Dy_{min}$ . Table 4.23 shows the different variable values of  $Dd_k$  in TPD at different state of aggregation, the corresponding yearly values are deduced by multiplying by the number of days during the year.

**Table 4.23:** Linearization parameters

	$Dd_{min} = Dd_0$	$Dd_1$	$Dd_2$	$Dd_3$	$Dd_{max} = Dd_4$
CGH	5 TPD	19 TPD	68 TPD	146 TPD	398 TPD
LOHC	3 TPD	11 TPD	40 TPD	85 TPD	398 TPD
LH	2 TPD	7 TPD	23 TPD	49 TPD	398 TPD

The sum of the Levelized cost of transforming and storing hydrogen  $LCOH_T$  and  $LCOH_S$  are defined using Equation 4.8, and the linear approximation expressed by Equation 4.39,, as shown by Equation 4.42.

$$(LCOH_T + LCOH_S) * Xy_{ij} = A_T * g_n(Xy_{ij}, \alpha_{tc}[t], s_k) + A_S * g_n(Xy_{ij}, \alpha_{sc}[t], s_k) + fVom_T * Xy_{ij}$$

$$\begin{cases} A_T = fCC_T * (CRF_T + OM_T) \\ A_S = fCC_S * (CRF_S + OM_S) \end{cases}$$

**Equation 4.42**

The fixed parameter related to the capital cost of transformation and storage  $CRF_T$  and  $CRF_S$  and the fixed operation and maintenance cost  $fVom_T$  are those defined by Equation 4.28, Equation 4.29, and Equation 4.30. The different parameters of function linearization  $\alpha_{sc}[t]$ ,  $\alpha_{tc}[t]$  and  $s_k$  depend on the SoT, as shown in Table 4.24.

**Table 4.24: Linearization parameters**

State of aggregation	CGH	LOHC	LH
Transformation sizing factor $\alpha_{tc}[t]$	0.8	0.7	0.65
Storage sizing factor $\alpha_{sc}[t]$	0.75	0.7	0.7
Segments middles in TPD			
$s_1$	[12 44	[7 26	[4 15
$s_2$	107	63	36
$s_3$	272]	242]	223]
$s_4$			

As the road cost (Equation 4.36) is expressed using the number of trucks  $Nt_y[t]$  (Equation 3.52 and Table 3.8), the definition of a ceiling number allows writing the number of trucks using an inequation, as shown in Equation 4.43.

$$\frac{Xy_{ij}}{m[t] * Nrt_y[t]} \leq Xy_{ij} < \frac{Xy_{ij}}{m[t] * Nrt_y[t]} + 1$$

**Equation 4.43**

Thus, Equation 4.43 allows writing the function  $Nt_y[t]$  as a constant  $k$  when  $Xy_{ij}$  is included in an equal interval  $]ct[t] * (k - 1), ct[t] * k]$  where  $ct[t] = m[t] * Nrt_y[t]$ .

As for compression and storage, in this case, two problems are equivalent, where the first problem is defined by Equation 4.44.

$$\min Nt_y[t]$$

$$Dy_{min} \leq Xy_{ij} \leq Dy_{max}$$

**Equation 4.44**

Furthermore, the second problem is defined by Equation 4.45.

$$\begin{aligned} \min h_n(Xy_{ij}) \\ Dy_{min} \leq Xy_{ij} \leq Dy_{max} \end{aligned}$$

---

**Equation 4.45**

Where  $h_n(Xy_{ij})$  is the sum of the approximation functions at each interval  $]ct[t] * (k - 1), ct[t] * k]$ . In this case, the approximation function is a constant equal to  $k$ , as expressed by Equation 4.46.

$$\begin{aligned} h_n(Xy_{ij}) &= \sum_{k=1}^n [k * \chi_{]ct[t]*(k-1),ct[t]*k}] \\ \chi_{]ct[t]*(k-1),ct[t]*k]} &= \begin{cases} 1 & \text{if } Xy_{ij} \in ]ct[t] * (k - 1), ct[t] * k] \\ 0 & \text{if not} \end{cases} \end{aligned}$$

---

**Equation 4.46**

Finally the sum of Levelized cost of transporting hydrogen  $LCOH_R$  is defined using Equation 4.8 and the linear approximation expressed by Equation 4.46, as shown in Equation 4.47.

$$\begin{aligned} LCOH_R * Xy_{ij} &= A_r * h_n(Xy_{ij}) \\ A_r &= (C_{Cab}) * (CRF_{Cab} + OM_{Cab}) + (C_{tra}) * (CRF_{tra} + OM_{tra}) + LC[t] + FC[t] \end{aligned}$$

---

**Equation 4.47**

The fixed parameters related to the truck capital cost and the fixed operation and maintenance costs, including fuel cost and labor cost, are those defined by Equation 4.34 and Equation 4.35.

### **I.3 Dynamic transport cost**

The annual cost can be further reduced in particular demand and distance regions by calculating the storage parameters daily. In fact, the capacity transported does not match the hydrogen demand at the destination point because of the fixed capacity of the trucks  $m[t]$ . So, in practice, the daily transported flow  $Trd_{ij}$  is the sum of the daily hydrogen demand at the destination point  $Xd_{ij}$  and the surplus capacity available for storage  $Std$ . At the next day  $d' = d + 1$ , the stored capacity of the previous day  $Std$  could be first used to fuel the demand  $Xd'_{ij}$ , before calculating the new daily hydrogen that needs to be transported  $Trd'_{ij}$ . This assumption benefits mainly liquid storage as liquid hydrogen or liquid hydrogen carrier. In fact, for both states, hydrogen is stored in tanks; this allows more flexibility to meet the demand than the compressed gas that is constrained by the tube fixed capacity.

Thus, the dynamic annual road transport cost  $Cd_R$  is associated with the daily transported capacity  $Trd_{ij}$ , and calculated using Equation 4.8 by summing  $Trd_{ij}$  over the year, as shown in Equation 4.48.

$$Cd_R = LCOH_R * \sum_{d,year} Trd_{ij}$$

**Equation 4.48**

As all the transported capacity has to be transformed as well in advance, thus applies that annual dynamic cost related to transformation  $Cd_T$  is formulated as well by summing  $Trd_{ij}$  over the year using Equation 4.8, as expressed in Equation 4.49.

$$Cd_T = LCOH_T * \sum_{d,year} Trd_{ij}$$

**Equation 4.49**

The dynamic annual cost of storage  $Cd_S$  is associated with the daily stored capacity  $Std$ , and is calculated using Equation 4.8 by summing  $Std$  over the year, as shown in Equation 4.50.

$$Cd_S = LCOH_S * \sum_{d,year} Std$$

**Equation 4.50**

### 1.3.1 Dynamic cost functions

Concerning dynamic transformation and storage costs, the same cost function defined in Equation 4.27, is used by replacing  $Xy_{ij}$  in transformation and storage cost respectively by  $Trd_{ij}$  and  $Std$  summed over the year, as shown in Equation 4.51.

$$Cd_T + Cd_S = \sum_{d,year} fCC_T * (CRF_T + OM_T) * (Trd_{ij})^{\alpha_{tc}[t]} + \sum_{d,year} fVom_T * Trd_{ij} + \sum_{d,year} fCC_S * (CRF_S + OM_S) * (Std)^{\alpha_{sc}[t]}$$

**Equation 4.51**

The different economic parameters used in Equation 4.51 are the same summarized in Table 4.22.  $fCC_T$  accounts for transformation capital cost and is defined by Equation 4.28,  $fCC_S$  accounts for storage capital cost and is defined by Equation 4.29,  $fVom_T$  accounts for variable operation and maintenance cost and is defined by Equation 4.30.

Concerning the costs associated with road transport, all the cost components are recalculated using daily parameters. Thus, the dynamic capital cost of the cab  $CCd_{cab}$  and the trailer  $CCd_{tra}$  are defined from the total daily number of trucks  $Nt_d[t]$  summed during the year, as expressed in Equation 4.52.

$$\begin{cases} CCd_{cab} = \sum_{d,year} Nt_d[t] * C_{Cab} \\ CCd_{tra} = \sum_{d,year} Nt_d[t] * (C_{und} + C_{tube}[t]) \end{cases}$$

**Equation 4.52**

This can be generalized as well for fixed operation and maintenance cost expressed as a percentage of the capital cost  $CCd_{cab}$  and  $CCd_{tra}$ , as shown in Equation 4.53.

$$\begin{aligned} O\&Md_{cab} &= \sum_{d,year} Nt_d[t] OM_{cab} * CCd_{cab} \\ O\&Md_{tra} &= \sum_{d,year} Nt_d[t] OM_{tra} * CCd_{tra} \end{aligned}$$

**Equation 4.53**

Other dynamic costs include the fuel cost  $FCd$  and labor cost  $LCd$ . In the case of daily analysis, each truck is used at its maximum annual capacity performing a daily roundtrip  $Nrt_d[ ]$  corresponding to the maximum on (Equation 3.51, Equation 3.55, and Table 3.8).

The new fuel cost  $FCd$  is then calculated by multiplying the daily fuel cost associated with each truck  $FC_d[t]$  (Equation 3.69) and the number of trucks  $Nt_d[t]$  (Equation 3.52, Equation 3.55 and Table 3.8) operating at the same SoT  $t$  summed over the year (Equation 4.34), as expressed in Equation 4.54.

$$\begin{aligned} FCd &= \sum_{d,year} FC_d[t] * Nt_d[t] \\ FC_d[t] &= 2 * \left[ \frac{CF_{RTT} * Th_d}{\frac{2 * d_{ij}}{S_a} + tt_{l/u}[t]} \right] * F_p * d_{ij} \end{aligned}$$

**Equation 4.54**

Using the same assumption, the dynamic labor cost  $LCd$  is deduced from the labor cost associated with each truck  $LC_d$  (Equation 3.70) and the number of trucks  $Nt_d[t]$  (Equation 3.52, Equation 3.55 and Table 3.8) operating at the same SoT  $t$ , as expressed in Equation 4.55.

$$LCd = \sum_{d,year} Nt_d[t] * LC_d[t]$$

$$LC_d[t] = \left[ \frac{CF_{RTT} * Th_d}{2 * d_{ij} + tt_{l/u}[t]} \right] * \left[ \frac{\frac{d_{ij}}{S_a} + tt_{l/u}[t]}{Nwh} \right] * TC_{driver} * \left( \frac{2 * d_{ij}}{S_a} + tt_{l/u}[t] \right)$$

**Equation 4.55**

Finally, using Equation 4.6, the total annual road transport dynamic cost  $Cd_R$  is expressed using Equation 4.52, Equation 4.53, Equation 4.54, and Equation 4.55, and Equation 4.35, as shown in Equation 4.56.

$$Cd_R = \sum_{d,year} [(C_{Cab}) * (CRF_{Cab} + OM_{Cab}) + (C_{tra}) * (CRF_{tra} + OM_{tra}) + LC_d[t] + FC_d[t]] * Nt_d[t]$$

$$\left\{ \begin{array}{l} C_{tra} = C_{und} + C_{tube}[t] \\ FC_d[t] = 2 * \left[ \frac{CF_{RTT} * Th_d}{2 * d_{ij} + tt_{l/u}[t]} \right] * F_p * d_{ij} \\ LC_d[t] = \left[ \frac{CF_{RTT} * Th_d}{2 * d_{ij} + tt_{l/u}[t]} \right] * \left[ \frac{\frac{d_{ij}}{S_a} + tt_{l/u}[t]}{Nwh} \right] * TC_{driver} * \left( \frac{2 * d_{ij}}{S_a} + tt_{l/u}[t] \right) \end{array} \right.$$

**Equation 4.56**

### 1.3.2 Linearization

The sum of the new Levelized cost of transforming, storing and transporting hydrogen respectively  $LCOHd_T$ ,  $LCOHd_S$  and  $LCOHd_R$  are defined using Equation 4.8 and the linear approximation  $g_n$  and  $h_n$  expressed by respectively Equation 4.39 and Equation 4.47, as shown in Equation 4.57.

$$\left\{ \begin{array}{l} LCOHd_T * \sum_{d,year} Trd_{ij} = A_T * \sum_{d,year} g_n(Trd_{ij}, \alpha_{tc}[t], s_k) + fVom_T * \sum_{d,year} Trd_{ij} \\ LCOHd_S * \sum_{d,year} Std = A_S * \sum_{d,year} g_n(Std, \alpha_{tc}[t], s_k) \\ LCOHd_R * \sum_{d,year} Trd_{ij} = \sum_{d,year} Ad_R * h_n(Trd_{ij}) \end{array} \right.$$

**Equation 4.57**

The linear approximation is defined; for transformation by replacing  $Xy_{ij}$  with  $Trd_{ij}$  in Equation 4.39; for storage by replacing  $Xy_{ij}$  with  $Std$  in Equation 4.39; and for road transport by replacing  $Xy_{ij}$  with  $Trd_{ij}$  in Equation 4.47. While  $A_T$ ,  $A_S$  and  $Ad_r$  are function independent of the transported or stored flow and defined, as shown in Equation 4.58

$$\begin{aligned}
 A_T &= fCC_T * (CRF_T + OM_T) \\
 A_S &= fCC_S * (CRF_S + OM_S) \\
 Ad_r &= (C_{cab}) * (CRF_{cab} + OM_{cab}) + (C_{tra}) * (CRF_{tra} + OM_{tra}) + LC_d[t] + FC_d[t]
 \end{aligned}$$

**Equation 4.58**

---

The fixed parameters related to cost of transformation, storage and transport are those defined by Equation 4.28, Equation 4.29, Equation 4.30, and Equation 4.56. The different parameters of function linearization  $\alpha_{sc}[t]$ ,  $\alpha_{tc}[t]$  and  $s_k$  depend on the SoT as presented in Table 4.24.

## II Optimization model

The three-stage model aims, for a network corresponding to the road one  $\mathcal{N}(\mathcal{N}, \bar{E})$ , to link a set of production nodes  $P \subset \mathcal{N}$  to a set of distribution nodes  $D \subset \mathcal{N}$  at the minimum cost using seven different states of transport (SoT)  $t$ . Thus, the general model results will give, for each edge (corresponding to a part or complete road)  $\bar{u}_{ij}$  linking two nodes  $i$  and  $j$ , the optimum annual flow  $Xy_{ij}[t]$  or the daily one  $Trd_{ij}[t]$  transported by each transport state  $t$ . This is done by linking three parallel models, as shown in where the first one is a general minimization cost along a given edge, the second one is the total flow optimization, and the third one is the minimum cost of all the network.

The first model gives the minimum cost  $Z(x_{ij}, d_{ij})[s, t]$  of transporting hydrogen from an initial state  $s$  to a transport state  $t$  for a given input flow  $x_{ij}$  and transport distance  $d_{ij}$ . Which gives as an output, the annual or daily flow  $Xy_{ij}[t]$  or  $Trd_{ij}[t]$  respectively transported by each transport state  $t$ . The second model gives the optimum flow  $Z_{i_p j_d}$  of transporting hydrogen from all the production plants  $i_p \in P$  to the distribution hubs  $j_d \in D$  for a given network  $\mathcal{N}(\mathcal{N}, \bar{E})$ . Which gives as an output the flow  $F_{i_p j_d}$  transported between each couple  $(i_p, j_d)$ . Finally, the last model gives the minimum flow cost  $C_{ij}$  of transporting hydrogen along the edge  $\bar{u}_{ij}$  for the given network flow  $F_{i_p j_d}$ . This allows calculating the final annual flow  $Xy_{ij}[t]$  (or daily flow  $Trd_{ij}[t]$ ) transported at each transport state  $t$  between each node couples  $i$  and  $j$ .

The models use the definition of the different linear programming (LP) expressed at its canonical form by:

$$\begin{aligned} & \text{minimize } c^T * x \\ & \text{subject to } A * x \leq b \\ & x \geq 0 \end{aligned}$$

This formulation allows writing the LP problem in its standard form as defined by:

$$\begin{aligned} & \text{minimize } c^T * x \\ & \text{subject to } A * x + s = b \\ & s \geq 0 \\ & x \geq 0 \end{aligned}$$

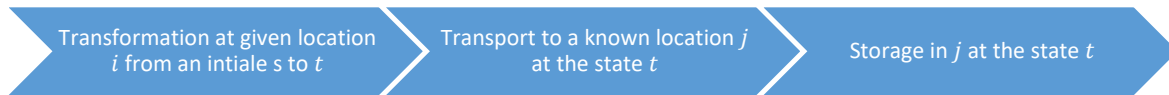
In both definitions,  $x$  is called the vector of variables (to be determined)  $c$  and  $b$  are vectors of known coefficients, and  $A$  is a matrix of known coefficients. The expression to minimize is called the objective function, in this case  $c^T * x$ , while the inequalities are called constrains in which the objective function has to be optimized, in this case:  $\begin{cases} A * x \leq b \\ x \geq 0 \end{cases}$

From the LP definition, different sub definitions are distinguished depending on the variables. Thus, an integer linear programming (ILP) is defined as a linear programming (LP) in which the variables  $x$  is restricted to be integers, and a mixed-integer linear programming (MILP) is defined as a LP in which some of its variables  $x$  are integers

## II.1 Mathematical formulation of the minimum cost for a given $(x_{ij}, d_{ij})$

Figure 4.3 shows the step used for modeling the minimum cost for an annual input flow and distance transport coordinates  $(x_{ij}, d_{ij})$  and a given initial state of aggregation  $s$ . First, for an input flow of hydrogen  $x_{ij}$ , the flow is transformed at a given location  $i$  from an initial state  $s$  to a SoT  $t$ , before being transported to a known destination  $j$  over a distance  $d_{ij}$ , the hydrogen is then stored at the destination  $j$  at the transported state  $t$ . The stored hydrogen can be transported again or distributed for consumption.

**Figure 4.3:** Steps for hydrogen transport via trucks



The minimum cost for input coordinates  $(x_{ij}, d_{ij})$  and a given initial state of aggregation  $s$  is formulated as a LP to identify the optimum combination of trucks at different states of aggregation  $t$ . Thus, the variable to be determined is the annual flow transported by each truck at different SoT  $t$  between the two locations  $Xy_{ij}[t]$ .

### II.1.1 The objective function

The cost associated with each transport state  $t$  is broken down into three types of costs. The initial cost is related to the transformation from  $s$  to  $t$ , the second cost is linked to transport cost using the SoT  $t$ , and the third cost expresses the final storage at location  $j$ .

The linear approximation of transforming and storing hydrogen (Equation 4.42) allows to write the first and the third cost, as expressed by Equation 4.59.

$$\begin{aligned} & (LCOH_T[t] + LCOH_R[t]) * Xy_{ij}[t] \\ & = A_T * g_n(Xy_{ij}[t], \alpha_{tc}[t], s_i) + A_S * g_n(Xy_{ij}[t], \alpha_{sc}[t], s_i) + fVom_T[t] * Xy_{ij}[t] \end{aligned}$$

**Equation 4.59**

$A_T$  and  $A_S$  are parameters associated with capital cost and variable operation and maintenance cost of transformation and storage, respectively (Equation 4.42), and  $g_n$  is the sum of the linear approximations as defined by Equation 4.39.

The linear approximation of road transport (Equation 4.47) allows to write the second cost is expressed by Equation 4.60

$$LCOH_R * Xy_{ij} = A_r * h_n (Xy_{ij})$$

**Equation 4.60**

---

$A_r[t]$  is the parameter associated with capital cost and variable operation and maintenance cost of each truck operating at SoT  $t$ , plus the logistics and fuel cost associated with each of them (Equation 4.47) and  $h_n$  is the sum of the linear approximations as defined by Equation 4.46.

Thus, the objective function to minimize is expressed as the sum of costs  $c_{ij}[t]$  associated with each SoT, and transport capacity  $Xy_{ij}[t]$ , as shown in Equation 4.61

$$\sum_{t \in T_s} c_{ij}[t] * Xy_{ij}[t] = \sum_{t \in T_s} (LCOH_R[t] + LCOH_T[s, t] + LCOH_S[t]) * Xy_{ij}[t]$$

$T_s = \{2,3,4,5,6,9,10\}$  corresponding to the SoT

**Equation 4.61**

---

### II.1.2 Constrains and ILP formulation

The flow is not associated with a direction of transport, therefore  $Xy_{ij}[t]$  is always positive. Moreover, each flow  $Xy_{ij}[t]$  associated with each SoT cannot exceed the total input flow to transport  $x_{ij}$  which can be translated in Equation 4.62.

$$\begin{cases} Xy_{ij}[] \leq x_{ij} \\ Xy_{ij}[t] \geq 0 \end{cases}$$

**Equation 4.62**

---

The LP problem is brought to its standard form by replacing the inequation, by the equation associated with the total flow balance. In fact, the total flow transported by the trucks at different states of aggregation must meet the total flow input is expressed in Equation 4.63.

$$x_{ij} = \sum_{t \in T_s} Xy_{ij}[t]$$

$$Xy_{ij}[t] \geq 0$$

$T_s = \{2,3,4,5,6,9,10\}$  corresponding to the SoT

**Equation 4.63**

---

The simplification of this problem to an ILP is done by considering the capacity and the distance as a discrete variable defined by a variable flow step  $\Delta x$  and a fixed distance step  $\Delta d$ , as shown by Equation 4.64.

$$\begin{aligned} x_{ij} &= \Delta x * n \\ Xy_{ij}[t] &= \Delta x * i_t \quad \text{with } (i_t, n, d) \in \mathbb{N}^3 \\ d_{ij} &= \Delta d * d \end{aligned}$$

**Equation 4.64**

The distance step  $\Delta d$  is independent of the cost optimization and is chosen constant equal to 1 km for a distance range reaching up to 500 km. The flow step is assumed variable depending on the distance step and the total flow to transport. In fact, in one hand, fixing  $\Delta x$  to a low constant step equal for instance to 1 kg/ day could be time-consuming as the total flow can exceed

500,000 kg/ day in high demand scenarios. In the other hand, fixing  $\Delta x$  to a high constant step equal for instance to 2500 kg, will not catch the cost variation at low demand scenarios where the use of truck at low capacities below 500 kg is relevant

Thus, at low demand, the lowest capacities that can be transported by one truck are 350 kg and 668 kg, respectively, corresponding to 180 bar and 250 bar. Therefore, a capacity step  $\Delta m$  of 250 kg is chosen. In the case of medium demand, the truck capacities corresponding to 1100 kg and 1230 kg allow fixing the capacity step  $\Delta m$  to 1000 kg. Finally, in case of high demand, the truck capacity step  $\Delta m$  is chosen equal to 2500 kg.

Finally,  $\Delta x$  is expressed as the product of one truck capacity step  $\Delta m$  and the annual round trip of a CGT of a maximum total loading and unloading time  $tt_{l/u}^{max}$  set equal to two hours.

$$\Delta x = \frac{\Delta m}{Ty_d} * \left[ \frac{S_a * Av.}{2 * \Delta d * p + S_a * tt_{l/u}^{max}} \right]$$

**Equation 4.65**

At the maximum distance chosen of 500 km, the flow step  $\Delta x$  is found out to vary between 0.5 TPD at low demand, 1 TPD at medium demand, and reaches 1.7 TPD at high demand.

Thus, LP can be reformulated as the ILP shown by Equation 4.66.

$$Z(x_{ij}, d_{ij})[s, t] = \min \Delta x \sum_{t \in T_s} c_{ij}[t] * i_t$$

$$n = \sum_{t \in T_s} i_t$$

$$(i_t, n) \in \mathbb{N}^{t+1}$$

**Equation 4.66**

### II.1.3 Dynamic formulation

In the case of daily transport, Equation 4.61 is expressed as the sum of two costs  $ct_{ij}[t]$  and  $cs_j[t]$ . The first one is associated with each daily transported and transformed flow  $Trd_{ij}[t]$ , while the second one is associated with each daily stored capacity  $Std[t]$  at different SoT, as shown in Equation 4.67.

$$\sum_{t \in T_s} \sum_{d, year} (ct_{ij}[t] * Trd_{ij}[t] + cs_j[t] * Std[t])$$

$$= \sum_{t \in T_s} \left( (LCOHd_R + LCOHd_T) * \sum_{d, year} Trd_{ij} + LCOHd_s * \sum_{d, year} Std \right)$$

$T_s = \{2,3,4,5,6,9,10\}$  corresponding to the SoT

**Equation 4.67**

The total flow demand is met using the daily transported and stored capacities using different states of aggregation summed over the year, as expressed in Equation 4.68.

$$x_{ij} = \sum_{t \in T_s} \sum_{d, year} Trd_{ij}[t] + Std[t]$$

$$Trd_{ij}[t] \geq 0$$

$$Std[t] \geq 0$$

$T_s = \{2,3,4,5,6,9,10\}$  Corresponding to the SoT

**Equation 4.68**

Finally, following the same ILP formulation shown in Equation 4.66, the linear problem expressed in Equation 4.67 and Equation 4.68 can be reformulated as an integer linear problem, as shown in Equation 4.69.

$$Z(x_{ij}, d_{ij})[s, t] = \min \Delta x \sum_{t \in T_s} \sum_{d, year} (ct_{ij}[t] * id_t + cs_j[t] * jd_t)$$

$$n = \sum_{t \in T_s} \sum_{d, year} id_t + jd_t$$

$$(id_t, jd_t, n) \in \mathbb{N}^{t+2}$$

Equation 4.69

## II.2 Mathematical formulation of the optimum flow

Figure 4.4 shows the step used for the modeling of the optimum flow for a given set of production and demand coordinates and input capacities  $(i_p, j_d) \in (P, D)$ . First, for an input production plant located in  $i_p$  of total capacity  $p_{i_p}$  hydrogen is produced at an initial state 0/1 and stored at the same state. Then, hydrogen is transformed from its initial state 0/1 to the transport state  $t$  to be transported to the final location  $j_d$  at different SoT  $t$  to meet the demand  $d_{j_d}$  of the destination hub.

Figure 4.4: Steps for hydrogen flow



The mathematical formulation to identify the optimum total flow to link hydrogen production nodes  $i_p \in P$  of total capacity  $p_{i_p}$  to the distribution hubs  $j_d \in D$  of demand  $d_{j_d}$  is formulated as linear programming (LP) to identify the total flow  $F_{i_p j_d}$  transported on the road network.

### II.2.1 The objective function

As all the trucks at different SoT use the same road infrastructure, the optimum total flow  $F_{i_p j_d}$  between the production and demand nodes is considered independent from the state of aggregation  $t$ . Thus, only the cost related to the transport distant  $d_{i_p j_d}$  are considered, including fuel cost  $FC$  and labor cost  $LC$ .

The linear approximation of road transport (Equation 4.47) allows writing the cost associated with the transported flow, as expressed by Equation 4.70.

$$LCOH_R * F_{i_p j_d} = A_r * h_n (F_{i_p j_d})$$

Equation 4.70

$A_r$  is associated with road transport cost, including logistic and fuel cost (Equation 4.47) and  $h_n$  is the sum of the linear approximations as defined by Equation 4.46.

Thus the objective function of the linear problem for the input set of production nodes  $i_p \in P$  and demand nodes  $j_d \in D$  that gives the optimum cost  $Z_{i_p j_d}$  of transporting hydrogen from  $i_p$  to  $j_d$  is shown in Equation 4.71.

$$Z_{i_p j_d} = \sum_{i_p \in P} \sum_{j_d \in D} LCOH_R * F_{i_p j_d}$$

---

**Equation 4.71**

### II.2.2 Constrains

The main constraints are divided on capacity constraints related to the production and distribution inputs and mass balance constraints related to the conversion of the flows entering and leaving the different nodes.

If the node is a production node ( $i_p \in P$ ) it is assumed that a hydrogen flow  $p_{i_p}$  can be produced at the initial condition 0/1 from a total installed capacity  $p_{i_p, max}$ . Thus, the total production  $p_{i_p}$  should not exceed the maximum installed capacity, as shown in Equation 4.72.

$$p_{i_p} \leq p_{i_p, max}$$

---

**Equation 4.72**

If there is also a local consumption, then the flow  $d_{i_p}$  is consumed at the final condition 7. Thus, the total production  $p_{i_p}$  is set equal to local consumption  $d_{i_p}$  and the total flow leaving the node  $i_p$ , as expressed in Equation 4.73.

$$p_{i_p} - d_{i_p} = \sum_{j_d \in N-P} F_{i_p j_d}$$

---

**Equation 4.73**

Finally, if the node is a consumption node ( $j_d \in D$ ) it is assumed that a hydrogen flow  $d_{j_d}$  is consumed at final condition  $t = 7$  and is equal to the total oncoming flows to the node  $j$ , as shown in Equation 4.74.

$$d_{j_d} = \sum_{i_p \in N-D} F_{i_p j_d}$$

---

**Equation 4.74**

### II.3 Mathematical formulation of the minimum road network cost

The mathematical formulation to identify the minimum edge flow  $x_{ij}$  to transport the hydrogen from a node  $i \in N$  at the initial state of aggregation  $s$  to a node  $j \in N$  at the final state of aggregation  $t$  is formulated as a linear optimization problem. The optimum cost is the minimum cost defined by Equation 4.66 (Equation 4.69 in case of daily calculation) to transport the hydrogen from the initial state  $s$  to a final SoT  $t$ .

In fact, for each edge, if the flow is transported between two storage edges  $(i, j) \in N - H^2$ , both states of aggregation  $s$  and  $t$  are states of transport  $(s, t) \in T_s^2$ . The optimum cost is consequently the minimum cost  $Z(x_{ij}, d_{ij})[s, t]$  defined by Equation 4.66 (Equation 4.69).

If the flow is transported between a production node  $i \in D$  to another non-production node  $j \in N - P$ , then the initial state of aggregation is at the initial state of hydrogen production state 0, and the final state is the SoT  $t \in T_s$ . The optimum cost is consequently the minimum cost  $Z(x_{ij}, d_{ij})[0, t]$ .

Finally, if the flow is transported between a non-demand node  $i \in N - D$  to another demand node  $j \in D$ , then the initial state of aggregation is a SoT  $t \in T_s$  and the final state of hydrogen demand is at the delivery condition 7. The optimum cost is consequently the minimum cost  $Z(x_{ij}, d_{ij})[s, 7]$ .

Thus, the objective function for giving the minimum cost of the road network is defined using Equation 4.75.

$$C_{ij} = \sum_{s \in T_s} \left( \sum_{i \in P} \sum_{j \in N-P} Z(x_{ij}, d_{ij})[0, t] + \sum_{(i,j) \in N-H^2} Z(x_{ij}, d_{ij})[s, t] + \sum_{i \in N-D} \sum_{j \in D} Z(x_{ij}, d_{ij})[t, 7] \right)$$

**Equation 4.75**

The input distance  $d_{ij}$  is determined for each edge as its Euclidian distance.

$$d_{ij} = d(i, j) = |i - j|$$

**Equation 4.76**

The flow  $x_{ij}$  is determined by the mass balance flow between the nodes as the sum of the flows entering the nodes  $i$  are equal to the sum of the flow leaving  $j$ .

This can be expressed using the flow  $F_{i_p j_d}$  between the different sets of production and demand nodes. In fact, all the flows  $F_{i_p j_d}$  passing by the edge  $(i, j)$  are summed up, as shown by Equation 4.77.

$$x_{ij} = \sum_{(i_p, j_d) \in I(i, j)} F_{i_p j_d}$$
$$I(i, j) = \{(i_p, j_d) \mid (i_p, j_d) \cap (i, j) \neq \{0\}\}$$

**Equation 4.77**

---

# CHAPTER FIVE

## 5 MODEL RESULTS

### **Abstract**

This chapter aims to present the model results that give the minimum cost of transporting hydrogen using road infrastructure in France and Germany. Thus, first, the Levelized cost of transporting hydrogen is given for different flow and transport distance in the case of France and Germany in order to investigate the transport states used and the different cost shares. These results are then implemented within a flow transport model in order to investigate the minimum cost of hydrogen transport for different production, demand, and infrastructure scenarios. Key findings are that the low demand scenarios corresponding to the year 2030 have the lowest infrastructure deployment cost for France and Germany varying around 862 M€, while the total cost increases for the demand year 2050 to an average of 7042 M€. In both cases, the minimum cost results correspond to distributed production plant scenarios. The results show as well that hydrogen is equally transported using low to medium pressurized tanks and higher pressurized tanks for the minimum cost results in 2030, while LOHC as a state of transport and storage is slowly introduced at low demand and reaches a share of 50% by 2050.

## Model results

### I MODEL RESULTS

<i>I.1 Results for the minimum cost</i> .....	156
I.1.1 Results corresponding to the case of France .....	156
I.1.2 Sensitivity analysis of electricity cost, comparison to the case of Germany.....	158
I.1.3 Share of compression, transformation and road transport cost .....	159
<i>I.2 Results of the optimum cost</i> .....	164
I.2.1 Standard optimum cost .....	164
I.2.2 Optimum Dynamic costs.....	165
I.2.3 Comparison.....	167

### II INFRASTRUCTURE MINIMUM COST

<i>II.1 Cost analysis</i> .....	169
<i>II.2 Share analysis</i> .....	173

### III FLOW RESULTS

<i>III.1 Demand scenarios comparison</i> .....	176
<i>III.2 Road infrastructure scenarios comparison</i> .....	180
<i>III.3 Production scenarios comparison</i> .....	182

## Acronyms

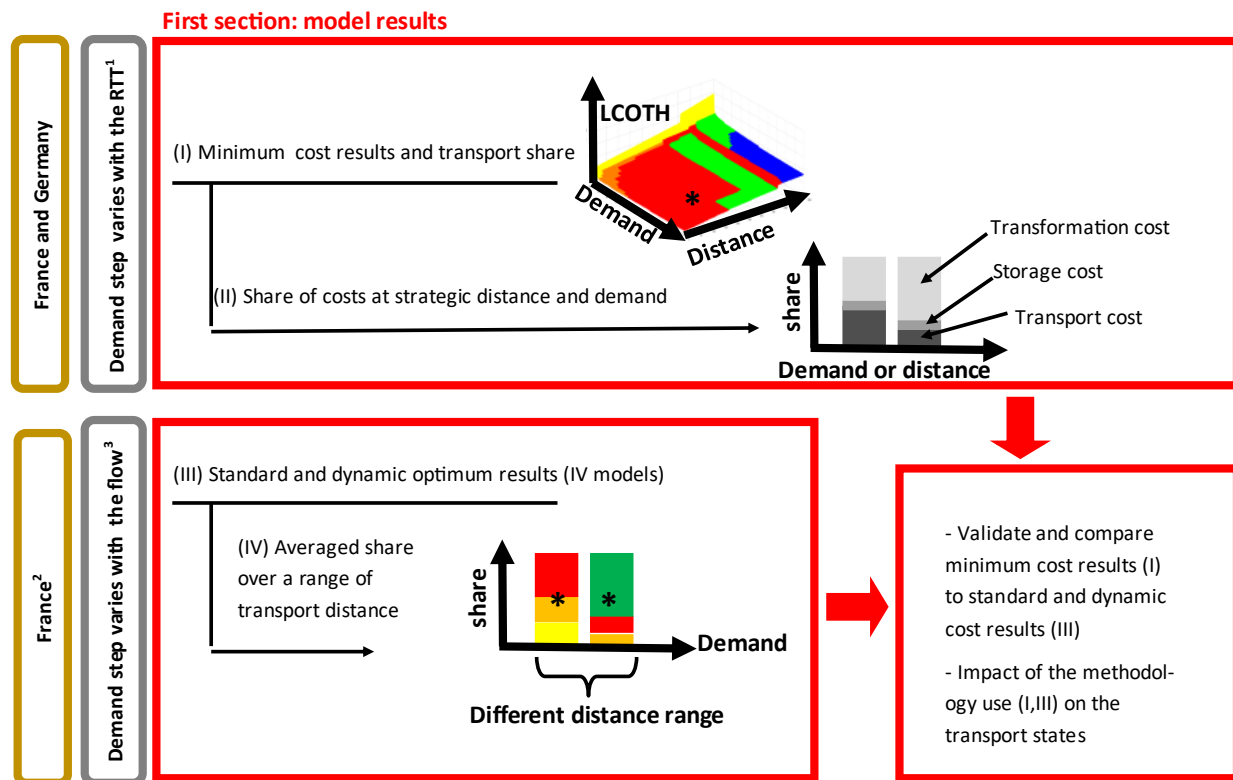
RTT	Road transport truck
LCOTH	Levelized cost of transporting hydrogen
SoT	State of transport
CGH	Compressed gas hydrogen
LH	Liquid hydrogen
LOHC	Liquid organic hydrogen carrier
OP	Standard optimization
DY	Dynamic optimization
SD	Standard deviation
NRW	North Rhine-Westphalia
IDF	Île-de-France
BOR	Border
$S_1 - S_{p9}$	Production, demand and infrastructure scenarios
D1 - D12	Main demand hubs
P1 – P73	Distributed production hubs

## Nomenclature

Parameter		First appearance	Unit
$D_{ij}$	Flow difference between scenarios $S_2$ and $S_3$	Equation 5.78	-
$F_{2ij}$	Flow of the scenario $S_3$	Equation 5.78	-
$F_{3ij}$	Flow of the scenario $S_3$	Equation 5.78	-

**T**he fifth chapter is divided in three subsections that aim to validate, compare, and analyze the results as summarized in Figure 5.1. In the first section (Figure 5.1), the different models introduced in chapter IV are run in parallel using different modeling tools depending on the type of data processed. Thus, the output used for parallel modeling calculations and implemented manually are compared and investigated. The results include a minimum cost comparison (I in Figure 5.1) and two optimum cost calculation methods (III in Figure 5.1) at different transport distances and hydrogen demand for France and Germany. The different transport states used (I and IV in Figure 5.1) and the corresponding cost-shares (II in Figure 5.1) are also investigated to explain the results.

**Figure 5.1:** Different results section, a specification for the model results



\* The different colors depend on the state of transport as compressed gas, liquid hydrogen, or liquid bounded to a carrier ■ low CGT , ■ medium CGT , ■ high CGT , ■ LOHC , ■ LH.

<sup>1</sup> In the minimum cost comparison, the demand step is chosen equal to the capacity transported by each Road transport truck (RTT)

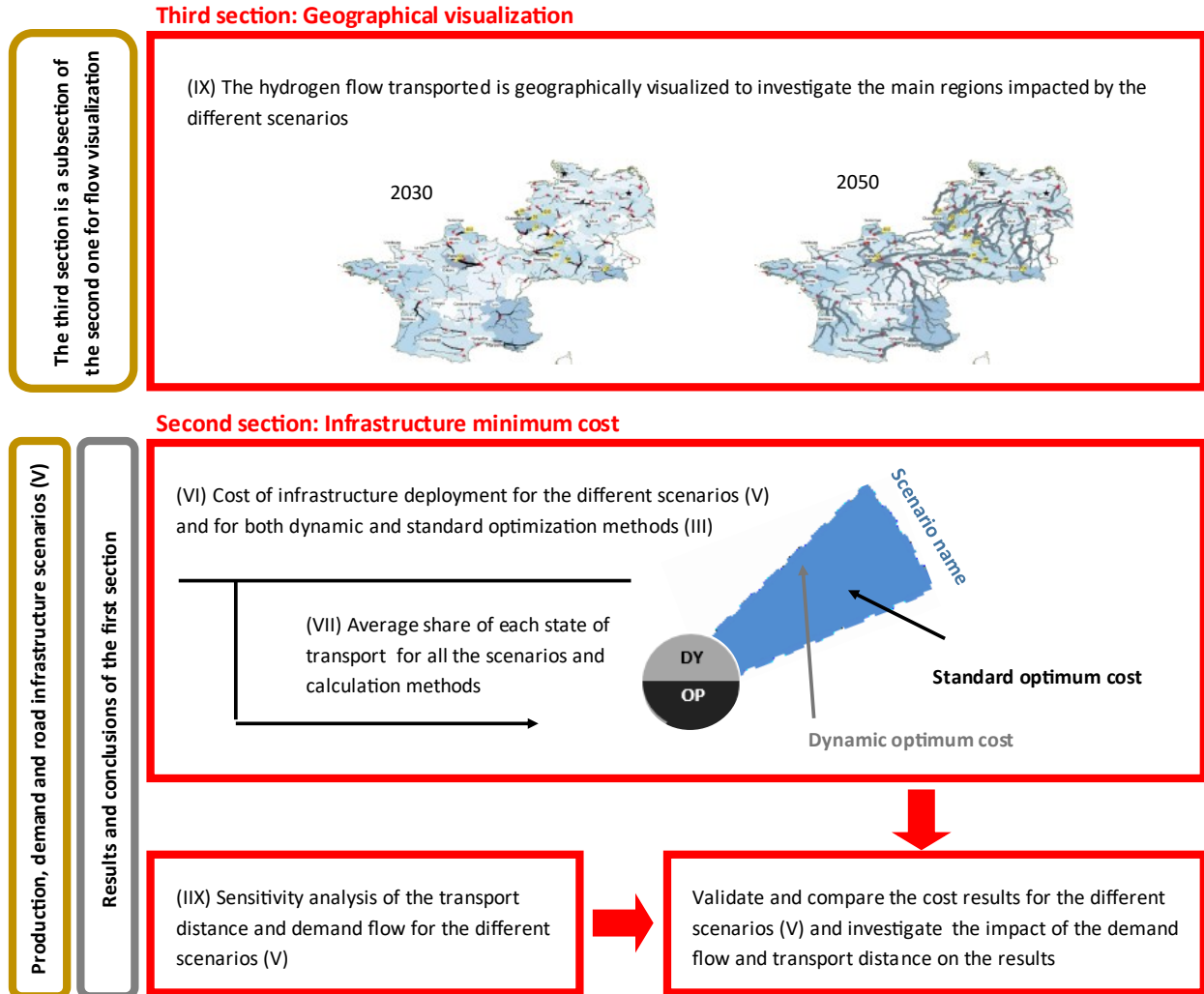
<sup>2</sup> Only the results of France are shown as it allows the use of LH state; nevertheless, the calculations are performed for both countries.

<sup>3</sup> The demand step is fixed for all RTT, and chosen equal to 0.5 TPD at low demand, 1 TPD at medium demand and reaches 1.7 TPD at high demand (chapter IV)

In the second section ( Figure 5.2), the first section outputs are applied to hydrogen transported in France and Germany for different production and demand scenarios (V in Figure 5.2). The results allowed the estimation of the total infrastructure deployment cost for the different scenarios and both calculation methods (VI in Figure 5.2). As for the first section, the different share of transport states used (VII in Figure 5.2) along with a sensitivity analysis of transport distance and hydrogen flow (IIX in Figure 5.2) is performed to interpret the results. Finally, the third section ( Figure 5.2) shows the geographical visualization of the essential results and focuses

on the hydrogen flow change with the road infrastructure, production, and demand frameworks (IX in Figure 5.2).

**Figure 5.2:** Different results section, a specification for the infrastructure results



## I Model results

As introduced in the literature review (Chapter I), the cost of hydrogen infrastructure was investigated by exploring the minimum cost between different transport pathways (Yang & Ogden, 2007) or via a cost optimization using linear programming. Thus, in this chapter, both methods results = are presented to investigate the optimization method impact on reducing the cost. Moreover, the two optimum calculation methods introduced in chapter IV are analyzed; a standard one where hydrogen stored and transported are coupled and calculated annually under an annual hydrogen flow, and a dynamic one where transported capacity is decoupled from the stored one and calculated daily.

### I.1 Results for the minimum cost

To check the validity and the coherence of the results, the capacity step  $dxt$  was the chosen variable depending on the way of transporting hydrogen. This capacity step corresponds to the truck capacity, which corresponds to the minimum cost at each state of transport SoT, as each truck is used as its optimum capacity.

Figure 5.1 shows the Levelized cost of transporting hydrogen  $LCOTH$  for a distance  $d_{ij}$  reaching 500 km and a maximum daily demand  $Dd_j$  of 100 TPD. The different colours correspond to the corresponding state of transport used. To better visualize the different distance and demand areas where each SoT was used, the second figure shows the color range at different distance and demand. For the sake of consistency of the results, a cost difference below 0.2% was neglected. Meaning, that in the case where the cost difference between two SoT was below 0.2%, only the SoT corresponding to the similar SoT in the neighborhood distance and demand coordinates were chosen.

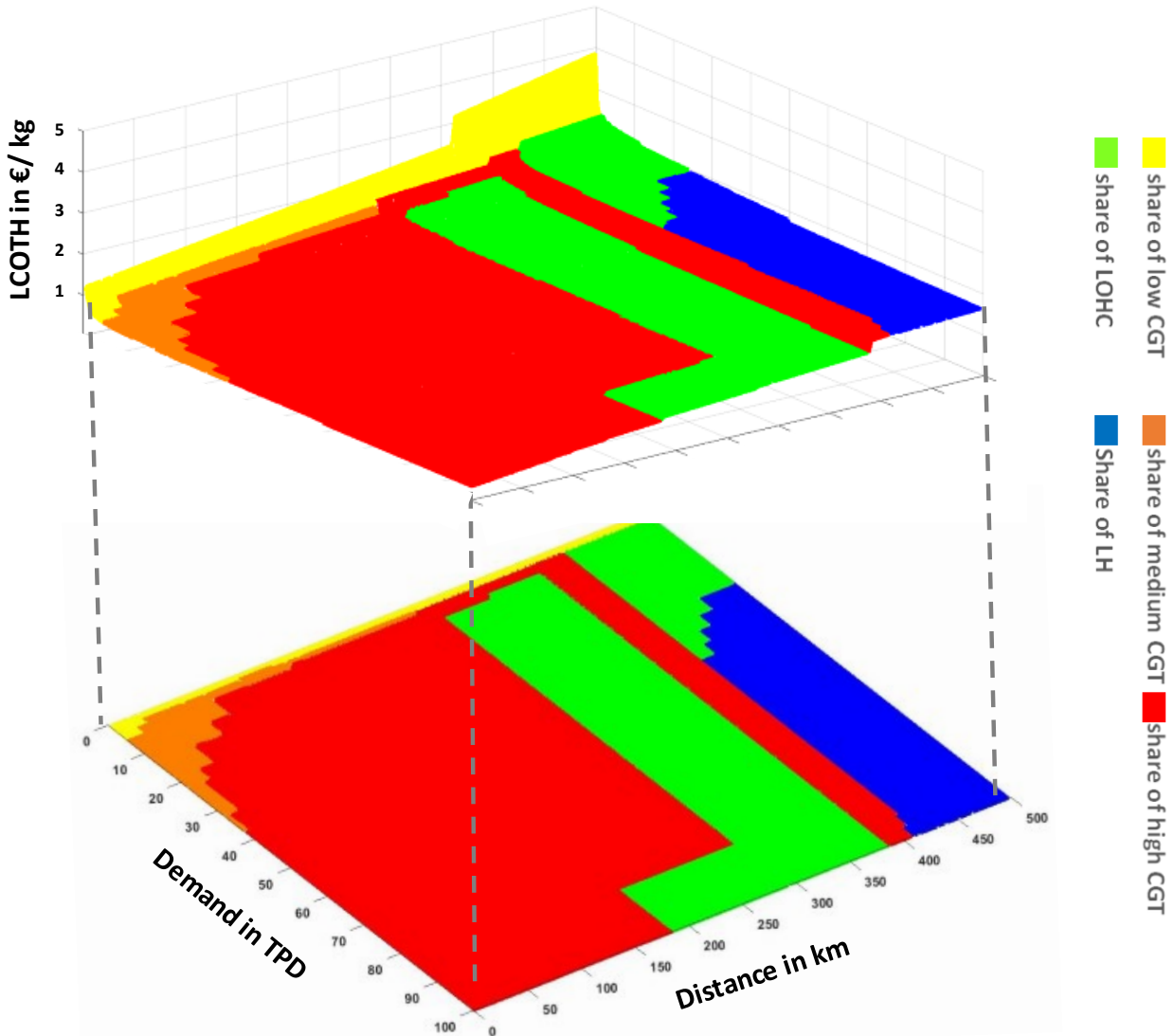
#### I.1.1 Results corresponding to the case of France

The first results shown in Figure 5.3 are those of France where the total transporting cost  $LCOTH$  is below 4 €/ kg for the distance and demand range chosen. The higher cost occurs at low daily demand  $Dd_j$  below 2 TPD and high transport distance exceeding 400 km.

At low daily demand, the cost increases by more than 1 €/ kg compared to higher demand flows. These higher costs are associated with the use of compressed truck gas at low pressure levels as a transport option.

At high transport distances, the costs increase by more than 0.5 €/ kg compared to a low transport distance. LOHC is first used to transport daily demand below 30 TPD. Exceeding this value, LOHC is gradually replaced by liquid hydrogen for road transport up to 48 TPD, where all hydrogen is transported as a liquid.

**Figure 5.3:** Levelized cost of transporting hydrogen for France



LCOTH: Levelized cost of transporting hydrogen

Compressed hydrogen gas (CGH) at medium pressure level is used as a transition SoT between low and high pressure CGH for a transport distance reaching 75 km and a daily demand ranging between 2 and 30 TPD.

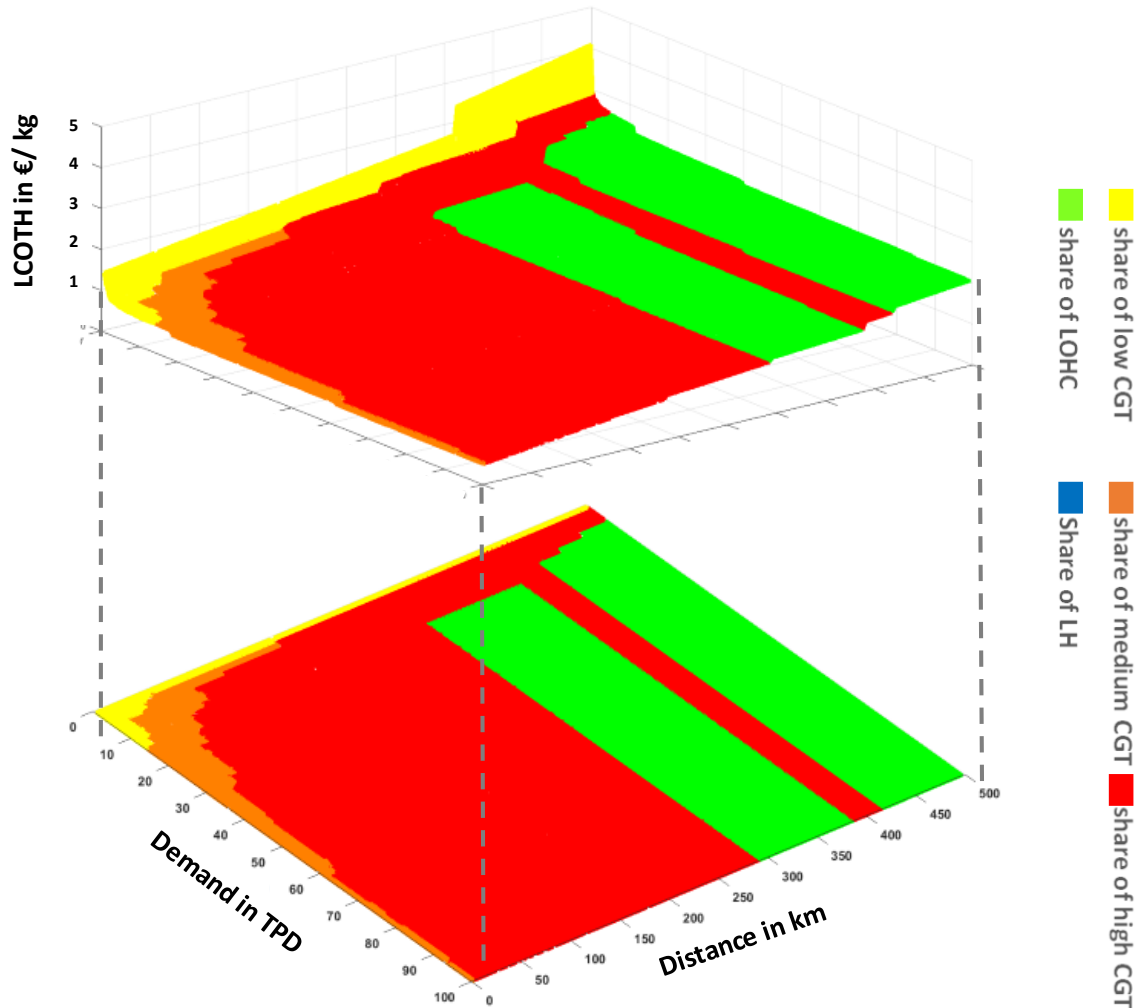
High pressure CGH is used for the main transport below 180 km, exceeding this distance, LOHC gradually replaces it, and above 300 km, it is mostly replaced by LOHC.

An exception around 400 km is noticeable, when usually LOHC should be used and is replaced by CGH at a high pressure level due to logistical costs as is detailed in the part on costs shares.

### 1.1.2 Sensitivity analysis of electricity cost, comparison to the case of Germany

The results of Figure 5.3 are compared to the German case, shown in Figure 5.4, which has different electricity costs. These results show the impact of higher electricity prices on hydrogen transformation (mainly liquefaction) and thus on total transport costs and the states of the transport used.

**Figure 5.4:** Levelized cost of transporting hydrogen for Germany



LCOTH: Levelized cost of transporting hydrogen

The higher electricity price chosen for Germany impacts on the cost of transporting hydrogen as the maximum value of LCOTH in the range of demand and distance studied exceeds 4 €/ kg.

This difference is more visible at a higher demand range above 50 TPD and a higher distance above 400 km. The cost in the German case exceeds 2 €/ kg, while it is below 1.75 €/ kg in France.

This difference in price at higher demand and distance also impacts the SoT chosen, as liquid hydrogen, which has a higher energy demand, is not chosen as a transport option in the German case and was replaced by LOHC.

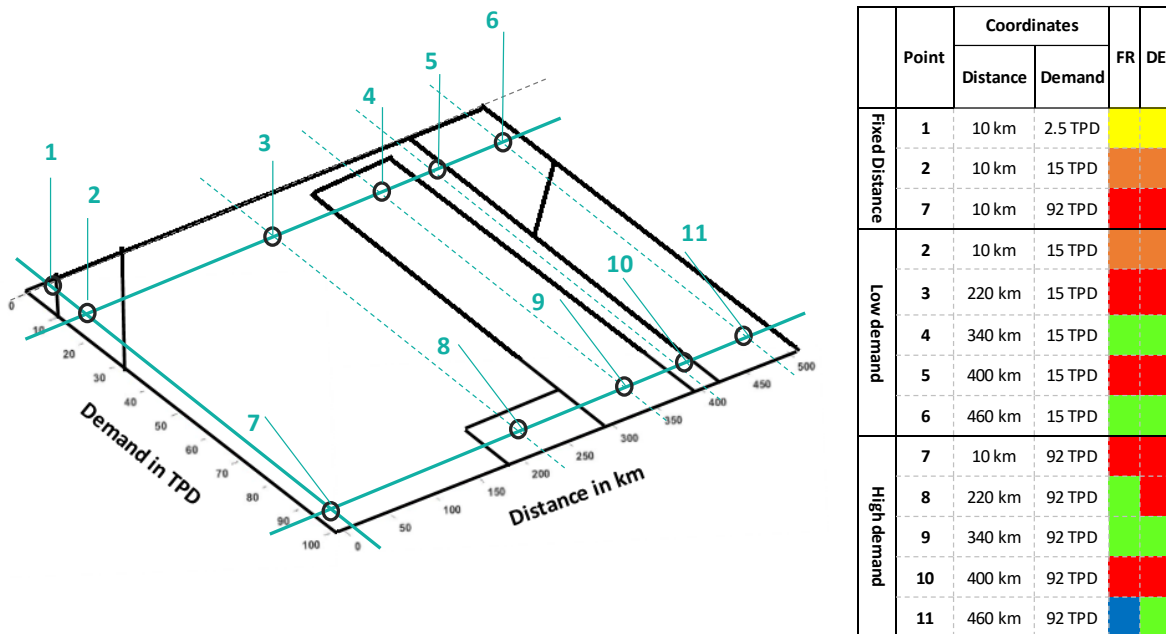
As in the French case, and despite higher hydrogen transport costs, the use of low and medium CGH occurs in the same distance and demand ranges. At a distance between 200 and 300 km and demand above 87 TPD, the use of LOHC in the French case was replaced using high pressure CGH. This choice of the transport state with lower energy needs is noticeable in all the transition regions (where the change of SoT occurs) that apply lower electricity prices.

Finally, the same exception also occurs around 400 km, where high pressure CGH seems to have an advantage over LOHC.

### 1.1.3 Share of compression, transformation and road transport cost

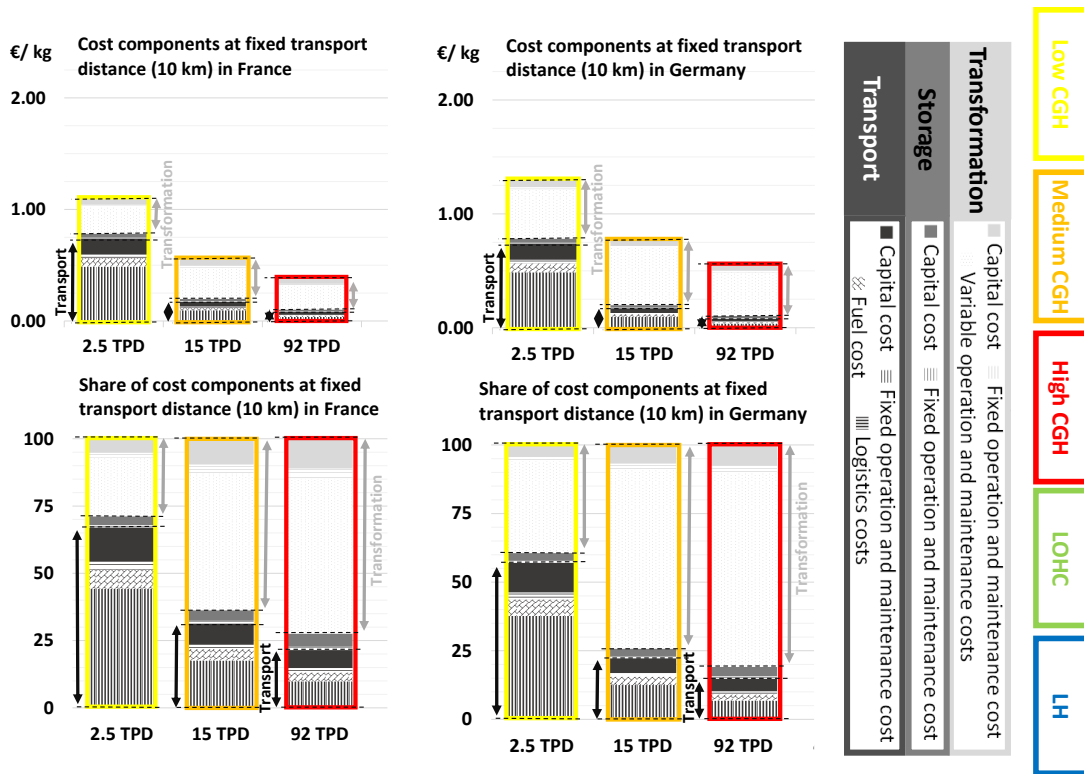
To proof check the validity of the results and to explain the different results obtained, the cost was broken down into different shares associated with the transformation, road transport, and storage. These shares were calculated at strategic points where the state of transport changed for France and Germany, as shown in Figure 5.5.

**Figure 5.5:** Points of cost shares calculation



The first line passes by points 1, 2, and 7 and corresponds to the costs and cost shares for a fixed distance 10 km (Figure 5.6), where the hydrogen is transported as CGH at a similar SoT for both countries.

**Figure 5.6:** Costs at a fixed distance of 10 km



For both countries, at fixed distance groups of 10 km, the costs related to transporting hydrogen are the same. This cost decreases with the increase of transported capacity, which decreases the share of transport costs from 67% and 57% in France and Germany, respectively, to 21% and 15%, respectively (Figure 5.6).

This cost decrease is related to the use of CGH at a higher pressure level. In fact, switching to medium pressure CGH at 15 TPD, and then to 92 TPD at high pressure CGH increases the capacities transported, which reduces the CGH needed, and thus the number of round trips and the number of drivers needed.

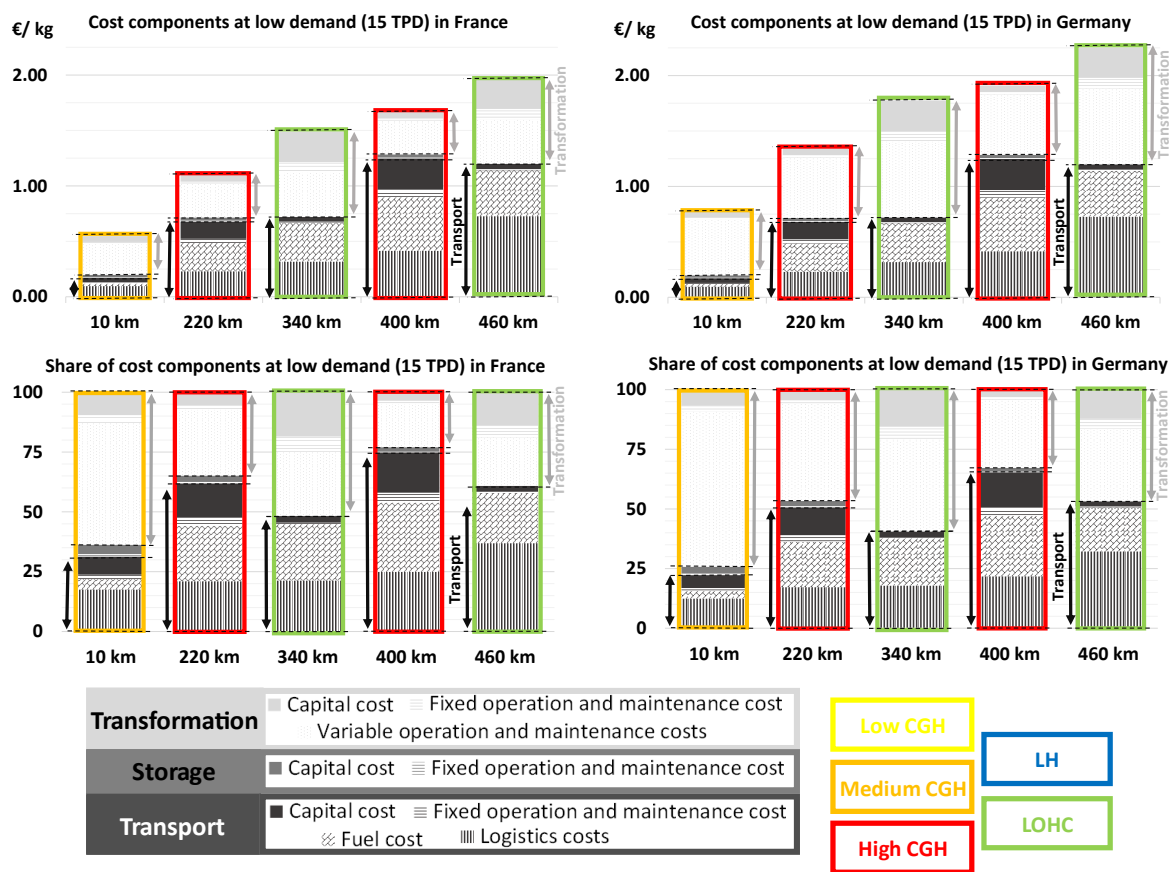
The use of higher pressure level CGH is made possible thanks to the economy of scale. The increase in energy demand due to the increase of pressure level is balanced by the increase of hydrogen quantity as well. Thus, the Levelized cost of variable operation and maintenance cost that includes transformation cost is mainly constant.

The decrease in transport cost in relation to fixed transformation cost increases the share of transformation cost in France from 29% to 72%.

The higher electricity cost in Germany increases the variable operation and maintenance cost related to compression, and this results in a higher share of transformation cost of 11% at low and medium CGH and 9% at high pressure CGH.

The second comparison corresponds to the line passing by points 2, 3, 4, 5, and 6 (Figure 5.5) corresponding to the costs and cost shares at a low fixed demand of 15 TPD (Figure 5.7). The hydrogen is transported as CGH and LOHC, and similar results can be seen for both countries.

**Figure 5.7:** Cost at low demand of 15 TPD



At fixed low demand of 15 TPD, and below a transport distance of 220 km, CGH is used to transport hydrogen. The increase of the distance in both countries increases the number of round trips and driver working hours, and, because of limited truck annual availability, increases the number of trucks as well and, thus, the capital cost of transport. Consequently, the share of transport increase from 31% to 62% in France, and from 22% to 51% in Germany. This difference between the two countries comes from the difference in electricity prices.

This increase in transport costs can be reduced by switching to a higher SoT capacity and/ or SoT with lower investment costs. Thus, at 340 km, the use of LOHC reduces the capital cost of transport by lowering the cost of the LOHC tube trailers. Consequently, even with higher fuel and logistics costs due to the increase of the transport distance, the total transport cost is kept constant equal to 0.7 €/ kg. The cost increased only because of the increase of transformation and investment cost associated with the use of de- and hydrogenation process estimated at 0.3 €/ kg compared to 0.1 €/ kg for high CGH.

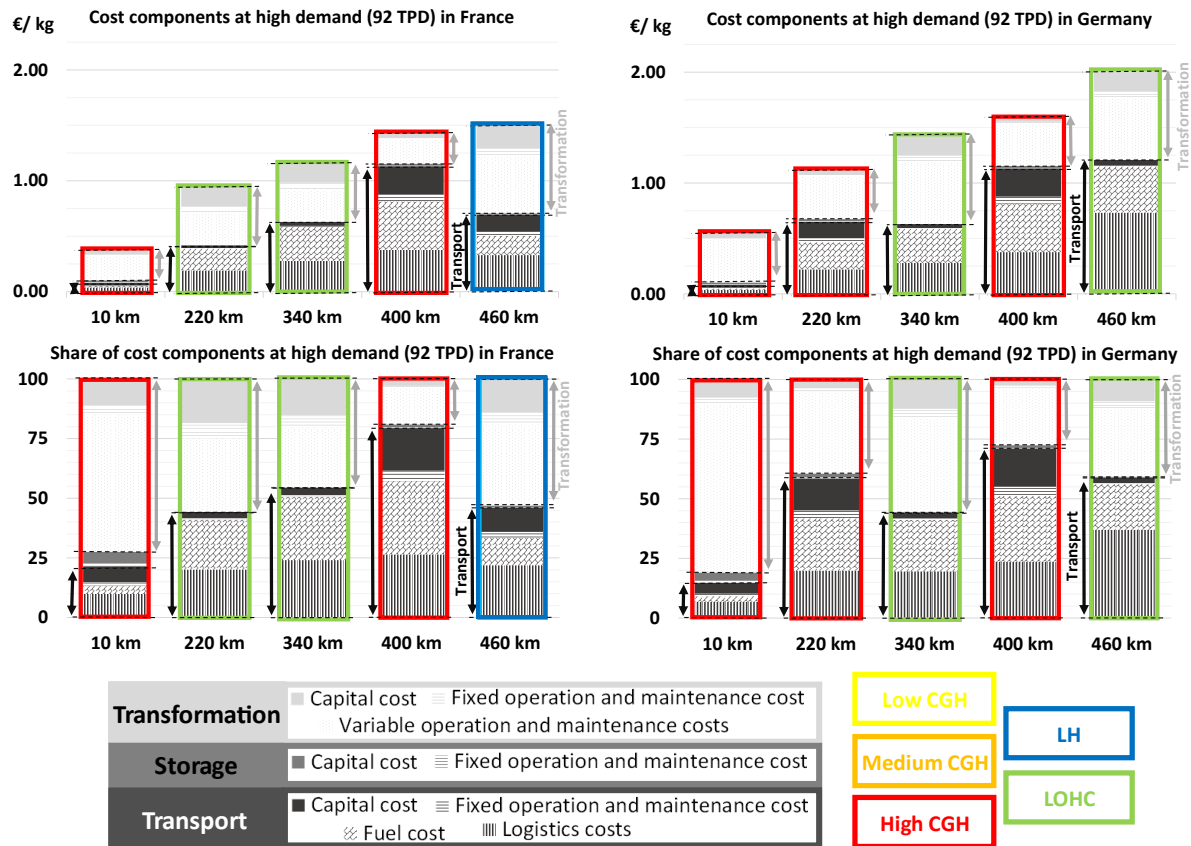
From 400 km, the logistics costs are doubled because of the use of two simultaneous drivers, independently of the choice of the SoT, accounting for a new cost of 0.4 €/ kg and 0.7 €/ kg for high pressure CGH and LOHC, respectively.

Therefore, at 400 km, continuing using LOHC will still maintain the transport cost above 1 €/ kg, which will increase the total cost to 1.8 €/ kg. Thus, the increase in logistics costs forces the re-use of CGH with lower transformation costs.

The same behavior is noticeable in the transition between 400 km and 460 km and between 220 km and 340 km as switching from high pressure CGH to LOHC leads to constant total transport cost of 1.2 €/ kg because of lower investment costs on the tube trailers.

Finally, the third line passes by points 7, 8, 9, 10, and 11 corresponding to the costs and cost shares at a high fixed demand of 92 TPD (Figure 5.8). The hydrogen is transported using all the states of transport, and differences in results are noticed between France and Germany at transport distances of 220 km and 460 km.

**Figure 5.8: Costs at high demand of 92 TPD**



As seen for the comparison at a fixed distance, switching from a low demand of 15 TPD to 92 TPD promotes the use of hydrogen at a higher transport state with higher transformation costs because of the economy of scale (high pressure CGH and LOHC, and LH in the case of France at high transport distance).

In fact, for both countries, the results show that high pressure CGH is used at 10 km transport distance, while LOHC is preferred at 340 km. With the increase of the distance, the switch to a SoT with higher energy content is not automatic in the case of Germany, because the higher electricity prices will result in higher transformation costs. For instance, an increase of 0.2 €/ kg for CGH and 0.3 €/ kg for LOHC is seen for variable operation and maintenance transformation cost in Germany compared to France.

Thus, in Germany, high pressure CGH is still an optimal option over LOHC at a transport distance of 220 km; And LOHC is still an optimal option over LH at a transport distance of 460 km.

As for the case of low demand, the logistics costs are doubled from 400 km, which applies the re-use of high pressure CGH that has lower transformation cost.

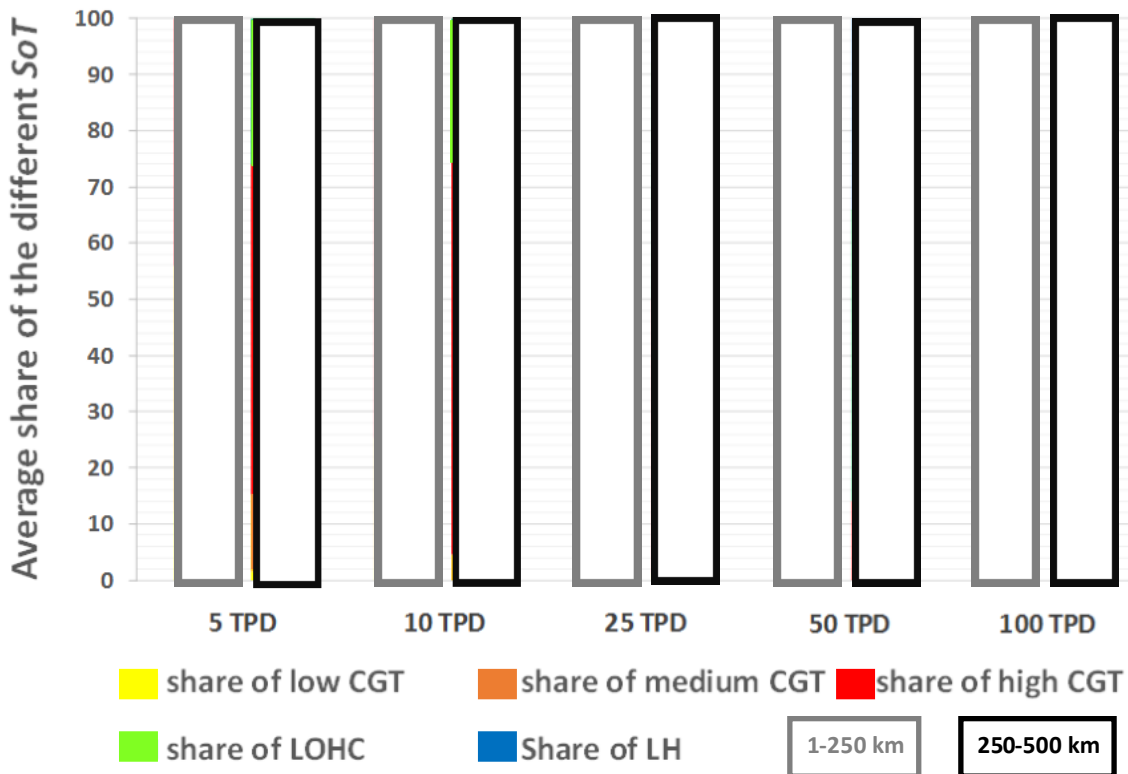
## 1.2 Results of the optimum cost

The optimum cost results, in contrast to the minimum costs one, are obtained using the linear optimization problem to allow the transport of a given flow at different SoT at the same time and thus minimizing further the total costs. These results are broken down into two model results and compared to each other. The first one, the standard optimization problem, uses linear cost functions calculated based on the annual technical assessment of coupled transported and stored flow capacities. The second one, the dynamical optimization problem, uses linear cost functions calculated based on the daily technical assessment of decoupled transported and stored flow capacities, giving priority to the use of stored excess capacity due to its lower cost.

### 1.2.1 Standard optimum cost

Figure 5.9 shows the average share of SoT calculated for two ranges of distances of 1-250 km, and 250-500 km at five different flow transported corresponding to 5, 10, 25, 50, and 100 TPD. These results correspond to the optimization cost using the standard cost function based on a coupled technical and economic assessment.

**Figure 5.9:** Average share of SoT for the standard optimization problem in%



As expected, the increase of the demand and the range distance increase the use of SoT with higher transported capacity. For instance, at the range distance below 250 km and low demand of 5, 10 TPD, and 25 TPD, only compressed gas trucks are used. Thus, to transport a total flow of 5 TPD, 10 TPD, and 25 TPD, respectively, low pressure CGH is used at a share of 12.4%, 2.2%, and 1.2%, medium pressure CGH is used at a share of 43.6%, 23%, and 7.3% respectively, and high pressure CGH is used at a share of 44%, 74.8%, and 91.5%, respectively. These results also show the gradual switch from low and medium pressure CGH at 5 TPD to high pressure CGH at 25 TPD. At medium demand of 50 TPD, high pressure CGH is widely used as well at a share of 96.7%, but LOHC also starts to be used at a low distance range with a share of 2%. Finally, with the increase of the demand at higher flow, the use of LOHC increases as well to reach, for instance, 10% at 100 TPD transported flow.

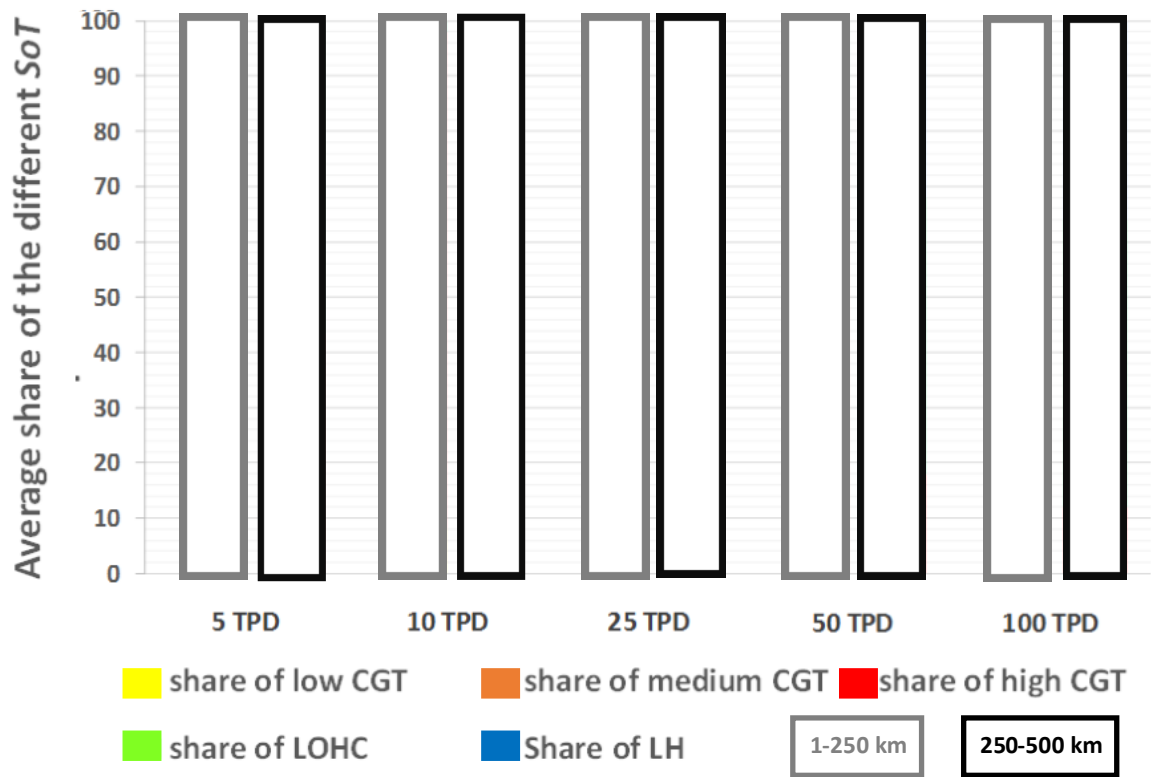
Concerning the distance range above 250 km, mainly high pressure CGH is used at low demand, while liquid transport is used at medium and high transported flow. Besides the use of high pressure CGH, medium pressure CGH share decreases at low demand with the increase of transported flow from 13.6% to 4.5% at 5 and 10 TPD, respectively. From a transported flow of 25 TPD, most of the flow is transported using liquid states. Thus, LOHC share increases from 42.2% to 52% and then to 54%, at a transported flow of 25, 50, and 100 TPD respectively, while LH share increases from 8% to 34% and then 34.2% at a transported flow of 25, 50, and 100 TPD respectively.

Finally, the impact of logistics costs is still noticeable, as high pressure CGH is still used at the share of 12% even with a high transported capacity of 100 TPD. This limits mainly the use of the transported liquid form, as the use of LOHCT and LH increase with only 3.8% and 0.3% respectively, while the transported flow doubled to 100 TPD.

### *1.2.2 Optimum Dynamic costs*

Figure 5.10 shows the average share of SoT calculated for two ranges of distance of 1-250 km, and 250-500 km at five different transported flows corresponding to 5, 10, 25, 50, and 100 TPD. This result corresponds to the optimization cost using the dynamic cost function based on a decoupled technical and economic assessment.

**Figure 5.10:** Average share of *SoT* for the dynamic optimization problem in%



As for standard linear optimization, a more significant demand and range distance increase the use of *SoT* with higher transported capacity. For instance, at the range distance below 250 km and low demand of 5, 10, and 25 TPD, mainly compressed pressure gas trucks are used. Thus, to transport a total flow of 5 TPD, 10 and 25 TPD, low and medium pressure CGH are used at a share of 36%, 8 and 2%, respectively and high pressure CGH is used at a share of 62%, 90%, and 96%, respectively. These results show the gradual switch as well from low and medium pressure CGH at 5 TPD to high pressure CGH at 25 TPD. At medium and high demand of 50 and 100 TPD, the high pressure CGH share decreases to 74 and 72%, respectively, while being replaced by LOHC that reaches a share of 26 and 28%, respectively.

Concerning the distance range above 250 km, mainly LOHC is used at low demand below 25 TPD, while both liquid transport states are represented at medium and high transported flows. Below 25 TPD, the LOHC share increases from 57% to 66% and 62% at a transported flow of 5 and 25 TPD, respectively, while LH share increases from 4% to 32% and 36% at a transported flow of 50 and 100 TPD, respectively.

Finally, as noticed for standard linear optimization, the impact of logistics costs is noticeable as well, as high pressure CGH is still used at a share of 12% even with a high transported capacity of 100 TPD.

### 1.2.3 Comparison

Table 5.1 and Table 5.2 show the impact of decoupling storage and transport capacities on reducing the cost by using the liquid state to transport hydrogen, mainly LOHC, at large distances above 200 km. From the overall result available in Annex (Table A.18, Table A.19, and Table A.20), the main difference between dynamic and standard optimization happens at low demand. Thus, the comparison of the simple cost minimum results focuses on low transported capacities of 5, 10, and 25 TPD.

First, Table 5.1 uses the results show in Annex (Table A.18, Table A.19, and Table A.20) to sum up the cost reduction using the optimum cost and the dynamic optimum cost methods compared to a simple cost minimum cost comparison. Then Table 5.2 uses the tables in Annex (Table A.18, Table A.19, and Table A.20) to sum up the results for LOHCT at an average distance between 250 and 500 km.

**Table 5.1:** Impact of the cost calculation methodology on the minimum cost

		1 - 100 km			100 - 200 km			200 - 300 km			
		5 TPD	10 TPD	25 TPD	5 TPD	10 TPD	25 TPD	5 TPD	10 TPD	25 TPD	
(1)		7.38%	6.02%	1.79%	8.49%	2.57%	1.12%	3.45%	1.47%	1.56%	
(2)		11.12%	10.24%	7.19%	12.58%	5.90%	3.98%	6.73%	5.71%	3.51%	
		300 - 400 km			400 - 500 km						
		5 TPD	10 TPD	25 TPD	5 TPD	10 TPD	25 TPD				
(1)	Cost decrease using optimum cost	3.37%	1.69%	0.97%	2.25%	2.10%	1.00%				
(2)	Cost decrease using dynamic optimum cost	6.06%	0.79%	0.96%	9.95%	8.64%	3.96%				

From the results of Table 5.1, it is clear that at demand flow below 10 TPD and low transport distance below 100 km, both approaches allow a high cost reduction ranging between 6.0% and 10.2% at 10 TPD, and between 7.4% and 11.1% at 5 TPD. Thus, the principal cost reduction comes from the use of the linear optimization method, independently of the cost function methodology calculation.

The impact of the use of the dynamical method that uses a cost function calculated from decoupled transport and storage capacities increases with the increase of hydrogen flow. Thus, at 25 TPD, 7.2% (2) cost reduction is achieved compared to only 1.8% (1) at a transported distance below 100 km. Another parameter that promotes the use of the second methodology is low flow demand below 10 TPD, transported over a long distance above 400 km. In this case, between

8.6% and 10.0% reduction is performed using the dynamic method, compared to a reduction ranging between 2.1% and 2.3% using a standard linear optimization method.

Finally, as introduced in the minimum cost results, the use of two drivers for the truck transport double the logistical costs. Thus, a compressed gas truck is again used instead of LOHC at distances around 400 km, even at a higher demand. At the linear optimization method, the restrained use of LOHC at this range distance does not achieve significant cost reductions. Thus, the cost reduction, for both methodologies, and all transported flow ranges below 25 TPD is minimized at transport distance between 300 km and 400 km.

**Table 5.2:** Impact of the cost calculation methods on the use of LOHC

Transported flow	Minimum cost	Optimum cost	Dynamic optimum cost
5 TPD	23.4%	22.2%	56.7%
10 TPD	27.5%	26.0%	66.0%
25 TPD	30.2%	46.9%	62.0%

Table 5.2 shows that, at low demand and for range distance between 250 and 500 km, the dynamic optimization method uses the highest share of LOHC of transporting 5, 10, and 25 TPD. Moreover, in the three cases, this SoT represented the majority compared to compressed gas or liquid hydrogen.

In fact, in the dynamic optimization method, the stored capacity is decoupled from the transported one in technical assessment and is not equal to the hydrogen demand. Thus, the assessment is performed daily, which allows the storage of the surplus hydrogen transported at the end of the first day and not consumed, and it can be made available for local consumption for future use. By allowing this, storage is favored over transport, and liquid storage benefits from this, as it enables more flexibility because of the pumped liquid stored in tanks with flexible size, while compressed hydrogen is still restrained by its tube capacity.

To conclude, while the standard linear optimization method is performed in all range cases as it allows a significant cost reduction, the dynamic optimization is only restrained at low demand, at a low distance below 250 km or a high transport distance above 400 km.

## II Infrastructure minimum cost

Depending on the range of transport distance and hydrogen flow, the methodology of cost optimization with and without dynamic analysis introduced before was applied for the different case scenarios introduced in chapter 3 and summarized in Table 5.3.

**Table 5.3:** Different scenarios for infrastructure cost calculation

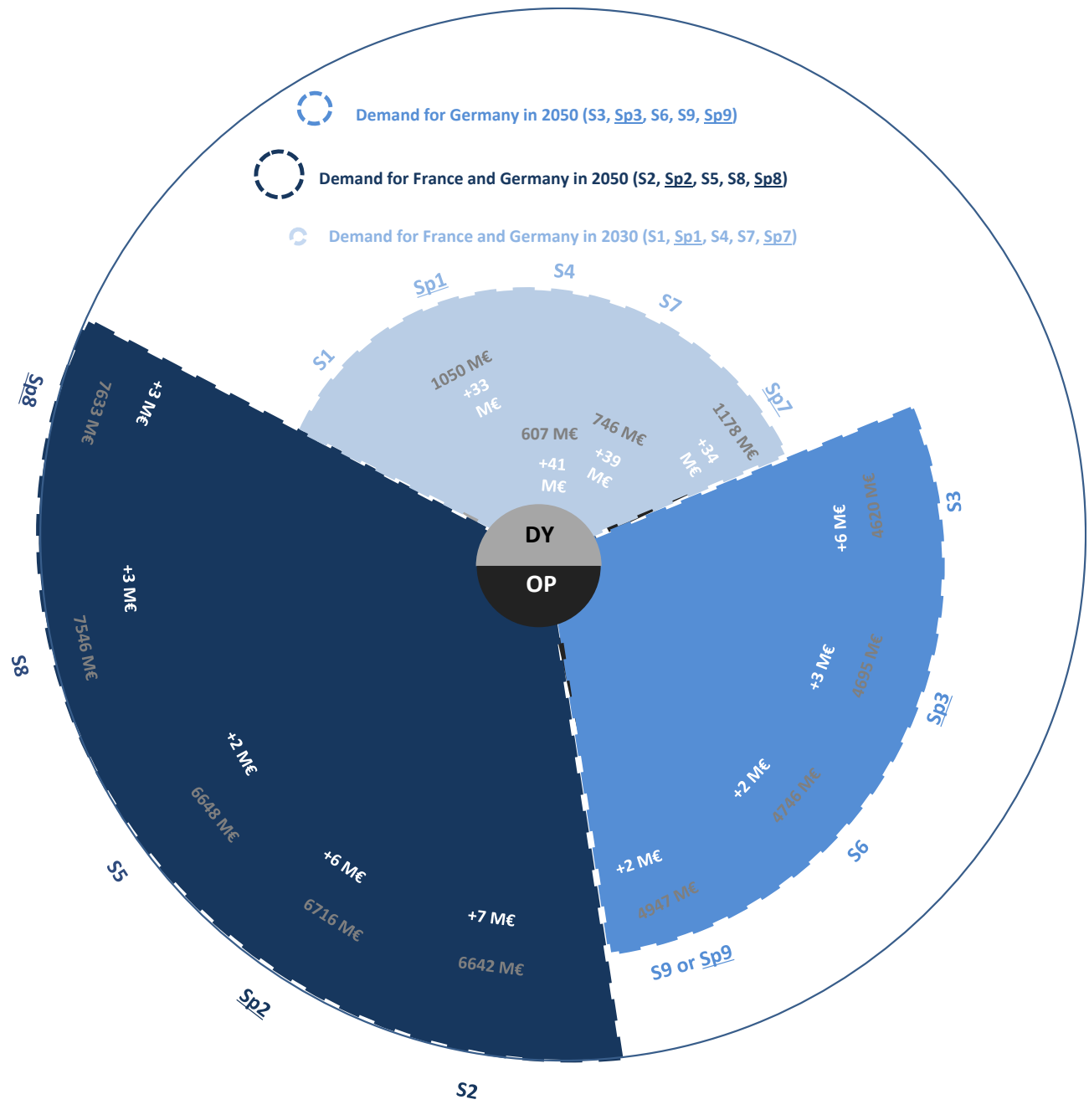
	Demand scenario	Production scenario		Road infrastructure
	Year	Distribution	Cost	Country
<i>S1</i>	2030	Distributed, 73 production plants	-	G & F
<i>Sp1</i>			Included	
<i>S2</i>	2050		-	G & F
<i>Sp2</i>			Included	
<i>S3</i>			-	G
<i>Sp3</i>			Included	
<i>S4</i>	2030	Distributed, 35 production plants	-	G & F
<i>S5</i>	2050		-	G
<i>S6</i>			-	
<i>S7</i>	2030	centralized, 22 production plants	-	G & F
<i>Sp7</i>			Included	
<i>S8</i>	2050		-	G & F
<i>Sp8</i>			Included	
<i>S9</i>			-	G
<i>Sp9</i>			Included	

### II.1 Cost analysis

The three steps model was then used to calculate the cost of the hydrogen infrastructure associated with each scenario, as summarized in Figure 5.11. This figure shows the cost of the hydrogen infrastructure deployment for different scenarios (Table 5.3) using standard **OP** optimization and dynamic **DY** optimization models. The minimum total cost corresponding to dynamic optimization is shown in grey for each scenario (**634 M€**), while the cost increase due to the use of the standard optimization model is shown in black (**+38 M€**). The scenarios are organized in three cost categories; a low cost range corresponding to the scenarios at low demand for France and Germany in 2030 (*S1*, *Sp1*, *S4*, *S7*, *Sp7*); a medium cost range corresponding to the scenarios at high demand for Germany in 2050 (*S3*, *Sp3*, *S6*, *S9*, *Sp9*); and a high cost range corresponding to the scenarios at high demand for France and Germany in 2050 (*S2*, *Sp2*, *S5*, *S8*, *Sp8*).

The overall results show that the model results are more sensitive to low demand scenarios, while the difference between costs is reduced at high demand scenarios independently of the production plant distribution and the calculation method.

**Figure 5.11:** Cost of the hydrogen infrastructure associated with the scenarios studied using standard and dynamic optimization method



Concerning the demand scenario impact, Figure 5.11 shows that the low demand scenarios corresponding to the year 2030 have the lowest infrastructure deployment cost for France and Germany varying around 862 M€, while the increase of the demand in 2050 increases the infrastructure cost to an average of 7042 M€. Despite a cost increase of 717% between the two years, this is still below the demand increase of 1088% due to the economy of scale. The result shows as well that an average of 65% of the infrastructure deployment cost in 2050 occurs in Germany, this is due to the demand difference of 10% and the higher electricity price.

Concerning the production scenario impact, Figure 5.11 shows that the scenarios with distributed production plants have a lower infrastructure cost compared to the centralized one. Thus, the minimum cost of a hydrogen infrastructure is achieved in 2050 using the distributed one with 73 production plants, and in 2030 using the distributed one with only 35 production plants. In fact, at low demand corresponding to the year 2030, the increase in the number of distributed production plants increases the number of low distances over which low hydrogen capacities are transported. Indeed, the distance is the main parameter that increases the transport cost at low demand and transport distance as discussed in the cost-share (Figure 5.6); hence, the use of a lower number of distributed production plants is cost-effective at low demand.

Concerning the method calculation, low demand scenarios are mainly affected using dynamic optimization as a cost reduction averaging 39 M€ is achieved compared to standard optimization. As presented in the dynamic model results, the method benefits mainly hydrogen flow transported at low demand, which explains the results obtained. Thus, at higher demand in 2050, the cost-reduction achieved using the dynamic optimization is minimal. Scenarios S2 and Sp2 (S3 and Sp3) represent an exception; this is explained by the higher number of production plants that reduce the flow delivered to low demand hubs.

The flow transported and the transport distance mainly affect the cost difference between the different scenarios. Thus, Figure 5.12 presents the average transport distance and the average hydrogen flow, along with the maximal standard deviation (SD) for the scenarios for France and Germany in 2030 and 2050. The figure displays the infrastructure costs as well to underline the impact of the flow and the distance.

**Figure 5.12:** Average and maximal standard deviation (SD) of transport distance and flow

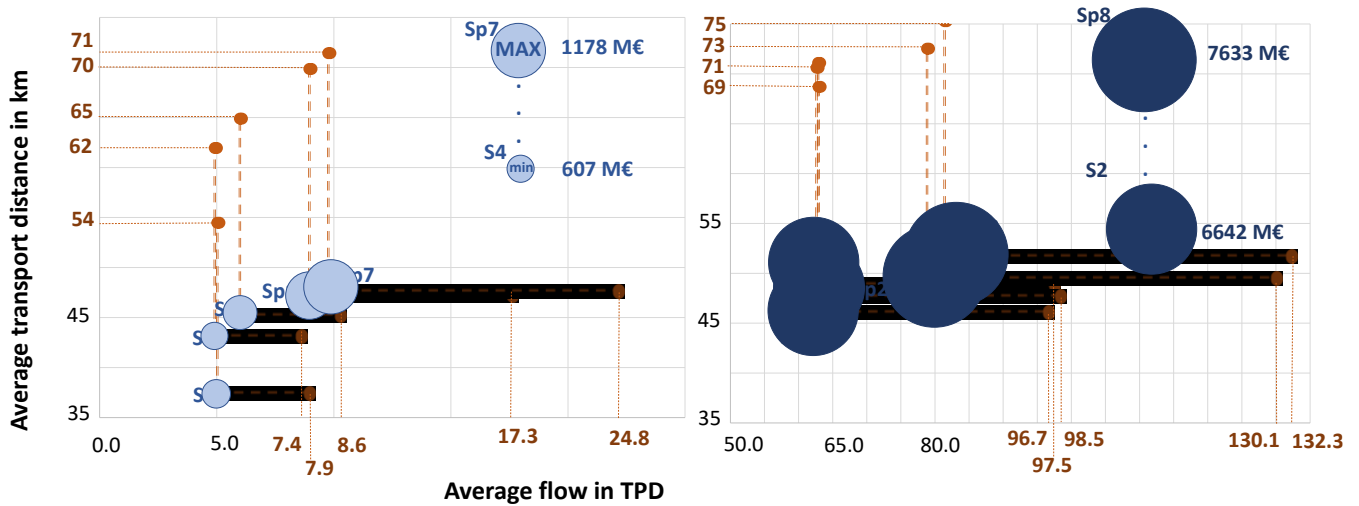


Figure 5.12 shows that the cost increase can be explained by the increase of the hydrogen flow, while the transport distance difference reflects the cost difference between the scenarios.

In 2030, for instance, the maximum transport distance SD reflects the production plant distribution, as the lowest maximum SD of 54 km corresponds to the scenario with the highest production plants S1 in contrast to S7. The impact of the infrastructure cost is proportional to the transported flow as S4, with the lowest maximum flow SD of 7.4 TPD, corresponds to the minimum cost scenario. Key finding is that the inclusion of production cost increases the total cost by increasing the maximum flow SD to 24.8 TPD and the maximum distance SD to 71 km. In the meantime, the average distance difference between the highest and lowest production plants (S1 and S7) is reduced from 11 km to only 1 km (between Sp1 and Sp7).

In 2050, the total cost can be explained as well by the transported flow. However, the impact of the production cost inclusion is different. Thus, S2 and Sp2 (as for S8 and Sp8) have a marginal cost difference due to an average flow difference of less than two TPD in 2050, in contrast to 16 TPD in 2030.

The impact of the transport distance can be seen in the cost variation between the scenarios. Thus, at low demand, a significant difference of the maximum transport distance SD ranging between 54 and 71 km results in a bigger disparity between the scenarios costs. In contrast, in 2050, the cost variation between the scenarios is marginal as for the maximum transport distance SD that ranges between 69 and 75 km.

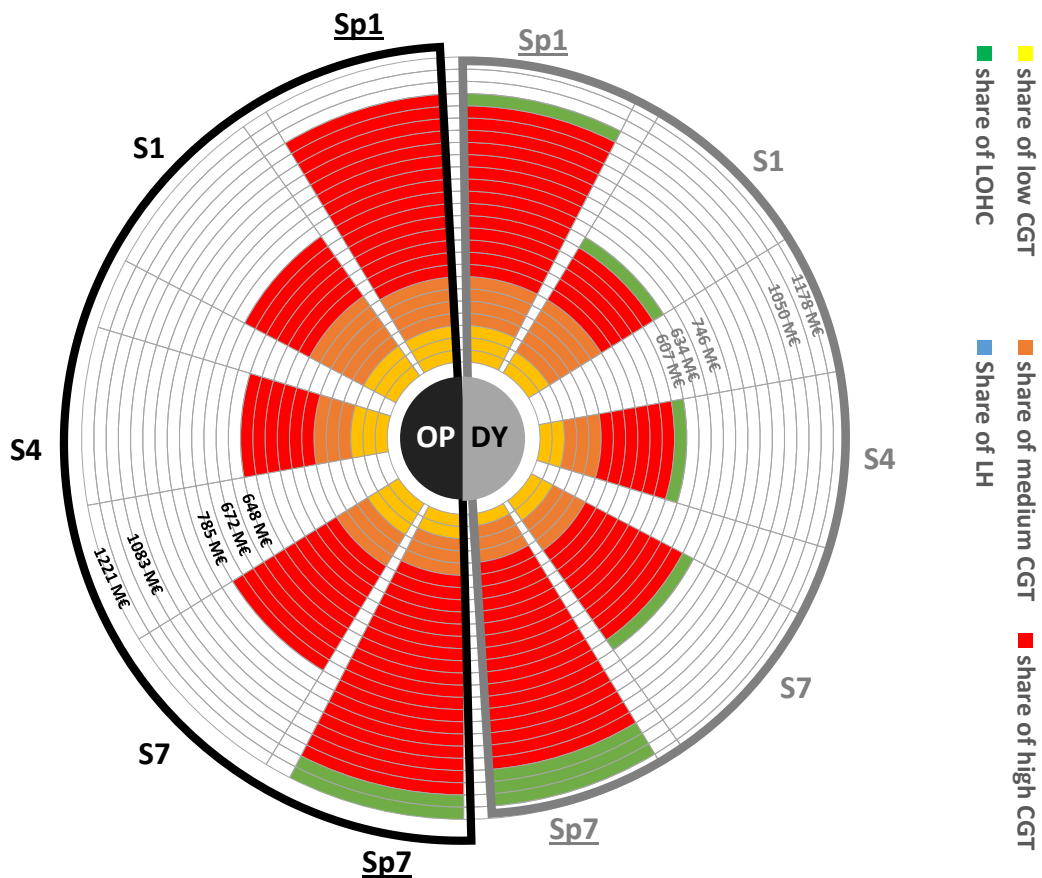
The results also show the dependency between the production and the demand scenarios. In fact, the choice of the production scenario impact on the average transport distance and

hydrogen flow, as the increase of the number of production plants decreases the transport distance ranges over which hydrogen is transported while decreasing the hydrogen flow because of more accessible production sites. Simultaneously, increasing the demand scenarios from 2030 to 2050 increases the hydrogen flow, and because of the limited number of production plants, it increases the transport distance, as more hydrogen has to be transported from remote nodes.

## II.2 Share analysis

As introduced in the cost analysis, the model calculation and production cost inclusion are more sensitive to low demand scenarios. Thus, the average shares of the transport states on the low demand scenarios are calculated for the whole infrastructure and summarized in Figure 5.13.

**Figure 5.13:** Share of the transport states at low demand scenarios



Concerning the standard optimization method that results in higher costs, all the hydrogen is transported as compressed gas except for centralized production that includes production cost. In the case when production cost is not included in the total transport cost, most hydrogen is

transported using low and medium pressure CGH for distributed production (S1 and S4) and using high pressure CGH for centralized production (S7).

Including production cost increases the hydrogen flow (Figure 5.12), allowing the use of RTT with higher capacities. Thus, the share of high pressure CGH in all case scenarios with production increases, and LOHC is even introduced as a SoT in the case of the Sp7 scenario. This difference between the two scenarios regarding the use of LOHC can be explained by higher transport distances, as shown in Figure 2.1 and Figure 5.4. This introduction of LOHC in standard optimization, however, in contrast to the dynamic one, increases the total transport cost, which explains the higher cost for Sp7 compared to Sp1.

Using dynamic optimization allows the improvement of the infrastructure cost by using LOHC storage and transport that shows more daily flexibility. Thus, for all scenarios, a share of low and high pressure CGH is replaced by LOHC, while medium pressure CGH maintains its share.

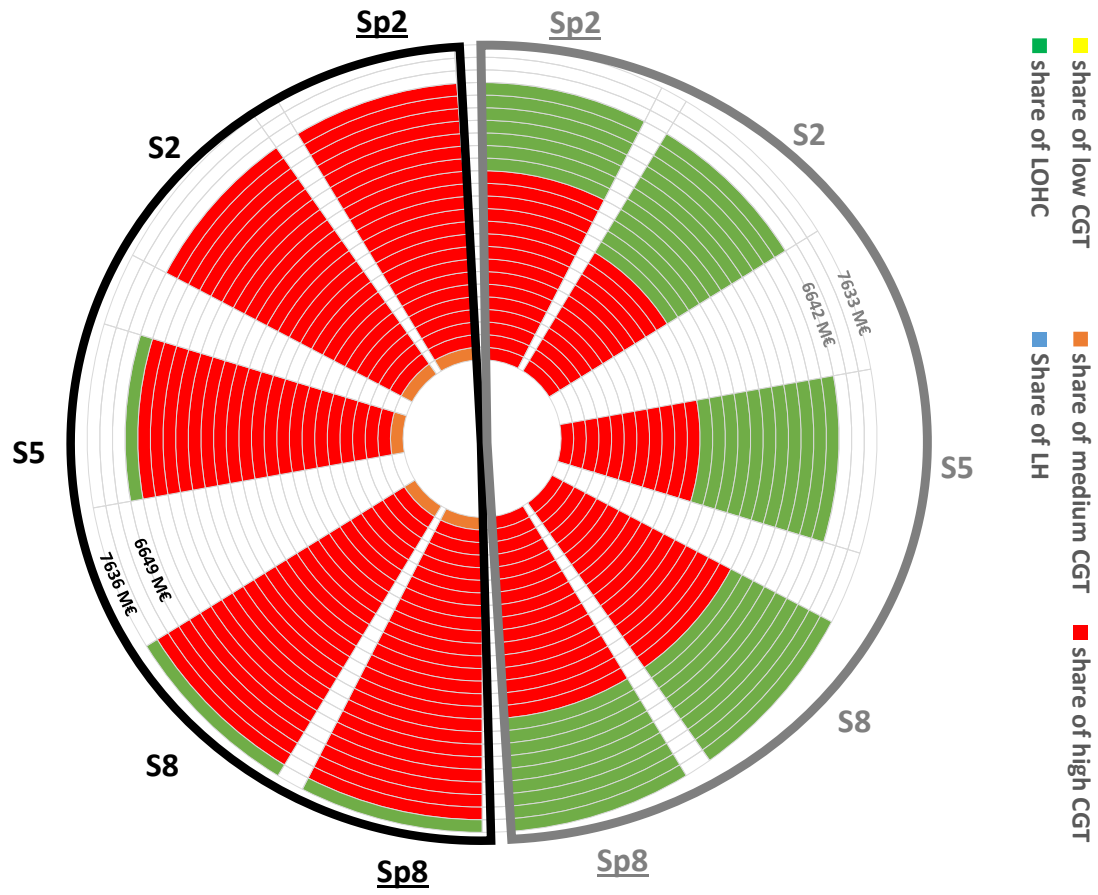
Concerning the results at high hydrogen penetration, the results showed a small variation between the costs using standard and dynamic optimization. However, concerning the share of different transport states, the results showed a significant variation for LOHC share but with lower cost impact, as shown in Figure 5.14.

These results for the year 2050 confirm the results previously observed with the case scenario S7 and the impact of LOHC as a SoT in both methods. At standard optimization, the use of LOHC comes with higher costs for S5 and S8, while using dynamic optimization, the use of LOHC contributes to reductions in costs.

As concluded in Table 5.1 and Table 5.2, the contribution of LOHC in reducing the transport cost is more relevant to the transport at a low hydrogen flow. Thus, the principal cost reduction can be attributed to medium pressure CGH replacement with LOHC in dynamic optimization. The high LOHC share did not, however, have any impact on the cost suggesting that this SoT can be used interchangeably with high pressure CGH at high hydrogen penetration.

Finally, for both hydrogen penetration scenarios, the choice of the different SoT is flow and distance related (Figure 2.1 and Figure 5.4). Thus, at standard optimization, a low to medium flow requires the use of low to high pressure CGH, while a medium to high flow applies the use of a medium to high pressure CGH and LOHC. Furthermore, LOHC share is increased with dynamic optimization. Two exceptions are Sp7 at low demand and S2 (Sp2) at high demand because of the transport distance. On the one hand, the maximum transport distance for scenario Sp7 is 413 km, which applies the use of LOHC even at low demand and without dynamic optimization and increases the cost. On the other hand, the high number of production plants in S2 and Sp2 minimizes the transport distance and therefore limits the use of LOHC even at high penetration, which leads to lower infrastructure cost.

Figure 5.14: Share of the transport states at high demand scenarios



### III Flow results

The flow result section provides the intermediate results that allow the presentation of the transported flow in France and Germany for different scenarios.

The results for all the scenarios are found in the annex (Figure F.1 - Figure F.15) and show that the hydrogen flow is impacted by three parameters, namely the hydrogen demand, the production cost, and the road infrastructure while it is less sensitive to the production distribution. Thus, a comparison is made between the flow demand of the two years 2030 and 2050 in the first part. Then, the hydrogen transported in the German case, as an isolated road infrastructure, is investigated. Finally, the impact on the introduction of the cost production on the flow is explored.

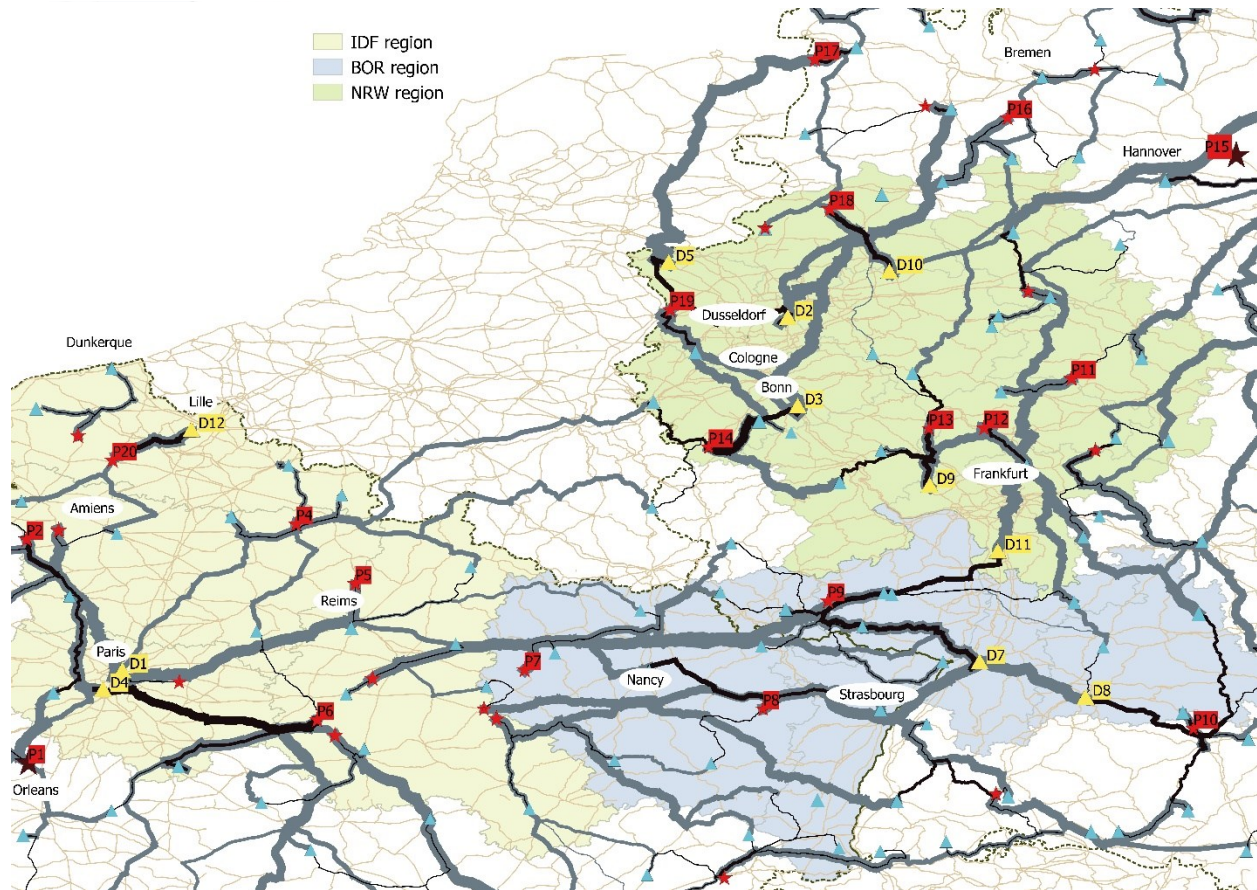
#### III.1 Demand scenarios comparison

For the demand scenarios comparison between 2030 and 2050, the French and German cases with 73 distributed production plants are chosen, corresponding to scenarios  $S_1$  (Figure F.1) and  $S_2$  (Figure F.2). For this case study, the impact of the electricity price is not considered, and the costs associated with production are taken as constant to investigate only the optimum transport network.

An analysis of regions with high demand allows a focus on three central regions as presented in Figure 5.15: western Germany, mainly the North Rhine-Westphalia (NRW in green in Figure 5.15) with six main distribution hubs, the North of France, mainly Île-de-France (IDF in yellow in Figure 5.15) with three main distribution hubs. The region close to the border between the countries (BOR in blue in Figure 5.15) with two main distribution hubs was added as well to highlight the hydrogen transport at the border.

Eleven out of the twelve main distribution hubs are located in the studied region (in Figure 5.15, the hubs are organized from the largest to the smallest demand from D1 to D12). These hubs correspond to a demand above 10 TPD by 2030 and 120 TPD by 2050. Both hydrogen flows corresponding to  $S_1$  and  $S_2$  are shown, in Black for the year 2030 and in grey for the year 2050.

**Figure 5.15: Hydrogen transport at high demand regions**



In the NRW region, the demand is satisfied by local production in 2030, the production plant P19 west of Dusseldorf covers both the demand of D5 and D2, while P14 south of Bonn covers the demand at D3. Meanwhile, D9 and D10 demand are covered using production from P13 and P18, respectively. The only exception is the hub demand D11 that exports hydrogen from the South of Germany at the French Border P9 (Figure 5.15).

By 2050, the demand exceeds the regional production capacity, and hydrogen has to be exported to satisfy the demand, from the North of Germany at the production plant P17 and from East of Germany at production plants P15 and P16. In the meantime, the increase of the demand at the border also pushes the hydrogen to flow from North and East to South and West. Thus, D11 is no longer exporting hydrogen from the South of Germany.

Concerning the flow in 2030, all the hydrogen transported to the main demand hubs in the NRW region does not exceed 50 TPD, while it reaches more than 100 TPD by 2050.

Table 2.4 shows the amount of hydrogen transported between the different production plants and the demand hubs located in NRW. A share of 75% - 100% corresponds to the case where a high flow is transported between a production plant  $P_i$  and a demand hub  $D_i$  in 2030, and the number corresponds to the share of hydrogen transported via the road ( $P_i, D_i$ ).

By 2050, 75% - 100%, 25% - 75%, and 0% - 25% correspond, respectively, to a high flow, medium flow, and low flow transported between the production and demand nodes  $P_i$  and  $D_i$ . For both years, the grey cell corresponds to the case when the road ( $P_i, D_i$ ) is not used to transport hydrogen.

**Table 5.4:** Share of hydrogen transport in the NRW region in%

	D2		D3		D5		D9		D10		D11	
	2030	2050	2030	2050	2030	2050	2030	2050	2030	2050	2030	2050
P9											100	
P11												60
P12							54	100				40
P13							100	46				
P14			100									
P15										12		
P16		58								28		
P17						100						
P18		42		57						60		
P19	100			43	100							

In 2030, for all the six demand hubs located in NRW D2, D3, D5, D9, D10 and D11, only one production plant is needed each time to cover the hydrogen demand, in contrast to 2050 when only D5 is fueled at 100% using the production plant P17.

In 2050, D2, D3, D9, and D11 are fueled using equally two distinct production plants: P16 at 58% and P18 at 42% in the case of demand hub D2; P18 at 57% and P19 at 43% in the case of demand hub D3; P12 at 54% and P13 at 46% in the case of demand hub D9; P11 at 60% and P12 at 40% in the case of demand hub D11. In the meantime, D10 with lower hydrogen demand than D2, D3, D5, and D9 needs to be connected to the three production plants P15, P16, and P18 to cover the total demand.

In IDF, the main region has great wind potential and none of the hydrogen production for both years is imported from surrounding regions, except from production P1 near Orleans. In the center of the region, the distribution hubs D1 and D4 are supplied using one production point P6 located east in 2030. In the same year, the demand hub D12 located in the North has its hydrogen transported from P20 only.

The case in the North does not change by 2050 because of lower demand, and the hydrogen is transported from P20. In the Central region, P6 does not cover the demand in D1 and D4 by 2050 anymore, and more hydrogen has to be transported from P1 south, P2 north, P4, and P5 west.

Concerning the flow in 2050, the hydrogen transported to the main demand hubs in the IDF region is transported at a flow exceeding 100 TPD, as noticed in the NRW region.

In 2030, because of higher demand at D1, the flow from P10 to D1 and D4 exceeds 50 TPD in 2030.

Table 5.5 shows the amount of hydrogen transported between the different production plants and the demand hubs located in IDF. The same notations and legend introduced for Table 2.4 are kept.

**Table 5.5:** Share of hydrogen transport in IDF region in%

	D1		D4		D12	
	2030	2050	2030	2050	2030	2050
P1				13		
P2		36				
P3				87		
P4		10				
P5		42				
P6	100	11	100			
P20					100	100

In 2030, all hydrogen for the demand hubs of D1 and D4 are covered by only one production plant P6.

By 2050, D1, with the highest hydrogen demand in France and Germany, needs to transport hydrogen from three more additional hydrogen production plants. Thus, the hydrogen demand is transported as well from P2 at 36%, from P4 at 10%, and from P5 at 42%. Meanwhile, the P6, which was used to cover both D1 and D4 at 100% in 2030, only covers D1 at a share of 11%. The increased hydrogen demand explains this, so the hydrogen is transported from P6 to South West.

For D4, the main demand by 2050 is covered by P3 at 87% that was used to cover the demand in Amiens.

In the BOR region, mainly, no exchange at the border happens in 2030. On the one hand, P7 and P8 allow the supply of all the distribution on the French side of the border. On the other hand, P9 and P10 are used to cover the demand on the German side of the border, including the main distribution hubs D7 and D8, and two minor demand hubs in France.

By 2050, the increase of demand allows hydrogen to circulate from the French to the German border. D8 absorbs the total production from P9, and hydrogen has to be exported from France to cover the demand at D7 and all the hubs near the border.

Concerning the flow in 2030, all the hydrogen transported to the main demand hubs in the BOR region does not exceed 50 TPD, while it reaches more than 100 TPD by 2050.

Table 5.6 shows the amount of hydrogen transported between the different production plants and the demand hubs located in BOR. The same notations and legend introduced for Table 2.4 are kept.

**Table 5.6:** Hydrogen transport in BOR region

	D7		D8	
P8		53		
P9	100	47		100
P10			100	

As for the other regions, the demand is covered by using one production plant each time in 2030, P9 in case of the demand hub D7 and D11, and P10 in case of the demand hub D8.

The production plant P10 is no longer used for fueling the region by 2050 because of the increase of demand in the South of Germany. It can be noticed as well, that P9 is used in 2050 to cover the demand of D8 and 47% of the demand in D7, while the rest is fueled from P8 located in France.

### III.2 Road infrastructure scenarios comparison

As shown in the general results section on the BOR region, the main exchange at the border happens by 2050 when the hydrogen demand is eleven times greater than in the year 2030. This exchange occurs from France to Germany, as more hydrogen is exported from France to Germany, as shown in Figure 5.15 and Table 5.6.

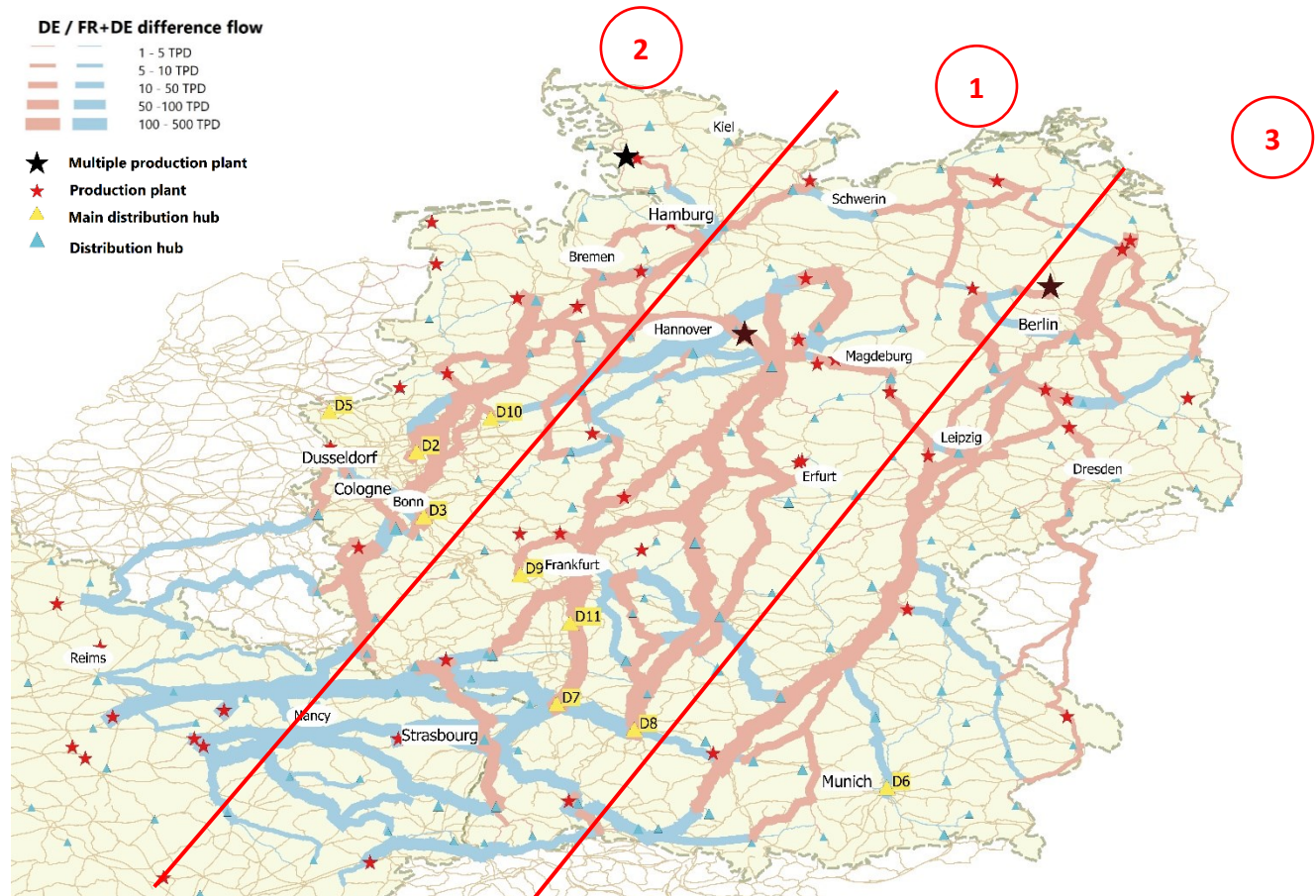
Thus, the scenario  $S_2$  (Figure F.2) is compared to the transport of hydrogen in Germany as an isolated case  $S_3$  (Figure F.3) to investigate the impact of open exchange at the border between France and Germany on the transport of hydrogen. To visualize the variation results, the flow difference  $D_{ij}$  is represented by a blue color (Figure 5.16) in case of higher flow  $F_{2ij}$  in the scenario  $S_2$ , and by red colour (Figure 5.16) in case of higher flow  $F_{3ij}$  in the scenario  $S_3$ , as shown by Equation 5.78

$$D_{ij} = F_{2ij} - F_{3ij} \quad \text{if } F_{2ij} > F_{3ij}$$

$$D_{ij} = F_{3ij} - F_{2ij} \quad \text{if } F_{2ij} < F_{3ij}$$

Equation 5.78

Figure 5.16: Difference of flow between the isolated case of Germany (DE) and the case of an open border between France and Germany (FR+DE)



The result flow difference  $D_{ij}$  can be divided into three regions that depend on the multiple production plants with the highest hydrogen production and the change of flow.

The region 1 is the Central region that has a big production plant located east of Hannover, and four main distribution hubs, D7, D8, D9, and D11.

The region 2 is the western region that has a big production plant corresponding to the closest point to offshore wind farms and four main distribution hubs, D2, D3, D5, and D10.

Finally, region 3 is the eastern region that has a big production plant located north of Berlin and only one main distribution hub D6.

For region 1, in the case of  $S_2$  where both countries are considered, the hydrogen is flowing from France to the South of Germany and from West to East within Germany (from region 1 to region 2). The main production point is used to cover the demand at the West (Region 2), while the main demand in D7 and D8 are covered by exporting hydrogen from France. In contrast, in  $S_3$  where only Germany is considered, the hydrogen is flowing from North to South within Germany as the main production point is used to cover the primary demand within the same region 1 in D7, D8, D9, and D11.

For region 2, in the case of  $S_2$ , there is a marginal export from France and from region 2 to fuel the main demand around Dusseldorf and Cologne in D2, D3, and D5. In the case where only Germany is considered, the demand is covered with the production in the same region 2. For both scenarios, the primary production at the North is not used.

For region 3, in the case of  $S_2$ , the flow is more distributed within the region except for a marginal export from region 1 to region 3. While in  $S_3$ , the hydrogen is flowing from North to South. Nevertheless, the main distribution at the North is not used for both scenarios.

In conclusion, the configuration of isolated hydrogen transported within Germany changes how the hydrogen is flowing within the country, as hydrogen is transported from North to South to cover the consumption at the border of France, and from East to West to cover the most populated region around Dusseldorf and Cologne at the Belgian/ Dutch border. Nevertheless, switching between both configuration scenarios does not have an impact on reducing the overproduction on the North, as only one main production plant of three is used in both scenarios.

### III.3 Production scenarios comparison

As shown in the general results in the annex (Figure F.1 - -Figure F.15), including production cost impact mainly on the flow imported from France. In 2050, the high flow transported, and the limited production capacity does not allow significant changes when the hydrogen production cost is introduced. In contrast, the low demand flow in 2030 offers more flexibility for hydrogen hubs to import hydrogen from less expensive production plants.

The case of France and Germany with 73 distributed production nodes is chosen for instance to investigate the impact of including the production cost in the scenario  $Sp_1$  (Figure F.10) and  $Sp_2$  (Figure F.11) compared respectively to  $S_1$  (Figure F.1) and  $S_2$  (Figure F.2). Thus, this comparison allows deducing the share of imports in the total hydrogen consumption per country, as summarized in Table 5.7.

**Table 5.7:** Share of import in total hydrogen consumption per country

	$S_1$	$Sp_1$	$S_2$	$Sp_2$
Consumption year	2030		2050	
Hydrogen cost included	No	Yes	No	Yes
Share of import in Germany (from France)	0.93%	87.97%	10.13%	33.67%
Share of import in France (from Germany)	3.60%	0.11%	3.17%	5.30%

In 2030 and without hydrogen production cost inclusion, the share of imports in France is higher than in Germany as the demand hubs on the French side of the border are closer to the German production plant P9 (Figure 5.15). Nevertheless, the imports are still marginal below 3.60% in both countries. Including the hydrogen production cost, however, increases the total transport cost in Germany compared to France (Chapter V, I.1.3). As the fixed transformation operation and maintenance cost represent the main cost share at low hydrogen demand and transport distance below 350 km (Figure 5.7), the total cost in Germany can be further reduced by importing hydrogen from France. The low demand as well implies more import potential due to the higher production capacities. Thus, the hydrogen imported from France increases drastically to reach 87.97% of the total hydrogen consumption within Germany. In parallel, lower production cost in France reduces the hydrogen import from Germany by 97.00% in  $Sp_1$  in comparison to  $S_1$ .

In 2050 and without hydrogen production cost inclusion, opposite effects are seen, as more imports are needed in Germany than in France. The higher hydrogen demand in the NRW region cannot be covered by local production and import from the North of France is needed (Figure 5.15). This is especially true in the case of production cost inclusion because of lower hydrogen costs in France. However, the high demand and the limited production capacities constrain the imported flow to a maximum limit of 33.67% of the total consumption in Germany. Another effect of the limited production capacities is also the increase of imports in France, even with higher production costs. In fact, the cost reduction achieved from hydrogen export from France to Germany balances the slight cost increase due to hydrogen export from Germany.

To visualize the flow imported from France to Germany in the case of production cost inclusion, Figure 5.17 represents the main corridor used to export hydrogen from France in 2030 (black in Figure 5.17) and 2050 (grey in Figure 5.17).

**Figure 5.17: Main corridor used to export hydrogen from France to Germany in 2030 and 2050**

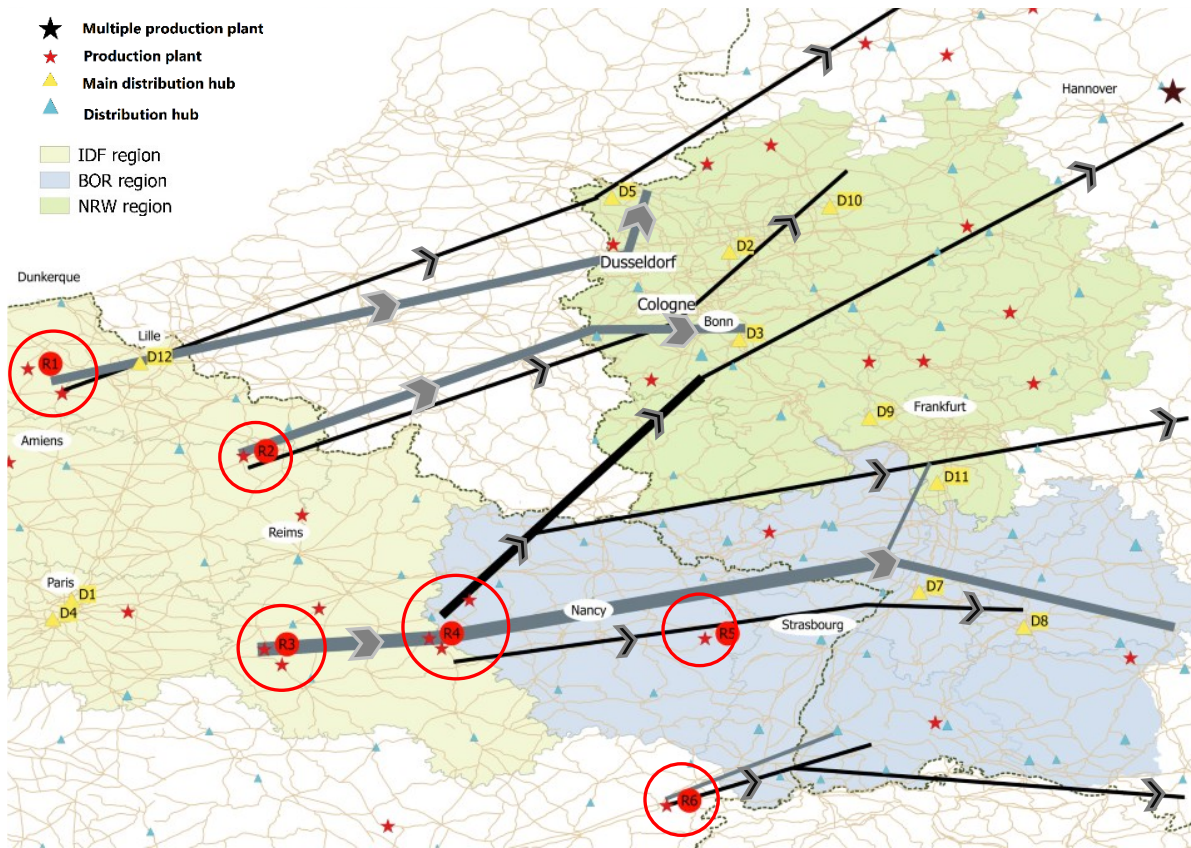


Figure 5.17 underlines the effect of the fixed hydrogen production in France on limiting the hydrogen flow exported to Germany. In 2050, all the hydrogen exported from France is used to supplement the high demand hubs in Germany. Thus, hydrogen production plants located in the regions R1 and R2 in the North of France are used to fuel the demand in the NRW region and the main demand hubs D5 and D3. In parallel, the production plants in the West of France located in R3 and R4 are used to export hydrogen within the BOR region from France to Germany and fuel the main demand hubs D7 and D8.

In 2030, and due to low demand, the export of hydrogen from France to Germany covers most of the German demand. Thus, not only hydrogen production in the North of France located in R1 and R2 are used to cover the demand in NRW and the main demand hubs D2, D5, and D10, but are also used to export hydrogen to the North of Germany. In the meantime, hydrogen production located in R4 and R5 are used to supply North West and western Germany with hydrogen while covering the main demand in BOR and the South of NRW region.

# CONCLUSION

**H**ydrogen via fuel cell electric vehicles represents an alternative to conventional fuel in order to find a balance between the increasing demand on road transportation and the necessity to lower the carbon emissions. Besides being environmentally friendly, hydrogen for mobility could improve the viability of standard electric vehicles by reducing the refueling time and increasing the driving range. Nonetheless, the physical and chemical properties of hydrogen make the use of this energy carrier at its standard pressure and temperature conditions inefficient, which opens the debate on the optimum technologies that could be used to transport and store hydrogen.

The complexity of hydrogen transport restrains the deployment of adequate infrastructure at the national and European level and restrains investment only to the regions where hydrogen is produced for industry. This aspect is one of the barriers that could explain why hydrogen is still not directly targeted by policies to decarbonize the mobility sector compared, for example, to biofuels.

Therefore, this thesis aims to shed light on technologies that could be used to transport hydrogen in order to achieve an optimum infrastructure deployment for mobility. Thus, first, the technologies to transport and store hydrogen at different states of aggregation are investigated, including compressed and liquid states, by assessing technically and economically the feasibility and the energy requirements. In the second part, these solutions are included to transport hydrogen at the national level for different production and demand scenarios and investigate the impact of a common European hydrogen market between France and Germany.

## *Scientific motivation*

The work developed used linear programming to minimize the cost at different states of aggregation, and geographical distribution to visualize the different flows transported in France and Germany. To our knowledge, a coupled cost optimization and geographical visualization at this scale level that included various states of aggregation have not yet been simultaneously treated in the dedicated hydrogen infrastructure literature.

The scientific objective of this thesis was to investigate seven different options and three states of aggregation. In addition to compressed gas and liquid hydrogen, liquid organic hydrogen carrier as novelty storage and transport option is considered as well. Furthermore, five different pressure levels were considered, at a low pressure level of 180 and 250 bar, a medium pressure

level of 350 bar, and at a high pressure level of 500 and 540 bar. These states were compared and optimized at different transport and demand ranges.

Another novelty of the work resides on the fact that the detailed transport analysis and optimization were coupled with geographical visualization at the scale of France and Germany that differ by their energy and power systems, which allows investigating the results in the scope of a single European hydrogen market.

### *Modeling approach*

The general model aims to link a set of production nodes to a set of distribution nodes along the road infrastructure at the minimum cost using different transport cost functions corresponding to the seven states of transport. Thus, the model output for each edge gives the optimum capacity transported by each state using three parallel models where the first one is a general minimization cost along a given edge, the second one is the total flow optimization, and the third one is the minimum cost of the entire network.

The first model gives the minimum cost of transporting hydrogen from an initial state to a transport state for a given input flow and transport distance, which gives as an output, depending on the optimization method, the annual or daily flow transported by each transport state. The second model gives the optimum flow transported over the network for different production and demand scenarios. Finally, the last model gives the minimum flow cost of transporting hydrogen along the edge for the different network flows.

The model uses as framework the road infrastructure and the hydrogen production and demand scenarios. It assumes that hydrogen is produced using future wind power projections and that hydrogen demand is driven by mobility and population frameworks.

### *Lesson learned about hydrogen storage and transport technologies*

Besides comparing different transport and hydrogen storage options, the study aims to minimize the annual cost using a standard and a dynamic method that optimizes independently the capacities transported and stored. This aims to give a guideline about the technologies that could be used at different flow and transport distance ranges, independently on the production and demand scenarios.

The cost of transporting hydrogen was found out to increase with the demand flow due to transformation energy requirements, and with the trucks transport distance due to fuel and logistic costs. This impacted on the state of transport as low to medium compressed hydrogen with lower energy requirements are promoted at low demand. Meanwhile, at higher demand, the total transport distance traveled to deliver hydrogen could be reduced by increasing the capacity transported by every single truck, and thus promoting liquid transport states with higher energy densities. In this case, mainly liquid organic hydrogen carrier is used at high transport

distance, while liquid hydrogen benefits mainly for energy systems with lower electricity cost due to the higher energy requirements.

The annual cost of transporting hydrogen could be further reduced by using linear optimization to allow hydrogen transport at different states of aggregation at the same time. This method benefits mainly to daily demand below 50 TPD. In this case, hydrogen is transported using equally compressed gas at low to medium and high pressure levels for transport distances below 250 km, while liquid states and compressed gas at high pressure levels are preferred for higher distances.

In reality, if the costs are calculated annually, the technical analysis can be performed daily to identify the number of trucks needed at each transport state. In this case, the total annual cost is further reduced by decoupling the daily stored and transported capacities. In fact, storing hydrogen can be cheaper than transporting it, and therefore, it could be economically beneficial to store hydrogen for an amount of period before transporting it. This dynamic optimization profits to liquid states where hydrogen is not stored in fixed tube capacities, but pumped into tanks. This promotes the use of liquid hydrogen carrier, compared to liquid hydrogen that has lower energy requirements and lower investment costs when it comes to the transport tubes.

Thus, at low demand and transport distance below 25 TPD and 250 km, respectively, liquid organic hydrogen carrier is used at a small share instead of compressed hydrogen at low and medium pressure levels, while it represented the share majority at higher transport distance. However, when it comes to the cost, the impact of the optimization method is more relevant at low demand and transport distance below 25 TPD and 250 km, respectively, or high transport distance above 400 km.

#### *Infrastructure deployment in France and Germany*

Both methods of cost optimization with and without dynamic analysis were then coupled to a flow optimization and geographic visualization for different scenarios. Fifteen scenarios were analyzed that differed by production distribution and cost, hydrogen demand, and infrastructure location in France and Germany.

The results showed a dependency between the model frameworks, mainly production and demand scenarios. In fact, increasing the production plants distribution decreases the transport distance ranges and the hydrogen flow because of more accessible production sites. Simultaneously, increasing the hydrogen demand increases the hydrogen flow, and the transport distance as more hydrogen has to be transported from remote nodes.

#### **Demand is the cost-driven parameter**

The demand has the highest impact on the cost as its increase increases the infrastructure deployment cost in France and Germany to a median of 7,039 M€ in 2050 compared to 766 M€ in 2030.

The main demand and eleven out of the twelve main distribution hubs are located in three main regions: western Germany around the North Rhine-Westphalia, North of France, including Île-de-France region, and the border between the two countries.

In western Germany, the demand is satisfied by local production in 2030, while export is needed to satisfy the demand in 2050, mainly from the North and West of Germany. The north of France has great wind potential, and none of the hydrogen production for both years is imported from surrounding regions. However, up to four production plants are needed to cover, for instance, the main demand hub located in the North West of Paris. Finally, marginal exchange at the border is noticeable in 2030, while more than 10% of hydrogen demand in 2050 at the German side border is covered via export from France.

#### **Infrastructure choice impacts on the hydrogen distribution**

The result showed that an average of 65% of the infrastructure deployment cost in 2050 occurs in Germany. This is due to higher demand and higher electricity prices. This difference was further explored by investigating Germany as an isolated case.

Thus, switching from the reference case where hydrogen is transported within a single European market, to a case where Germany is taken as an isolated infrastructure showed a change of hydrogen flow, which impacted on the transport distance and thus increased the total cost. In the isolated case, hydrogen is transported from North to South to cover the consumption at the border of France, and from East to West to cover the most populated region around Dusseldorf and Cologne at the Belgian/ Dutch border. Nevertheless, switching between both configurations does not have an impact on reducing the overproduction on the North West of Germany, as only one main production plant out of three northern production sites is used in both scenarios.

#### **Production cost increases the hydrogen exchange at the border**

The scenarios with distributed production plants have a lower infrastructure cost compared to the centralized one, independently on the road infrastructure and demand scenarios. However, low demand scenarios are more impacted when including the cost of hydrogen production as the total cost increases because of an increase in the maximum flow and distance standard deviations by 16 TPD and 6 km, respectively.

Including production cost, impacted as well on the flow imported from France at low demand scenarios. In 2050, the high flow transported, and the limited production capacity does not allow significant changes when the hydrogen production cost is introduced. In contrast, the low demand flow in 2030 offers more flexibility for hydrogen hubs to import hydrogen from less expensive production plants.

This export in 2030 is due to the increase of fixed transformation operation and maintenance cost in Germany that represented the main cost share at low hydrogen demand and transport distance below 350 km.

#### **Calculation method benefits for low demand scenarios**

Finally, the same conclusion can be made towards the impact of the optimization method choice as low demand scenarios are mainly impacted using dynamic optimization by achieving a cost reduction averaging 39 M€ compared to standard optimization.

In fact, at low demand, using dynamic optimization allows the improvement of the infrastructure cost by using liquid organic hydrogen carrier storage and transport that shows more daily flexibility. Thus, for all low demand scenarios, a small share of compressed gas at low and medium pressure level are replaced. In contrast, significant variation for liquid organic hydrogen carrier share was noticeable at high hydrogen penetration; however, with small cost impact. Thus, a choice of an adequate technology to transport hydrogen is more critical at the early stage of infrastructure deployment.

#### *Main contributions and further improvements*

The main study target was first to optimize the choice of the technology to store and transport hydrogen. In these regards, conclusions could be made towards the optimal technologies to be used at different demand flow, and perspectives can be suggested in order to improve the results:

- By including various pressure levels for compressed hydrogen, besides the liquid states of aggregation, the results allowed to cover different ranges of hydrogen demand and transport distance. However, the results took into account only the road infrastructure to transport hydrogen. Thus, including other modes of transport using railways and pipeline system could reduce further the costs.
- Concerning transport and storage technologies, the results showed that compressed gas truck at high pressure level is a better option independently of the hydrogen penetration scenarios. In contrast, liquid hydrogen is the less cost-effective option. However, the scenarios took into account only the mobility sector that is more distributed. Thus, a more complex energy system that takes into account the localized industry sector with higher hydrogen consumption could increase the share of liquid hydrogen.
- At earlier stage of infrastructure deployment, low and medium compressed gas or liquid organic hydrogen carrier are the two alternatives besides compressed hydrogen at high pressure level. The first option is already developed and commercialized, while the second option is still at the research stage but with lower investment cost and better storage flexibility. In this case, another criterion that could change the results and have

to be addressed is multi-objective optimization, including mainly the environmental aspect. In fact, in the short term perspective, the transport of hydrogen via truck would be performed using heavy-duty with conventional consumption. Thus, higher transported capacities would reduce the total carbon emissions.

The optimization model results were then included in different scenarios that took into account different production, distribution, and infrastructure. This allowed concluding to the impact of the hydrogen penetration shares, the production potential and effect, and hydrogen distribution in the case of France and Germany. Meanwhile, several perspectives can be suggested in order to improve mainly the proposed production and demand frameworks:

- The scenarios were investigated in the scope of two shares of hydrogen penetration scenarios, a low one of 2.4% in 2030, and a high one of 28.5% in 2050. The results showed that the choice of transport technologies is more critical at the early stage of hydrogen penetration, where the demand is low. In reality, the infrastructure will be deployed gradually so that the initial choice of technology will impact how the infrastructure choice will involve. In this scope, a temporal optimization could be included to investigate the impact of temporal discretization on the choice of the transport and storage technologies.
- Hydrogen production capacities and locations, based on proton exchange membrane technology from wind power, were used only as a model framework favorizing distributed production scenarios compared to localized ones. Thus, including more electricity sources and hydrogen production technologies as a decision variable could improve further the costs.
- In the case of France, potential wind location matched population dispersion, which allowed better hydrogen distribution. However, this consideration was taken in the perspective of comparison to the case of Germany. In reality, more electricity sources for hydrogen production would be more appropriate to the French energy system. Nuclear power will remain in the electricity landscape, even with a lower share. Moreover, hydrogen production is driven mainly by regional initiatives including different sources of electricity, an excellent example of that is la Manche project with maritime power.
- The case of Germany with higher wind potential suffers from a disparity between production and eventual consumption locations, with the main population and industry based on the South. Thus, the hydrogen share increase in mobility does not absorb the wind production in the north of Germany, and thus even in the isolated German case without hydrogen export from France. However, the case of industry, which represents the main hydrogen consumption currently, is not taken into account in the analysis, which could be addressed in future analysis.

## A1. Hydrogen production

Table A.1 shows the capacity factor for the last ten years (starting from the reference year 2016) for France and Germany and both onshore and offshore technologies.

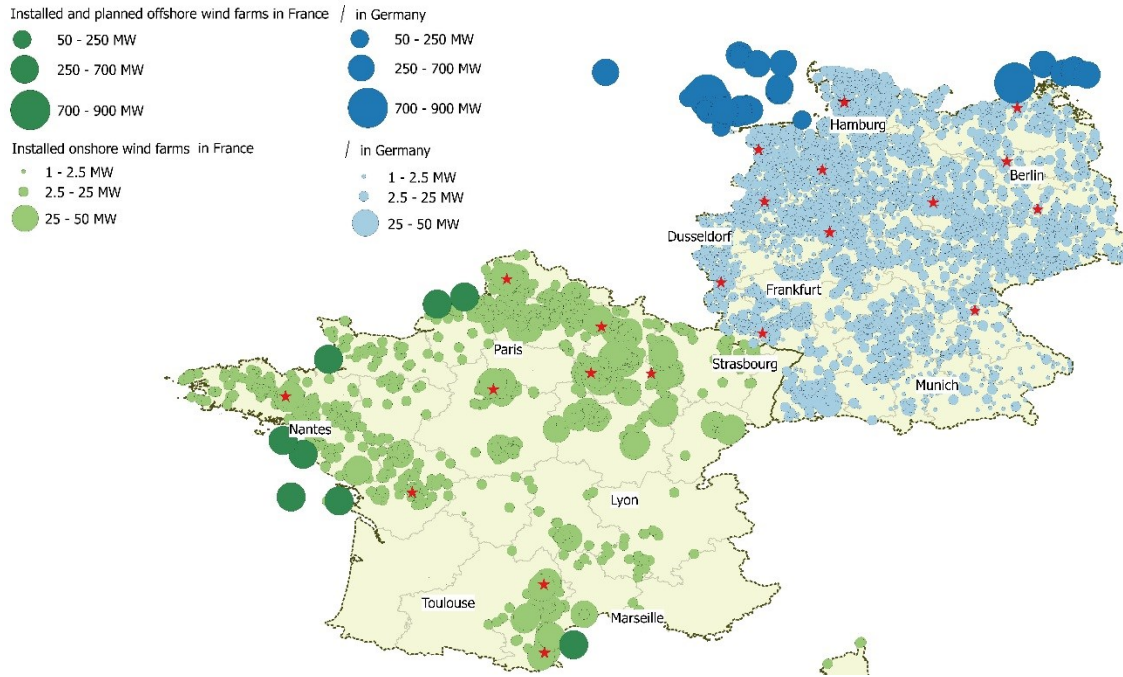
**Table A.1:** Onshore and offshore wind capacity factor in France and Germany from 2006 to 2016 (McCarty, Hord et al. 1981)

year	Germany		France	
	offshore	onshore	offshore	onshore
	$CF_{windOff,G}$	$CF_{windOn,G}$	$CF_{windOff,F}$	$CF_{windOn,F}$
2006	0.32	0.18	0.44	0.24
2007	0.36	0.22	0.48	0.26
2008	0.36	0.20	0.45	0.25
2009	0.32	0.18	0.44	0.24
2010	0.29	0.17	0.44	0.23
2011	0.35	0.20	0.43	0.23
2012	0.34	0.19	0.46	0.25
2013	0.32	0.18	0.46	0.24
2014	0.34	0.18	0.45	0.23
2015	0.36	0.21	0.47	0.25
2016	0.30	0.17	0.43	0.22

Figure A.1, Figure A.2, and Figure A.3 show hydrogen production for four different scenarios corresponding to centralized production and distributed production. The first one corresponds to nine and twelve production plants in France and Germany, respectively (Figure A.1).

For the second one option, a high distribution resulting in the maximum number of production plans of 32 and 41 for France and Germany respectively (Figure A.2); a low one corresponding to 15 and 20 production plants in France and Germany respectively (Figure A.3).

**Figure A.1: Centralized hydrogen production**



Based on the database summed in Table 2.2

**Figure A.2: Low distributed hydrogen production**

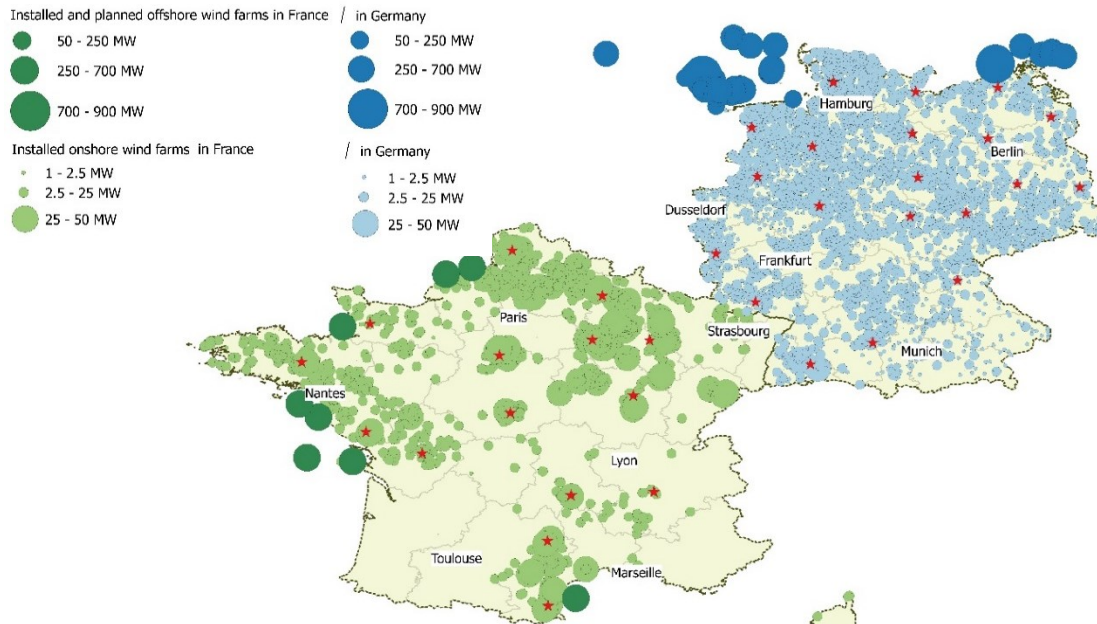
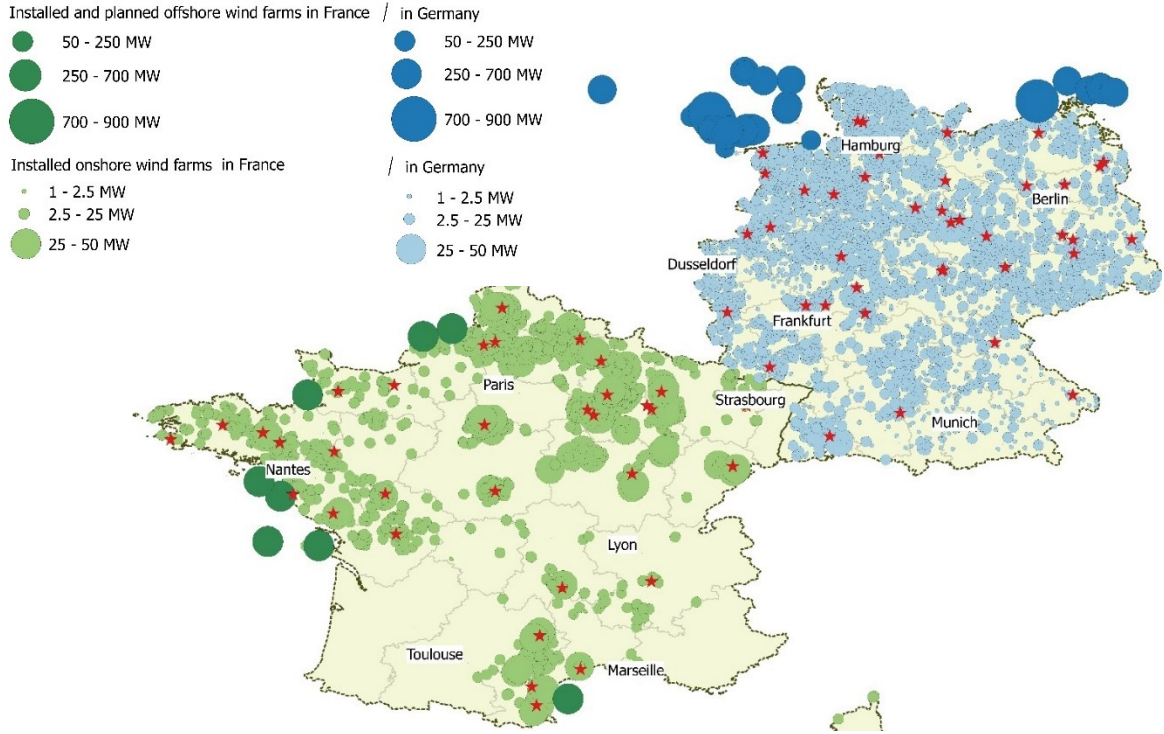


**Figure A.3: High distributed hydrogen production**

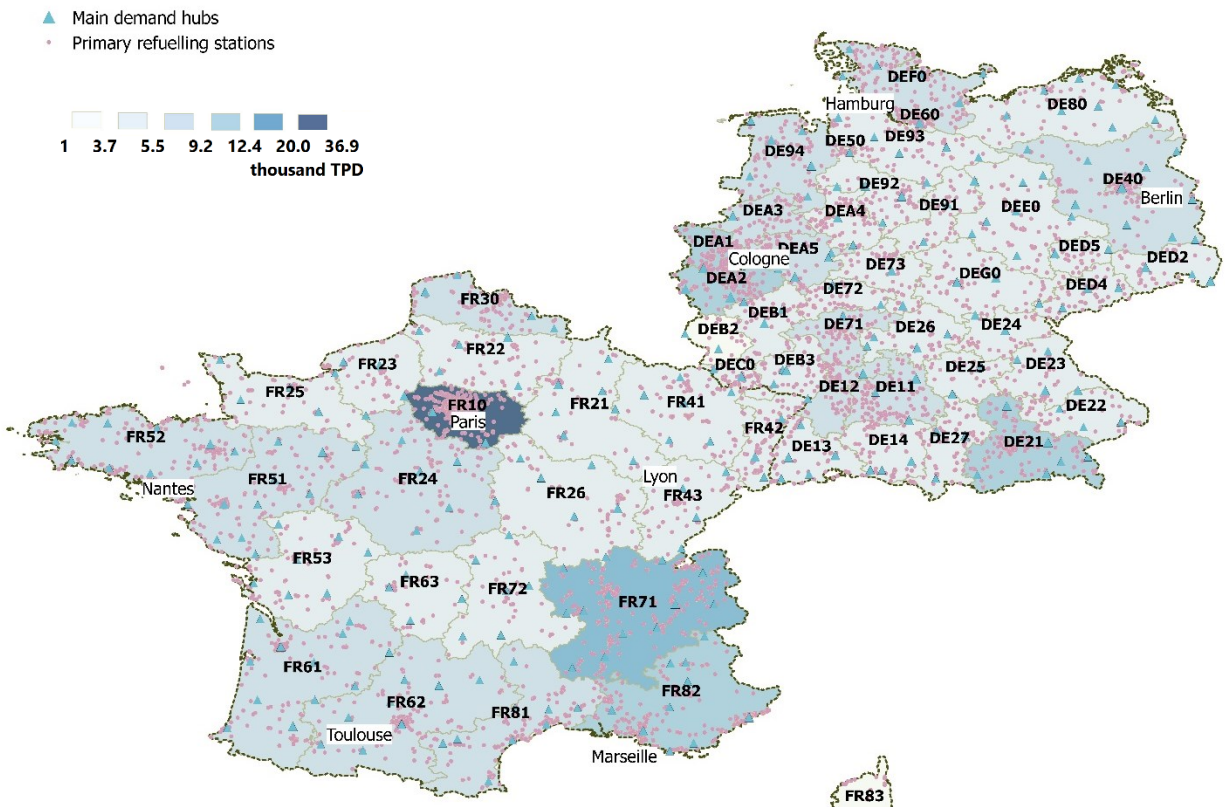


Based on the database summed in Table 2.2

## A2. Hydrogen demand

For hydrogen demand, two scenarios were considered corresponding to two different hydrogen penetration rates by 2030 and 2050. Figure A.4 shows the regional demand by 2030 along with the NUTS-2 region titles and the main demand hubs located along the primary refuelling stations in France and Germany. A more detailed summary for both years is shown in Table A.12.

**Figure A.4:** Main demand hubs and regional demand by 2030



Based on the database summed in Table 2.2

Table A.12 shows the regional demand for France and Germany for both years scenarios in TPD.

**Table A.2:** Regional demand in TPD by 2030 and 2050

ID	Name	2030	2050	ID	Name	2030	2050
DE11	Stuttgart	9.92	115.08	FR10	Île de France (NUTS 2013)	24.66	308.78
DE12	Karlsruhe	6.73	78.11				
DE13	Freiburg	5.42	62.91	FR21	Champagne-Ardenne (NUTS 2013)	2.71	34
DE14	Tübingen	4.44	51.57				
DE21	Oberbayern	11.18	129.77	FR22	Picardie (NUTS 2013)	3.93	49.19
DE22	Niederbayern	2.95	34.28				
DE23	Oberpfalz	2.66	30.89	FR23	Haute-Normandie (NUTS 2013)	3.78	47.38
DE24	Oberfranken	2.58	29.96				
DE25	Mittelfranken	4.24	49.17	FR24	Center (NUTS 2013)	5.24	65.64
DE26	Unterfranken	3.18	36.93				
DE27	Schwaben	4.5	52.2	FR25	Basse-Normandie (NUTS 2013)	3	37.62
DE30	Berlin	8.58	99.54				
DE40	Brandenburg	6.06	70.27	FR26	Bourgogne (NUTS 2013)	3.33	41.71
DE50	Bremen	1.64	18.99				
DE60	Hamburg	4.36	50.55	FR30	Nord-Pas-de-Calais (NUTS 2013)	8.29	103.87
DE71	Darmstadt	9.56	110.92				
DE72	Gießen	2.53	29.41	FR41	Languedoc-Roussillon (NUTS 2013)	5.68	71.09
DE73	Kassel	2.96	34.32				
DE80	Mecklenburg	3.93	45.6	FR42	Provence (NUTS 2013)	10.21	127.91
DE92	Hannover	5.2	60.3				
DE93	Lüneburg	4.14	48.07	FR43	Franche-Comté (NUTS 2013)	2.4	30.02
DE94	Weser-Ems	6.08	70.59				
DEA1	Düsseldorf	12.61	146.3	FR51	Pays de la Loire (NUTS 2013)	7.6	95.2
DEA2	Köln	10.78	125.06				
DEA3	Münster	6.37	73.93	FR71	Rhône-Alpes (NUTS 2013)	13.34	167.1
DEA4	Detmold	5.02	58.2				
DEA5	Arnsberg	8.77	101.73	FR53	Poitou-Charentes (NUTS 2013)	3.67	45.97
DEB1	Koblenz	3.63	42.09				
DEB2	Trier	1.3	15.06	FR61	Aquitaine (NUTS 2013)	6.9	86.39
DEB3	Rheinhessen-Pfalz	4.95	57.46				
DEC0	Saarland	2.43	28.15	FR62	Midi-Pyrénées (NUTS 2013)	6.14	76.93
DED2	Dresden	3.91	45.32				
DED4	Chemnitz	3.57	41.45	FR63	Limousin (NUTS 2013)	1.5	18.75
DED5	Leipzig	2.48	28.75				
DEE0	Sachsen-Anhalt	5.47	63.5	FR52	Bretagne (NUTS 2013)	6.72	84.18
DEF0	Schleswig-Holstein	6.97	80.84				
DEG0	Thüringen	5.29	61.39	FR72	Auvergne (NUTS 2013)	2.77	34.69
DE91	Braunschweig	3.89	45.19				
DE	Total Germany	243.69	2827.89	FR	Total France	203.11	2543.69

### A3. Technical parameters

The different thermodynamic parameters associated with hydrogen are presented in Table A.3, Table A.4, and Table A.5.

First, Table A.3 (McCarty et al., 1981b) represents the thermodynamics properties used for work calculation at different inlet pressure levels  $P_i$ . These parameters include the heat capacity at constant pressure  $C_p$ , the heat capacity at constant volume  $C_v$ , the specific volume  $\vartheta_i$  and the isothermal compressibility  $\beta_T$ .

**Table A.3:** Heat capacities and isothermal compressibility of hydrogen at 300 K and different inlet pressure (McCarty et al., 1981b).

$P_i$ in bar	<b>1.01325</b>	<b>2</b>	<b>5</b>	<b>10</b>	<b>20</b>	<b>25</b>	<b>60</b>	<b>60</b>	<b>100</b>	<b>160</b>	<b>180</b>
$C_p$ in J/K	14.31	14.32	14.33	14.33	14.36	14.37	14.45	14.45	14.54	14.54	14.57
$C_v$ in J/K	10.18	10.18	10.19	10.19	10.20	10.20	10.22	10.22	10.25	10.3	10.31
$\vartheta_i$ in m <sup>3</sup> /kg	12.13	6.19	2.48	1.24	0.63	0.50	0.26	0.21	0.13	0.09	0.08
$-1/\beta_T$ in MPA	0.10	0.20	0.50	1.01	2.02	2.53	5.15	6.22	10.62	17.63	20.08
$P_i$ in bar	<b>200</b>	<b>240</b>	<b>250</b>	<b>300</b>	<b>350</b>	<b>400</b>	<b>450</b>	<b>500</b>	<b>540</b>	<b>550</b>	<b>700</b>
$C_p$ in J/K	14.70	14.75	14.76	14.62	14.87	14.91	14.94	14.97	15.00	15.00	15.06
$C_v$ in J/K	10.33	10.36	10.36	10.40	10.44	10.46	10.52	10.55	10.59	10.59	10.69
$\vartheta_i$ in m <sup>3</sup> /kg	0.07	0.06	0.06	0.05	0.04	0.04	0.04	0.03	0.03	0.03	0.03
$-1/\beta_T$ in MPA	22.58	27.75	29.11	35.89	43.04	50.50	58.27	66.32	67.99	74.65	101.21

Table A.4 shows then the specific enthalpy  $h_{n,i}$  for normal hydrogen  $n$  and an inlet pressure  $P_i$ , and the specific entropy  $s_{n,i}$  for the same conditions.

**Table A.4:** Specific enthalpy and entropy of normal hydrogen at 300 K and different pressure. (McCarty et al., 1981b)

$P_i$ in bar	<b>1.01325</b>	<b>5</b>	<b>9</b>	<b>15</b>	<b>20</b>	<b>25</b>	<b>30</b>	<b>35</b>	<b>40</b>
$h_{n,i}$ in kJ/kg	4226.90	4228.60	4230.20	4232.80	4234.90	4337.10	4239.30	4241.60	4243.90
$s_{n,i}$ in kJ/kg	70.57	63.99	61.56	59.45	58.25	57.33	56.57	55.93	55.38
$P_i$ in bar	<b>45</b>	<b>50</b>	<b>55</b>	<b>60</b>	<b>100</b>	<b>150</b>	<b>200</b>	<b>300</b>	<b>400</b>
$h_{n,i}$ in kJ/kg	4246.20	4248.50	4250.80	4253.20	4373.30	4300.30	4329.20	4391.50	4458.20
$s_{n,i}$ in kJ/kg	54.378	54.448	54.051	53.688	51.549	49.841	48.624	46.90	45.68

Finally, Table A.5 shows the specific enthalpy  $h_{n,f}$  and  $h_{p,f}$  for normal hydrogen  $n$  and para hydrogen  $p$ , respectively, at saturated liquid conditions of atmospheric pressure; and the specific entropy  $s_{n,f}$  and  $s_{p,f}$  for the same final conditions.

**Table A.5:** Enthalpy and entropy of para and normal hydrogen at saturated liquid conditions of atmospheric pressure (McCarty et al., 1981b)

$h_{n,f}$ in kJ/ kg	$h_{p,f}$ in kJ/ kg	$s_{n,f}$ in kJ/ kg	$s_{p,f}$ in kJ/ kg
270.9	-258.8	17.093	7.848

To allow a comparison between the different liquefaction plants and processes, the input conditions are brought to the atmospheric pressure. The missing plants and process data were calculated using the equations (Table A.6), and all the parameters summarized in

Table A.7 (the calculated one are bolded in green):

**Table A.6:** Parameters and equation listing for liquefaction work calculation

Parameter	Definition	Equation
$\dot{W}_p$	ideal work of compression	Equation 3.16
$\dot{W}_{pc}$	real compression work	Equation 3.32
$\eta_{pc}$	real compression efficiency	
$\dot{W}_{ideal,L}$	ideal work of liquefaction	Equation 3.22
$\dot{W}_l$	real liquefaction work	Equation 3.41Equation 3.39
$\eta_l$	Real liquefaction efficiency	
$\dot{W}_s$	System overall real work	Equation 3.42

**Table A.7:** Exergy efficiency and total process work of the plants in the study

	Baker & Shaner (1978)	WE-NET H <sub>2</sub> -Claude (1997)	WE-NET He-Brayton (1997)	WE-NET Ne-Brayton (1997)	Quack (2001)
Capacity in TPD	250	300	300	300	170
<b>Feed steam state in bar</b>					
$P_i$	1.01325	1.01325	1.01325	1.01325	1.0132
<b>Ideal work in kWh/ kg</b>					
$\dot{W}_{ideal,L}$	3.91	3.92	3.92	3.92	3.94
$\dot{W}_p$	NAN	NAN	NAN	NAN	NAN
<b>Real work in kWh/ kg</b>					
$\dot{W}_l$	10.85	8.53	8.69	8.58	6.93
$\dot{W}_{pc}$	NAN	NAN	NAN	NAN	NAN
$\dot{W}_s$	10.85	8.53	8.69	8.58	6.93
<b>Efficiency in%</b>					
$\eta_l$	36.0	46.0	45.1	45.7	56.8
$\eta_{pc}$	NAN	NAN	NAN	NAN	NAN
$\eta_s$	<b>36.0</b>	<b>46.0</b>	<b>45.1</b>	<b>45.7</b>	56.8

	Valenti & Macchi (2008)	Baker & Shaner (1978)	WE-NET H <sub>2</sub> -Claude (2004)	SINTEF MR (2010)	Shimko He-Brayton (2008)
Capacity in TPD	860	300	300	86	50
Feed steam state in bar					
$P_i$	60	1.01325	1.01325	21	1.01325
Ideal work in kWh/ kg					
$\dot{W}_{ideal,L}$	2.56	3.91	3.94	2.95	3.89
$\dot{W}_p$	1.61	NAN	NAN	1.13	NAN
Real work in kWh/ kg					
$\dot{W}_l$	5.29	10.85	8.72	6.2 - 6.5	8.73
$\dot{W}_{pc}$	2.22	NAN	NAN	1.47	NAN
$\dot{W}_s$	7.51	10.85	8.72	7.67 – 7.97	8.73
Efficiency in%					
$\eta_l$	48.3	36	45.2	44.7 - 47.1	44.6
$\eta_{pc}$	76.9	NAN	NAN	76.9	NAN
$\eta_s$	54.7	36	45.2	50.9 - 52.6	44.6

	Inglostadt plant (1992)	Leuna (2007)	Paraxaire (2002)	Paraxaire (2005 status)	Paraxaire (Futur status)
Capacity in TPD	4.4	5	20-36	30 - 300	30 – 300
Feed steam state in bar					
$P_i$	20	24	20	20	20
Ideal work in kWh/ kg					
$\dot{W}_{ideal,L}$	2.95	2.87	2.95	2.95	2.95
$\dot{W}_p$	1.13	1.22	1.13	1.13	1.13
Real work in kWh/ kg					
$\dot{W}_l$	13.6	11.9	12.5-15	14	11
$\dot{W}_{pc}$	1.47	1.59	1.47	1.57	1.57
$\dot{W}_s$	15.07	13.49	13.97 – 16.47	15.57	12.57
Efficiency in%					
$\eta_l$	21	23.6	19,7	21,1	26,8
$\eta_{pc}$	76,9	76,9	76,9	76,9	76,9
$\eta_s$	26.5	29.9	29.2 – 24.8	26.4	32.7

(David O. Berstad et al., 2010; Bracha et al., 1994; Fukano et al., 2007; Krasae-in, 2013; Kuendig et al., 2006; Klaus Ohlig & Decker, 2000; K Ohlig & Decker, 2014) and own calculation IEK-STE 2016

Finally, Table A.8 sum up the results obtained from the literature review of the liquefaction work at different input pressure level

**Table A.8:** Specific work of liquefaction at different inlet pressure

$P_i$ in bar	1.013	20	180	250	350	500	540
$\dot{w}_s(P_i)$ kWh/ kg	12	10.53	9.24	9.03	8.81	8.58	8.53
$\eta_s$ in%	33.4	27.9	23.1	21.3	21.6	20.7	20.5

Table A.9 shows the matrix of transformation work  $\dot{w}_s[t, t']$  from a state  $St$  to a new state  $St'$ , with  $t$  corresponding to the column index, and  $t'$  the line index. For compressed gas hydrogen, the pressure level used are 1.013 bar [ $t = t' = 0$ ] and 20 bar [ $t = t' = 1$ ] at the production; 180 bar [ $t = t' = 2$ ], 250 bar [ $t = t' = 3$ ], 350 bar [ $t = t' = 4$ ], 500 bar [ $t = t' = 5$ ] and 540 bar [ $t = t' = 6$ ] for the transport; 700 bar [ $t = t' = 7$ ] and 875 bar [ $t = t' = 8$ ] for dispensing hydrogen. For the other states of aggregation [ $t = t' = 9$ ] correspond to liquid organic hydrogen carrier and [ $t = t' = 10$ ] for saturated liquid hydrogen.

**Table A.9:** Matrix of transformation work  $\dot{w}_s[t, t']$

$t \backslash t'$	0	1	2	3	4	5	6	7	8	9	10
0	0	1.47	2.75	2.97	3.19	3.42	3.47	3.63	3.76	6.02	12
1	0	0	1.07	1.24	1.42	1.62	1.66	1.81	1.93	4.31	10.53
2	0	0	0	0.16	0.34	0.52	0.56	0.7	0.82	3.8	9.24
3	0	0	0	0	0.18	0.38	0.42	0.57	0.69	3.71	9.03
4	0	0	0	0	0	0.2	0.24	0.39	0.51	3.62	8.81
5	0	0	0	0	0	0	0.05	0.2	0.34	3.53	8.58
6	0	0	0	0	0	0	0	0.15	0.29	3.51	8.53
7	0	0	0	0	0	0	0	0	0.15	3.44	8.36
8	0	0	0	0	0	0	0	0	0	3.39	8.24
9	0	0	0	0	0	0	0	0	0	0	8.2
10	0	0	0	0	0	0	0	0	0	0	0

Table A.10 shows the different parameters of the tube trucks found in the literature. The parameters include the state of aggregation, the pressure, the total loading and unloading time.

The shade of orange varies with the design tube pressure, from a lighter corresponding to low operating pressure to a darker corresponding to a high operating pressure, while the blue color corresponds to liquid hydrogen, and the green to liquid organic hydrogen carrier.

**Table A.10:** State of aggregation, pressure, capacity and loading/ unloading time of the different tube trucks from literature

State of aggregation	CGH	LH	CGH	LH	CGH	
Design pressure $P_t$ in bar	200	1	162	1	200	200
Total net truck capacity $m^t$ in kg	250	4000	244	4000	368	555
Loading and unloading time $tt_{l/u}^t$ in hours	2	4	1	3	2	-
Source	(Amos, 1998)		(Steward, Ramsden, & Zuboy, 2008)		(Zerhusen, 2013)	

State of aggregation	CGH						LH
Design pressure $P_t$ in bar	180	250	400	520	165.5	500	7 - 9
Total net truck capacity $m^t$ in kg	280	560	700	940	300	1100	More than 3000
Loading and unloading time $tt_{l/u}^t$ in hours	-	-	-	-	1 - 1.5	1	2 - 4
Source	(Barckholtz et al., 2013)			(Tamhankar, 2014)			

Name from source	LINCOLN TITAN			HEXAGON LINCOLN TITAN V			-	
State of aggregation	CGH							
Design pressure $P_t$ in bar	250	350	540	250	350	540	180	350
Total net truck capacity $m^t$ in kg	554	728	1040	720	907	1350	300	800
Loading and unloading time $tt_{l/u}^t$ in hours	-	-	-	-	-	-	-	-
Source	(Baldwin & Newhouse, 2013; Composites, 2006)						(Weil, 2012)	

State of aggregation	LCOH	
Design pressure $P_t$ in bar	8	-
Storage density $wt - \%$	3.7	5.2
Total net truck capacity $m^t$ in kg	916	1500
Loading and unloading time $tt_{l/u}^t$ in hours	1.5	2
Source	(Ahluwalia et al., 2011)	(Teichmann et al., 2012)

#### A4. Economic parameters

Table A.11 and Table A.12 were used to convert the different literature costs to the modeling cost of the year 2016.

Table A.11 shows the annual inflation rate for France, Germany, and USA to the reference year 2010, and Table A.12, the annual average exchange rate between the EUR and USD that was used to convert the different literature costs to the modeling cost of the year 2016.

**Table A.11:** Annual inflation rate to the reference year 2010 (OECD 2017)

Year y	1990	1991	1992	1993	1994	1995	1996	1997	1998
<i>France</i>	73.5	75.4	76.9	78.2	78.9	79.8	80.9	81.6	82.4
<i>Germany</i>	75.2	77.5	81.6	85.0	86.8	88.5	89.1	89.3	89.9
<i>USA</i>	66.0	68.2	69.7	71.4	72.9	74.4	75.8	77.1	77.9
Year y	1999	2000	2001	2002	2003	2004	2005	2006	2007
<i>France</i>	82.6	83.8	85.5	87.3	88.9	90.4	92.1	94.1	96.5
<i>Germany</i>	90.1	89.7	90.9	92.1	93.2	94.2	94.8	95.1	96.7
<i>USA</i>	79.1	80.9	82.7	84.0	85.7	88.0	90.9	93.7	96.2
Year y	2008	2009	2010	2011	2012	2013	2014	2015	2016
<i>France</i>	98.8	98.9	100.0	100.9	102.1	102.9	103.5	104.6	98.8
<i>Germany</i>	97.5	99.2	100.0	101.1	102.6	104.6	106.6	108.7	97.5
<i>USA</i>	98.0	98.8	100.0	102.1	103.9	105.6	107.5	108.7	110

**Table A.12:** Annual average exchange rate EUR/USD (OECD 2017)

Year y	1990	1991	1992	1993	1994	1995	1996	1997	1998
<i>EUR/USD</i>	127.3	123.9	129.8	117.1	119.0	130.8	127.0	113.4	112.1
Year y	1999	2000	2001	2002	2003	2004	2005	2006	2007
<i>EUR/USD</i>	106.6	92.4	89.6	94.6	113.1	124.4	124.4	125.6	137.1
Year y	2008	2009	2010	2011	2012	2013	2014	2015	2016
<i>EUR/USD</i>	147.1	139.5	132.6	139.2	128.5	132.8	132.9	111.0	110.7

Table A.13 shows the electric prices for France  $Ce^{FR}$  and Germany  $Ce^{DE}$  for different annual production capacities. These costs included all the taxes and levies and corresponded to the year 2016.

**Table A.13:** Electricity cost in € \*/kWh (Eurostat 2017)

Band	IA	IB	IC	ID	IE	IF	IG
Maximum annual consumption in MWh	20	500	2000	20000	70000	150000	-
$Ce^F$ in € */kWh	0.1703	0.1357	0.1110	0.0921	0.0773	0.0642	0.055
$Ce^G$ in € */kWh	0.27775	0.2246	0.1966	0.16985	0.13645	0.11785	0.11

The capital cost of transformation was writing using a sizing factor  $\alpha_{sc}$  to scale the cost form a base known case cost  $C_b$  of a system that has a size  $S_b$  (Tribe & Alpine, 1986), as shown in the equation below.

$$C = C_b \left( \frac{S}{S_b} \right)^{\alpha_{sc}}$$

Table A.14 lists the economic assumption for the different parameters used to calculate the cost parameters for different transformation, including compression, liquefaction, and de- and hydrogenation.

**Table A.14:** Economic assumptions for capital cost of transformation

Parameter	Definition	Value	Unit	Source
<b>Compression</b>				
$C_{b,c}$	Base compressor cost	1164	€/kW	(Tribe & Alpine, 1986), (Drennen & Rosthal, 2007)
$S_{b,c}$	Base compressor size	4000	kW	
$\alpha_{sc}$	Sizing factor	0.8	NAN	
<b>Liquefaction</b>				
$C_{b,L}$	Base liquefier cost	47895	€/ (kg/h)	(Tribe & Alpine, 1986), (Drennen & Rosthal, 2007)
$S_{b,L}$	Base liquefier size	1167	€	
$\alpha_{sc}$	Sizing factor	0.65	NAN	
<b>De- and hydrogenation</b>				
$C_{b,h}$	Base de- and hydrogenation cost	31881	€ * (kg/h)	(Teichmann et al., 2012), (Yamaguchi, 2003), (Ahluwalia et al., 2011)
$S_{b,h}$	Base de- and hydrogenation size	11574	(kg/h)	
$\alpha_{sc}$	Sizing factor	0.7	NAN	

The capital cost of storage used the same methodology (Tribe & Alpine, 1986) to scale a base known case cost  $C_{tube}[t]$  of a system that have a capacity  $m[t]$  using factor  $\alpha_{sc}[t]$ . The three parameters depended on the state of transport and aggregation, as shown in Table A.15

**Table A.15: Economic assumption for the capital cost of storage**

State of aggregation	CGH					LOHC	LH
sizing factor $\alpha_{sc}[t]$	0.75					0.7	0.7
Storage pressure $Pt$ in bar	180	250	350	500	540	1	1
Index $t$ of SoT	2	3	4	5	6	9	10
Total net truck capacity $m[t]$ in kg	350	668	885	1100	1230	1500	3600
Cost of the tube trailer $C_{tube}[t]$ in €	385,000	525,000	689,000	1,056,991	1,197,500	57,087	1,732,500
Base source*	[1]	[2]	[2]	[3]	[2]	[4]	[3]

\*The base costs calculation is taken from the source listed below; however, some costs were adjusted, when the cost was underestimated or unknown.

[1]: Own calculation

[2]: (Baldwin & Newhouse, 2013; Composites, 2006)

[3]: (Tamhankar, 2014)

[4]: (Ahluwalia et al., 2011)

Table A.16 shows the parameters that were used to calculate the different road transportation cost and variable operation and maintenance costs, including those of transformation and transport.

**Table A.16: truck and variable cost parameters**

Parameter	Definition	Value	Unit	Source
$C_w$	water cost	1164	€/kW	(Intratec, 2017)
$TC_{driver}$	driver wage	32.0	€ */ hour	[[26],1]
$F_p$	unit fuel cost	1.4 /2.1	€ */ km	[[26],2]
$C_{Cab}$	Cabin truck cost	107740.0	€ *	[[26],2]
$C_{und}$	Undercarriage cost	69826.0	€ *	

The NPV method was used to express the annual cost functions. The parameters used for calculation are shown in Table A.17 for compression function calculation, for liquefaction function calculation, for de- and hydrogenation function calculation, and road transport function calculation. For  $CRF$  calculation the interest rate  $i_{dr}$  was taken equal to 6%.

**Table A.17: Economical assumption for compression**

Parameter	Definition	Value	Unit
<b>Economical assumption for compression</b>			
$yn_{Tc}$	Depreciation period for compressor	20	Years
$yn_{Sc}$	Depreciation period for compression storage	12	Years
$CRF_{Tc}$	Capital recovery factor of the compressor	8.7	%
$CRF_{Sc}$	Capital recovery factor of the compression storage	11.9	%
$CF_{Tc}$	Capacity factor of compressor	90	%
$CF_{Sc}$	Capacity factor of compression storage	90	%
$OM_{Tc}$	Share of $O\&M_{Tc}$ to the capital cost	3	%
$OM_{Sc}$	Share of $O\&M_{Sc}$ to the capital cost	3	%
<b>Economical assumption for liquefaction</b>			
$yn_{Tl}$	Depreciation period for the liquefier	20	Years
$yn_{Sl}$	Depreciation period for liquefaction storage	12	Years
$CRF_{Tl}$	Capital recovery factor of the liquefier	8.7	%
$CRF_{Sl}$	Capital recovery factor of liquefaction storage	11.9	%
$CF_{Tl}$	Capacity factor of liquefier	70	%
$CF_{Sl}$	Capacity factor of compression storage	70	%
$OM_{Tl}$	Share $O\&M_{Tl}$ to the capital cost	3	%
$OM_{Sl}$	Share of $O\&M_{Sl}$ to the capital cost	3	%
<b>Economical assumption for de- and hydrogenation</b>			
$yn_{Th}$	Depreciation period for the de- and hydrogenation	20	Years
$yn_{Sh}$	Depreciation period for LOHC storage	20	Years
$CRF_{Th}$	Capital recovery factor of the de- and hydrogenation	8.7	%
$CRF_{Sh}$	Capital recovery factor of LOHC storage	11.9	%
$CF_{Th}$	Capacity factor of de- and hydrogenation	80	%
$CF_{Sh}$	Capacity factor of LOHC storage	70	%
$OM_{Th}$	Share of $O\&M_{Th}$ to the capital cost	3	%
$OM_{Sh}$	Share of $O\&M_{Sh}$ to the capital cost	3	%
<b>Economical assumption for road transportation</b>			
$yn_{cab}$	Depreciation period for truck cab	8	Years
$yn_{tra}$	Depreciation period for truck trailer	12	Years
$CRF_{cab}$	Capital recovery factor of the truck cab	16.1	%
$CRF_{tra}$	Capital recovery factor of the truck cab	11.9	%
$CF_{tr}$	Capacity factor of the truck	90	%
$OM_{cab}$	Share of $O\&M_{cab}$ to the capital cost	3	%
$OM_{tra}$	Share of $O\&M_{tra}$ to the capital cost	3	%

## A5. Results

Table A.18, Table A.19, and Table A.20 show the average share of SoT and the average cost for different transport distance, and for transported low flow of 5, 10, and 25 TPD, medium flow of 50 TPD, and high flow of 70 and 100 TPD.

Table A.18 corresponds to a minimum cost comparison of the cost of the different pathways (similar to Odgan methodology for instance)

**Table A.18:** Minimum cost option at different transported flow

	Distance range	Average cost in	Average CGH share	Average LOHCT share	Average LHT share
5 TPD	1 - 100 km	1,412,246 €/year	100.00%	0.00%	0.00%
	100 - 200 km	2,075,023 €/year	100.00%	0.00%	0.00%
	200 - 300 km	2,426,240 €/year	100.00%	0.00%	0.00%
	300 - 400 km	3,039,907 €/year	100.00%	0.00%	0.00%
	400 - 500 km	4,040,940 €/year	41.40%	58.60%	0.00%
10 TPD	1 - 100 km	2,592,163 €/year	100.00%	0.00%	0.00%
	100 - 200 km	3,567,155 €/year	100.00%	0.00%	0.00%
	200 - 300 km	4,615,155 €/year	100.00%	0.00%	0.00%
	300 - 400 km	5,597,053 €/year	100.00%	0.00%	0.00%
	400 - 500 km	7,792,481 €/year	26.30%	73.70%	0.00%
25 TPD	1 - 100 km	5,394,891 €/year	100.00%	0.00%	0.00%
	100 - 200 km	7,905,626 €/year	100.00%	0.00%	0.00%
	200 - 300 km	10,419,641 €/year	100.00%	0.00%	0.00%
	300 - 400 km	12,857,351 €/year	89.00%	11.00%	0.00%
	400 - 500 km	17,356,092 €/year	19.20%	64.60%	16.20%
50 TPD	1 - 100 km	10,224,077 €/year	100.00%	0.00%	0.00%
	100 - 200 km	15,242,315 €/year	100.00%	0.00%	0.00%
	200 - 300 km	19,971,610 €/year	58.00%	42.00%	0.00%
	300 - 400 km	23,758,171 €/year	11.00%	89.00%	0.00%
	400 - 500 km	31,201,845 €/year	19.20%	0.00%	80.80%

Table A.19 is based on a cost minimization problem using a linear integer problem using cost functions calculated from a coupled stored and transported capacities based on a yearly technical assessment.

**Table A.19:** Optimum cost option for coupled storage and transport at different transported flow

	Distance range	Average cost in	Average CGH share	Average LOHCT share	Average LHT share
5 TPD	1 - 100 km	1,315,178 €/year	100.00%	0.00%	0.00%
	100 - 200 km	1,912,676 €/year	100.00%	0.00%	0.00%
	200 - 300 km	2,345,258 €/year	100.00%	0.00%	0.00%
	300 - 400 km	2,940,876 €/year	100.00%	0.00%	0.00%
	400 - 500 km	3,952,153 €/year	44.40%	55.60%	0.00%
10 TPD	1 - 100 km	2,445,043 €/year	100.00%	0.00%	0.00%
	100 - 200 km	3,477,657 €/year	100.00%	0.00%	0.00%
	200 - 300 km	4,548,208 €/year	100.00%	0.00%	0.00%
	300 - 400 km	5,503,965 €/year	91.00%	9.00%	0.00%
	400 - 500 km	7,632,170 €/year	43.90%	56.10%	0.00%
25 TPD	1 - 100 km	5,300,131 €/year	100.00%	0.00%	0.00%
	100 - 200 km	7,817,969 €/year	100.00%	0.00%	0.00%
	200 - 300 km	10,259,156 €/year	100.00%	0.00%	0.00%
	300 - 400 km	12,733,860 €/year	60.40%	39.60%	0.00%
	400 - 500 km	17,185,044 €/year	11.10%	77.80%	11.10%
50 TPD	1 - 100 km	10,107,887 €/year	100.00%	0.00%	0.00%
	100 - 200 km	15,074,530 €/year	100.00%	0.00%	0.00%
	200 - 300 km	19,739,160 €/year	40.00%	60.00%	0.00%
	300 - 400 km	23,760,020 €/year	20.00%	80.00%	0.00%
	400 - 500 km	30,961,667 €/year	11.10%	0.00%	88.90%

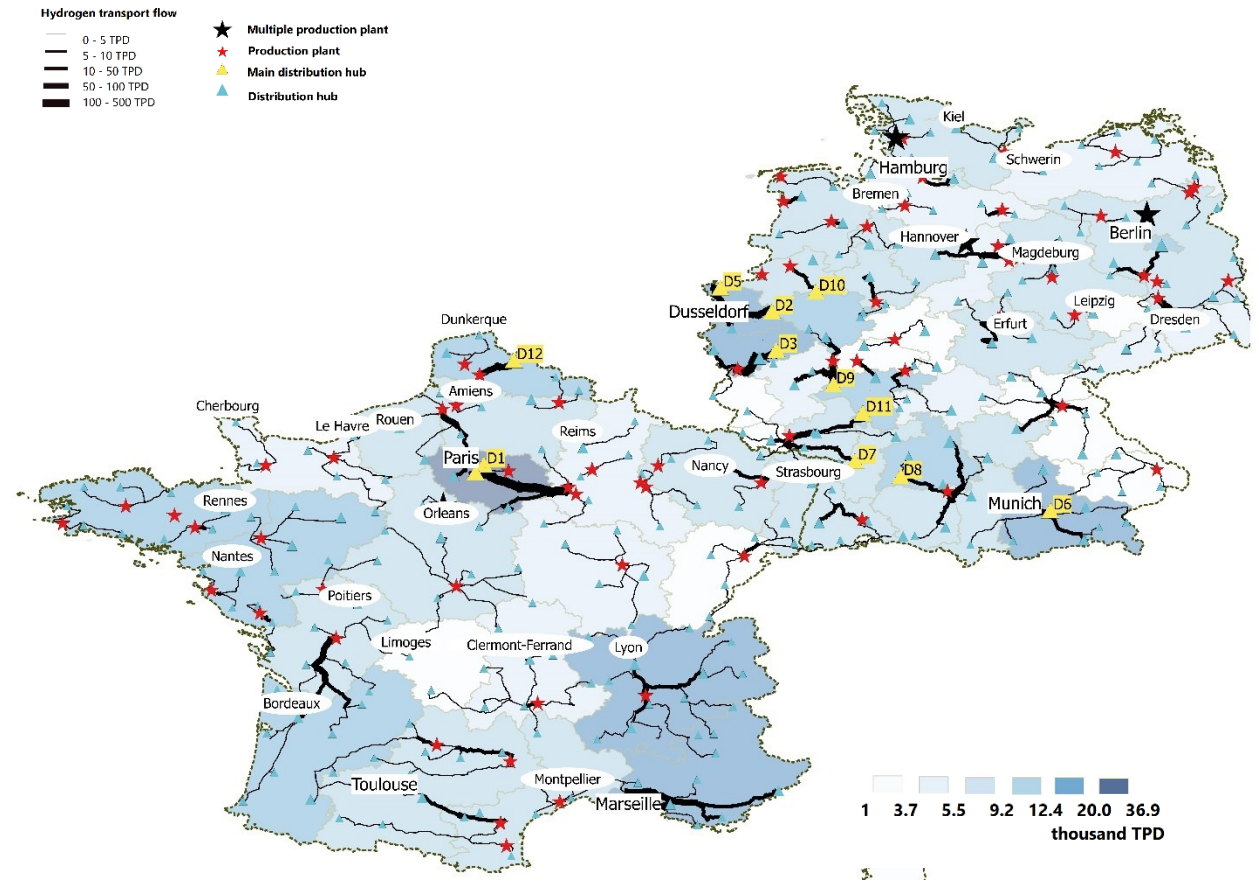
Finally, Table A.20 is based on a cost minimization problem using a linear integer problem using cost functions calculated from a decoupled stored and transported capacities based on a daily technical assessment.

**Table A.20:** Optimum cost option for decoupled storage and transport at different transported flow

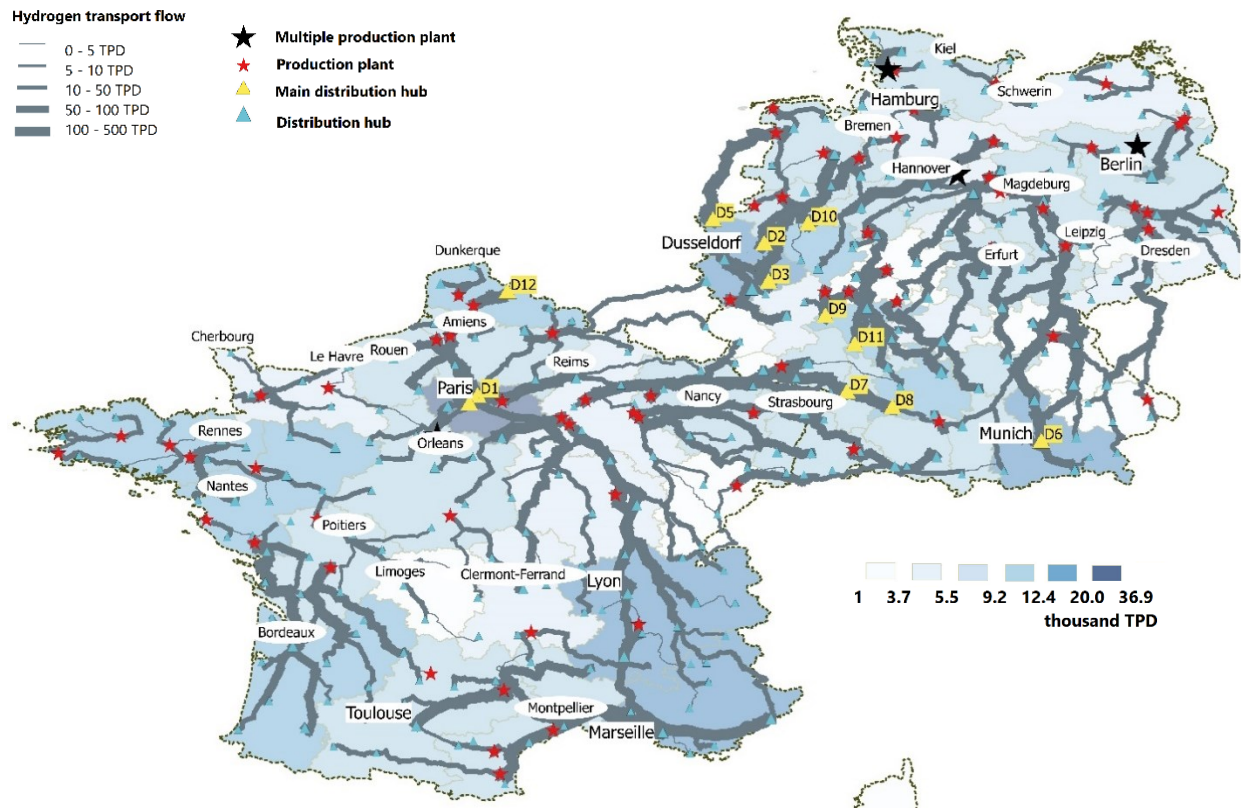
	Distance range	Average cost in	Average CGH share	Average LOHCT share	Average LHT share
5 TPD	1 - 100 km	1,255,242 €/year	100.00%	0.00%	0.00%
	100 - 200 km	1,813,937 €/year	100.00%	0.00%	0.00%
	200 - 300 km	2,262,875 €/year	90.00%	10.00%	0.00%
	300 - 400 km	2,855,658 €/year	20.00%	80.00%	0.00%
	400 - 500 km	3,639,064 €/year	20.00%	80.00%	0.00%
10 TPD	1 - 100 km	2,326,707 €/year	100.00%	0.00%	0.00%
	100 - 200 km	3,356,623 €/year	100.00%	0.00%	0.00%
	200 - 300 km	4,351,743 €/year	90.00%	10.00%	0.00%
	300 - 400 km	5,552,600 €/year	20.00%	80.00%	0.00%
	400 - 500 km	7,119,413 €/year	20.00%	80.00%	0.00%
25 TPD	1 - 100 km	5,006,948 €/year	100.00%	0.00%	0.00%
	100 - 200 km	7,590,934 €/year	100.00%	0.00%	0.00%
	200 - 300 km	10,053,973 €/year	90.00%	10.00%	0.00%
	300 - 400 km	12,733,860 €/year	20.00%	80.00%	0.00%
	400 - 500 km	16,669,493 €/year	20.00%	70.00%	10.00%
50 TPD	1 - 100 km	9,739,683 €/year	100.00%	0.00%	0.00%
	100 - 200 km	14,976,410 €/year	80.00%	20.00%	0.00%
	200 - 300 km	19,653,850 €/year	10.00%	90.00%	0.00%
	300 - 400 km	23,998,470 €/year	20.00%	80.00%	0.00%
	400 - 500 km	30,895,560 €/year	20.00%	0.00%	80.00%

Figure F.1 - Figure F.15 show the different hydrogen flow transported in France and Germany in 2030 and 2050 for the different scenarios.

**Figure F.1: Hydrogen flow for scenario  $S_1$**



**Figure F.2: Hydrogen flow for scenario  $S_2$**



**Figure F.3: Hydrogen flow for scenario  $S_3$**

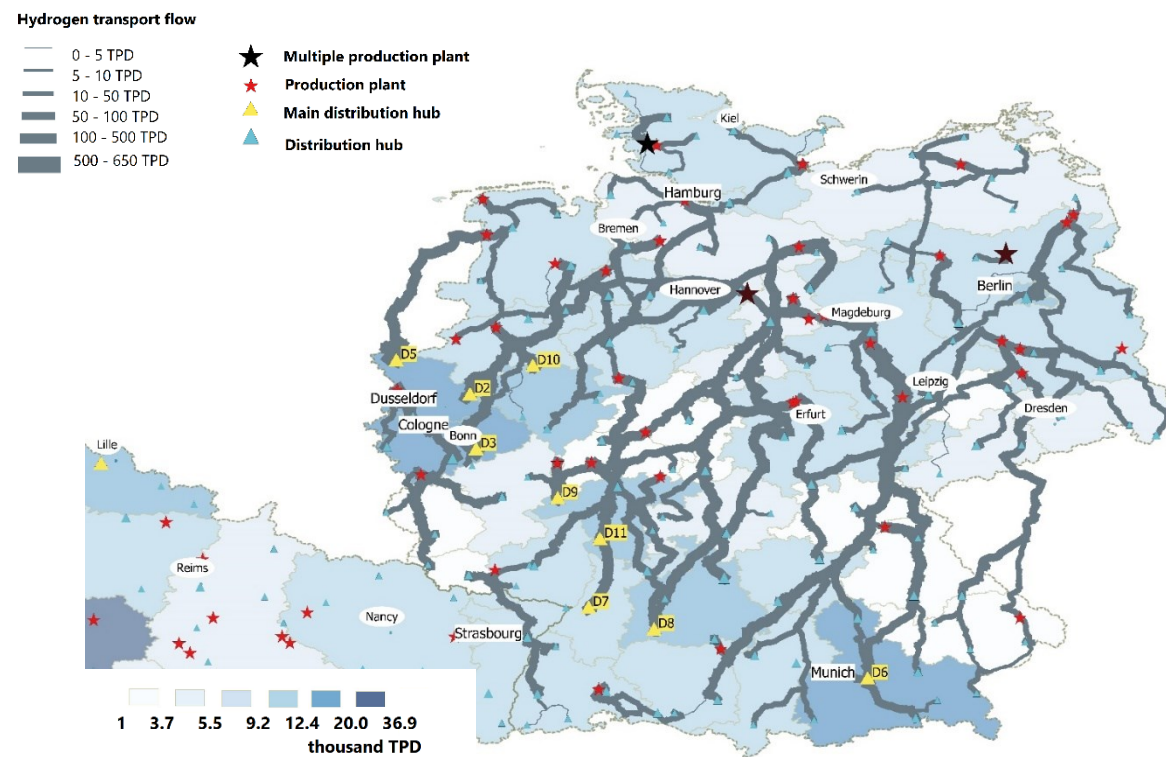


Figure F.4: Hydrogen flow for scenario  $S_4$

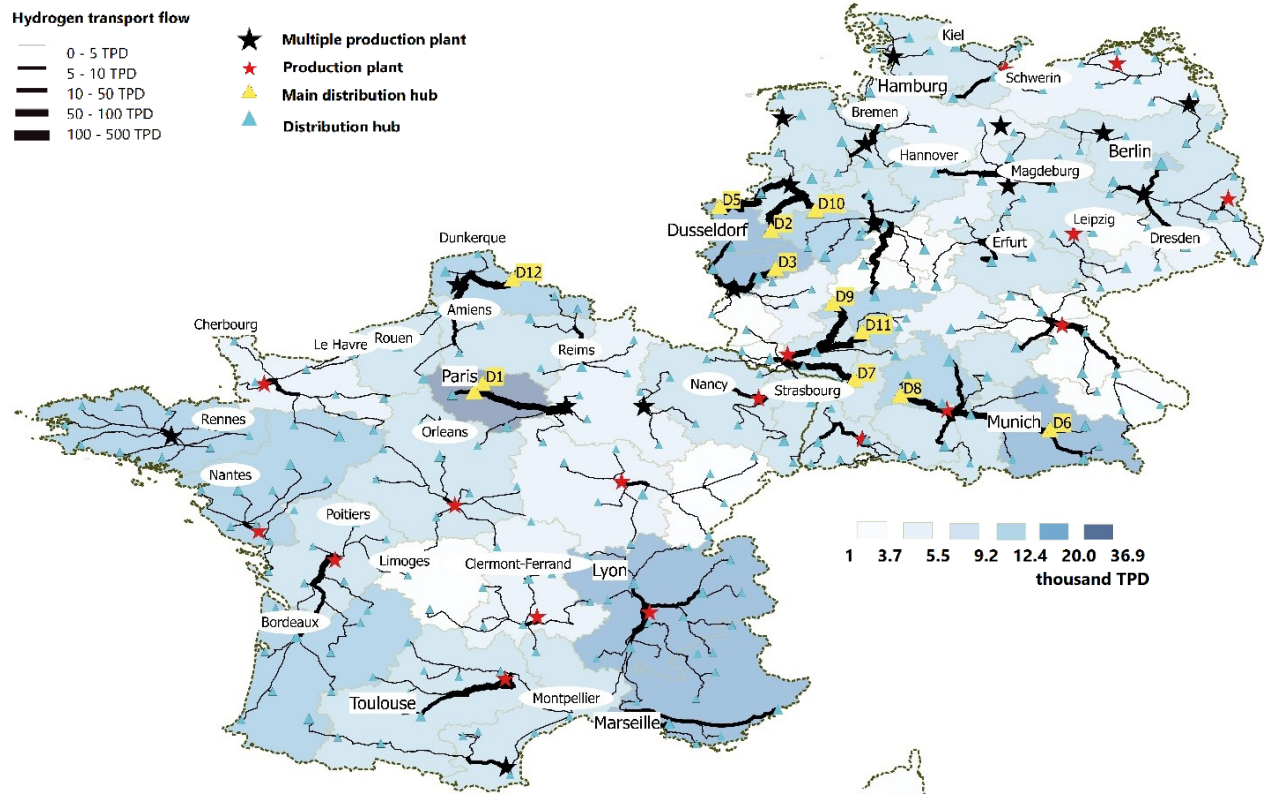


Figure F.5: Hydrogen flow for scenario  $S_5$

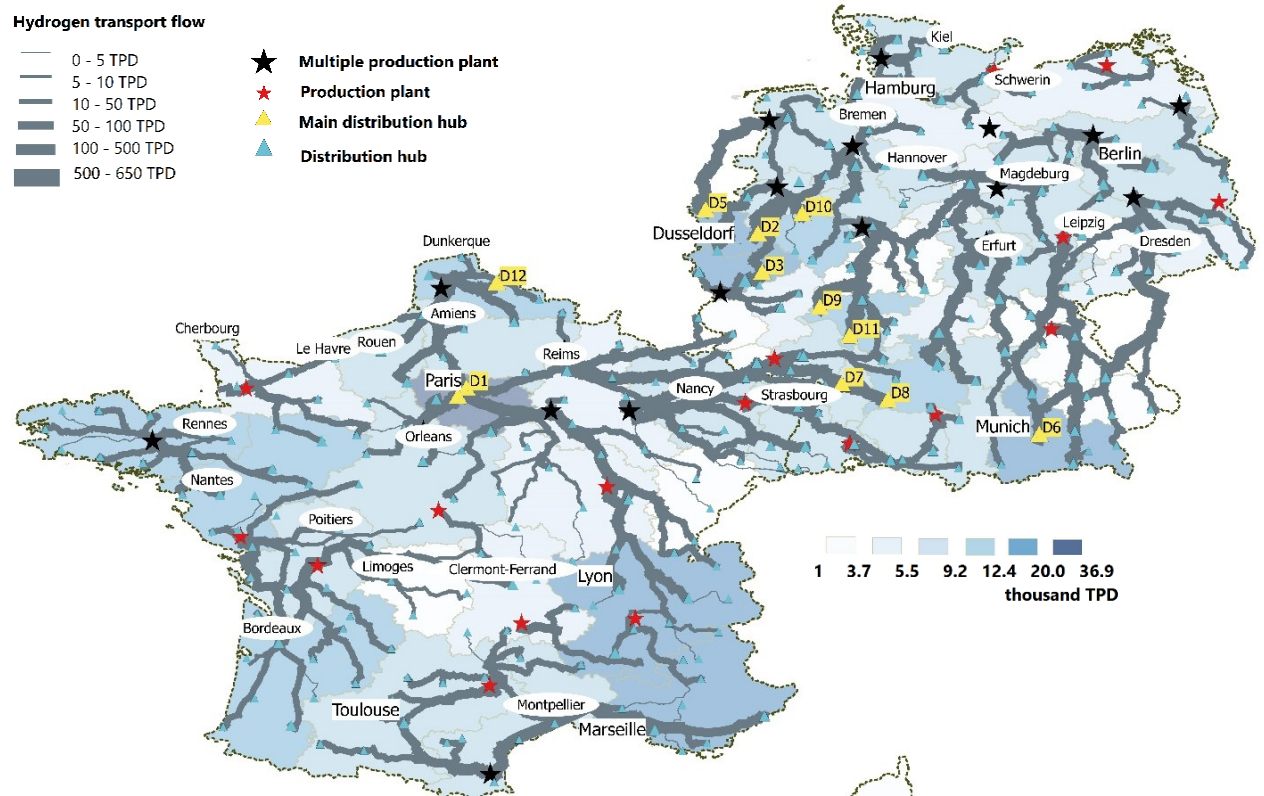


Figure F.6: Hydrogen flow for scenario  $S_6$

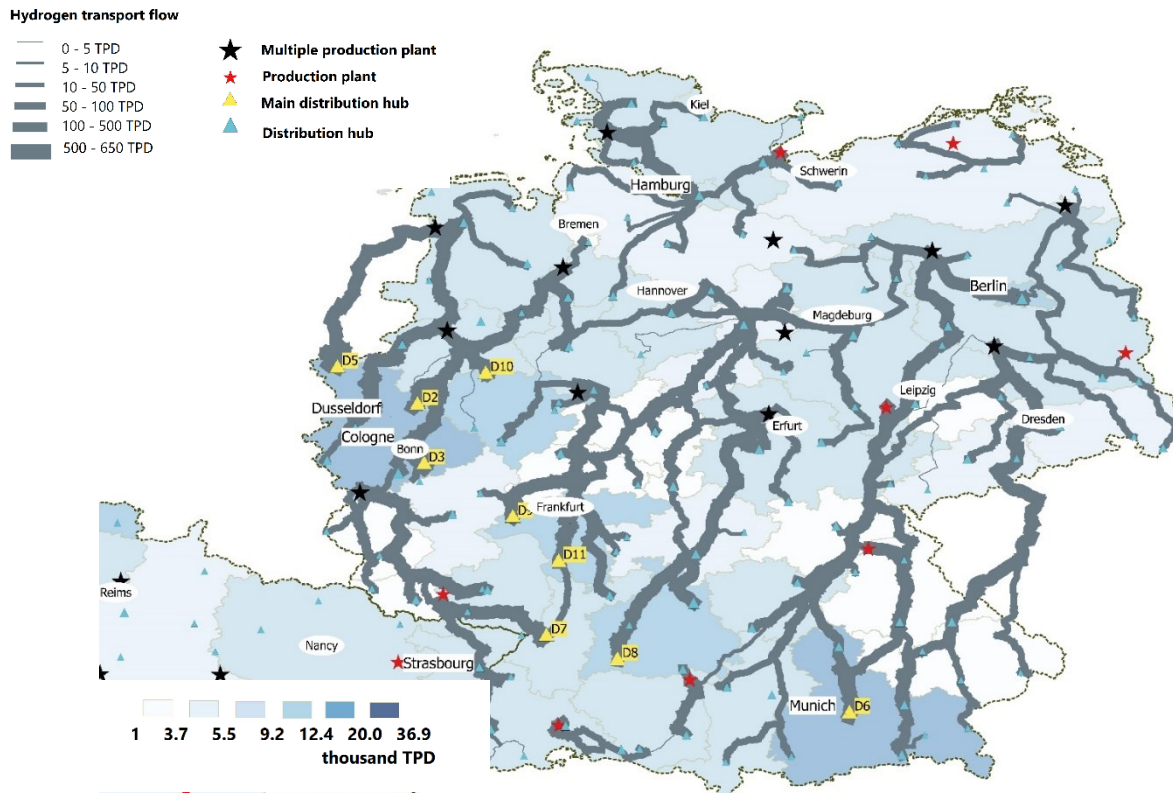


Figure F.7: Hydrogen flow for scenario  $S_7$

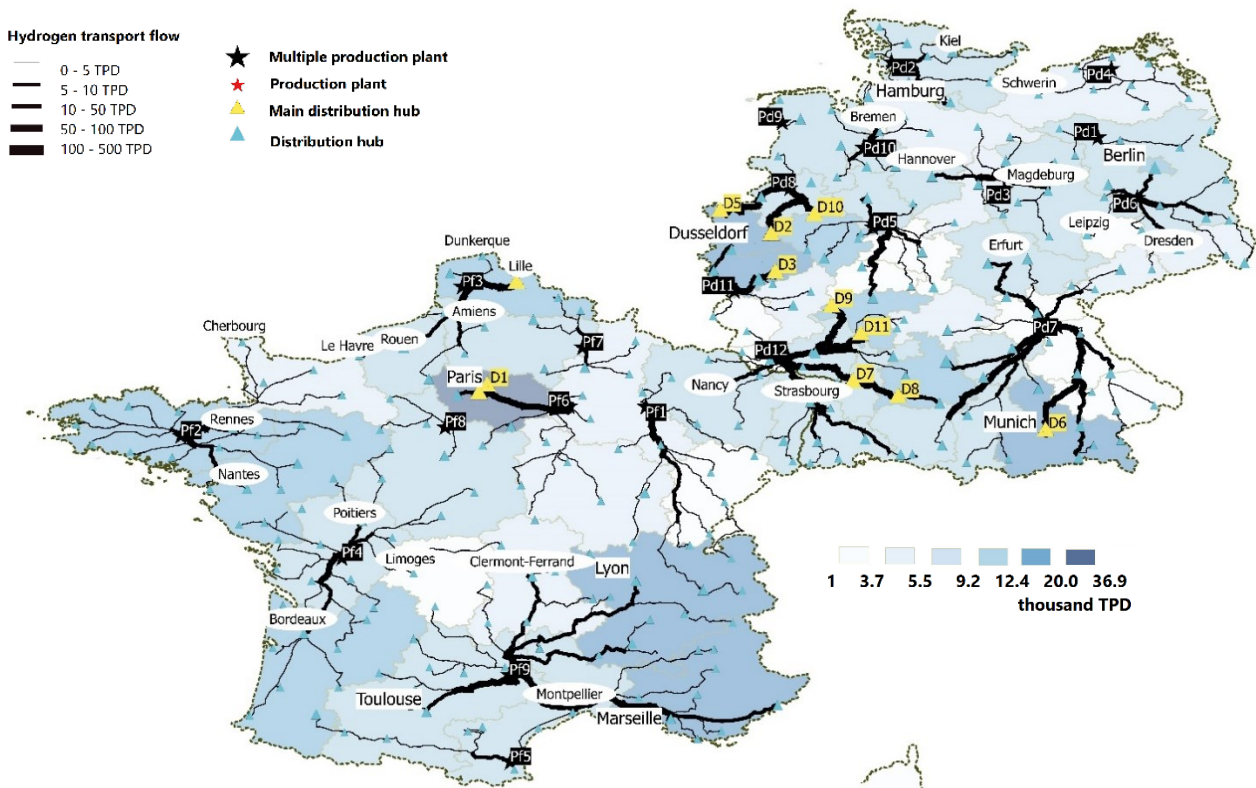


Figure F.8: Hydrogen flow for scenario  $S_8$

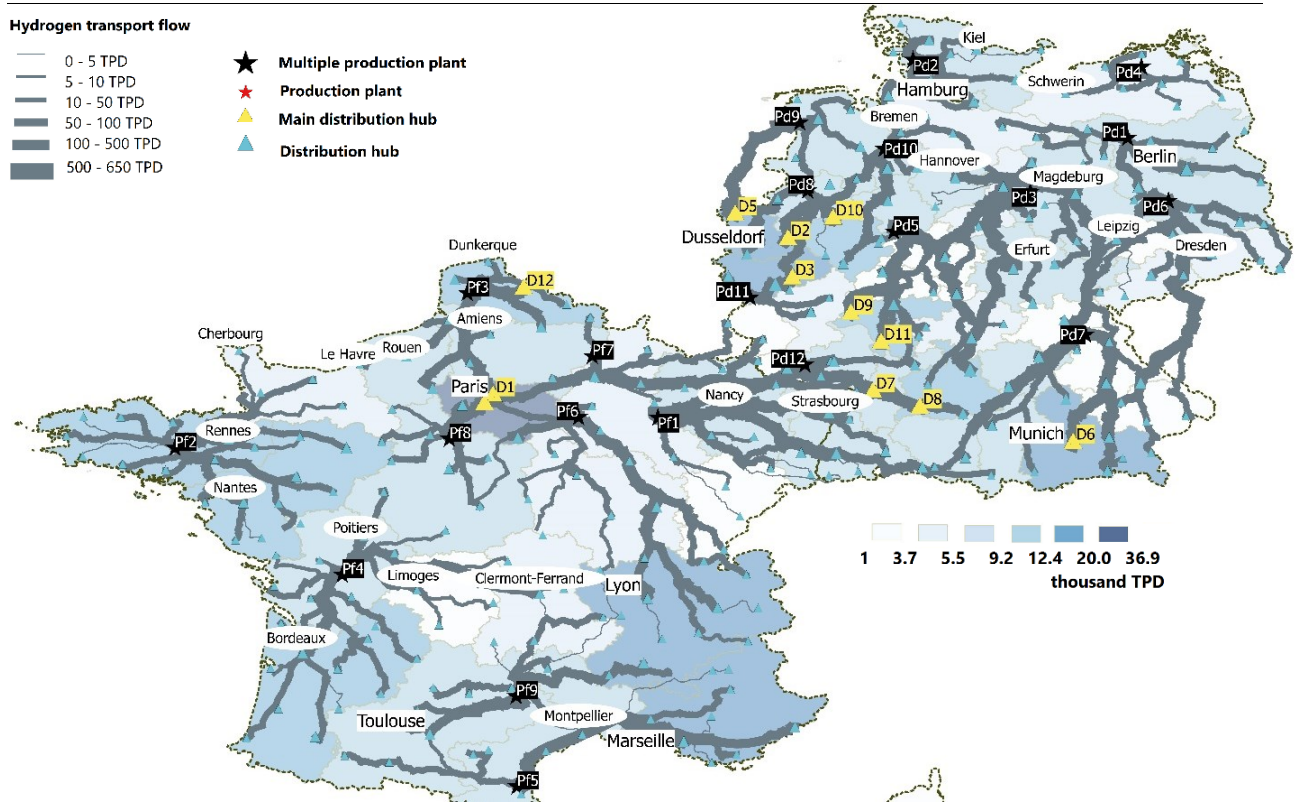


Figure F.9: Hydrogen flow for scenario  $S_9$

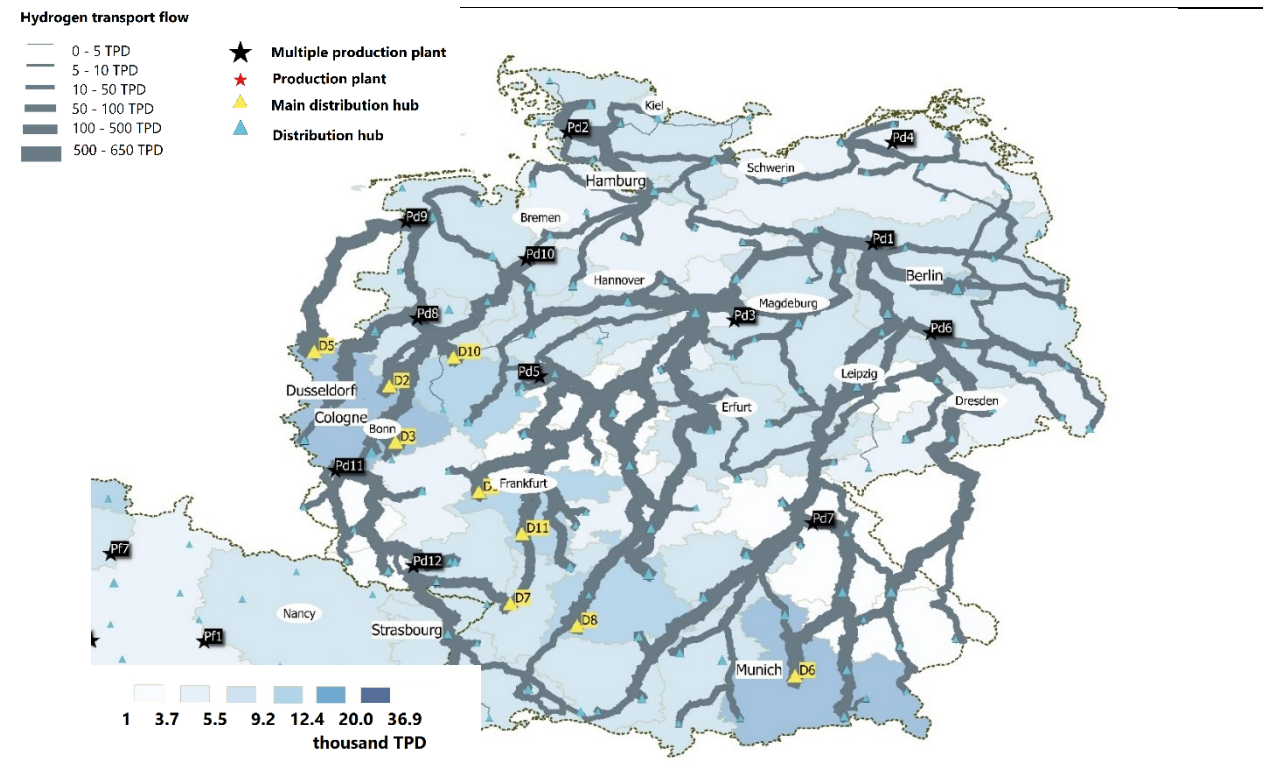


Figure F.10: Hydrogen flow for scenario  $Sp_1$

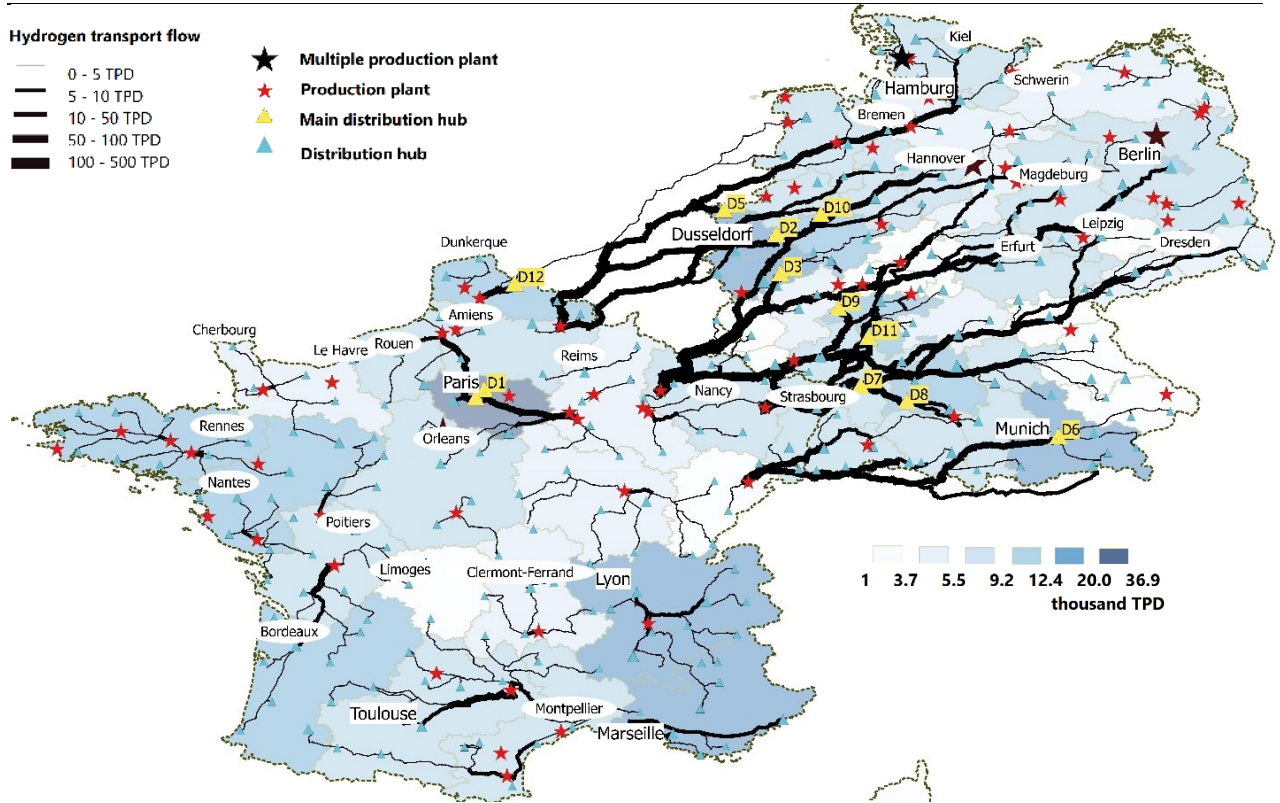


Figure F.11: Hydrogen flow for scenario  $Sp_2$

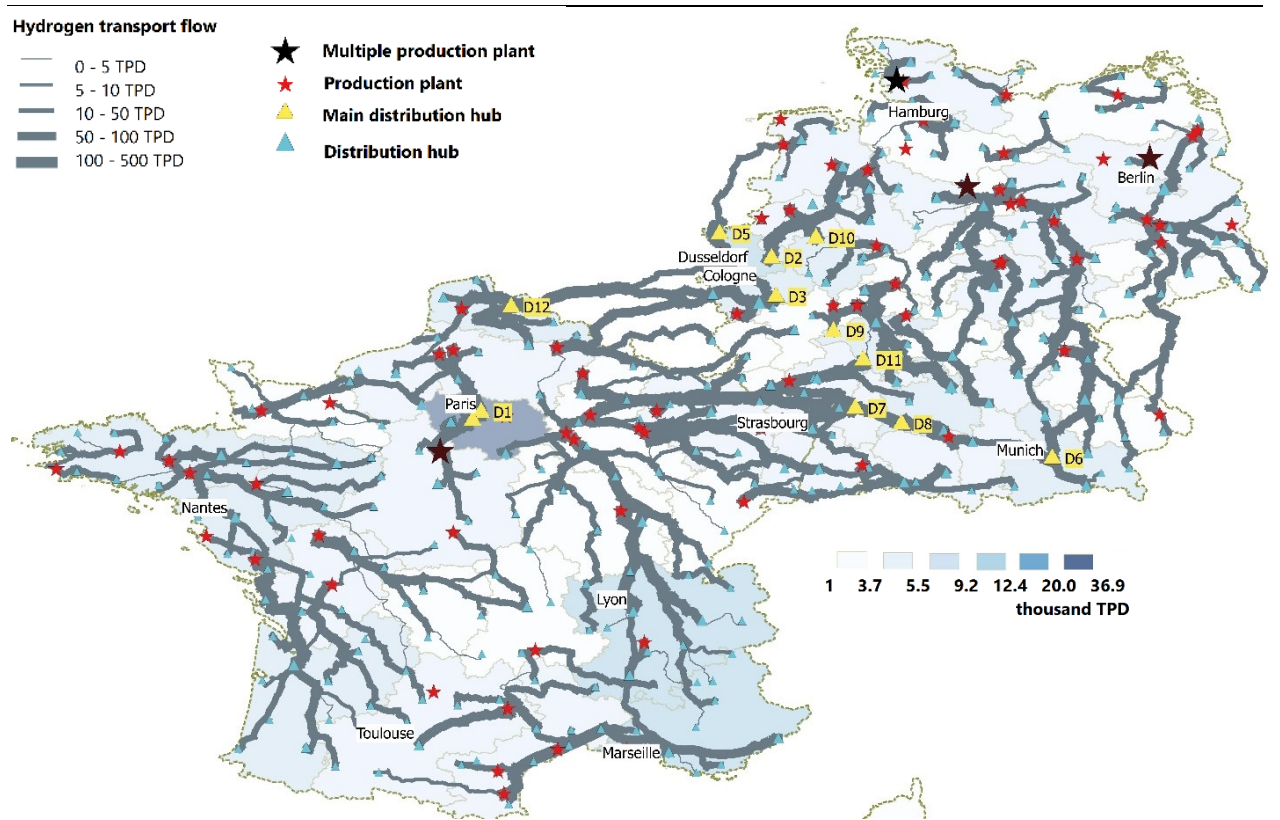


Figure F.12: Hydrogen flow for scenario  $S_{p3}$

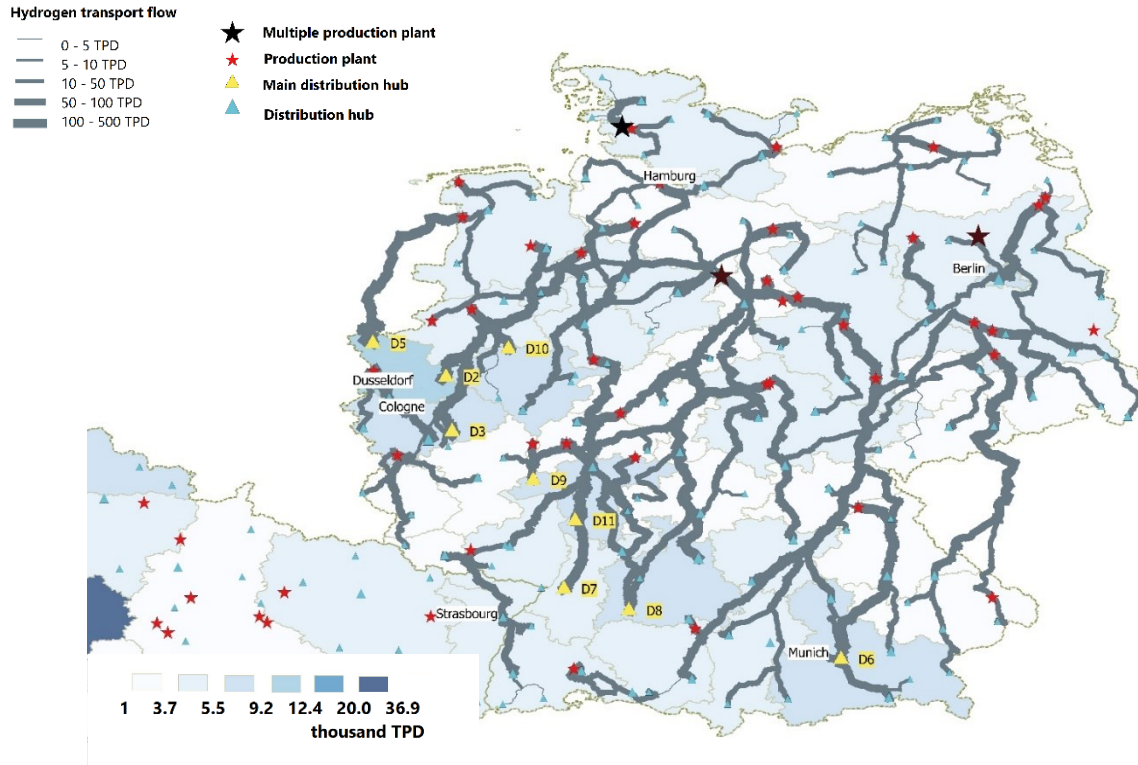


Figure F.13: Hydrogen flow for scenario  $Sp_7$

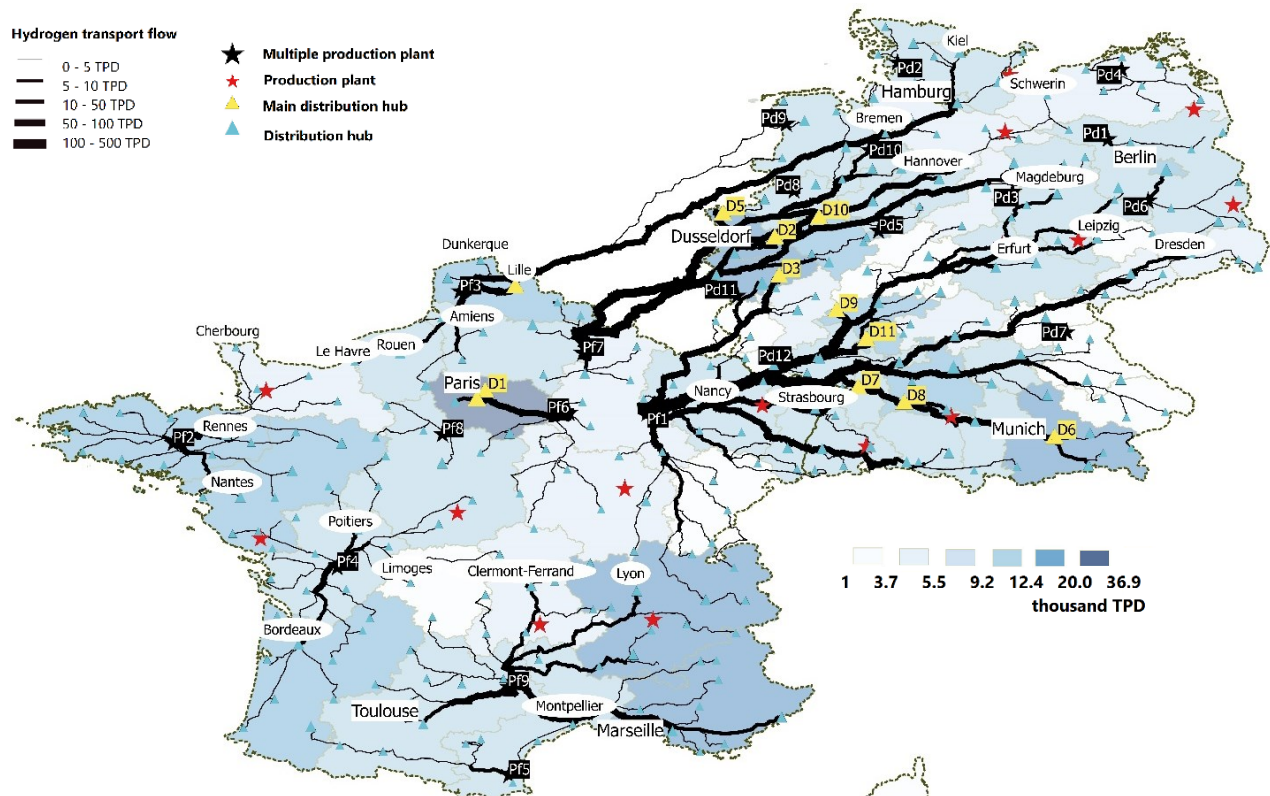


Figure F.14: Hydrogen flow for scenario  $Sp_8$

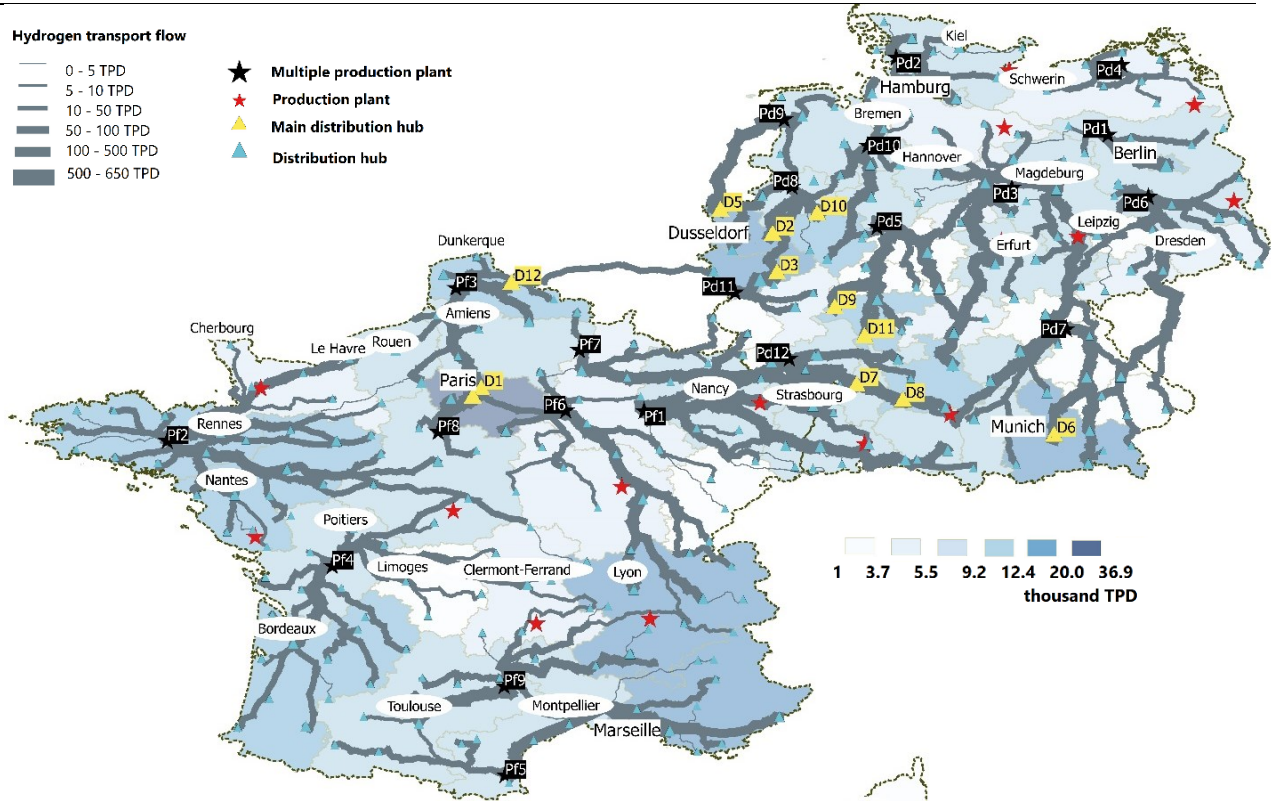
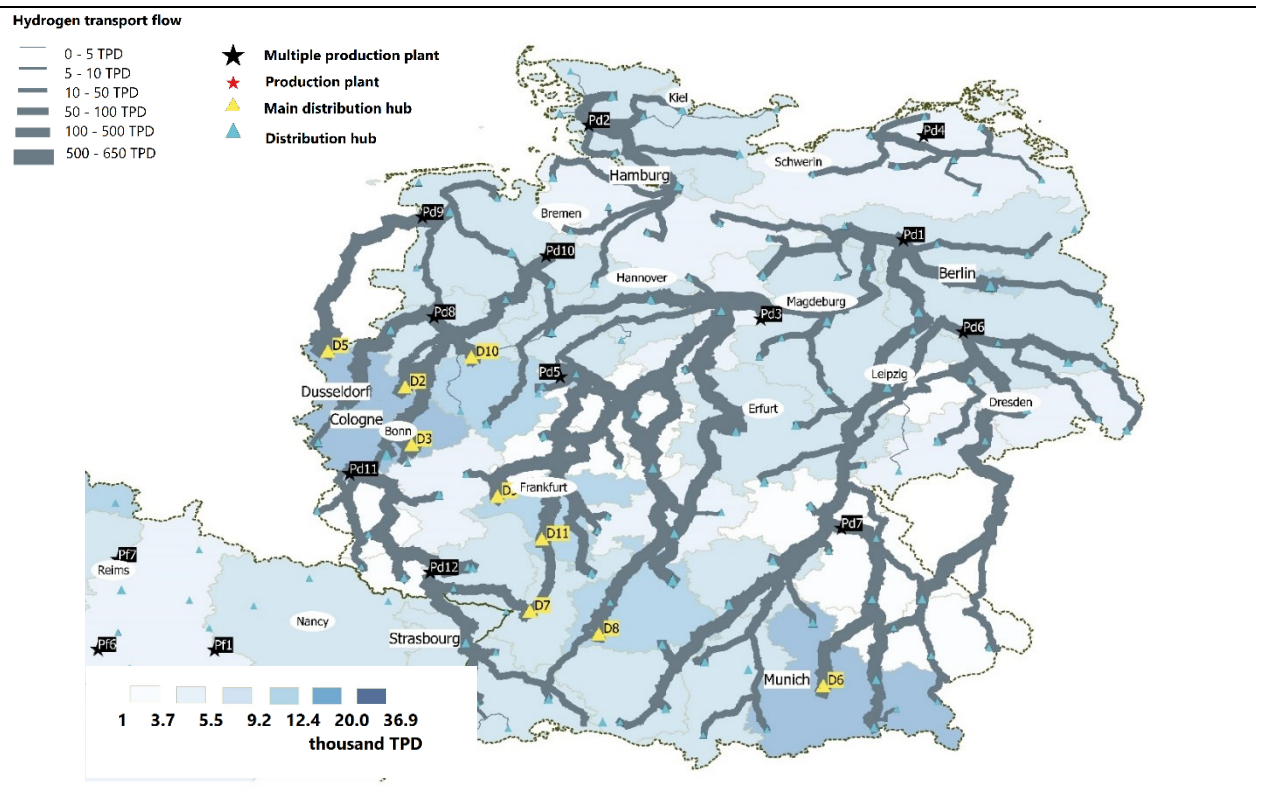


Figure F.15: Hydrogen flow for scenario  $Sp_9$



# REFERENCE

- AFHYPAC (2018a) *Développons l'Hydrogène pour l'économie française*. Association français pour l'hydrogène et les piles combustibles.  
[http://www.afhypac.org/documents/actualites/pdf/Afhypac\\_Etude%20H2%20Fce\\_VDEF.pdf](http://www.afhypac.org/documents/actualites/pdf/Afhypac_Etude%20H2%20Fce_VDEF.pdf).
- AFHYPAC (2018b) *L'HYDROGÈNE : DÉFI NATIONAL, ENJEUX TERRITORIAUX*. Association français pour l'hydrogène et les piles combustibles.  
[http://www.afhypac.org/documents/Enjeux%20territoriaux\\_def\\_BD.pdf](http://www.afhypac.org/documents/Enjeux%20territoriaux_def_BD.pdf).
- AGENCY, I. E. (2015) *Energy and Climate Change–World Energy Outlook Special Report*. International Energy Agency Paris.
- AGORA (2017) *Transforming the Transport Sector: 12 Insights into the Verkehrswende*. Agora Verkehrswende. [https://www.agora-verkehrswende.de/fileadmin/Projekte/2017/12\\_Thesen/Agora-Verkehrswende-12-Insights\\_EN\\_WEB.pdf](https://www.agora-verkehrswende.de/fileadmin/Projekte/2017/12_Thesen/Agora-Verkehrswende-12-Insights_EN_WEB.pdf).
- AGORA (2018) *Energiewende 2030: Megatrends, Targets, Strategies and a 10-Point Agenda* Agora Energiewende. [https://www.agora-energiewende.de/fileadmin2/Projekte/2017/Big\\_Picture/134\\_Big-Picture\\_EN\\_WEB.pdf](https://www.agora-energiewende.de/fileadmin2/Projekte/2017/Big_Picture/134_Big-Picture_EN_WEB.pdf).
- AL-SHARAFI, A., SAHIN, A. Z., AYAR, T. & YILBAS, B. S. (2017) Techno-economic analysis and optimization of solar and wind energy systems for power generation and hydrogen production in Saudi Arabia. *Renewable and Sustainable Energy Reviews*, 69, 33-49.
- ALMANSOORI, A. & BETANCOURT-TORCAT, A. (2016) Design of optimization model for a hydrogen supply chain under emission constraints-A case study of Germany. *Energy*, 111, 414-429.
- ALMANSOORI, A. & SHAH, N. (2006) Design and operation of a future hydrogen supply chain: snapshot model. *Chemical Engineering Research and Design*, 84:6, 423-438.
- ALMANSOORI, A. & SHAH, N. (2009) Design and operation of a future hydrogen supply chain: multi-period model. *international journal of hydrogen energy*, 34:19, 7883-7897.
- ALMARAZ, S. D.-L., AZZARO-PANTEL, C., MONTASTRUC, L. & BOIX, M. (2015) Deployment of a hydrogen supply chain by multi-objective/multi-period optimization at regional and national scales. *Chemical Engineering Research and Design*, 104, 11-31.
- ALMARAZ, S. D.-L., AZZARO-PANTEL, C., MONTASTRUC, L. & DOMENECH, S. (2014) Hydrogen supply chain optimization for deployment scenarios in the Midi-Pyrénées region, France. *International Journal of Hydrogen Energy*, 39:23, 11831-11845.
- AMOS, W. A. (1999) *Costs of storing and transporting hydrogen*. National Renewable Energy Lab., Golden, CO (US).
- ANDRÉ, J., AURAY, S., BRAC, J., DE WOLF, D., MAISONNIER, G., OULD-SIDI, M.-M. & SIMONNET, A. (2013) Design and dimensioning of hydrogen transmission pipeline networks. *European Journal of Operational Research*, 229:1, 239-251.
- ANDRÉ, J., AURAY, S., DE WOLF, D., MEMMAH, M.-M. & SIMONNET, A. (2014) Time development of new hydrogen transmission pipeline networks for France. *International Journal of Hydrogen Energy*, 39:20, 10323-10337.
- ANEX, R. P., et al. (2010) Techno-economic comparison of biomass-to-transportation fuels via pyrolysis, gasification, and biochemical pathways. *Fuel*, 89, S29-S35.
- ANG, A. (2009) *Evaluation of active management of the Norwegian government pension fund–global*. London Business School.

- BARBIR, F. (2005) PEM electrolysis for production of hydrogen from renewable energy sources. *Solar Energy*, 78:5, 661-669.
- BARTELS, J. R., PATE, M. B. & OLSON, N. K. (2010) An economic survey of hydrogen production from conventional and alternative energy sources. *International Journal of Hydrogen Energy*, 35:16, 8371-8384.
- BELLOTTI, D., RIVAROLO, M., MAGISTRI, L. & MASSARDO, A. (2015a) Thermo-economic comparison of hydrogen and hydro-methane produced from hydroelectric energy for land transportation. *International Journal of Hydrogen Energy*, 40:6, 2433-2444.
- BELLOTTI, D., RIVAROLO, M., MAGISTRI, L. & MASSARDO, A. F. (2015b) Thermo-economic comparison of hydrogen and hydro-methane produced from hydroelectric energy for land transportation. *International Journal of Hydrogen Energy*, 40:6, 2433-2444.
- BESSARABOV, D., et al. (2017) South African hydrogen infrastructure (HySA infrastructure) for fuel cells and energy storage: Overview of a projects portfolio. *International Journal of Hydrogen Energy*, 42:19, 13568-13588.
- BHATTACHARYYA, R., MISRA, A. & SANDEEP, K. (2017) Photovoltaic solar energy conversion for hydrogen production by alkaline water electrolysis: conceptual design and analysis. *Energy Conversion and management*, 133, 1-13.
- BLANCO, H., NIJS, W., RUF, J. & FAALJ, A. (2018) Potential for hydrogen and Power-to-Liquid in a low-carbon EU energy system using cost optimization. *Applied Energy*, 232, 617-639.
- BOUDRIES, R. (2013) Analysis of solar hydrogen production in Algeria: Case of an electrolyzer-concentrating photovoltaic system. *International Journal of Hydrogen Energy*, 38:26, 11507-11518.
- BOUDRIES, R. & DIZENE, R. (2011) Prospects of solar hydrogen production in the Adrar region. *Renewable energy*, 36:11, 2872-2877.
- BOUWMEESTER, M. C. & OOSTERHAVEN, J. (2017) Economic impacts of natural gas flow disruptions between Russia and the EU. *Energy policy*, 106, 288-297.
- BRAUNSDORF, P. (2018) *Country Overview Germany*. International Infrastructure Workshop Boston, <https://www.energy.gov/sites/prod/files/2018/10/f56/fcto-infrastructure-workshop-2018-1-braunsdorf.pdf>.
- BREY, J., CARAZO, A. & BREY, R. (2012) Using AHP and binary integer programming to optimize the initial distribution of hydrogen infrastructures in Andalusia. *International Journal of hydrogen energy*, 37:6, 5372-5384.
- BRÜCKNER, N., OBESSER, K., BÖSMANN, A., TEICHMANN, D., ARLT, W., DUNGS, J. & WASSERSCHIED, P. (2014) Evaluation of Industrially Applied Heat-Transfer Fluids as Liquid Organic Hydrogen Carrier Systems. *ChemSusChem*, 7:1, 229-235.
- BRUNET, J. & PONSSARD, J.-P. (2016) Policies and deployment for fuel cell electric vehicles an assessment of the normandy project.
- BURGER, B. (2018) Net Public Electricity Generation in Germany in 2018. Fraunhofer institute for solar energy systems ISE. [https://www.ise.fraunhofer.de/content/dam/ise/en/documents/News/Stromerzeugung\\_2018\\_2\\_en.pdf](https://www.ise.fraunhofer.de/content/dam/ise/en/documents/News/Stromerzeugung_2018_2_en.pdf).
- CAPROS, P., et al. (2016) EU Reference Scenario 2016-Energy, transport and GHG emissions Trends to 2050.
- CFR (2019) *Political Instability in Algeria*. Council Foreign relations. <https://www.cfr.org/report/political-instability-algeria>.
- COMMISSION, E. (2007) *Communication from the Commission to the European Council and the European Parliament: An Energy Policy for Europe*. Commission of the European Communities. <https://eur-lex.europa.eu/legal-content/EN/TXT/PDF/?uri=CELEX:52007DC0001&from=EN>.

- COMMISSION, E. (2009) Renewable energy directive. IN UNION, T. E. P. A. T. C. O. T. E. (Ed.) 2009/28/EC. <https://eur-lex.europa.eu/legal-content/EN/TXT/HTML/?uri=CELEX:32009L0028&from=EN>.
- COMMISSION, E. (2011) *White Paper—Roadmap to a Single European Transport Area—Towards a Competitive and Resource Efficient Transport System*. European Commission.
- COMMISSION, E. (2012) *Energy roadmap 2050*, Publications Office of the European Union.
- COMMISSION, E. (2014) Communication from the Commission to the European Parliament, the Council, the European Economic and Social Committee and the Committee of the Regions—A policy framework for climate and energy in the period from 2020 to 2030, COM (2014) 15 final, Brussels, 22.1. 2014.
- COMMISSION, E. (2015) *EU transport in figures*.
- COMMISSION, E. (2018) *Revised renewable energy directive*.
- CORBETTA, G., HO, A. & PINEDA, I. (2015) *Wind energy scenarios for 2030*. European Wind Energy Association. <https://www.ewea.org/fileadmin/files/library/publications/reports/EWEA-Wind-energy-scenarios-2030.pdf>.
- COUNCIL, N. R. (2004) *The hydrogen economy: opportunities, costs, barriers, and R&D needs*, National Academies Press.
- DATALAB (2018) *Chiffres du climat ;France et monde ; Edition 2017*.
- DEMIR, M. E. & DINCER, I. (2017) Cost assessment and evaluation of various hydrogen delivery scenarios. *International Journal of Hydrogen Energy*.
- DEMIR, M. E. & DINCER, I. (2018) Cost assessment and evaluation of various hydrogen delivery scenarios. *International Journal of Hydrogen Energy*, 43:22, 10420-10430.
- DUMAN, A. C. & GÜLER, Ö. (2018) Techno-economic analysis of off-grid PV/wind/fuel cell hybrid system combinations with a comparison of regularly and seasonally occupied households. *Sustainable Cities and Society*, 42, 107-126.
- EOLIENNE, F. E. (2017) *La transition énergétique*. <http://fee.asso.fr/politique-de-leolien/la-transition-energetique/>.
- ESSO (2016) *essofuelfinder*. <https://wholesalefuels.esso.de/de-DE/>.
- EUROPE, W. (2018) Wind in Power 2017. Annual Combined Onshore and Offshore Wind Energy Statistics. [windeurope.org/wp-content/uploads/files/about-wind/statistics/WindEurope-Annual-Statistics-2017.pdf](http://windeurope.org/wp-content/uploads/files/about-wind/statistics/WindEurope-Annual-Statistics-2017.pdf).
- EUROPEAN-COMMISSION (2018a) *EU energy in figures*. European Commission. [https://ec.europa.eu/energy/sites/ener/files/pocketbook\\_energy\\_2018\\_web.pdf](https://ec.europa.eu/energy/sites/ener/files/pocketbook_energy_2018_web.pdf).
- EUROPEAN-COMMISSION (2018b) *EU transport in figures*. European Commission. <https://ec.europa.eu/transport/sites/transport/files/pocketbook2018.pdf>.
- Eurostat (2016a) Passenger road transport on national territory, by type of vehicles registered in the reporting country. <http://ec.europa.eu/eurostat/web/transport/data/database>. 7th Mai 2016.
- Eurostat (2016b) Population projections data. STATISTICS, E., <http://ec.europa.eu/eurostat/web/population-demography-migration-projections/population-projections-data>. 7th Mai 2016.
- EUROSTAT (2017a) *NUTS regions in France*. European statistics. <http://ec.europa.eu/eurostat/documents/345175/7451602/nuts-map-FR.pdf>. 26th January 2018
- EUROSTAT (2017b) *NUTS regions in Germany*. European statistics. <http://ec.europa.eu/eurostat/documents/345175/7451602/nuts-map-DE.pdf>. 26th January 2018.
- EUROSTAT (2018a) *Population on 1 January by NUTS 2 region*. European statistics. <http://ec.europa.eu/eurostat/tgm/table.do?tab=table&init=1&language=en&pcode=tgs00096&plugin=1>. 12th June 2018.

- Eurostat (2018b) Stock of vehicles by category and NUTS 2 regions. STATISTICS, E., [http://appsso.eurostat.ec.europa.eu/nui/show.do?dataset=tran\\_r\\_vehst&lang=en](http://appsso.eurostat.ec.europa.eu/nui/show.do?dataset=tran_r_vehst&lang=en). 7th Mai 2018.
- FCH-JU (2019) *Hydrogen roadmap Europe*. FUEL CELLS AND HYDROGEN. [https://www.fch.europa.eu/sites/default/files/Hydrogen%20Roadmap%20Europe\\_Report.pdf](https://www.fch.europa.eu/sites/default/files/Hydrogen%20Roadmap%20Europe_Report.pdf).
- FIKRT, A., et al. (2017) Dynamic power supply by hydrogen bound to a liquid organic hydrogen carrier. *Applied Energy*, 194, 1-8.
- FRAILE, D., LANOIX, J.-C., MAIO, P., RANGEL, A. & TORRES, A. (2015) Overview of the market segmentation for hydrogen across potential customer groups, based on key application areas. *CertifHy Proj*, 1-32.
- FUELLCELLTODAY (2013) *Fuel Cells and Hydrogen in Norway*.
- GÖKÇEK, M. & KALE, C. (2018) Techno-economical evaluation of a hydrogen refueling station powered by Wind-PV hybrid power system: A case study for İzmir-Çeşme. *International Journal of Hydrogen Energy*, 43:23, 10615-10625.
- GOUV (2017) *Plan climat*. Le ministère de la Transition écologique et solidaire. [https://www.ecologique-solidaire.gouv.fr/sites/default/files/2017.07.06%20-%20Plan%20Climat\\_0.pdf](https://www.ecologique-solidaire.gouv.fr/sites/default/files/2017.07.06%20-%20Plan%20Climat_0.pdf).
- GOVERNEMT (August 2017) *Plan Climat*. <http://www.gouvernement.fr/action/plan-climat>.
- GRASS (2003) Geographic Resources Analysis Support System. *GRASS GIS 7.7.svn*. <https://grass.osgeo.org/grass77/manuals/index.html>.
- GRUBB, M., VROLIJK, C. & BRACK, D. (1997) *The Kyoto Protocol: a guide and assessment*, Royal Institute of International Affairs Energy and Environmental Programme.
- GUANDALINI, G., CAMPANARI, S. & ROMANO, M. C. (2015) Power-to-gas plants and gas turbines for improved wind energy dispatchability: Energy and economic assessment. *Applied Energy*, 147, 117-130.
- H2 (2018) Hydrogen Refueling Stations Worldwide. H2STATIONS, <https://www.netinform.net/h2/h2stations/h2stations.aspx>.
- H2 (2019a) *Hydrogen cars, All models at a glance*. <https://h2.live/en/wasserstoffautos>. 19/02/2019.
- H2 (2019b) *Network expansion, The latest update for Germany*. H2. <https://h2.live/en/netzausbau>. 03/02/2019.
- HAN, J.-H., RYU, J.-H. & LEE, I.-B. (2012) Modeling the operation of hydrogen supply networks considering facility location. *International Journal of Hydrogen Energy*, 37:6, 5328-5346.
- HAN, J.-H., RYU, J.-H. & LEE, I.-B. (2013) Multi-objective optimization design of hydrogen infrastructures simultaneously considering economic cost, safety and CO2 emission. *Chemical Engineering Research and Design*, 91:8, 1427-1439.
- HE, C., SUN, H., XU, Y. & LV, S. (2017) Hydrogen refueling station siting of expressway based on the optimization of hydrogen life cycle cost. *International Journal of Hydrogen Energy*, 42:26, 16313-16324.
- HIDROGENOARAGON (2018) *H2PiyR, Hydrogen Corridor for the Pyrenean Region*. Hidrogenoaragon. [http://hidrogenoaragon.org/en/proyectos/h2piyr\\_en/](http://hidrogenoaragon.org/en/proyectos/h2piyr_en/). 02/05/2018.
- HIT (2014) *NATIONAL IMPLEMENTATION PLAN FOR HYDROGEN REFUELING INFRASTRUCTURE 3rd final edition*. [www.hit-tent.eu](http://www.hit-tent.eu).
- HO, A., MBISTROVA, A. & CORBETTA, G. (2016) *The European offshore wind industry - key trends and statistics 2015*. the European Wind Energy Association. <https://www.ewea.org/fileadmin/files/library/publications/statistics/EWEA-European-Offshore-Statistics-2015.pdf>.
- HOFFMANN, J. (2019) On the outlook for solar thermal hydrogen production in South Africa. *International Journal of Hydrogen Energy*, 44:2, 629-640.

- HOLLMULLER, P., JOUBERT, J.-M., LACHAL, B. & YVON, K. (2000) Evaluation of a 5 kWp photovoltaic hydrogen production and storage installation for a residential home in Switzerland. *International Journal of Hydrogen Energy*, 25:2, 97-109.
- HONDA (2018) *Clarity Fuel Cell 2018* <https://automobiles.honda.com/clarity-fuel-cell#>. 19/02/2019.
- HWANGBO, S., LEE, S. & YOO, C. (2017) Optimal network design of hydrogen production by integrated utility and biogas supply networks. *Applied energy*, 208, 195-209.
- HWANGBO, S., NAM, K., HAN, J., LEE, I.-B. & YOO, C. (2018) Integrated hydrogen supply networks for waste biogas upgrading and hybrid carbon-hydrogen pinch analysis under hydrogen demand uncertainty. *Applied Thermal Engineering*, 140, 386-397.
- HYDROGENEUROPE (2018) *Project WindGas Falkenhagen*. <https://hydrogeneurope.eu/index.php/project/windgas-falkenhagen>. 13/09/2018.
- HYUNDAI (2019) *Hyundai NEXO*. <https://www.hyundai.de/Modelle/NEXO.html>. 19/02/2019.
- HYWAY (2018) *Premier cluster de déploiement de flottes captives de véhicules hybrides électriques à hydrogène*. <https://www.tenerrdis.fr/uploads/2017/04/rapport-final-hyway-public.pdf>.
- IEA (2009) *Transport Energy and CO<sub>2</sub>, Moving Toward Sustainability*.
- IEA (2015) *Technology Roadmap: Hydrogen and Fuel Cells*. International Energy Agency, IEA. <http://www.iea.org/publications/freepublications/publication/technology-roadmap-hydrogen-and-fuel-cells.html>.
- IEA (2017) *Key world energy statistics*. International Energy Agency. <https://www.iea.org/publications/freepublications/publication/KeyWorld2017.pdf>.
- IEA (2019) *Hydrogen, Tracking Clean Energy Progress*. <https://www.iea.org/tcep/energyintegration/hydrogen/>.
- JONES, D., SAKHEL, A., BUCK, M. & GRAICHEN, P. (2019) *The European Power Sector in 2018, Up-to-date analysis on the electricity transition*. Sandbag, Agora Energiewende.
- JUNG, C., NAGEL, L., SCHINDLER, D. & GRAU, L. (2018) Fossil fuel reduction potential in Germany's transport sector by wind-to-hydrogen. *International Journal of Hydrogen Energy*, 43:52, 23161-23167.
- KIKUCHI, Y., ICHIKAWA, T., SUGIYAMA, M. & KOYAMA, M. (2019) Battery-assisted low-cost hydrogen production from solar energy: Rational target setting for future technology systems. *International Journal of Hydrogen Energy*, 44:3, 1451-1465.
- KIM, M. & KIM, J. (2016) Optimization model for the design and analysis of an integrated renewable hydrogen supply (IRHS) system: Application to Korea's hydrogen economy. *International Journal of Hydrogen Energy*, 41:38, 16613-16626.
- KOTAY, S. M. & DAS, D. (2008) Biohydrogen as a renewable energy resource—prospects and potentials. *International Journal of Hydrogen Energy*, 33:1, 258-263.
- L-B-SYSTEMTECHNIK (2008) *European hydrogen energy roadmap (HyWays)*. [http://ieahydrogen.org/Activities/National-Documents/Task-18/HyWays\\_External\\_Document\\_02FEB2006.aspx](http://ieahydrogen.org/Activities/National-Documents/Task-18/HyWays_External_Document_02FEB2006.aspx).
- LEVENE, J. (2005) *Economic Analysis of Hydrogen Production from Wind: Preprint*. National Renewable Energy Laboratory (NREL), Golden, CO. <https://www.nrel.gov/docs/fy05osti/38210.pdf>.
- LI, Z., GAO, D., CHANG, L., LIU, P. & PISTIKOPOULOS, E. N. (2008) Hydrogen infrastructure design and optimization: a case study of China. *International Journal of Hydrogen Energy*, 33:20, 5275-5286.
- LIN, Z., CHEN, C.-W., OGDEN, J. & FAN, Y. (2008) The least-cost hydrogen for Southern California. *International Journal of Hydrogen Energy*, 33:12, 3009-3014.
- LIN, Z., OU, S., ELGOWAINY, A., REDDI, K., VEENSTRA, M. & VERDUZCO, L. (2018) A method for determining the optimal delivered hydrogen pressure for fuel cell electric vehicles. *Applied energy*, 216, 183-194.

- MARKILLIE, R. (2015) *Hydrogen mobility Europe launched with €32M funding*. <http://www.itm-power.com/news-item/hydrogen-mobility-europe-launched-with-e32m-funding>. 20/02/2019.
- MAROUFMASHAT, A., FOWLER, M., KHAVAS, S. S., ELKAMEL, A., ROSHANDEL, R. & HAJIMIRAGHA, A. (2016) Mixed-integer linear programming based approach for optimal planning and operation of a smart urban energy network to support the hydrogen economy. *International Journal of hydrogen energy*, 41:19, 7700-7716.
- MASSON-DELMOTTE, V., et al. (2018) IPCC, 2018: Summary for Policymakers. *Global Warming of*, 1.
- MERCEDES-BENZ (2019) *Electric intelligence by Mercedes-Benz*. <https://www.mercedes-benz.fr/passengercars/mercedes-benz-cars/models/e-mobility/project-eq/experience-eq/electric-intelligence.module.html>. 15/02/2019.
- MORENO-BENITO, M., AGNOLUCCI, P. & PAPAGEORGIOU, L. G. (2017) Towards a sustainable hydrogen economy: Optimization-based framework for hydrogen infrastructure development. *Computers & Chemical Engineering*, 102, 110-127.
- MOTOR1 (2018) *Kia E-Niro review*. <https://fr.motor1.com/reviews/296979/autonomie-kia-e-niro-voiture-electrique-essai/>. 12/02/2019.
- MOTORS, T. (2019a) *Tesla Model S*. <https://www.tesla.com/models>. 12/02/2019.
- MOTORS, T. (2019b) *Tesla Model X*. <https://www.tesla.com/modelx>. 10/02/2019.
- NIKOLAIDIS, P. & POULLIKKAS, A. (2017) A comparative overview of hydrogen production processes. *Renewable and sustainable energy reviews*, 67, 597-611.
- NISSAN (2019) *2019 Nissan Leaf*. <https://www.nissanusa.com/vehicles/electric-cars/leaf.html>. 12/02/2019.
- NISTOR, S., DAVE, S., FAN, Z. & SOORIYABANDARA, M. (2016) Technical and economic analysis of hydrogen refueling. *Applied Energy*, 167, 211-220.
- NREL (2015) H2A: Hydrogen Analysis Production Models. *Future Central Hydrogen Production from PEM Electrolysis version 3.101* version 3.101 ed. <https://www.nrel.gov/hydrogen/h2a-production-models.html>.
- NUNES, P., OLIVEIRA, F., HAMACHER, S. & ALMANSOORI, A. (2015) Design of a hydrogen supply chain with uncertainty. *International Journal of Hydrogen Energy*, 40:46, 16408-16418.
- NYKVIST, B. & NILSSON, M. (2015) Rapidly falling costs of battery packs for electric vehicles. *Nature climate change*, 5:4, 329.
- OPSM (2019) Bonn Hauptbahnhof, Bonn Beuel. <https://www.openstreetmap.org/#map=16/50.7354/7.1127>.
- OPSD (2018) Renewable power plants DE. [https://data.open-power-system-data.org/renewable\\_power\\_plants/](https://data.open-power-system-data.org/renewable_power_plants/). 29th March 2018.
- PFEIFFER, A., MILLAR, R., HEPBURN, C. & BEINHOCKER, E. (2016) The '2 C capital stock' for electricity generation: Committed cumulative carbon emissions from the electricity generation sector and the transition to a green economy. *Applied Energy*, 179, 1395-1408.
- POSTGRESQL (1996) PostgreSQL IN GROUP, T. P. G. D. (Ed.). <https://www.postgresql.org/>.
- The Wind Power (2016) Total installed capacity by country. POWER, T. W., [http://www.thewindpower.net/country\\_list\\_en.php](http://www.thewindpower.net/country_list_en.php). 5th September 2017.
- PREGGER, T., GRAF, D., KREWITT, W., SATTLER, C., ROEB, M. & MÖLLER, S. (2009) Prospects of solar thermal hydrogen production processes. *International journal of hydrogen energy*, 34:10, 4256-4267.
- REDDI, K., ELGOWAINY, A. & SUTHERLAND, E. (2014) Hydrogen refueling station compression and storage optimization with tube-trailer deliveries. *International Journal of Hydrogen Energy*, 39:33, 19169-19181.
- REIS, A. (2010) *The role of Battery Electric Vehicles, Plug-in Hybrids and Fuel Cell Electric Vehicles*.

- REUß, M., GRUBE, T., ROBINIUS, M., PREUSTER, P., WASSERSCHIED, P. & STOLTEN, D. (2017) Seasonal storage and alternative carriers: A flexible hydrogen supply chain model. *Applied energy*, 200, 290-302.
- REZAEI-SHOUROKI, M., MOSTAFAEIPOUR, A. & QOLIPOUR, M. (2017) Prioritizing of wind farm locations for hydrogen production: a case study. *International Journal of Hydrogen Energy*, 42:15, 9500-9510.
- RICHARDSON, L. (2012) Beautiful Soup. IN RICHARDSON, L. (Ed.) *Beautiful Soup 3*. March 2012 ed. <https://www.crummy.com/software/BeautifulSoup/>.
- RIIS, T., HAGEN, E. F., VIE, P. J. & ULLEBERG, Ø. (2006) Hydrogen production and storage—R&D priorities and gaps. *IEA Hydrogen Implementing Agreement (HIA)*, International Energy Agency (IEA), Paris.
- ROBINIUS, M., et al. (2017) Linking the power and transport sectors—Part 1: The principle of sector coupling. *Energies*, 10:7, 956.
- SABIO, N., GADALLA, M., GUILLÉN-GOSÁLBEZ, G. & JIMÉNEZ, L. (2010) Strategic planning with risk control of hydrogen supply chains for vehicle use under uncertainty in operating costs: a case study of Spain. *International journal of hydrogen energy*, 35:13, 6836-6852.
- SDAA (2010) Global Roads Open Access Data Set. CENTER, S. D. A. A., <http://sedac.ciesin.columbia.edu/data/set/groads-global-roads-open-access-v1/data-download>.
- SHHP (2006) *Hydrogen for transport in the Scandinavian region*. The Scandinavian Hydrogen Highway Partnership. <http://www.scandinavianhydrogen.org/shhp/about-shhp/>. 02/18/2018.
- SHI, L., QI, S., QU, J., CHE, T., YI, C. & YANG, B. (2019) Integration of hydrogenation and dehydrogenation based on dibenzyltoluene as liquid organic hydrogen energy carrier. *International Journal of Hydrogen Energy*, 44:11, 5345-5354.
- SIEMINSKI, A. (2014) International energy outlook. *Energy Information Administration (EIA)*, 18.
- SIMBECK, D. & CHANG, E. (2002) Hydrogen supply: cost estimate for hydrogen pathways—scoping analysis. *National Renewable Energy Laboratory*, 71.
- SPATIALREFERENCE (2013) *Spatial reference list*. <http://spatialreference.org/ref/epsg/>. 2017.
- STEPHENS-ROMERO, S. D., BROWN, T. M., KANG, J. E., RECKER, W. W. & SAMUELSEN, G. S. (2010) Systematic planning to optimize investments in hydrogen infrastructure deployment. *International Journal of Hydrogen Energy*, 35:10, 4652-4667.
- STERN, J., PIRANI, S. & YAFIMAVA, K. (2009) *The Russo-Ukrainian gas dispute of January 2009: a comprehensive assessment*, Oxford Institute for Energy Studies.
- STERN, J., ROGERS, H., YAFIMAVA, K., PIRANI, S., EL-KATIRI, L., HONORE, A., HENDERSON, J., HASSANZADEH, E. & DICKEL, R. (2014) Reducing European Dependence on Russian Gas—distinguishing natural gas security from geopolitics.
- STILLER, C., BÜNGER, U., MØLLER-HOLST, S., SVENSSON, A. M., ESPEGREN, K. A. & NOWAK, M. (2010) Pathways to a hydrogen fuel infrastructure in Norway. *International journal of hydrogen energy*, 35:7, 2597-2601.
- STOLTEN, D. (2016) *Hydrogen Science and Engineering: Materials, Processes, Systems and Technology*, 2 Volume Set, John Wiley & Sons.
- SUN, H., HE, C., WANG, H., ZHANG, Y., LV, S. & XU, Y. (2017) Hydrogen station siting optimization based on multi-source hydrogen supply and life cycle cost. *International Journal of Hydrogen Energy*, 42:38, 23952-23965.
- TAMHANKAR, S. (2014) *Terminal Operations for Tube Trailer and Liquid Tanker Filling: Status, Challenges and R&D Needs*. DOE Hydrogen Transmission and Distribution Workshop, Golden, CO.
- THEWINDPOWER (2018) Calvados (France). POWER, T. W., [https://www.thewindpower.net/windfarm\\_en\\_16522\\_calvados.php](https://www.thewindpower.net/windfarm_en_16522_calvados.php). 05/04/2018.

- THOMAS, M. (2016) *TRAN COMMITTEE - THE WORLD IS CHANGING. TRANSPORT, TOO.*  
<http://www.europarl.europa.eu/committees/en/supporting-analyses-search.html>.
- TOYOTA (2019) *2019 TOYOTA MIRAI FUEL CELL ELECTRIC VEHICLE.*  
<https://ssl.toyota.com/mirai/fcv.html>.
- TURNER, J. A. (2004) Sustainable Hydrogen Production. *Science*, 305:5686, 972-974.
- WIND POWER (2017) Datasets countries. [https://www.thewindpower.net/country\\_list\\_en.php](https://www.thewindpower.net/country_list_en.php). 5th September 2017.
- WOO, Y.-B., CHO, S., KIM, J. & KIM, B. S. (2016) Optimization-based approach for strategic design and operation of a biomass-to-hydrogen supply chain. *International Journal of Hydrogen Energy*, 41:12, 5405-5418.
- WULF, C., REUß, M., GRUBE, T., ZAPP, P., ROBINIUS, M., HAKE, J.-F. & STOLTEN, D. (2018) Life Cycle Assessment of hydrogen transport and distribution options. *Journal of cleaner production*, 199, 431-443.
- XU, X., XU, B., DONG, J. & LIU, X. (2017) Near-term analysis of a roll-out strategy to introduce fuel cell vehicles and hydrogen stations in Shenzhen China. *Applied Energy*, 196, 229-237.
- YANG, C. & OGDEN, J. (2007) Determining the lowest-cost hydrogen delivery mode. *International Journal of Hydrogen Energy*, 32:2, 268-286.
- ZAITSAU, D. H., EMEL'YANENKO, V. N., PIMERZIN, A. A. & VEREVKIN, S. P. (2018) Benchmark properties of biphenyl as a liquid organic hydrogen carrier: Evaluation of thermochemical data with complementary experimental and computational methods. *The Journal of Chemical Thermodynamics*, 122, 1-12.
- ZHENG, J., LIU, X., XU, P., LIU, P., ZHAO, Y. & YANG, J. (2012) Development of high pressure gaseous hydrogen storage technologies. *International Journal of Hydrogen Energy*, 37:1, 1048-1057.

**Titre :** Modélisation et optimisation du transport de l'Hydrogène à différents états d'agrégations en France et en Allemagne

**Mots clés :** hydrogène comprimé, hydrogène liquide, transport d'hydrogène, modélisation, optimisation des coûts, visualisation géographique

**Résumé :** L'hydrogène vert pour la mobilité représente une alternative au carburant conventionnel dans l'optique d'un système énergétique basé sur le développement durable. Néanmoins, les propriétés thermodynamiques compliquent l'utilisation de ce vecteur d'énergie à ses conditions standards de pression et de température, ce qui ouvre le débat sur les technologies qui peuvent optimiser le transport et le stockage.

Par conséquent, cette thèse vise à apporter la lumière sur ces solutions et de modéliser l'infrastructure au coût minimal associée à plusieurs scénarios qui diffèrent par la production et la demande en Allemagne et en France entre 2030 et 2050.

Pour cela, le bilan énergétique est modélisé afin de déduire les coûts de transport. Ces coûts sont ensuite introduits dans un modèle linéaire pour

optimiser les capacités d'hydrogène à transporter entre les sites de production et de distribution.

En parallèle, une visualisation géographique est associée au modèle, où les circulations de l'hydrogène en Allemagne et en France sont référencées dans un système d'information géographique.

Les résultats ont montré que l'hydrogène comprimé à haute pression est la meilleure option commune à tous les scénarios. À court terme, les coûts de déploiement de l'infrastructure peuvent être amorties, en remplaçant le transport et le stockage du gaz comprimé à faible et moyenne pression par les liquides organiques porteurs d'hydrogène. Enfin, les scénarios analysés ont montré une meilleure répartition géographique de l'hydrogène en France, contrairement à l'Allemagne qu'a connue une disparité entre les éventuels points de production et de consommation.

**Title :** Optimization of the infrastructure cost of hydrogen transported at different states of aggregation in France and Germany

**Keywords :** hydrogen compressed gas, hydrogen liquid states, hydrogen transport infrastructure, modeling, cost optimization, geographical visualization

**Abstract:** Hydrogen for mobility represents an alternative to conventional fuel to achieve a future energy system based on sustainable development. Nevertheless, the thermodynamic properties of hydrogen make the use of this energy carrier at its standard pressure and temperature conditions inefficient, opening the debate on the optimal technologies that can be used to transport and store the hydrogen.

Therefore, this thesis aims to shed light on adequate hydrogen transport and storage technologies and to model the optimal infrastructure for different production and demand scenarios in France and Germany, between 2030 and 2050.

To this end, using the energy requirements associated to hydrogen transformation, the costs of processing, storing, and transporting hydrogen using trucks are deduced. Then, a

model is developed to optimize the transported hydrogen capacities between the production and distribution sites. In parallel, a geographical visualization is associated with the model where all the flows of hydrogen transported in Germany and France are geo-referenced based on the distribution of expected demand and hydrogen production.

The overall results showed that compressed gas at high-pressure level is a better common option for all the scenarios studied. Concerning early-stage infrastructure deployment, costs could be further minimized by substituting compressed gas at low to medium pressure levels for liquid organic hydrogen carrier. Finally, the results of the scenarios analyzed showed a better geographical distribution of hydrogen in France. In contrast, the case of Germany suffered from a disparity between production and eventual consumption locations.